# Final Report

## DSE Group 12 - Wings For Aid

**TU**Delft

# Final Report

by

## DSE Group 12 - Wings For Aid

| Student Name | Student Number |
|---|---|
| Bram Buijvoets | 4793110 |
| Joep de Boer | 4877160 |
| Martijn van Dongeren | 5083486 |
| Luc Gemassmer | 5025362 |
| Bram Meijerink | 4997328 |
| Alberts Osis | 5057531 |
| Daniel Tromborg | 5000106 |
| Yoni Verhulst | 5107121 |
| Jose Villalta Alas | 5095077 |
| Georgi Rulev | 5079403 |

**Changelog**

| Version | Notes |
|---|---|
| 1.0 | Draft, Submitted 15-06-2022 |
| 1.1 | Final, Submitted 21-06-2022 |

| | |
|---|---|
| Principal Tutor: | Ir. J.A. (Joris) Melkert |
| Coaches: | Dr. E. (Erdem) Akay & S. (Stavrow) Bahnam MSc |
| Project Timeline: | April 16 - June 23, 2022 |
| Faculty: | Faculty of Aerospace Engineering, Delft |

Cover Image: Own library

**TU**Delft

This report was written by a group of 10 aerospace engineering students at the Technical University of Delft. This project has been completed for the Design Synthesis Exercise and the final stage of the bachelors degree. We were tasked with designing a unmanned aerial vehicle that can perform according to the requirement of our client, Wings For Aid.

The Design Synthesis Exercise has been a testament to all the hard work we have devoted to our studies during our Bachelors degree. However we would not have been able to finish this 10 week long project without the help of numerous individuals. As a group we would like to sincerely thank our tutors, Joris Melkert, Erdem Akay and Stavrow Bahnam for all the support and guidance they have provided us with. During the weekly meetings with them we could discuss all our concerns and get advice on how to continue with the design exercise. Without their insights, we would not have been able to come up with the produced result. We would like to thank Barry Koperberg and the Wings For Aid foundation for the three meetings that we were able to schedule during the project. These meetings gave us more insights in how Wings for Aid exactly operates and this kept motivating us to come up with a good design solution.

*Bram Buijvoets, Joep de Boer, Martijn van Dongeren, Luc Gemassmer, Bram Meijerink, Alberts Osis,*
*Daniel Tromborg, Yoni Verhulst, Jose Villalta Alas, Georgi Rulev*
*DSE Group 12*
*Delft, June 2022*

This summary covers three phases during the design. It starts with the preliminary design which describes the main requirements and analyses the market. It also determines initial design parameters and includes a trade-off between different concept designs. During the detailed design phase, the methodology and tools for the final design as well as the final design itself are discussed. Finally in the post DSE design phase, a manufacturing and development plan are presented along with technical recommendations.

## I. Preliminary design phase

### Requirements

First the user requirements are defined. These are requirements that come directly from the user in addition to the mission need statement. The most important user requirement is the driving requirement WFA-REQ-USE-09: The aircraft shall fit in a 20 ft container under transport conditions. This requirement influences the design more than average and is therefore a driving requirement.

As the user requirements do not describe all the things that the system shall adhere to, more requirements are needed. These are either technical requirements or constraints. Every requirement is given a unique identifier consisting out of five elements from which can be derived what kind of requirement it is. Next to the driving user requirement, there are also key/driving requirements which are either constraints or technical requirements:

- WFA-REQ-USE-09: For Wings for Aid it is important that the aircraft fits in a 20 ft container. The dimensions of the container limit the design and therefore this requirement is a driving requirement.
- WFA-UREQ5-SysCo-FI-1: For the customer it is important that the total aircraft has a lower unit cost than € 15,000. This is limiting and something the customer specifically asked for. Therefore this is a key requirement.
- WFA-UREQ19-SysCo-OP-6: The 24 hour operation implies that the aircraft can fly at night. So this is a limiting requirement directly from the customer and thus a key requirement.
- WFA-REQ-SysCo-OP-2: The unmanned requirement is given by the customer and it heavily influences the design. So it is both a key and driving requirement.
- WFA-UREQ1-SysTe-FP-1: The range requirement is also a limiting requirement from the customer, so it must also be seen as a key requirement. However, the range also influences the design more than average so it is a driving requirement as well.
- WFA-UREQ3-SysTe-PD-1: The payload requirement is just like the range requirement a limiting request from the customer and drives the design significantly and is therefore a key and driving requirement.
- WFA-UREQ8-SysTe-SB-1 and WFA-UREQ8-SysTe-SB-2: The stability of the aircraft was also limited by a request from the customer and should be considered very thoroughly during designing. This influences the design more than average and are therefore key and driving requirements.
- WFA-UREQ14-SysCo-OP-3-1, WFA-UREQ11-SysTe-FP-1-5, WFA-UREQ11-SysTe-FP-1-6, WFA-UREQ11-SysTe-FP-1-7: The conditions in which the aircraft should perform are prescribed by the customer. The design will be influenced by the terrain in which it operates, thus creating key and driving requirements.
- WFA-UREQ20-SysTe-PD-1: The total deployment payload for the whole mission is also described by the customer. It also influences the mission profile of a single aircraft and is thus a key and a driving requirement.

### Market analysis

In the market analysis the current and future markets were investigated. The market Wings for Aid is operating in is the Humanitarian Last mile logistics with a market value of $ 1 Billion currently. The customer expects that Wings for Aid can attain a yearly revenue of $ 20 Million and thus a market share of 2%.

The competitors of Wings for Aid were analysed and compared to the characteristics of the Wings for Aid aircraft. It was concluded in the end that Wings for Aid has significant advantages over its competitors in terms of payload and range, but also the fact that the aircraft can carry up to 10 packages makes it a very versatile aircraft over the competitors.

Furthermore the future market and possible market opportunities were investigated. It was expected that the market will grow in the future due to two reasons. Firstly, the market for last mile logistics is expected to grow by about $ 92.32 Billion in 7 years. Secondly, it is expected that in the long term last mile aid will become increasingly more important due to climate change. This brings with it floods, extreme weather conditions and heat, which makes these locations harder to reach, which is where last-mile aid delivery comes into play. Finally several market opportunities next to humanitarian aid delivery were found. The first being medical delivery drones, as this is a relatively large market, and the payload boxes of the aircraft could easily be adjusted to deliver medical supplies. The second option could be military usage, since the aircraft is cheap compared to other military vehicles, it can be used with low risk. Finally the drone could also be used for commercial purposes, where individual boxes may be dropped with food or clothing in remote locations around the globe.

## Initial determination of design parameters

During the preliminary design phase, already some important design parameters are determined. The aircraft weight is found by iterating between Class I and Class II weight estimations. By generating a Wing loading-Power loading diagram, the wing area and required power can be found. The parameters that are determined during this phase are tabulated in Table 1

**Table 1:** Preliminary design values.

| Parameter | Value |
|---|---|
| $W_{fuel}$ $[kg]$ | 116 |
| $OEW$ $[kg]$ | 333 |
| $MTOW$ $[kg]$ | 649 |
| $S_w$ $[m^2]$ | 10.9 |
| $P_{req}$ $[kW]$ | 58 |
| $P_{req}$ $[hp]$ | 78 |

## Design trade-off

For the design trade off, six different design concepts have been considered, as shown in figures 5.2 - 5.7. The different concepts are subjected to a trade-off which is evaluated in the following criteria: Structural mass, drag, manufacturing costs, Appearance, Mission robustness and operability. The results of the trade off are shown in Table 2. Because concept 1 has the highest score it was decided to continue with this conceptual design. The design itself is however not fixed and may change during the detailed design.

**Table 2:** Final trade-off table considering all the scores from the previous tables.

| Concept | Structural mass | Drag | Manu. Cost | Appearance | Mission robustness | Operability | Score |
|---|---|---|---|---|---|---|---|
| Concept 1 | 3 | 4 | 5 | 4 | 4 | 4 | 63 |
| Concept 2 | 3 | 4 | 5 | 3 | 4 | 4 | 62 |
| Concept 3 | 3 | 2 | 3 | 3 | 3 | 2 | 44 |
| Concept 4 | 2 | 4 | 4 | 3 | 3 | 4 | 51 |
| Concept 5 | 3 | 4 | 3 | 2 | 1 | 4 | 47 |
| Concept 6 | 4 | 2 | 3 | 3 | 4 | 3 | 53 |

| Poor (1) R | Bad (2) O | Satisfactory (3) Y | Good (4) LG | Excellent (5) G |
|---|---|---|---|---|

# II. Detailed design phase

## Design methodology and tools

In order to ensure that the detailed design is accurate and realistic, verification and validation (V&V) is performed on each subsystem design. V&V allows the design team to have confidence in the numerical solutions obtained from the created tools. This confidence is what ensures that the aircraft is compliant with the design requirements and specifications, and that the right aircraft has been designed for this specific mission. Verification is performed on two levels: code and system. Each engineering department makes use of their own developed design tools, therefore the following generalised unit tests are performed on the each code:

- **U.1**: Visual inspection that equations are inputted correctly. The test is a pass when at least 2 team members have verified the equations inputted into the code.
- **U.2**: A code function to check that the mathematical sign convention is used properly. The test passes when the expected mathematical sign for a value corresponds to the analysed parameter.
- **U.3**: Visual inspection that correct values and units are inputted. The test is passed when at least 2 team members have verified the values and units inputted into the code.
- **U.4**: Print statements that parameters are within correct order of magnitude. The test passes when the values are within the expected order of magnitude according to 2 team members.

System verification ensures that the code works as intended by the user. In order to check this, initial condition and extreme value tests are applied to verify the system code.

### Aerodynamics

The characteristics of the flow is crucial for an accurate airfoil performance analysis. When performing the airfoil selection, flow conditions at three crucial stages are considered; take-off, cruise and payload deployment. Airfoils from a sample of aircraft with similar mission and performance characteristics were selected as an initial analysis batch, due to the airfoil characteristics and large experimental data set. A variety of performance indicators were used in order to evaluate which airfoil performs the best in the case of the mission profile; $C_{m_\alpha}$, $C_m$, $C_l$, $C_d$, $C_{l_{max}}$, $\alpha_{stall}$, $C_{l_0}$.

XFLR5 was used to perform both 2D airfoil an 3D wing analysis. The analysis of these airfoil are performed using the geometry of the final wing planform. The lift coefficient vs. drag coefficient curve of various airfoils have been displayed in Figure 2
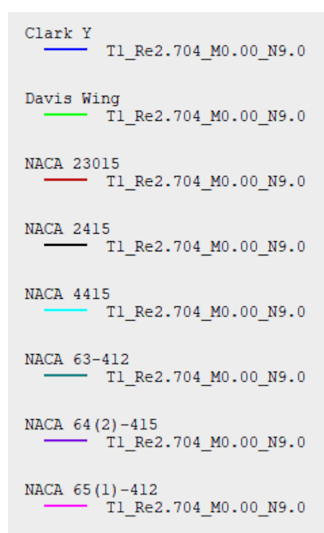


**Figure 1:** Legend for Colours in the 2D Airfoil Analysis
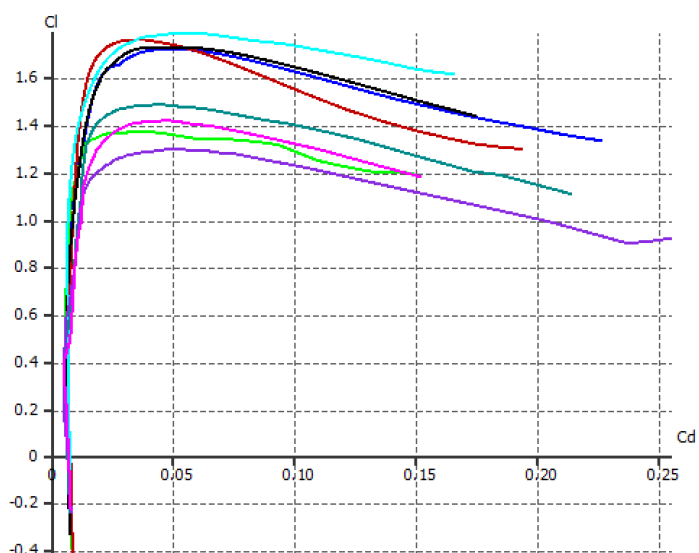
**Figure 2:** $C_l$ VS. $C_d$ Airfoil

After comparing the various airfoils, it was concluded that the NACA $2415$ airfoil had the best combination of characteristics. It presented high lift to drag ratio, less negative moment coefficients, and high lift coefficient at zero angle of attack. Furthermore, a 3D wing analysis was conducted in order to analyse how the airfoil would perform using the final wing geometry. Besides the main wing airfoil, the empennage airfoil also requires analysis.

When selecting an airfoil for both the vertical and horizontal stabilisers, two main factors are crucial: The ability to generate lift in both directions and low drag characteristics. Therefore a symmetrical airfoil with a lower max thickness to chord ratio is typically selected. Historically airfoils such as the NACA 0012 and NACA 0009 have been used as empennage airfoils. The airfoils have a symmetrical profile with respectively a maximum of 12% and 9% chord thickness at 30.9% of the chord. Within the scope of this initial detailed design, a NACA 0009 airfoil is chosen. It is concluded that it is more critical to have a low drag airfoil due to the need for energy efficient optimisation.

In addition, a drag analysis of the aircraft was performed in order to obtain an estimate for the drag coefficient of the aircraft. This process was broken into two parts whereby the zero-lift drag coefficient ($C_{D_0}$) and the lift-induced drag coefficient $C_{D_i}$ were estimated. The breakdown of the zero-lift drag coefficient of the main aircraft components can be found in Table 3 while the total aircraft drag coefficient as a function of the lift coefficient is represented by Equation 1.

**Table 3:** Contribution of different aircraft components to zero-lift drag coefficient

| Component | $C_{D_0}$ Contribution |
|---|---|
| Wing | 0.00972 |
| Horizontal Tail | 0.00129 |
| Vertical Tail | 0.000850 |
| Fuselage | 0.0116 |
| Landing Gear | 0.00590 |
| Excrescence and Leakage | 0.00294 |
| **Total** | **0.0323** |

$$C_D = 0.0323 + 0.0452 \cdot C_L^2 \tag{1}$$

**Materials & structures**

The structural design of the aircraft depends on the loads the aircraft experiences during operation. To determine these loads, certain motions such as turning and rotation were investigated. From the load cases, shear, moment, and torsional loading diagrams were generated for the aircraft wing and fuselage. This was than put into numerical which calculate shear stress, normal stress, twist and deflection. These models were then used to design a wingbox that has an optimal weight while ensuring no yielding or buckling occurs. In addition, a preliminary design analysis for the fuselage was performed. For the structures considered, it was decided that aluminium alloy AL7075 (T6) would be used due to its high strength.

**Stability and control**

To size the empennage, the stability and control of the aircraft had to be evaluated. For this purpose a software code was written, which takes as an input several geometric and aerodynamic parameters and as the output gives the horizontal tail surface area and optimal wing position. The program works by first constructing a scissor plot. This plot indicates the allowed C.G. ranges for different horizontal tail surface areas. The program also makes a loading diagram. This diagram shows how the aircraft's C.G. location shifts in different loading conditions, and is used to find the minimum and maximum C.G. location of its mission profile. This loading diagram was then used to construct a plot which shows the C.G. range vs. Wing position. Finally an algorithm was made which combined the latter graph with the scissor plot to find an optimal horizontal tail surface area and wing position, which still allows for sufficient stability and controllability.

**Performance and propulsion**

To design an aircraft that complies with the take-off and landing distance, the mission time and the amount of fuel necessary for the it, a performance analysis is necessary. To perform this analysis, an engine and propeller model are used. The model for the engine is based on performance data of the UL260i. This is considered a benchmark engine, of which the properties are well known and researched. A polynomial regression is then performed on the available data to obtain the fuel flow as a function of RPM and power. The propeller model is based on the efficiency data with respect to the advance ratio of a standard propeller. Additionally a function is created to correct propeller efficiency when not flying at optimum design velocity. These models are then implemented together to create a general function to evaluate the engine and propeller performance. Newton's method is used to optimise for either fuel flow or power available. This will then give the required insight into the thrust and fuel flow for the flight performance tools. These tools are created to calculate the performance during every phase of flight: take-off, climb, cruise, descent and landing. Code is written for each of these phases that takes as an input certain aircraft and engine parameters, such as weight, wing surface area and mass flow. It then outputs other parameters like the fuel consumed, the time taken and the horizontal distance travelled. These tools are then combined to calculate the characteristics of a whole mission profile. Calculating the aircraft performance provides us the opportunity to optimize our design during the detailed design phase while still adhering to all relevant requirements.

# Detailed Design

**Fuselage design**

For the design of the fuselage inside out approach was used wherein the fuselage is designed around the components which in this case were mostly the payload. This means that the cargo configuration was one of the main design parameters in fuselage design. Additionally, it was found beneficial for stability purposes to reduce the length of the fuselage which resulted in a wide and rather short design with a 2-3-3-2 cargo box configuration as shown in Figure 3. Finally, structural analysis of the fuselage was performed where bending and torsional stresses and deformations were evaluated. An example, of a structural design concept is provided in Figure 4.
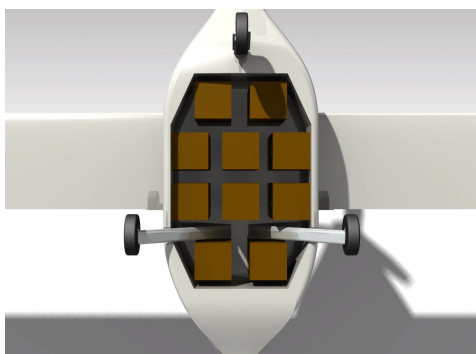


**Figure 3:** Cargo configuration of the aircraft



**Figure 4:** An example of the structural configuration of the fuselage

**Main wing design**

The planform geometry is defined using the wing area generated from the mission design point. Furthermore, the aspect ratio defines the wing span and root chord. The maximum dimensions of the wing are constrained by the dimensions of a $20\ ft$ container. Finally The rest of the parameters were

defined based on the aerodynamic analysis performed in XFLR5. In the figures below, The geometry and aerodynamic characteristics at cruise are tabulated.

**Table 4:** Wing Planform Geometry

| Parameter | Symbol | Value | Unit |
|---|---|---|---|
| Wing Area | $S$ | 11.43 | $m$ |
| Wing Span | $b$ | 10.14 | $m$ |
| Root Chord | $C_r$ | 1.13 | $m$ |
| Taper Ratio | $\lambda$ | 1 | $-$ |
| Quarter Chord Sweep | $\Lambda_{1/4}$ | 0 | $\circ$ |
| Max Thickness to Chord Ratio | $t/c_{max}$ | 0.15 | $-$ |
| Aspect Ratio | A | 9 | $-$ |
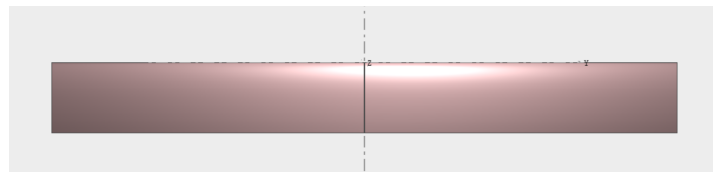


**Figure 5:** Final Wing Planform

**Table 5:** Final Wing Characteristics at Cruise Conditions

| Angle of attack | $C_{L_{max}}[-]$ | $C_{L_0}[-]$ | $C_{m_{cruise}}[-]$ | $\alpha_{stall}[\circ]$ | $\frac{C_L}{C_D}_{cruise}[-]$ |
|---|---|---|---|---|---|
| 6.2 | 1.63 | 0.3 | -0.28 | N.A. | 24.5 |

As for the design of the wingbox, the conceptual design as presented in Figure 6 was selected whereby the wingbox (in orange) can be seen within the selected airfoil design. The design parameters for the designed wingbox can be found in Table 6.
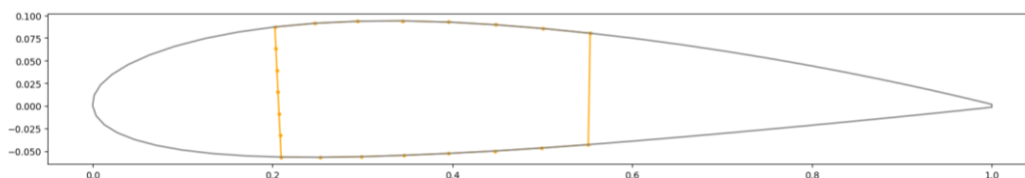


**Figure 6:** Conceptual wingbox design

**Table 6:** Design parameters of wingbox

| Design parameters | Concept 1 |
|---|---|
| Material | Aluminium 7075 (T6) |
| Spar chord-wise positioning | $0.2$ and $0.6$ |
| Maximum thickness | $1.4\ mm$ |
| Minimum thickness | $0.6\ mm$ |
| Side panel to horizontal panel thickness ratio | 1.8 |
| Number of stringers | 7 on top, 5 on bottom |
| Stringer cross-sectional area | $3.8 \cdot 10^{-5}\ m^2$ |
| Rib spacing | $0.3\ m$ |

| Mass | 26.8 $kg$ per wing |
|------|---------------------|

## Empennage design

For the empennage sizing both the horizontal and vertical tail were sized. The horizontal tail was sized using the aforementioned methods. The final horizontal tail dimensions are presented below.

**Table 7:** Sizing for horizontal tail

| $S_h$ $[m^2]$ | 2.13 |
|---------------|------|
| $b_h$ $[m]$ | 2.53 |
| $c_h$ $[m]$ | 0.84 |

With the sizing of the empennage as indicated by the table above, the driving requirement that the aircraft shall fit inside a 20 ft container is not met. Therefore, cuts are required in the empennage in order to make it fit. It is desirable to have the amount of cuts minimized, therefore it has been chosen to change the empennage configuration from a conventional to a H-tail. This ensures that the vertical tails will fit inside the container. The vertical tail is shiften below the horizontal tail until it just fits in the container. The sizing for the H-tail can be found in Table 8.

**Table 8:** Sizing for the H-tail

| Horizontal tail | | Vertical tail | |
|-----------------|-------|----------------------------------|-------|
| **Parameter** | **Value** | **Parameter** | **Value** |
| $S_h$ $[m^2]$ | 2.13 | $S_v$ $[m^2]$ | 0.89 |
| $b_h modular$ $[m]$ | 2.20 | $b_v$ $above\ horizontal\ tail$ $[m]$ | 0.71 |
| $b_h nonmodular [m]$ | 0.32 | $b_v$ $under\ horizontal\ tail$ $[m]$ | 0.45 |
| $c_h$ $[m]$ | 0.84 | $c_v$ $[m]$ | 0.77 |

## Undercarriage design

From the trade off performed during the project, a tricycle configuration was chosen. This was chosen for ground stability as well as the added ground clearance when compared to a tail dragger configuration. The landing gear was entirely constrained by both the shipping container and static load requirements on the nose landing gear. The internal dimensions of the container constrain the wheel track to 2.3m. The following diagrams show the geometry of the landing gear.
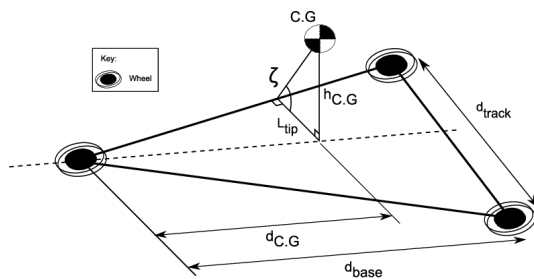


**Figure 7:** Landing Gear Geometry [42]
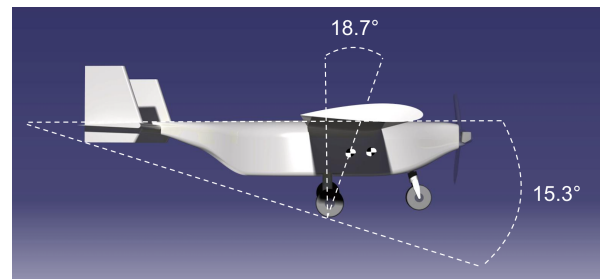


**Figure 8:** Aircraft Side-on View Displaying Scrape Angle

**Table 9:** Landing Gear Configuration

| Parameter | Value | Unit |
|-----------|-------|------|
| $X_{Nose}$ | 0.1 | $m$ |
| $W_b$ | 1.45 | $m$ |
| $W_t$ | 2.3 | $m$ |
| $Z_{LG}$ | 0.6 | $m$ |

**Table 10:** Tire dimensions and Performance

| Parameter | Value | Unit |
|-----------|-------|------|
| $d_t$ | 0.34 | $m$ |
| $W_t$ | 0.17 | $m$ |
| $p_t$ | 20 | $Psi$ |

Given these geometries, the landing gear can expect a minimum static nose load of 8.2% of the MTOW at take-off and a maximum static nose load of 15.4% of the MTOW on landing. In order to fully assess the consequences of the design constraints a full structural analysis must be performed and verification drop tests conducted. When analysing the turning performance of the landing gear, turns of radius 1.85m can be performed with a deflection of 51.6 degrees from the nose wheel. This allows for tight turns while on the runway, ensuring that the aircraft can perform the mission in tight spaces. Furthermore as seen in Figure 7.19, the design has a scrape angle of 15.3 degrees, allowing for adequate clearance during the pitch-up maneuver at take off and during landing.

**Propulsion system**

The propulsion system is designed to be cost effective reliable and easy to maintain. The engine of choice is the AM13 from Aeromomentum. It is a converted Suzuki G13 (4-stroke) engine. With a max power of $100\ hp$ the aircraft has the ability to take off within $300\ m$. It can take low octane rated automotive gasoline which increases flexibility when fuel is hard to come by. The engine can operate for $2000\ hrs$ before overhaul is needed. This keeps operational cost low and downtime limited. The predicted fuel-efficiency is expected to be slightly better than the Rotax-912 ULS. The price point of the Rotax lies around double the price of the AM13 which costs $\$9,995$ making the AM-13 clearly more attractive. The propeller design is driven, next to cost and reliability, by the need for sufficient ground clearance and the ability to convert the engines power in to thrust. Due to the diameter limitation for ground clearance a three-bladed propeller is required for higher maximum thrust. The propeller will be fixed pitch and will be optimised for cruise minimizing the fuel required. The next steps in designing/implementing the propulsive system is obtaining data from the engine on a test bed. Additionally propeller manufactures will have to be consulted to research the possibility to use an off the shelve propeller and compared with benefit for developing a type specific propeller.

**Operation and planning**

The operation of the mission starts with an incoming aid delivery request. This request can come from anywhere in the world. To transport the drones and Forward Operating Base an aircraft can be used. However using an aircraft is expensive, so it is recommended to transport the base and the first few drones by aircraft and ship the other drones over seas and by train. This also allows the local crew to prepare the base before all drones arrive and the drone deliveries start. The dropping mission is performed by the aircraft in 4.7 hours. This is not a complete mission as this does not include resupplying and refueling. In total the complete mission takes 5:27 hours. This means that an aircraft can perform 4.4 missions in a 24 hours period and can drop $881\ kg$ of payload per day. To meet the performance of the Hercules C-130, which can drop $20,000\ kg$, 23 aircraft are needed. To cover for the maintenance period of the aircraft, 6 additional planes are needed to prevent the loss of sufficient capacity. The direct control for short range id done by RC. For long range a flight plan can be uploaded to the aircraft which the aircraft will follow automatically. In this way the airplane can be controlled by the ground operator even if direct control is not available.

# III. Post DSE phase

## Production Plan

In the production plan, the manufacturing, assembly and integration plan from the start to the delivery of the customer was made. This was done using a flow chart containing manufacturing steps, tasks and subtasks connected by arrows to indicate the order. The first step in the process is to order the necessary parts. These contain blank materials and also pre-manufactured parts. It was assumed that smaller structural parts like stringers and ribs will be manufactured by an external supplier, while the larger parts that are harder to transport, like fuselage and wing skin, will be manufactured by Wings for Aid themselves. The next step is to prepare the parts. In the case of pre-manufactured parts they only have to go through quality control, while the blank materials will have to go through the necessary processing to get to the desired shape. The third step is to assemble the subassemblies, which are the wing, fuselage, landing gear and empennage. Then these subassemblies will be moved to the assembly line to assemble the final aircraft. Here the aircraft body, engine and landing gear will be assembled, and finally moved to a hangar. The final step is delivery to the customer.

Furthermore, production methodology was considered. Line production was chosen as a method of manufacturing, which is the most used manufacturing method for aircraft. This method utilises routine forming to increase the efficiency of the working. Furthermore quality control is implemented after every step (process-based quality control) using non-destructive tests. Finally lean manufacturing was also considered for production.

## Future project development

For the post-DSE phase, a project design and development logic diagram, as well as a project Gantt chart were made. These diagrams contain the recommended steps to take from the current design until it is a working aircraft that can be delivered to the customer. In the beginning, more detailed design and analysis need to be performed before production can begin. Company development was also part of the post-DSE plans. The final steps are developing operations and logistics, and performing the production plan. From the Gantt chart, the estimated launch date for the aircraft was Q4 2024. Lastly, technical recommendations were made for each engineering department. The most important ones are listed below:

### Aerodynamic
- WFA-AERO-REC-01: Complete further analysis on empennage airfoil selection.
- WFA-AERO-REC-02: Conduct in depth analysis of subsystem interactions, ie. wing, fuselage, empennage, landing gear. Optimise geometry between these sections to provide minimum drag while still optimising weight and structural performance.
- WFA-AERO-REC-03: Construct complete drag budget using CFD to characterise drag coefficients at each stage in the flight profile.

### Structures
- WFA-STRUC-REC-01: Create complete CAT model for structural analysis. With this complete model FEM (Finite Element Method) analysis can be done and a more detailed design can be made.
- WFA-STRUC-REC-02: Consider bending and torsional stiffness in the design process.
- WFA-STRUC-REC-03: Consider more stress considerations and failure modes such as inter-rivet buckling, fatigue failure, impact damage, shear buckling, and stress.

### Flight performance & propulsion
- WFA-PP-REC-01: Further research into a better fitting engine.
- WFA-PP-REC-02: Further research into a specific propeller design.
- WFA-PP-REC-03: Further research into propeller performance characteristics.

### Stability & control
- WFA-SC-REC-01: Find other static stability derivatives in lateral direction using the DATCOM method, to assess the lateral static stability.
- WFA-SC-REC-02: The subsystems should be correctly positioned by sizing the inside of the fuselage, which will give a more accurate C.G. OEW location.
- WFA-SC-REC-03: Dynamic stability should be analysed by using the equations of motion to calculate the eigenvalues corresponding to all the eigenmotions.

### Operations
- WFA-OPS-REC-01: Complete analysis of optimum distribution center locations to reduce logistical challenges.
- WFA-OPS-REC-02: Develop a complete operating profile program that allows the operator to input the package delivery location and receive the flight performance plan, fuel required, contingency plans as well as if the current operating range is feasible.

# Contents

| | | |
|---|---|---|
| $CG$ | Centre of gravity | - |
| $MAC$ | Mean aerodynamic chord | m |
| $MNS$ | Mission Need Statement | - |
| $MTOW$ | Maximum take off weight | N |
| $OEW$ | Operational empty weight | N |
| $POS$ | Project objective statement | - |
| $ROC$ | Rate of climb | m/s |
| $RPM$ | Rounds per minute | 1/minute |
| $ZFW$ | Zero fuel weight | N |

| | | |
|---|---|---|
| $\alpha$ | Angle of attack | rad |
| $\alpha_c$ | Experimental constant for buckling analysis | - |
| $\alpha_T$ | Thrust angle | deg |
| $\epsilon$ | Downwash angle | rad |
| $\Gamma_0$ | Vortex strength constant | $m^2/s$ |
| $\gamma_0$ | Climb angle | deg |
| $\Lambda_m$ | Sweep angle at position of maximum thickness | rad |
| $\mu$ | Viscosity | $Ns/m^2$ |
| $\nu$ | Poisson ratio | - |
| $\rho$ | Density | $kg/m^2$ |
| $\rho_g$ | Radius of gyration | m |
| $\sigma_y$ | Yield stress | MPa |
| $\sigma_{cc}$ | Crippling stress | MPa |
| $\sigma_{cr}$ | Critical buckling stress | MPa |
| $\tau$ | Shear stress | MPa |
| $\theta$ | Twist angle | rad |

| | | |
|---|---|---|
| $(x/c)_m$ | Position of maximum thickness | - |
| $\bar{c}$ | Mean aerodynamic chord | m |
| $\bar{x}_{ac}$ | Aerodynamic centre location | /MAC |
| $\bar{x}_{cg}$ | Centre of gravity location | /MAC |

| | | |
|---|---|---|
| $\bar{x}_{np}$ | Neutral point location | /MAC |
| $\frac{t}{c}$ | Average thickness-to-chord ratio | - |
| $\sigma_{11}$ | Tensile stress | Pa |
| $\sigma_{12}$ | Shear stress | Pa |
| $A_m$ | Enclosed area | $mm^2$ |
| $A_s$ | Stringer cross sectional area | $mm^2$ |
| $AR$ | Aspect ratio | - |
| $b$ | Wingspan | m |
| $b_h$ | Horizontal tail span | m |
| $b_p$ | Plate width | m |
| $b_v$ | Vertical tail span | m |
| $C$ | Boundary condition constant | - |
| $C_D$ | Drag coefficient | - |
| $c_h$ | Horizontal tail chord | m |
| $C_L$ | Lift coefficient | - |
| $C_m$ | Moment coefficient | - |
| $c_v$ | Vertical tail chord | m |
| $C_{D_0}$ | Zero-lift drag coefficient | - |
| $C_{D_i}$ | Lift-induced drag coefficient | - |
| $C_{D_{misc}}$ | miscellaneous drag coefficient | - |
| $C_f$ | Skin fricion coefficient | - |
| $C_{L_h}$ | Tail lift coefficient | - |
| $C_{L_{\alpha_{A-h}}}$ | Aircraft-less-tail lift curve slope | 1/rad |
| $C_{L_\alpha}$ | Lift curve slope | 1/rad |
| $C_{l_\beta}$ | Change in rol moment coefficient due to change in angle of slideslip | 1/rad |
| $C_{L_{A-h}}$ | Aircraft-less-tail lift coefficient | - |
| $C_{L_{max}}$ | Maximum lift coefficient | - |
| $C_{L_{takeoff}}$ | Lift coefficient at take-off | - |
| $C_{m_\alpha}$ | Change in pitching coefficient due to change in angle of attack | 1/rad |
| $C_{m_{ac}}$ | Moment coefficient about aerodynamic center | - |
| $C_{n_\beta}$ | Change in yaw moment coefficient due to change in angle of slideslip | 1/rad |
| $C_{n_r}$ | Change in yaw moment coefficient due to change in yaw rate | 1/(rad/s) |

| | | |
|---|---|---|
| $C_{Y_\beta}$ | Change in side force coefficient due to change in angle of slideslip | 1/rad |
| $D$ | Drag | N |
| $D_p$ | Propeller diameter | m |
| $E$ | Youngs modulus | MPa |
| $e$ | Oswald efficiency factor | - |
| $E_t$ | Tangent modulus | GPa |
| $F$ | Force | N |
| $f$ | Fuselage slenderness ratio | - |
| $f$ | Mean stress at failure | MPa |
| $F_{fric}$ | Friction force | N |
| $FF$ | Component form factor | - |
| $G$ | Shear Modulus | GPa |
| $h_{screen}$ | Screen height | m |
| $I_{xx}$ | Moment of inertia around x axis | $m^4$ |
| $I_{xy}$ | Product moment of inertia around x and y axes | $m^4$ |
| $I_{yy}$ | Moment of inertia around y axis | $m^4$ |
| $IF$ | Interference factor | - |
| $L$ | Lift force | N |
| $l$ | Length of the flow | m |
| $L_e$ | Effective stringer length | m |
| $l_h$ | Horizontal tail length | m |
| $l_v$ | Vertical tail length | m |
| $M$ | Mach number | - |
| $M_x$ | Moment about x direction | Nm |
| $N$ | Compressive end load per width | N/inch |
| $n$ | Experimental constant for buckling analysis | - |
| $n$ | Load factor | - |
| $P$ | Power | W |
| $P_a$ | Power available | W |

| | | |
|---|---|---|
| $P_r$ | Power required | W |
| $P_{br}$ | Break power | W |
| $q_b$ | Varying shear flow | N/m |
| $q_{s0}$ | Constant shear flow | N/m |
| $R$ | Radius | m |
| $Re$ | Reynolds number | - |
| $S$ | Wing surface area | $m^2$ |
| $s$ | Length of section | m |
| $S_h$ | Horizontal tail surface area | $m^2$ |
| $S_{exp_{HT}}$ | Exposed horizontal tail area | $m^2$ |
| $S_{exp_{VT}}$ | Exposed vertical tail area | $m^2$ |
| $S_{exp_{wing}}$ | Exposed wing area | $m^2$ |
| $S_{ref}$ | Wing reference area | $m^2$ |
| $S_{wet}$ | Wetted area | $m^2$ |
| $T$ | Thrust | N |
| $T$ | Torsional moment | Nm |
| $t$ | Thickness | m |
| $T_{static}$ | Static thrust | N |
| $V$ | Velocity | m/s |
| $V_\infty$ | Freestream velocity | m/s |
| $V_{LOF}$ | Lift off velocity | m/s |
| $V_x$ | Shear force in x direction | N |
| $V_y$ | Shear force in y direction | N |
| $W$ | Weight | N |
| $W_b$ | Wheel Base, Distance between nose and main nomunitm | |
| $w_e$ | Skin width | mm |
| $W_t$ | Wheel track, Distance between main wheels nomunitm | |
| $y$ | Spanwise position along the wing | m |
| $Z_{LG}$ | Distance between ground and fuselage | m |

Natural and humanitarian disasters lead to the forced displacements of large groups of people. Destruction of infrastructure, supply chains and access to essential goods forces these displaced individuals to seek out necessary aid to survive. Typical large distribution centers present challenges with regards to health, safety and logistics. Therefore the organisation, Wings For Aid, has produced a concept for the "last mile" aid distribution. DSE Group 12, Wings for Aid, has produced a full system design to fulfil the needs and requirement of the client Wings For Aid and their aid delivery concept. The aircraft is an unmanned aerial vehicle fully capable of tackling the logistical and distribution issues surrounding the "last mile" delivery of aid. When a nation's infrastructure is not sufficient to allow for adequate distribution using conventional methods, government organisations, as well as non-government organisations, such as the Red Cross, can request Wings For Aid to perform the operation utilising our system. The aircraft specialises in the pinpoint delivery of ten 20 kg aid packages within an effective operational radius of 250 km from the ground station.

This project aims to solve the "last mile" delivery problem for areas that are hard to reach. The final report addresses the detailed design of the system. First the description of the project is presented and the market is analysed. Also the requirements are presented again and a summary is given of the preliminary design phase. Then the design methodology is presented where every sub department gives an overview of the tools they used to get to their design and how these tools are verified. Then they all present their detailed design where the results of the tools are shown. Afterwards, the ability of the aircraft to perform the mission is analysed with regards to different criteria, like reliability, safety sustainability, etc. Finally, in the last part of the report the post DSE activities like manufacturing plan and the post DSE Gantt chart is presented.

## 2.1. Project Objective

Before the project can start, first the project has to be defined. This can be done by the mission need statement (MNS) and the project objective statement (POS).

The mission need statement describes the need and mission in general terms. The mission need statement for this project is defined as: *Deliver aid in a timely and affordable manner to small groups of people in disaster struck areas*.

A project objective statement describes what the system does and how it will be designed. The project objective statement is defined as *The project team will design a low-cost, easily transportable, unmanned aircraft that can deliver a total payload of 100 to 200 kg of aid packages within an effective range of 250 km, by 10 students in 10 weeks*.

This project aims to produce a comprehensive system overview of the initial design. This overview, which is contained in the content of this final report, will cover all aspects of the design, prototyping, manufacture and implementation of said system. This system is being designed for the customer Wings For Aid, which is currently testing a proof of concept system, designated the MiniFreighter 8/500FW. This design study acts as an avenue for the organisation to test new and unconventional solutions which also may act as a product to solve the issue of "last mile" aid delivery.

## 2.2. Project Organization

In the initial stage of the project, a team structure was established in order to ensure organisation and work distribution for the following stages; both managerial and engineering roles were created. Within each of theses roles, associated responsibilities were assigned. The detailed breakdown of role responsibilities can be found in Table 2.1. Furthermore to have an overall understanding of the interaction between internal and external parties, an organogram was created. The organogram can be observed in Figure 2.1.
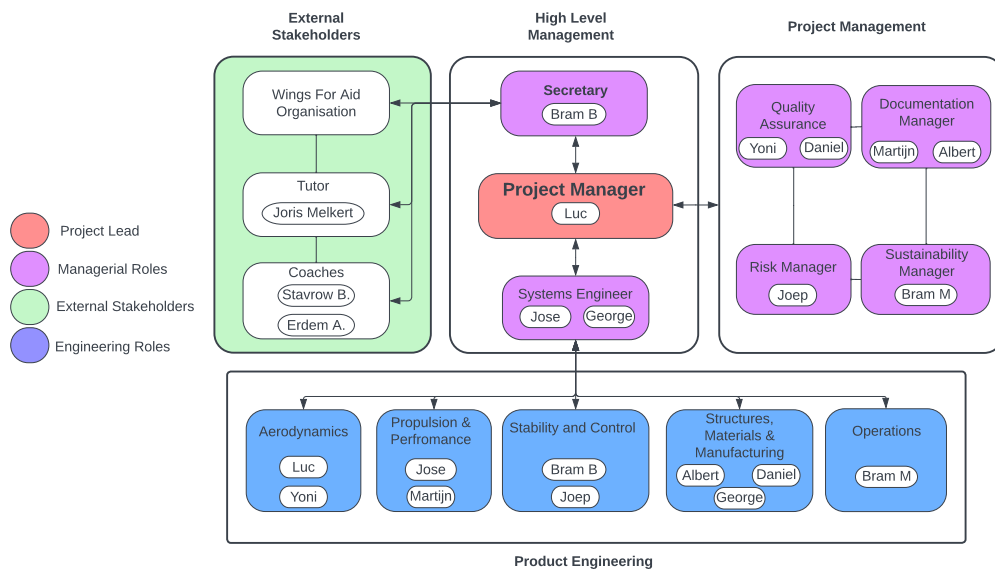


**Figure 2.1:** Project Organogram

**Table 2.1:** Responsibility Breakdown of Organisational Roles

| Role | Responsibilities | Assigned Individuals |
|---|---|---|
| *External Stakeholders* | | |
| **Project Mentor and Coaches** | - Provide systems engineering support<br>- Supervise design process | - Joris Melkert<br>- Erdem Akay<br>- Stavrow Bahnam |
| **External Client** | - Provide top level design requirements<br>- Provide industry knowledge and suport | - Wings For Aid |
| *Management Department* | | |
| **Project Manager** | - Keep overview of completed tasks, required deliverables and deadlines<br>- Organise and lead daily meetings | - Luc Gemassmer |
| **Secretary** | - Compose record of meeting minutes<br>- Project contact channel for principle tutor, coaches and TAs<br>- Schedule Status Meetings<br>- Responsible for submitting final documents | - Bram Buijvoets |
| **Systems Engineers** | - Inform management group of engineering design option updates<br>- Ensure final design meets all top level requirements | - Jose Villalta Alas<br>- George Rulev |
| **Quality Assurance Manager** | - Ensure that referencing and latex standards are met, utilising correct formatting styles throughout the document | - Yoni Verhulst<br>- Daniel Tromborg |
| **Risk Manager** | - Identify risks and contigency stratagies | - Joep de Boer |
| **Sustainability Manager** | - Check design meets sustainability standards and create sustainable project practices | - Bram Meijerink |
| **Documents Manager** | - Organises communication pathways<br>- Ensure project updates are properly submitted in the logbook<br>- Organising file storage | - Martijn van Dongeren<br>- Alberts Osis |
| *Engineering Department* | | |
| **Aerodynamics** | - Designing lifting bodies<br>- Responsible for the drag budget | - Luc Gemassmer |
| **Performance & Propulsion** | - Designing of propulsion system<br>- Designing for flight performance | - Jose Villalta Alas<br>- Martijn van Dongeren<br>-Joep de Boer |
| **Stability & Control** | - Designing control and stability subsystems of the aircraft | - Bram Buijvoets<br>-Yoni Verhulst |
| **Structures & Materials** | - Designing load carrying structures<br>- Choosing appropriate materials for structures and manufacturability | - Alberts Osis<br>- Daniel Tromborg<br>- George Rulev |
| **Operations** | - Account for maintenance needs of the aircraft<br>- Account for different mission profiles | - Bram Meijerink |

## 3.1. Current Market

Before an analysis can be conducted the market of Wings for Aid must be defined first. Fortunately, the customer has already performed extensive market research. Wings for Aid is operating in "Humanitarian logistics" which has a market value of approximately $3.65 Billion. This market is however quite vast, thus the market needs to be segmented. Wings for Aid takes care of the "Last mile delivery" meaning the last part of the delivery to the actual destination. Note that this market segment is not limited to aerial delivery. This part of the humanitarian logistics market has a value of approximately $ 1 Billion according to the customer. Wings for Aid strives to take approximately a 2% market share in this segment, meaning a yearly revenue of $20 Million. However this revenue assumes a fleet of 100 aircraft. Since the requirement is a fleet of 500 aircraft, it is expected that the market share will be higher, provided there is enough demand on the market. Not only is it important to understand the value of the current market, but potential customers of the service must also be identified. Currently the client Wings for Aid plans to utilise a service model where the aircraft and all equipment involved in the system belongs exclusively to the organisation. The service that they provide is then contracted out to customers; the mission location is identified and then carried out in an appropriate time frame. The main customers of this service will be large organisations involved with the distribution of aid to affected countries. Notable organisations include: The United Nations, The World Food Bank and The Red Cross.

## 3.2. Competitors

Wings for Aid has several competitors in the last mile delivery sector. The most important criteria to compare the competitors with are the range and maximum payload. The main competitors are tabulated in Table 3.1:

**Table 3.1:** Competitors of Wings for aid

| Company | Range [km] | Payload [kg] |
|---|---|---|
| **Wings for Aid** | 500 | 200 |
| Zipline [1] | 300 | 1.8 |
| Elroy Air [2] | 482 | 226 |
| UAV aid [3] | 300 | 10 |
| Pouncer drone (MK3) [4] | 100 | 100 |
| Swoop Aero Kite [5] | 180 | 5 |

As can be seen, Elroy Air is the closest competitor for both range and payload. Furthermore the company has the same goals as Wings for Aid, i.e. providing humanitarian aid in difficult to reach areas. Elroy Air currently has an annual revenue of $5,837,000, which is approximately a quarter of the estimated revenue of Wings for Aid. There are however differences in the way of operation. Firstly, Elroy Air sells the UAV's to commercial, defense and humanitarian customers, while Wings for Aid does not sell the drones themselves, but the service. Furthermore Elroy Air's drone is a VTOL aircraft, meaning it can vertically take off and land. The Wings for Aid aircraft is a conventional aircraft and drops the packages while still in the air, which is significantly faster than landing to deliver packages.The next closest competitor is the Pouncer drone. This drone is similarly to Wings for Aid able to deliver aid supplies to hard to reach areas. The difference between the Pouncer drone and Wings for Aid is that the Pouncer drone is an expendable drone, meaning it can only be used once. This means the drone can only be used for one delivery [6]. This is again a large difference with the Wings for Aid aircraft which functions as a conventional aircraft, able to perform multiple missions. In conclusion Wings for

---

[1]https://www.wsj.com/articles/amazon-alphabet-and-others-are-quietly-rolling-out-drone-delivery-across-america-11648872

[2]https://www.theverge.com/2022/1/26/22902351/elroy-air-chaparral-autonomous-vtol-electric-hybrid-cargo-plane

[3]https://www.aerosociety.com/news/multirole-lifesavers-a-new-approach-to-humanitarian-drones/

[4]https://www.dezeen.com/2017/02/23/edible-pouncer-drone-delivers-aid-victims-natural-disasters-conflict-technology-desi

[5]https://swoop.aero/media-releases/newly-unveiled-aircraft#:~:text=The%20Kit%20can%20travel%20up,of%20up%20to%205%20kgs.

[6]https://www.rtlnieuws.nl/tech/artikel/3935936/eetbare-drone-redt-mensen-van-de-honger

Aid separates itself from competitors in terms of its payload and range, and its operating characteristics. It is therefore expected that Wings for Aid can achieve its own place in the market.

## 3.3. Future Market

It is expected that the market will grow in the coming years, for two reasons. Firstly, the market for last mile logistics in growing yearly, and is expected to grow by about $92.32 Billion dollars from 2020 until 2027 [7]. Also, one of the main trends in this market is that autonomous vehicles are becoming increasingly more important [8]. Furthermore, it is expected that the number of people in need of aid will increase in the long term because of climate change. Climate change brings with it floods, rough weather conditions and extreme heat, which will effect more and more people over time. These conditions will also make these places hard to reach and therefore it is expected that services like Wings for Aid will have an increasing demand over time.

## 3.4. Market Opportunities

The current goal of Wings for Aid is limited to providing humanitarian aid in hard to reach areas. The aid packages contain aid supplies being food, water, blankets and tents. However since humanitarian disasters are not a constant occurrence, fleets of aircraft may eventually become underutilised. Therefore alternative market opportunities must be investigated, such that the aircraft can also be used effectively in the downtime. Currently the market for "Medical delivery drones" is quite a large market with a market size of $254.7 Million. Medical delivery drones are UAVs able to deliver medicines, vaccines and other life saving supplies in remote or hard to reach areas. It could be interesting for Wings for Aid to deliver medical supplies to hospitals as well, to possibly obtain a share in this market. For this purpose the amount of adjustments needed to the design are very limited. It might be required to increase the crumple zone of the box if vaccines are dropped. Otherwise the aircraft will operate in the same way as the original purpose. Currently the deployment package reaches a velocity of around $40\ km/h$ upon landing. For various medical suppliers this may be deemed a substantial risk for the delivery of life critical goods. Therefore in order to deliver these fragile products, the current design must be validated to insure significant safety factors or a different mechanism must be employed.

Another possible market opportunity could be military drones. The military drones market is a very large market with a size of $11.25 Billion in 2021 [9]. Military drones have a wide variety of purposes such as: intelligence, surveillance, reconnaissance but also search and rescue missions. By altering the fuselage of the Wings for Aid aircraft it could be used for one such purpose. The advantage of using the Wings for Aid aircraft here is the low price, meaning the risk is quite low when flying over hostile areas. The aircraft also has a large possibility of utilisation in the commercial goods delivery market. The total market is predicted to grow $1,522.4$ million USD in 2021 to $31,188.7$ million by 2028 [10]. The patented packages can be filled with a variety of different delivery goods and then brought directly to a central distribution center. Removing the procedure of landing the aircraft in order to deliver the payload reduces operation times and gets the package from point A to B in significantly shorter times. However in order for the aircraft to be feasible in this application, certification procedures must be heavily investigated. Furthermore both the dropping mechanism and procedure must be validated to ensure safety within civilian areas. Although this would largely be an issue in densely population areas, applications in remote environments would be more feasible due to reduced regulations. For example the system may be able to benefit farmers in remote areas with no access to crucial goods. The system may also be able to help researchers or isolated groups of individuals located far from society. The driving consideration when looking at civilian and commercial feasibility is the accuracy of the dropping mechanism as well as the certification of the aircraft. Therefore it is recommended that robust software is developed to predict the optimum drop time as well as certification is kept as a potential design factor.

---

[7]https://www.statista.com/statistics/1286612/last-mile-delivery-market-size-worldwide/

[8]https://supplychaingamechanger.com/what-are-the-trends-in-last-mile-logistics/

[9]https://www.fortunebusinessinsights.com/military-drone-market-102181

[10]URL: https://www.fortunebusinessinsights.com/drone-package-delivery-market-104332 [cited 21 June 2022]

## 3.5. SWOT Analysis

In Figure 3.1, a SWOT analysis was performed in order to find the strengths, weaknesses, opportunities and threats compared to the competition are analysed.

| Strengths | Weaknesses |
|---|---|
| S1 Autonomous vehicle<br>S2 Can carry multiple, large packages<br>S3 Relatively longer range than competitors<br>S4 Relatively bigger payload capability than competitors S5 Cheap material price<br>S6 Sell service instead of drone<br>S7 Can fit in 20 ft container | W1 Dependent on funding by UN, UNICEF etc.<br>W2 UAVs are still relatively immature technology<br>W3 Not VTOL<br>W4 Disassembly and assembly required for shipping |
| Opportunities | Threats |
| O1 Growing last mile logistics market<br>O2 Humanitarian aid in long term more important due to climate change<br>O3 Easy (crowd)funding<br>O4 Civilian use | T1 Possible new competition<br>T2 Enemies are a danger to the aircraft and equipment<br>T3 Possible new regulations could have an impact on the aircraft |

**Figure 3.1:** SWOT analysis

The most important strengths are S2 and S3. This is because the Wings for Aid aircraft is the only one in the competition capable of easily dropping at multiple locations which makes it a versatile option, especially for civilian use. The large payload and range are advantageous when the location is hard to reach. The most important weakness is W4. This namely requires trained crew to load and unload the aircraft, and it also makes the drone more prone to failure. The most important opportunity is O4. The aircraft could then be used in the downtime from already existing airport to increase the revenue. Finally the biggest threat is T2. When operating in violent countries, special precautions must be taken to protect the aircraft, equipment and crew.

## 3.6. Operation Locations

The client Wings For Aid, looks to implement the UAV in a variety of different locations and environments. In order to design a drone that has the capabilities of performing our mission in numerous locations, research into these environments and the available infrastructure must be completed. It has been stated by the client that current areas of notable interest are South Sudan, Haiti and Nepal; this is due to reoccurring natural or humanitarian crisis. Available infrastructure is a driving factor when analysing how the system shall be implemented in the chosen location. Therefore airports from these 3 countries have been analysed for average runway length and average mean elevation above sea level. Only airports that are designated as low traffic domestic airports have been compared; the surface ranges from paved asphalt to firm dirt. The results of this analysis have been tabulated in Table 3.2

**Table 3.2:** Average Airport statistics of various deployment locations

| Location | Number of Airports in Data Set | Runway Length [m] | Elevation[m] |
|---|---|---|---|
| South Sudan | 22 | 1443 | 542 |
| Haiti | 11 | 840 | 91 |
| Nepal | 24 | 657 | 1185 |

From this data, some baseline for requirements can be deduced. In order to have a system that is usable in a multitude of locations, utilising pre-existing airports, it must have a generally low take off and landing distance below 700m. Furthermore the system must be able to perform optimally at a large range of elevations.

This chapter describes the requirements. Requirements are statements which describe what the system must be able to perform. First the requirements that come directly from the client, or user requirement, are identified. After that, the system requirements will be identified since the user requirements do not cover all the requirements that an aircraft must adhere to. Some of the requirements will get the label of key, killer or driving requirement.

## 4.1. User Requirements

User requirements are requirements that come directly from the user in addition to the mission need statement. Every requirement is given a unique identifier consisting out of five elements from which can be derived what kind of requirement it is. The requirement identifier is built up as:

- The first part "WFA" refers to the project title "Wings for Aid"
- The second part is either titled "UREQX" or "REQX" whereby "X" is a number. This part of the identifier is included for traceability. If the system requirement is derived from a user requirement then "UREQX" is used. If the requirement was newly created in the requirements discovery tree, then "REQX" is used.
- The third part is either titled "SysCo" or "SysTe" depending on whether the requirement is a constraint or a technical requirement respectively.
- The fourth part refers to the requirement sub-category that the requirement belongs to. The sub-category that the abbreviation (such as "SEN") refers to can be found in the requirement discovery tree from the baseline report.
- The fifth part refers to the requirement number of the sub-category.

. The user requirements can be found in Table 4.1.

**Table 4.1:** User Requirements

| Requirement ID | Requirement | Type |
|---|---|---|
| WFA-REQ-USE-01 | The aircraft shall be able to operate for a total range of 500km. | |
| WFA-REQ-USE-02 | The aircraft shall have a deployment system for aid packages of 20 kg. | |
| WFA-REQ-USE-03 | The aircraft shall be able to carry 10 aid packages of 20 kg. | |
| WFA-REQ-USE-04 | The aircraft shall be unmanned. | |
| WFA-REQ-USE-05 | The unit cost of one aircraft shall be less than €15,000 . | |
| WFA-REQ-USE-06 | The operational cost of the aircraft, measured per kg of delivered goods, shall be less than that of the UH-1 helicopter. | |
| WFA-REQ-USE-07 | The operational cost of the aircraft, measured per kg of delivered goods, shall be in the range of 2 to 4 times the operational cost of a truck. | |
| WFA-REQ-USE-08 | The aircraft shall be as stable or more stable than a Cessna 172. | |
| WFA-REQ-USE-09 | The aircraft shall fit in a 20 ft container under transport conditions. | Driving |
| WFA-REQ-USE-10 | The aircraft shall be of modular design. | |
| WFA-REQ-USE-11 | The aircraft shall be able to operate in similar conditions as allowable for the UH-1 helicopter. | |
| WFA-REQ-USE-12 | The aircraft shall be able to accurately drop an aid package in a 25 m by 25 m drop zone from a height of 15 m. | |
| WFA-REQ-USE-13 | The aircraft shall be able to take-off and land in conditions of 100 m of visibility. | |
| WFA-REQ-USE-14 | The aircraft must be able to take-off and land in environment conditions stated to be expected in a humanitarian aid program. | |
| WFA-REQ-USE-15 | The aircraft shall be able to deliver aid packages 3 times in a 24 hours period including maintenance. | |
| WFA-REQ-USE-16 | The service ceiling of the aircraft shall be 10000 ft. | |
| WFA-REQ-USE-17 | The aircraft shall be able to fly in a swarm configuration. | |
| WFA-REQ-USE-18 | The aircraft shall operate when using low quality diesel or gasoline. | |
| WFA-REQ-USE-19 | The aircraft shall have a 24/7 operational window. | |
| WFA-REQ-USE-20 | The complete operation of multiple drones shall have the same aid deployment capacity as a C-130 Hercules. | |
| WFA-REQ-USE-21 | The aircraft shall be safe. | |

## 4.2. System Requirements and Constraints

As the user requirements do not describe all the things that the system shall cohere to, more requirements are needed. These are either technical requirements or constraints. The constraints can be found in Table 4.2 and the technical requirements in Table 4.3.

**Table 4.2:** Design constraints

| Requirement ID | Requirement | Type |
|---|---|---|
| WFA-UREQ5-SysCo-FI-1 | The aircraft unit cost excluding development costs and costs for setting up production shall be less than €15,000 | Key |
| WFA-UREQ9-SysCo-DIM-1 | The disassembled aircraft shall fit inside a 20 ft shipping container | |
| WFA-UREQ9-SysCo-DIM-1-1 | Parts that obstruct/collide with the container shall be removable, detachable or foldable | |
| WFA-UREQ14-SysCo-OP-3-1 | The aircraft shall be able to take off and land on low-quality ground paving | Key, Driving |
| WFA-UREQ15-SysCo-TI-1 | The aircraft shall be able to perform 3 round trips within 24 hours | |
| WFA-UREQ15-SysCo-TI-1-1 | The total maintenance time per day shall be less than 4 hours | |
| WFA-UREQ15-SysCo-TI-1-2 | The aircraft shall have a cruise speed of 34 m/s | |
| WFA-UREQ16-SysCo-OP-5 | The aircraft shall have an operational ceiling of 10000 ft | |
| WFA-UREQ18-SysCo-OP-1 | The propellant of choice shall be either low quality petrol or diesel | |
| WFA-UREQ18-SysCo-OP-1-1 | The aircraft propulsion system shall be able to operate using the low quality fuel of choice | |
| WFA-UREQ19-SysCo-OP-6 | The aircraft shall have a 24/7 operational window | Key |
| WFA-REQ-SysCo-TI-1-2-1 | The engine shall provide a power of at least 58 kW | |
| WFA-REQ-SysCo-TI-1-2-2 | The aircraft shall be able to carry the aerodynamics loads at cruise speed | |
| WFA-REQ-SysCo-TI-1-2-2-1 | The aircraft shall not flutter | |
| WFA-REQ-SysCo-TI-2 | The ground operations per day shall take a maximum of 4 hours | |
| WFA-REQ-SysCo-TI-2-1 | The payload reload time per cycle shall take a maximum of 1 hour | |
| WFA-REQ-SysCo-TI-2-2 | The refuel time per cycle shall take 10 minutes | |
| WFA-REQ-SysCo-OP-2 | The aircraft shall be an unmanned aerial vehicle | Key, Driving |
| WFA-REQ-SysCo-OP-2-1 | The aircraft shall accommodate for remote control | |
| WFA-REQ-SysCo-OP-3-2 | The aircraft shall be able to take of and land on high-quality ground paving | |
| WFA-REQ-SysCo-SA-1 | The aircraft engine start-up procedure shall be remote | |
| WFA-REQ-SysCo-SA-2 | The aircraft shall not navigate over housing during flight | |
| WFA-REQ-SysCo-SUS-1 | The aircraft shall emit a maximum of **[TBD]** kilograms of emissions over its specified life cycle | |
| WFA-REQ-SysCo-SUS-1-1 | The maximum emissions during the production of one aircraft unit shall be **[TBD]** kilograms | |
| WFA-REQ-SysCo-SUS-1-2 | The maximum emissions during one round trip of the aircraft shall be **[TBD]** kilograms | |
| WFA-REQ-SysCo-SUS-1-3 | The maximum emissions during end-of-life handling of one aircraft unit shall be **[TBD]** kilograms | |
| WFA-REQ-SysCo-SUS-2 | **[TBD]**% of the aircraft by mass shall be recyclable | |
| WFA-REQ-SysCo-SUS-2-1 | **[TBD]**% of the aircraft materials by mass shall be fully recyclable | |

**Table 4.3:** Technical requirements

| Requirement ID | Requirement | Type |
|---|---|---|
| WFA-UREQ1-SysTe-FP-1 | The aircraft shall have a range of 500 km | Key, Driving |
| WFA-UREQ1-SysTe-FP-1-1 | The aircraft shall accommodate for 65 kg of fuel | |
| WFA-UREQ3-SysTe-PD-1 | The aircraft shall be able to carry up to 200 kg of payload | Key, Driving |
| WFA-UREQ3-SysTe-PD-1-1 | The aircraft structure shall be able to carry the maximum payload weight of 200 kg | |
| WFA-UREQ3-SysTe-PD-1-2 | The aircraft structure shall have sufficient volume to carry maximum payload mass | |
| WFA-UREQ4-SysTe-SEN-1 | The aircraft shall have visual sensors | |
| WFA-UREQ4-SysTe-SEN-2 | The aircraft shall have attitude sensors | |
| WFA-UREQ4-SysTe-SEN-3 | The aircraft shall have atmospheric sensors | |
| WFA-UREQ4-SysTe-SEN-4 | The aircraft shall have positioning sensors | |
| WFA-UREQ8-SysTe-SB-1 | The aircraft shall have a least the same dynamic stability as a Cessna 172 | Key, Driving |
| WFA-UREQ8-SysTe-SB-2 | The aircraft shall have at least the same static stability as a Cessna 172 | Key, Driving |
| WFA-UREQ8-SysTe-SB-2-1 | The aircraft shall be as longitudinally statically stable as the Cessna 172 | |
| WFA-UREQ8-SysTe-SB-2-2 | The aircraft shall be as laterally statically stable as the Cessna 172 | |
| WFA-UREQ11-SysTe-FP-1 | The aircraft shall be able to perform the mission in the same conditions as the UH-1 helicopter | |
| WFA-UREQ11-SysTe-FP-1-1 | The aircraft shall be able to perform the mission under a gust spread of 15 kts | |
| WFA-UREQ11-SysTe-FP-1-5 | The aircraft shall be able to perform the mission in mountainous conditions | Key, Driving |
| WFA-UREQ11-SysTe-FP-1-7 | The aircraft shall be able to land on grass | Key, Driving |
| WFA-UREQ12-SysTe-FP-1 | The aircraft shall maintain an altitude as low as 50 m during the payload deployment phase | |
| WFA-UREQ12-SysTe-PD-1 | The payload shall not sustain damage on delivery | |
| WFA-UREQ12-SysTe-PD-2 | The payload shall land within a designated dropzone with dimensions 25x25 m | |
| WFA-UREQ13-SysTe-FP-1 | The aircraft shall be able to take off and land with minimum visibility of 100 m | |
| WFA-UREQ17-SysTe-PD-1 | The aircraft shall be able to fly in a swarm configuration | |
| WFA-UREQ17-SysTe-PD-1-1 | The aircraft shall be able to avoid midair collisions with other aircraft | |
| WFA-UREQ20-SysTe-PD-1 | The swarm of aircraft shall deploy at least 20000 kg of payload in the span of 24 hours | Key, Driving |
| WFA-REQ-SysTe-CT-1 | The aircraft shall have a communications system for the ground system and communication with other aircraft (swarms) | |
| WFA-REQ-SysTe-CT-1 | The aircraft shall have a communications system for the ground system | |
| WFA-REQ-SysTe-CT-1-2 | The communication system shall have a feedback mechanism | |
| WFA-REQ-SysTe-FP-3 | The rate of climb shall be at least 2.1 m/s | |
| WFA-REQ-SysTe-FP-4 | The runway length required for take off shall not exceed 500 m | |
| WFA-REQ-SysTe-FP-5 | The runway length for required for landing shall not exceed 500 m | |
| WFA-REQ-SysTe-FP-6 | The aircraft shall be able to take-off and land with a screen height of 15 m or less | |

# 4.3. Key and Driving Requirements

There are two special types of requirements. Key requirements come directly from the user needs. Driving requirements are requirements that shape the design more than average. They can be found in Table 4.2 and Table 4.3. This section describes why they are either Key and/or Driving.

- WFA-REQ-USE-09: For Wings for Aid it is important that the aircraft fits in a 20 ft container. The dimensions of the container limit the design and therefore this requirement is a driving requirement.
- WFA-UREQ5-SysCo-FI-1: For the customer it is important that the total aircraft has a lower cost than € 15,000. This is limiting and something the customer specifically asked for. Therefore this is a Key requirement.
- WFA-UREQ19-SysCo-OP-6: The 24 hour operation implies that the aircraft can fly at night. So this is a limiting requirement directly from the customer and thus a key requirement.
- WFA-REQ-SysCo-OP-2: The unmanned requirement is given by the customer and it heavily influences the design. So it is both a key and driving requirement.
- WFA-UREQ1-SysTe-FP-1: The range requirement is also a limiting requirement from the customer, so it must also be seen as a key requirement. However, the range also influences the design more than average so it is a driving requirement too.
- WFA-UREQ3-SysTe-PD-1: The payload requirement is just like the range requirement a limiting request from the customer and drives the design and is therefore a key and driving requirement.

- WFA-UREQ8-SysTe-SB-1 and WFA-UREQ8-SysTe-SB-2: The stability of the aircraft was also limited by a request from the customer and should be considered very thoroughly during designing. This influences the design more than average and are therefore key and driving requirements.
- WFA-UREQ14-SysCo-OP-3-1, WFA-UREQ11-SysTe-FP-1-5, WFA-UREQ11-SysTe-FP-1-6, WFA-UREQ11-SysTe-FP-1-7: The conditions in which the aircraft should perform are prescribed by the customer. The design will be influenced by the terrain in which it operates, thus creating key and driving requirements.
- WFA-UREQ20-SysTe-PD-1: The total deployment payload for the whole mission is also described by the customer. It also influences the mission profile of a single aircraft and is thus a key and a driving requirement.

This chapter presents the major design steps that has been made during the preliminary design phase. First some weight estimations have been made. After that, an initial required power and wing area has been found. Then different design concepts have been created and subjected to a trade-off.

## 5.1. Weight Estimations

It was aimed to make an estimate for the operating empty weight, fuel weight and the payload weight. By summing these weights, the value of the maximum take off weight is determined. Of course, the value for the payload is fixed to be 200 kg as specified by WFA-REQ-USE-03 from Table 4.1.

First a class I weight estimation was performed with preliminary fuel fractions. This resulted in a operating empty weight and fuel weight of 415 kg and 135 kg respectively. This results in a MTOW of 750 kg.

These values are being used as inputs for the class II weight estimation. The results from the class II weight estimation have been iterated until they converged. The results for the class II are an operating empty weight of 333 kg and a fuel weight of 116 kg which results in a maximum take off weight of 649 kg.

## 5.2. Wing Area and Power Determination

The required power at take-off and surface area of the main wing can be determined by creating a wing loading and power loading diagram. Since the aircraft is a propeller aircraft, the wing loading, $W/S$, is plotted on the x-axis and power loading, $W/P$, on the y-axis. Furthermore it is desired that the design point is located on the top right, as this results in the lowest required power and wing area for a mass from the weight iteration. However, the design point is constrained by multiple flight manoeuvres which force the design point to the bottom left. The considered manoeuvres are: stall speed, landing, take-off, cruise, climb rate and climb gradient. The developed wing loading diagram can be found in Figure 5.1.
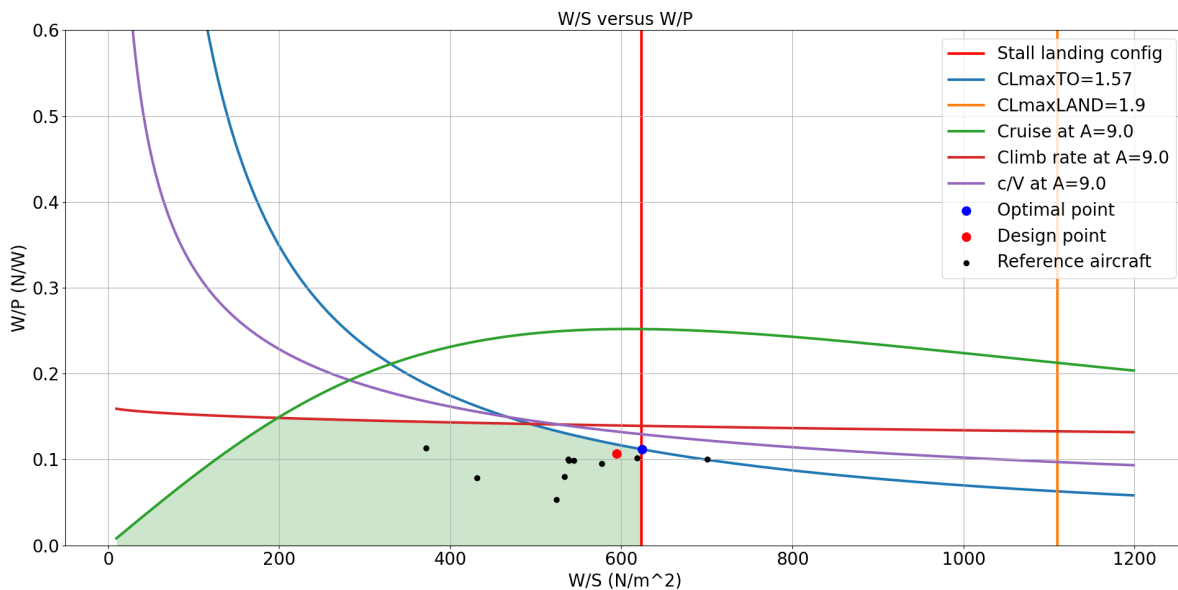


**Figure 5.1:** Wing loading - power loading diagram

As can be seen in Figure 5.1, $W/P = 0.11\ N/W$ and $W/S = 594\ N/m^2$. This results in a required power of $P_{req} = 58\ kW$ or $78\ hp$ and $S = 10.9\ m^2$

## 5.3. Overview of Design Concepts

In this section, the design concepts are presented. In Table 5.1 an overall configuration for each of the concepts is presented. Figures 5.2 to 5.7 show sketches to visually provide a high level overview of each of the concepts. At this stage it is not yet necessary to define the concepts on system level,

therefore only the higher level design options are considered. Further design choices will be made, once the overall design has been finalized and the detailed design phase can begin. It is also worth noting that the design concepts provided here might still be changed and new combinations might be created after new insights on the designs after trade-off and a more thorough analysis.

**Table 5.1:** Design concepts considered

| Component | Concept 1 | Concept 2 | Concept 3 | Concept 4 | Concept 5 | Concept 6 |
|---|---|---|---|---|---|---|
| Horizontal/ Vertical stabilizers | Conventional | V-tail | Double T-Tail | H-tail | Canard | Twin-boom tail |
| Fuselage configuration | Single | Single | Double | Single | Single | Triple |
| Wing location | High wing | High wing | High wing | High wing | High wing | High wing |
| Number and location of engines | Single, front mounted | Single, front mounted | Double, front mounted | Single, top mounted | Single, back mounted | Single, front mounted |
| Landing gear configuration | Taildragger | Tricycle | Double taildragger | Tricycle | Tricycle | Tricycle |

## 5.3.1. Conceptual Designs



**Figure 5.2:** Conventional concept (Concept 1)

This configuration has a single fuselage with a high wing and conventional empennage. There is only one engine and it is mounted in the front of the fuselage. The landing gear has a taildragger configuration. The configuration is shown in Figure 5.2.
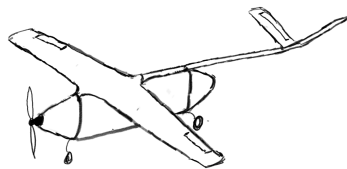


**Figure 5.3:** V-tail concept (Concept 2)

The aircraft has a single fuselage. The overall fuselage shape is inspired by the current Wings for Aid minifreighter 8/500FW. The wing configuration is a high wing and has a V-Tail as stabilizer. There is only one engine, mounted in the front. The landing gear has a tricycle configuration. The configuration can be found in Figure 5.3.
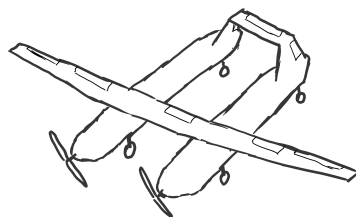


**Figure 5.4:** Twin fuselage concept (Concept 3)

The third concept is a double fuselage concept. It has a high wing and a double T-Tail. There are two engines and they are both mounted in the front of each fuselage. The landing gear is in the double taildragger configuration. A sketch of the configuration can be found in Figure 5.4.
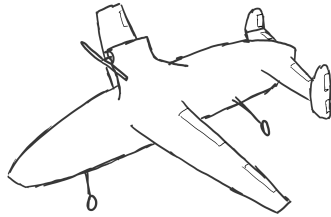
**Figure 5.5:** Top engine layout (Concept 4)

The fourth configuration is a single fuselage with a H-tail. The wing configuration is a high wing and the fuselage has one engine mounted on the top of the aircraft. It has a tricycle landing gear. The concept can be found in Figure 5.5.



**Figure 5.6:** Canard concept (Concept 5)

The fifth concept is a pusher aircraft based on the Cozy Mark IV by Aircraft Spruce and can be found Figure 5.6. The pusher refers to the aircraft which pushes air rather than the conventional tractor propeller. The aircraft has a semi-circular fuselage in the middle, storing aid packages. The wings have a large sweep angle to them and it has a canard configuration.
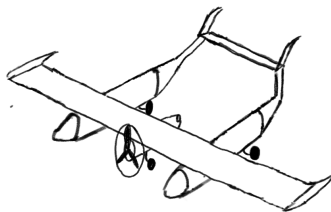


**Figure 5.7:** Triple fuselage (Concept 6)

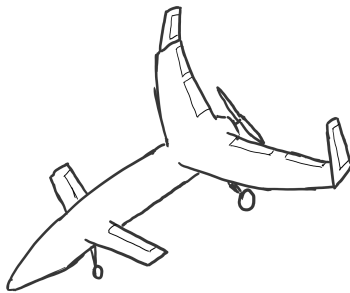The final concept is a triple fuselage engine inspired by the first design for the wings for aid aircraft, the Pipistrel Sinus. This concept uses the middle fuselage to house the engine, and two side fuselages to load the aid packages. The tail has a twin-boom configuration, with added vertical fins. The concept can be found in Figure 5.7.

## 5.4. Concept Selection

In this section the trade-off between the generated design concepts is presented. Prior to the trade-off, the selection criteria and weights should be specified. Then, the trade-off will be conducted by breaking down the selection criteria and performing a qualitative analysis on them. After performing the actual trade-off, a sensitivity analysis must be performed to verify the robustness of the trade-off. For a more elaborate and complete understanding of the trade-off process between the selection criteria the reader is directed to the previous report completed by the group [25].

### 5.4.1. Selection Criteria and Weights

For the trade-off between the generated concepts it is necessary to select certain distinguishing criteria relevant to the designs. These criteria reflect the most important aspects of the concepts that can be determined at this stage of the design to differentiate the designs and will thus determine what the final design will be. Furthermore weights must be given to the selection criteria, which is a measure of their impact on the mission. These weights will be given on a scale from 1 to 5, where 1 indicates low impact and 5 indicates great impact. The criteria weights are dependent on the ability to accurately attribute a score to the design, as well as their impact. As part of the trade-off sensitivity analysis, these selection criteria will later be adjusted to test how changes may affect the design chosen sensitivity analysis. The selection criteria and weights are summarized in Table 5.2.

**Table 5.2:** Selection criteria and weights

| Selection criteria | Weights |
|---|---|
| Structural mass | 5 |
| Drag | 2 |
| Manufacturing Cost | 4 |
| Appearance | 1 |
| Mission robustness | 2 |
| Operability | 2 |

Mass was attributed as one the most important and more accurately predictable criteria and therefore has the highest weight. This follows from the fact that mass is directly related to cost and other important parameters such as engine power and wing area, which are crucial aspects of the design. Second most important parameter is the manufacturing cost. It is generally important to keep the cost down, while it is also preferred that it is not financially attractive to shoot the aircraft down. The cost depends on the materials used and the production methods. To evaluate the manufacturing cost, the complexity and the shape of each of the concepts was considered. The drag is given a medium weight as this has a relatively large influence on the performance of the aircraft but it is quite difficult estimate at this stage of the design. A high drag will drive the required thrust up, which increases the mass and cost as well. The selection criteria for appearance follows from the goal WFA-GOAL-USE-1, which says that the aircraft should look friendly. Since this is difficult to evaluate and has limited effect importance on the choice of design a concept it only has been assigned a weight of 1. Mission robustness consists of multiple parameters influencing the dropping of the payload, take-off and landing. This includes the reliability, stability and ease of assembly. Finally the operability criteria is important to the mission as the client wants the aircraft to be easily transportable and fit in the allocated storage facility as well as being easily assembled on location. In multiple cases it happened that a high importance is given to a criteria but it is difficult to determine the performance of the concepts with regards to the criteria. This forces the assigned weight of an important criteria to be reduced, the drag estimation as an example.

### 5.4.2. Concept Trade-off

The design scores obtained from all selection criteria were taken and normalised. These normalized scores are used to create the trade-off table Table 5.3 where the final score of each of the design concepts is shown. Each selection criteria can be awarded a number between 1 to 5, where the higher the number, the better the design. The table makes use of 5 different colours to ease visual understanding. In order from lowest to highest scoring, these colours used are: red (R), orange (O), yellow (Y), Light green (LG) and green (G). The criteria weight column width in the table are proportional to the weights attributed to them in Table 5.2

**Table 5.3:** Final trade-off table considering all the scores from the previous tables.

| Concept | Structural mass | Drag | Manu. Cost | Appearance | Mission robust-ness | Operability | Score |
|---|---|---|---|---|---|---|---|
| Concept 1 | 3 | 4 | 5 | 4 | 4 | 4 | 63 |
| Concept 2 | 3 | 4 | 5 | 3 | 4 | 4 | 62 |
| Concept 3 | 3 | 2 | 3 | 3 | 3 | 2 | 44 |
| Concept 4 | 2 | 4 | 4 | 3 | 3 | 4 | 51 |
| Concept 5 | 3 | 4 | 3 | 2 | 1 | 4 | 47 |
| Concept 6 | 4 | 2 | 3 | 3 | 4 | 3 | 53 |

| Poor (1) R | Bad (2) O | Satisfactory (3) Y | Good (4) LG | Excellent (5) G |
|---|---|---|---|---|

From the final trade-off in Table 5.3 and the corresponding sensitivity analysis performed in [25] it is clear that concept 1 scores the best. It should however be noted that the configuration is not fixed and may change during further design iterations.

# 6 | Design Methodology & tools

This chapter discusses the design methodology and tools used to generate a detailed design of the aircraft. The tools are divided into the following four sections: Aerodynamics, structures, stability & control and power & performance. Furthermore the tools are verified according to the procedure from section 6.1.

## 6.1. Verification & Validation Procedure

Before the design methodology and tools are described, the general procedure in how these will be verified and validated is discussed. To ensure the design tools and their outcome result in an accurate and predictable model, verification and validation (V&V) of every system during design cycle is crucial. V&V allows the design team to have confidence in the numerical solutions obtained from the created tools. This confidence is what ensures that the aircraft is compliant with the design requirements and specifications, and that the right aircraft has been designed for this specific mission. The V&V procedure is broken down into code verification as documented on subsection 6.1.1, and system subsection 6.1.2.

### 6.1.1. Unit Tests Code Verification

The most basic form of verification test that is performed by the software interpreter in the form of error logs. Unit tests will be implemented to detect errors in calculation and/or communication between modules. Unit tests will therefore display a message stating what the unexpected event is, and where it is found within the code. This will be continuously performed as the script is being developed. In order to ensure this is properly verified, individuals from different engineering departments will check for the correct implementation of verification procedures for all tools used outside their department, as well as their own. Besides V&V this procedure will ensure that proper commenting and documentation is completed. Another type of code verification adopted by the tools is the use of print statements and visual inspections of analytical equations implemented in the code. The last, but most time-consuming form of code verification is hand calculations to ensure values have been properly calculated by the code. Each engineering department make use of their own developed design tools, the following general unit tests are performed on the code:
Unit tests

- **U.1**: Visual inspection that equations are inputted correctly. The test is a pass when at least 2 team members have verified the equations inputted into the code.
- **U.2**: A code function to check that the mathematical sign convention is used properly. The test passes when the expected mathematical sign for a value corresponds to the analysed parameter.
- **U.3**: Visual inspection that correct values and units are inputted. The test is passed when at least 2 team members have verified the values and units inputted into the code.
- **U.4**: Print statements that parameters are within correct order of magnitude. The test passes when the values are within the expected order of magnitude according to 2 team members.

### 6.1.2. System Code Verification & Validation

Verification of the system code ensures that the code works as intended by the user. Initial condition and extreme value tests are applied to verify the system code.

**Initial Condition Testing**
This type of system verification will consist of using the tools to simulate a sample scenario. This ensures that the units of code communicate all information within itself in the intended manner. The sample mission condition can mean a variety of things, for example, this would involve running a cruise sample mission to test the performance and propulsion cruise code. For structures, this could be the simulation of a generic wing-box design to display tool functionalities and feasibility.

**Extreme Value Testing**
The second form of system verification consists of extreme value testing. These tests are a measure of code robustness, as it consists on inputting nonsensical parameters into the code. For a code to pass this test, it requires the input of a nonsensical value, and the code producing a nonsensical result.

**System Validation**
Validation of the system ensures that the code represents reality to a certain degree of accuracy. Due to limited resources it is difficult to validate the code as no physical experiments can be conducted. The only validation tests that are performed are for aerodynamics. Where the airfoil data is compared to a wind tunnel test of the same airfoil. And the drag performance is compared to actual aircraft data.

## 6.2. Aerodynamics
In order to perform and maneuver optimally at each section in the mission profile, the aircraft needs to produce sufficient lift to counteract weight. The aircraft should be designed to optimise a high lift to drag ratio, allowing for an energy efficient design that utilises less fuel. The design of aerodynamic surfaces ensures that the aircraft is controllable and can perform flight maneuvers according to user and system requirements. This section will explain the methodology used to design relevant subsystems including the wing, control surfaces and high lift devices.

### 6.2.1. Airfoil Selection
The characteristics of the flow is crucial to an accurate airfoil performance analysis. When performing the airfoil selection flow conditions at three crucial stages are considered; take-off, cruise and payload deployment. Airfoils from a sample of transport aircraft were selected as an initial analysis batch, due to the airfoil characteristics and large experimental data set. Equation 6.1 defines the Reynolds number of the flow given specific characteristics.

<p align="center"><b>Table 6.1:</b> Reynolds numbers at various stages in flight profile</p>

$$Re = \frac{\rho V l}{\mu} \quad (6.1)$$

| Flight Part | Velocity [m/s] | Reynolds Number |
|---|---|---|
| Take-off | 26.09 | 2,069,320 |
| Cruise | 34.10 | 2,704,393 |
| Stall | 23.15 | 1,836,135 |

The Reynolds numbers in Table 6.1 are calculated with the corresponding flight velocities. These Reynolds numbers are used as inputs for analysis when comparing the performance of different airfoils. In order to complete this, the program XFLR 5 is used for a detailed analysis and to determine airfoil characteristics. When selecting an optimised airfoil for the aircraft wing, both two dimensional airfoil and three dimensional wing analysis will be conducted. The three dimensional wing analysis can be used as an indicator of performance, however there are different errors associated with its use which must be kept in mind; These errors are explained in subsection 6.2.5. Finally when conducting the analysis the following indicators and factors will be used to compare the results:

$C_{m_\alpha}$ - The derivative of the moment coefficient with respect to angle of attack is a crucial factor that affects the longitudinal stability and performance. In order to ensure static stability, this derivative value must be negative for the entire aircraft. Since the wing has a majority contribution to this factor, it is advantageous that it is also negative.

$C_m$ - The moment coefficient of the airfoil and wing influence the sizing of empennage and stability of the entire aircraft. In order to counteract the downwards pitching moment due to the wing, the tail must create negative lift. With a higher value of $C_m$, a larger downforce is required by the horizontal tail. Therefore it is optimal to look for an airfoil that has a low and negative $C_m$ value, allowing for a reduction in tail sizing and weight.

$C_l \backslash C_d$ - The ratio between lift coefficient $C_l$ and drag coefficient $C_d$ determines how aerodynamically efficient the airfoil is at a certain angle of attack. Higher values are desirable as they result in a more fuel efficient aircraft, improving emissions per kg of aid delivered as well as reducing costs.

$C_{l_{max}}$ - The max lift coefficient influences the design of the high lift devices and is an indicator for how slow the aircraft can fly before stalling.

$\alpha_{stall}$ - The stall angle provides a useful indicator of the range of possible angle of attacks. A higher stall angle of attack will also allow for greater flare out angle on landing as well as the take off angle.

$C_{l_0}$ - This indicator is used to characterise the amount of lift that is produced at lift off. This characterises how much incidence the wing should be designed with as well as directly influences the sizing of the high lift devices.

After the driving airfoil characteristics were identified, airfoil geometries are imported into XFLR5. Once geometries are registered within the program, a flow analysis is performed on the airfoils using cruise Reynolds number, viscus. The results of these analysis have been tabulated in Table 7.5. These values are at specific instances or maximums, and can't give a complete understanding of the performance over the entire operating range. Airfoils that have a larger drag bucket, are more desirable as they sustain a constant low drag coefficient while the lift coefficient increases with angle of attack. Furthermore airfoils that have a constant and high coefficient of lift to drag ratio are more desirable as they have a consistently more efficient flight performance. The Clark Y, Davis Wing, NACA $23015$, NACA $2415$, NACA $4415$, NACA $63_1 - 412$, NACA $64_2 - 415$, NACA $65_1 - 412$ were selected as airfoils to be analysed in this project. All of these airfoils have been historically used in stable and In order to observe these trends, the following XFLR 5 figures are analysed.
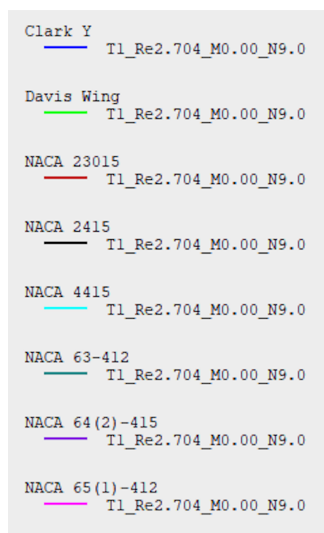


**Figure 6.1:** Legend for Colours in the 2D Airfoil Analysis
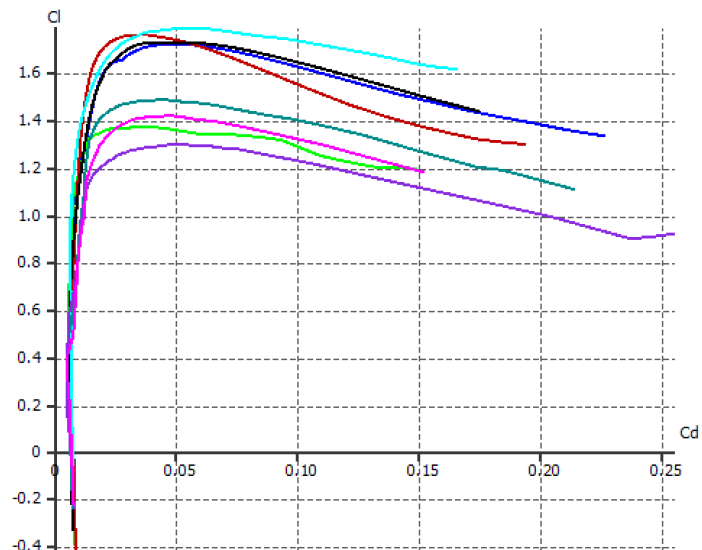
**Figure 6.2:** $C_l$ VS. $C_d$ Airfoil
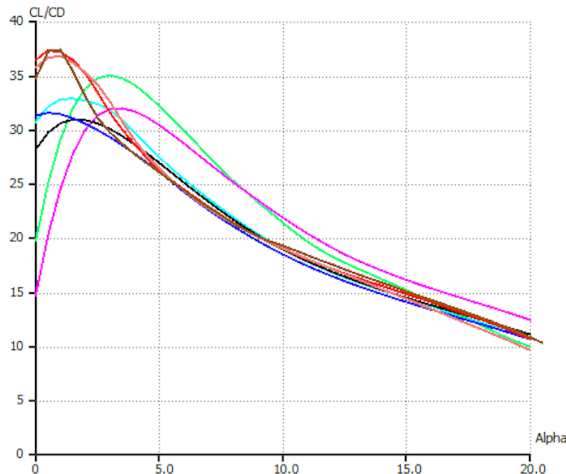
**Figure 6.3:** Cl/Cd VS. Alpha of Airfoils
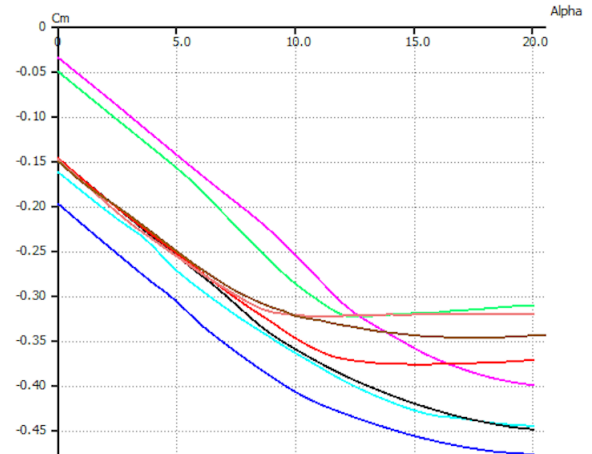


**Figure 6.4:** Cm VS. Alpha of Airfoils

The performance of these various airfoils is similar through the operating range. However the NACA 2415 performs well in all areas, maintaining a high lift to drag ratio at the chosen operating velocity as well as keeping a relatively low moment coefficient. This is important as it insures the horizontal tail section area is kept as low as possible. In order to check if this airfoil is still optimum in a three dimensional analysis, wing analysis is performed in XFLR5.
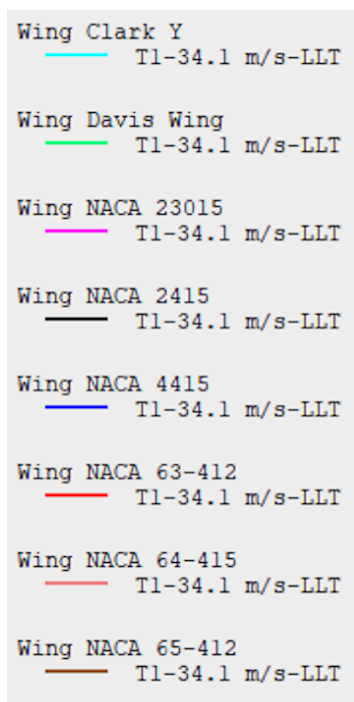


**Figure 6.5:** Legend for Wing Analysis of different airfoils
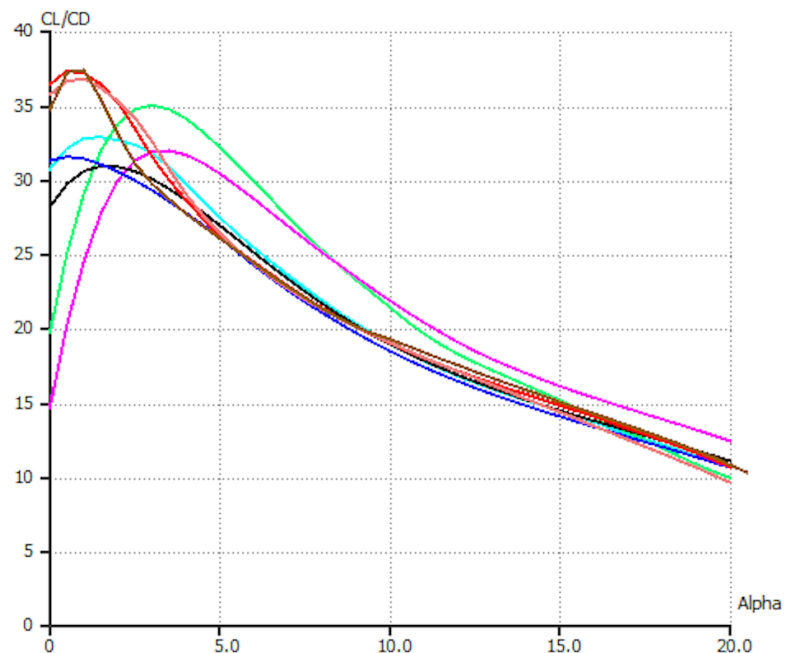


**Figure 6.6:** CL/CD VS. Alpha for various Wings

Comparison between Figure 6.3 and Figure 6.6 demonstrate that there is not considerable difference between the comparison of the 2D and 3D systems. The NACA 2415 still performs well in a wide range of situations. Although it does not perform the best in each performance indicator, overall it has a good

range in performance.

In order to estimate each airfoil performance with regards to wing tip stall characteristics, the induced angle of attack can be observed. If the induced angle of attack is considerably higher at the wing tips, the airfoil will stall and undesirable flight characteristics occur. Therefore it is more optimum that there is not a considerably larger induced angle. In Figure 6.8, the induced angle of the wing at each span wise position is graphed.
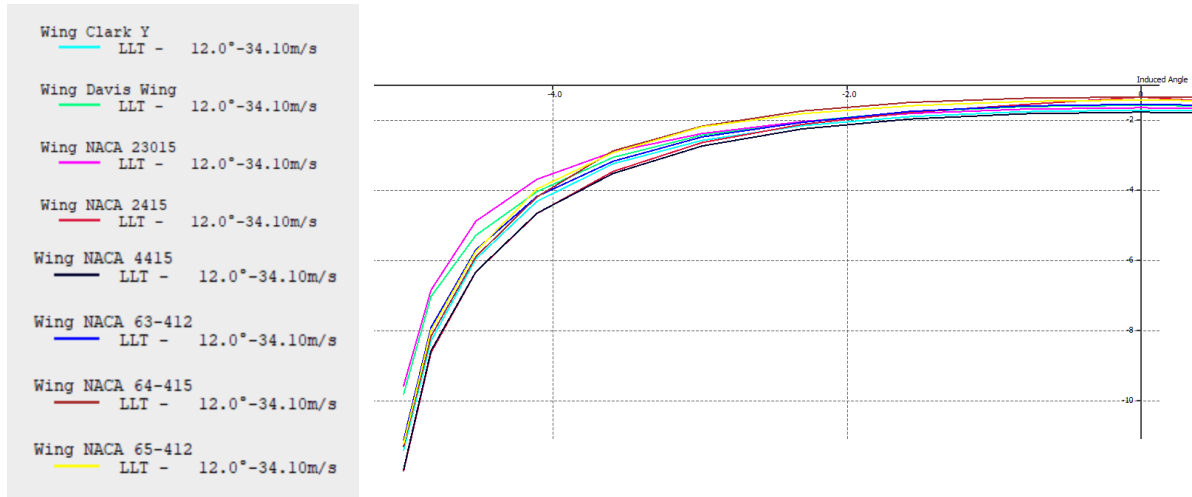


**Figure 6.7:** Legend for Wing Induced Angle of Attack



**Figure 6.8:** Wing Induced Angle of Attack

As the NACA 2415 has drastically high induced drag at the wing tips, additional considerations are required when designing the wing. In order to counteract the tip stalls, wing twist can be added. Due to the time constraints of this project, this has not been thoroughly investigated and should be performed in the next stages.

When selecting an airfoil for both the vertical and horizontal stabilisers, two main factors are crucial: the ability to generate lift in both directions and low drag characteristics. Therefore a symmetrical airfoil with a lower max thickness to chord ratio is typically selected. Historically airfoils such as the NACA 0012 and NACA 0009 have been used as empennage airfoils. The airfoils have a symmetrical profile with respectively a maximum of 12% and 9% chord thickness at 30.9% of the chord. Within the scope of this initial detailed design, a NACA 0009 airfoil is chosen. It is concluded that it is more critical to have a low drag airfoil due to the need for energy efficient optimisation.

At this stage of the project, an in depth analysis of the airfoil selection for both horizontal and vertical stabilisers is out of the scope. A NACA 0009 has been selected due to the symmetrical design, low thickness and resultant low drag. It is advised that a full in depth CFD analysis is conducted in order to determine the aerodynamic effects due to wing, fuselage and empennage interaction. Furthermore a dynamic stability analysis and effect of the empennage airfoil choice must be performed. These procedures will give a more complete understanding of system interactions.

### 6.2.2. Planform Design

During the planform design, not only the aerodynamics were considered, but also the manufacturability and structural effects. The initial wing characteristics are generated from both the wing surface area as well as the aspect ratio. When characterising the basic specifications of the wing planform, the following equations were used:

$$b = \sqrt{AR \cdot S} \qquad (6.2) \qquad \qquad C_r = \frac{2 \cdot S}{b(1 + \lambda)} \qquad (6.3)$$

### 6.2.3. Flap Design

Flap design is crucial to ensuring performance at take off and landing. The wing is not able to provide adequate lift by itself in a clean configuration. Therefore high lift devices are installed to generate an increase in lift at both these stages of the flight profile. In order to size the high lift devices, inputs of clean lift curve as well as required lift coefficient at take-off and landing are needed. Once the increase in lift coefficient is calculated, the span wise fraction of the high lift devices can be calculated using a rearrangement of Equation 6.4

$$\Delta C_{L_{max}} = 0.9 \cdot \Delta C_{l_{max}} \cdot \frac{SWF}{S} \cdot cos(\Lambda_{hinge}) \tag{6.4}$$

Depending on the flap type chosen, varying increases in the value of lift coefficient are achieved. These values are tabulated in Table 6.2

**Table 6.2:** Increase in lift coefficient for various flap styles

| Flap Type | $\Delta C_{l_{max}}$ |
|---|---|
| Plain | 0.9 |
| Split | 0.9 |
| Slotted | 1.3 |
| Fowler | 1.3 $c^{'}/c$ |
| Double Slotted | 1.6 $c^{'}/c$ |

Flaperons increase both aileron roll authority and allow for increased simplicity, reduced weight. Junker flaps are a small separate airfoil, positioned under the trailing edge of the wing. They are positioned in such a manner as to create "funnel" effects which introduce boundary layer flow back onto the wing surface. Junker flaps produce a larger increase in lift when deflected than plain and slotted flaps, however this comes with the consequence of larger induced drag. This flap design also has the consequence of high adverse yaw. This roll yaw coupling can lead to innately unstable dutch roll eigenmotions. Although this can be countered with some yaw dampers, it adds undesirable complexity to the system and increases the difficulty of manually controlled landings.

For the clean flap configuration, plain flap flaperons are utilised. These occupy 0.3% of the wing chord length. In order to achieve the increase in lift coefficient of 0.8, the flaps are deflected to 45 degrees. For the Junker Flap configuration, full flaperons are utilised. These extend outwards from the fuselage. They will utilise a Clark Y airfoil attached below the bottom side of the main wing. In order to determine the exact location of the airfoil, wind tunnel testing is required. A report by NASA investigating optimum placement of the control surfaces states that it should be placed roughly 0.05 times the chord length below the surface. Besides the placement, it was assumed from the clean configuration that a flap size of 0.3 times the mean aerodynamic chord would be used. Therefore the final dimensions of this surface would be chord length of $0.33\ m$ and a length of $4.1\ m$.

A recommendation that can be considered is the combination of theses two designs in a slotted flap configuration. This flap design allows for a low drag coefficient in cruise, but still retains the flow retention characteristics of the junker flap during deployment. However this will drastically raise the price of the wing component as slotted flaps require a significantly more complex deployment mechanism which extends the flap and re-energises the flow over the top surface of the wing.

### 6.2.4. Drag Coefficient Estimation

In order to evaluate the performance of the aircraft design, the drag coefficient is important to estimate. Determining the drag coefficient of the aircraft, as a function of the lift coefficient, was done using the methods as presented in the lecture slides of the course "Aerospace Design and Systems Engineering Elements II" (ADSEE II) [15]. For the zero-lift drag coefficient ($CD_0$), the component drag build-up method was used [15] while methods as presented in the lecture slides were used to determine the lift-induced drag coefficient ($CD_i$) [15].

The component drag build-up method [15] involves determining the zero lift drag coefficient of different aircraft components individually then summing them together. This is done by determining the flat plate skin friction coefficient ($C_f$), component form factor ($FF$), and interference factor ($IF$) and wetted area ($S_{wet}$) of each component then multiplying them together to get the drag contribution of the component. These contributions are then summed together, and divided by the wing reference area ($S_{ref}$) followed by the addition of drag from miscellaneous sources ($C_{D_{misc}}$). The general process is depicted in Equation 6.5 [15]. For this report, the main aircraft components considered were the wing, horizontal tail, vertical tail, and fuselage. The drag contribution due to the landing gear as well as excrescence and leakage were considered under miscellaneous drag sources.

$$C_{D_0} = \frac{1}{S_{ref}} \sum C_{f_c} \times FF_c \times IF_c \times S_{wet_c} + \sum C_{D_{misc}} \tag{6.5}$$

Before the coefficients were found, estimates for the wetted areas of the different aircraft components needed to be determined. This was mainly done using the lecture slides regarding drag from ADSEE II [15] whereby Equation 6.6, Equation 6.7, and Equation 6.8 were used for the wing, horizontal tail, and vertical tail respectively [15]. For the determination of the fuselage wetted area, the lecture slides could not be used as an unconventional design is used for the aircraft designed in this report. Therefore, to simplify the calculation of the wetted area, it was assumed that the fuselage comprises of three shapes: a trapezoidal prism, a rectangular cube, and a pyramid. The wetted area was then set equal to the calculated surface area of this simplified fuselage. Due to the simplifications used, and the fact that the wetted area is expected to be larger than just simply the surface area, it can be stated that the wetted area calculated for the fuselage was an underestimation. The calculated values for the wetted areas can be found in Table 6.4.

$$S_{wet_{wing}} = 1.07 \times 2 \times S_{exp_{wing}} \tag{6.6}$$

$$S_{wet_{HT}} = 1.05 \times 2 \times S_{exp_{HT}} \tag{6.7}$$

$$S_{wet_{VT}} = 1.05 \times 2 \times S_{exp_{VT}} \tag{6.8}$$

In order to determine the flat plate skin friction coefficient, the breakdown of laminar and turbulent flow for the different aircraft components was needed and can be found in Table 6.3 [15]. For this stage of the design, it was assumed that all of the aircraft components are designated under "General aviation - classic production metal". From there, the flat plate skin friction coefficient could be found using Equation 6.9 [15] and Equation 6.10 [15] whereby a weighted average for each component was found based on the laminar flow distribution found from Table 6.3.

$$Laminar : C_f = \frac{1.328}{\sqrt{Re}} \tag{6.9}$$

$$Turbulent : C_f = \frac{0.455}{(\log_{10} Re)^{2.58}(1 + 0.144M^2)^{0.65}} \tag{6.10}$$

**Table 6.3:** Laminar flow distribution of different aircraft components for different types of aircraft [15]

| Laminar flow | Fuselage (%) | Wing and tail (%) |
|---|---|---|
| General aviation - classic production metal | 0 | 10 |
| General aviation - smooth metal (no rivets or cracks) | 10 | 35 |
| General aviation - smooth molded composites | 25 | 50 |
| Sailplane - smooth molded composites | 35 | 70 |
| Civil jet - classic production metal | 5 | 10 |
| Military aircraft | 0 | 0 |

As for the component form factor, it could be found for the wing, horizontal tail, and vertical tail using Equation 6.11 [15]. It should be noted that $(x/c)_m$ is the position of the maximum thickness, $\frac{t}{c}$ is the

average thickness to chord ratio, and $\Lambda_m$ is the sweep angle at the position of the maximum thickness. Moreover, $f$ is the ratio of the fuselage length to the fuselage diameter.

$$FF_{wing,tail} = \left(1 + \frac{0.6}{(x/c)_m}(\frac{t}{c}) + 100(\frac{t}{c})^4\right)\left(1.34M^{0.18}(cos\Lambda_m)^{0.28}\right) \tag{6.11}$$

$$FF_{fuselage} = \left(1 + \frac{60}{f^3} + \frac{f}{400}\right) \tag{6.12}$$

As for the component interference factor, which is the drag contribution due to the boundary layer interaction at the interface of two parts [15], a table provided from the ADSEE II lecture slides was used to find the factor for each considered aircraft component. Table 6.4 displays all the factors and surface areas of the difference components considered for the zero-lift drag coefficient calculation. Table 6.5 shows the distribution of the zero-lift drag coefficient among the different aircraft components.

Table 6.4: Values used for the calculation of the zero-lift drag coefficient ($C_{D_0}$)

| Component | Wetted Area ($S_{wet}$) [m$^2$] | $C_{f_c}$ [-] | $FF_c$ [-] | $IF_c$ [-] |
|---|---|---|---|---|
| Wing | 23.4 | 0.00348 | 1.304 | 1 |
| Horizontal Tail | 3.4 | 0.00370 | 1.073 | 1.05 |
| Vertical Tail | 2.4 | 0.00347 | 1.068 | 1.05 |
| Fuselage | 18.5 | 0.00288 | 2.388 | 1 |

In order to determine the contribution of the landing gear to the zero-lift drag coefficient, the table provided in the lecture slides of ADSEE II was used [15]. This table stated that the value for $\frac{D/q}{Frontalarea}$ is 0.25 for a regular wheel and tire which is the case for the design of this report. To account for the drag contribution due to excrescence and leakage, this contribution is equal to 5-10% of the total zero-lift drag coefficient when considering propeller aircraft [15].

Table 6.5: Contribution of different aircraft components to zero-lift drag coefficient

| Component | $C_{D_0}$ Contribution |
|---|---|
| Wing | 0.00972 |
| Horizontal Tail | 0.00129 |
| Vertical Tail | 0.000850 |
| Fuselage | 0.0116 |
| Landing Gear | 0.00590 |
| Excrescence and Leakage | 0.00294 |
| **Total** | 0.0323 |

In addition, the lift-induced drag coefficient needs to be determined. For this calculation, Equation 6.13 was used where $AR$ is the aspect ratio and $e$ is the Oswald efficiency factor. This component of the aircraft drag coefficient is a function of the lift coefficient ($C_L$) which is not a constant. Therefore, in this section, the drag coefficient as a function of the lift coefficient will be determined and the drag polar will be displayed.

$$C_{D_i} = \frac{C_L^2}{\pi \cdot AR \cdot e} \tag{6.13}$$

The Oswald efficiency factor was found using Equation 6.14 which is the estimation method for straight wings [15]. As it can be seen from Equation 6.14, the wing aspect ratio is required to calculate the Oswald efficiency factor. This value is already known, but it should be mentioned that the wing tip shape has an effect on the effective aspect ratio. Since the Hoerner Wingtips were selected, which seem to look like a sharp rear corner wing tip, no change to the effective aspect ratio can be seen [15]. From Equation 6.14 it was determined that the Oswald efficiency factor of the aircraft is $0.783$.

$$e = 1.78(1 - 0.045AR^{0.68}) - 0.64 \tag{6.14}$$

Finally, an equation for the drag coefficient as a function of the lift coefficient could be determined with knowledge that the total drag coefficient is equal to the sum of the zero-lift drag coefficient and the lift-induced drag coefficient. The equation for the aircraft drag coefficient can be found in Equation 6.15. A graph depicting this relationship can be found in Figure 6.9.

$$C_D = 0.0323 + 0.0452 \cdot C_L^2 \tag{6.15}$$
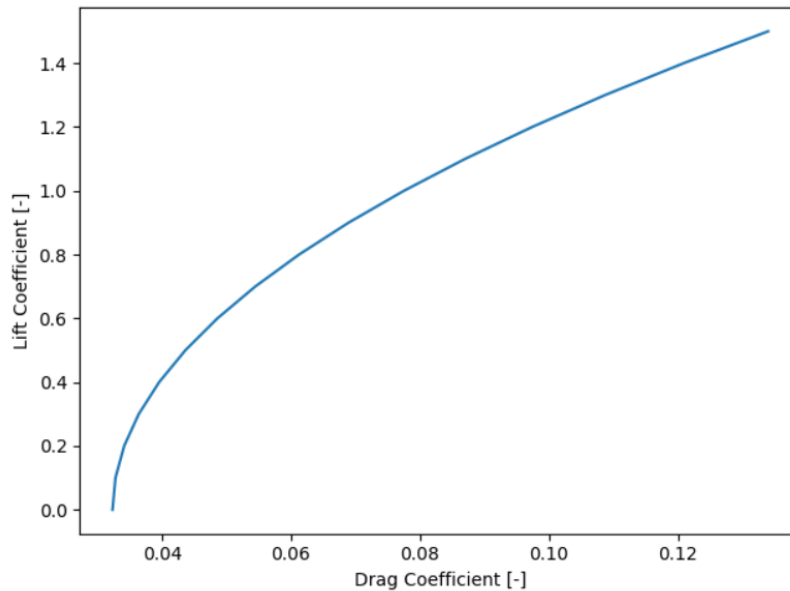


**Figure 6.9:** Drag polar

## 6.2.5. Verification and Validation

To determine certain aerodynamic parameters a python script was written. For this reason, verification and validation is performed in order to determine whether the script was written correctly and whether the method utilised is sufficiently accurate.

**Unit Tests**

Before any large verification tests were performed at the system level (and thus verifying the final results of the python script), smaller verification tests were performed. As the python script spanned hundreds of lines of code, multiple unit tests were performed.
Wing and Airfoil

In terms of unit testing in the wing and airfoil calculations, majority was performed on the wing planform code. Unit testing was performed on the basic functions that calculate wing geometry. This was done in order to ensure that outputs made sense. Furthermore these wing geometry parameters were then compared to existing aircraft to verify that the magnitude of the values was consistent. When comparing to the clients current aircraft, the MiniFreighter 8/500FW, the code predicts values that are significantly close. As the mission parameters are nearly identical, besides an increase in payload and different performance requirements, the outputs of the code can be verified.
Drag The first form of unit tests for drag that was conducted took the form of visual inspection of the equations inputted. This follows unit test U.1 as explained in section 6.1. The list of formulas that were visually inspected to ensure that they were inputted correctly is the following:

- Component wetted areas
- Air density with altitude
- Air temperature with altitude
- Dynamic viscosity

- Mach number
- Reynolds number
- Skin friction coefficients
- Form factor coefficients
- Oswald efficiency factor

Furthermore, as a lot of data describing the aircraft was necessary as input to all of these formulas, verification was needed for this too. In this case, verification was performed in the form of simple visual inspection that the values input into the code were indeed equal to those that described the aircraft. This follows unit test U.3 as described in section 6.1.

An additional form of unit testing was performed on all of the previously mentioned formulas. This form of unit testing involved performing calculations by hand and checking if the calculated value was close enough to that computed by the python script. This was done by conducting the entire calculation process by hand and noting down the calculated values from each formula on paper. Print statements were then implemented throughout the Python script such that each of the values calculated by hand could be compared with the Python script version.

**System Tests**
Airfoil
Airfoil system tests: In order to perform verification on the airfoil calculations, comparisons were made to literature data. When using viscid properties in the analysis, large errors become apparent before and significantly after stall. This makes the characterisation of each airfoils stall difficult and inaccurate. XFLR5 will not accurately predict rapid fluctuations in lift at stall. Therefore in order to get data on the stall regime, further wind tunnel testing is needed once a detailed design has been finalised.

Drag
As for performing verification on the system level, extreme-value tests were performed to verify the correct functioning of the python script. This was done by setting the wetted areas of each aircraft component and frontal area of the landing gear equal to zero for one test and equal to negative values of the actual aircraft areas for another test. By doing so, it is expected that the zero-lift drag coefficient should be equal to zero for the first test and a negative valued version of the initially calculated zero-lift drag coefficient for the second test. If the results of the python script are as expected, then the code clearly gives unfeasible values for unfeasible inputs, allowing users to easily identify a problem with their inputs. The results of the extreme-value tests can be found in Table 6.6 whereby the expected results were output by the python script and thus giving confidence in the code.

**Table 6.6:** Results of extreme-value tests for drag coefficient determination

| Extreme-value test | $C_{D_0}$ |
|---|---|
| Normal aircraft areas | 0.0323 |
| Zero aircraft areas | 0 |
| Negative aircraft areas | -0.0323 |

**Validation**
Airfoil
XFLR5 is a program that utilises different methods to perform both three dimensional and two dimensional analysis. When transitioning from a two dimensional airfoil analysis to a three dimensional wing analysis, a range of different changes are made. These impact the reliability of the program and its ability to characterise the viscid flow at high angles of attack where significant flow separation occurs. In three dimensional wing analysis, there are 4 different theories used: (LLT), (VM1), (VM2) and 3D Panel method. Each method has its benefits and downsides, performing more accurately at different stages in the operational profile. In Appendix B, Figure B.1 a comparison between the results of the 4 different methods is made. The wing planform is analysed using a Clark Y airfoil, due to the significant historical and experimental data available. Between the four methods at cruise a Reynolds number of $2.7 \cdot 10^6$ there is not significant deviation in the results. However Lifting Line Theorem (LLT) Provides

results over a greater range of angles of attacks. Utilising the panel methods of VM1, VM2 and 3D Panel method results in divergence at high angles of attack. The method is not able to compute results at these points as the errors become significantly large. Although all 4 methods have significant errors when modeling near stall characteristics, LLT presents a simple method which can roughly approximate the performance through the operating profile. Therefore LLT was chosen in the 3D wing analysis.

Drag

The first validation test involved the inspection of the drag polar curve to ensure if its shape corresponded to what was expected. As this drag polar encapsulates the final result of the aircraft drag coefficient determination, validation of its shape would provide confidence in the final results. It should first be mentioned that when inspecting Figure 6.9, the shape is indeed parabolic as expected. In addition, when comparing the drag polar of this report to that of the Cessna 172S [19], it can be seen that both the shape and the order of magnitude on both axes are very similar.
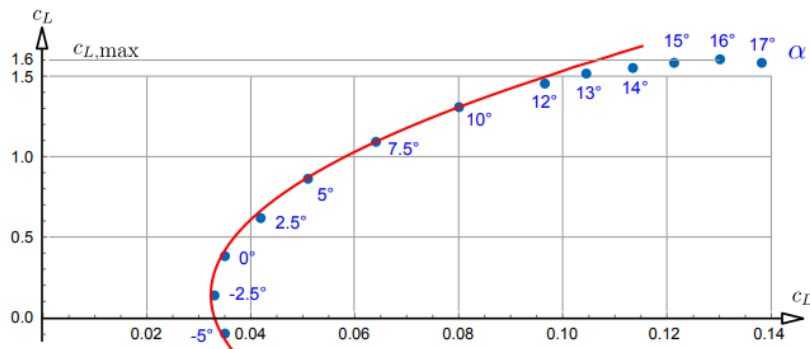


**Figure 6.10:** Drag polar of the Cessna 172S [19]

Additionally, the actual value of the calculated drag coefficient was validated. If the optimal lift coefficient for cruise is considered, which is equal to $0.86$, then a drag coefficient of $0.0657$ is found. When comparing this to the Wings For Aid MiniFreighter 8/500 FW aircraft, which has a claimed drag coefficient of $0.05$ [1], it can be seen that the calculated drag coefficient has the same order of magnitude and is relatively close in value. Comparison of the calculated drag coefficient with that of a Wings For Aid aircraft should give high confidence in the results as this aircraft performs the same mission as the aircraft being designed.

## 6.3. Flight Envelope

The flight envelope of an aircraft helps to determine the limits in structural performance at a specific velocity. This initial estimate will calculate the maximum loads experienced by the overall airframe due to both maneuvers and gust loading. These calculations will provide an ultimate load that the structure must be designed to handle. In the initial design stage of the aircraft, a detailed analysis of the flight performance and critical loading cases is not available. Therefore in order to formulate this diagram, methodologies from certification procedures such as CS-VLA, CS-23, CS-25 are used. Within a range CS-VLA is the closest category to which this aircraft performs in based off of the maximum take off weight.

The flight envelope is obtained from combining both the loading due to flight manoeuvres and the loading due to gusts. The highest positive load and lowest negative load are then determined to be the limits if the operational loads. Finally in order to calculate the ultimate load, these limits are multiplied by a factor of 1.5, allowing for adequate safety margins.

$$n = \frac{qC_{L_{max}}}{W/S} \tag{6.16}$$

---

[1]URL: https://www.ust-media.com/ust-magazine/UST035/26/ [cited 13 June 2022]

Equation 6.16 can be defined for both the clean configuration as well as the configuration with high lift devices. Furthermore Equation 6.16 forms the limit for positive loads at lower aircraft velocities. The maximum positive load factor that the aircraft must be able to handle stated by CS-VLA is 3.5. In comparison the maximum negative load factor is 1.5.

The gust loading diagram is defined by the following model. The gust load factor is assumed to be 1 before a gust affects the aircraft. The aircraft experiences a change in angle of attack due to both vertical and horizontal components of the gust.

$$\Delta n = \frac{\rho V C_{L_\alpha} u}{2\left(W/S\right)} \qquad (6.17)$$

$$u = K\hat{u} \qquad (6.18)$$

$$K = \frac{0.88\mu}{5.3 + \mu} \qquad (6.19)$$

$$\mu = \frac{2W/S}{\rho g \hat{c} C_{L_\alpha}} \qquad (6.20)$$

$\hat{u}$ Is calculated using statistical relations, changing with flight altitude and condition. After imposing both maneuver loading and gust loading in the same diagram, the maximum load factor can be identified. The maximum load of positive 3.5, calculated from the maneuver diagram is the most critical loading case. Taking into account the safety factor of 1.5, the structure must be able to then handle an ultimate load of 5.25.

## 6.4. Materials & Structures

Designing a strong and light structure that can carry all the loads the aircraft will experience during its life without failing is a crucial aspect of the design phase. Based on the estimated weight and cruise and landing conditions, several tools were developed to analyse the internal stresses of the wing, fuselage and landing gear for various geometries.

### 6.4.1. Material Selection

With the selection of materials for the aircraft, not only must the performance of the material under a variety of loading scenarios such as bending, shear and torsion be evaluated, but also the recyclability and production challenges must be analysed. Aircraft have been historically designed using wood, cloth, metal alloys and now the integration of carbon fibre reinforced composites has become increasingly popular. However these CFRPs pose challenges in areas of rapid, cheap manufacturing and the recyclability at the end of life. When comparing any two materials, specific stiffness and specific strength are two parameters that provide an excellent indicator of a materials mechanical performance with regards to weight. This is crucial for this aircraft as one of the main optimisation factors is weight. However when analysing specific loading cases, properties relating to the mechanics become more crucial. For example when looking at shear, shear modulus and shear strength are important to ensure that the part does not fail.

**Composites**
Composites involve the mixing of fibres and resin to form a solid piece of material. These are typically anisotropic materials with properties that depend mainly on the fibre orientation within the resin. Along the fibre direction, composites provide tremendous strength and stiffness. However, the same cannot be said regarding its load carrying capabilities along other directions.

As for the benefits of composite materials, these typically have a relatively high specific strength and specific stiffness along the fibre direction when comparing with most metals [2]. In addition, it is easier to construct an aerodynamic shape, resulting in a more drag efficient aircraft [3]. Therefore, since the material has good specific properties and can result in less drag for structures, composites are beneficial in achieving low weight aircraft structures. This can be concluded because the high specific

---

[2]URL:https://compositematerials.wixsite.com/home/single-post/2016-1-11-advantages-and-disadvantages-of-composites [cited 21 June 2022]

[3]URL:https://compositematerials.wixsite.com/home/single-post/2016-1-11-advantages-and-disadvantages-of-composites [cited 21 June 2022]

mechanical properties means that less material mass is required in order to meet sufficient mechanical performance. Moreover, by having a low drag design, less fuel mass is required for a mission.

Composites although providing tremendous strength, stiffness and low density, often lack the mechanical properties to provide structural reinforcement when loads are applied out of the fibre plane. They are also brittle in comparison to metal alloys, which then require additional structural measures to prevent catastrophic failure. Furthermore manufacturing methods for composites are often more time consuming, cost intensive and involve large amounts of quality assurance testing. If the driving requirement of meeting a unit cost of 15,000 euro (WFA-UREQ5-SysCo-FI-1) is to be adhered to, composites can still be utilised but not to a large degree. If manufacturing costs as well as raw material costs decrease within the next coming years, iterations can be done on the wing and fuselage to add composite sections. Furthermore additive manufacturing and large scale composite production should be investigated. Composite welding for wingboxes may be a viable solution if the technology is proven accurate, reliable and

**Metal Alloys**
Within the family of aluminum alloys used in the aerospace industry, 3 prominent series are used; 2XXX, 6XXX and 7XXX. AL - 2024 is one of the most widely used alloys with high fatigue resistance. 2024 is an AL - Cu Alloy, which is most commonly utilised in locations where high tension is required. It is typically used in a plate format and is implemented as fuselage tension structures, wing shear webs and ribs. Another widely utilised material is AL 6061, which is easily welded and manipulated; therefore it is typically used in home builds [37].

When looking towards future material applications, 3rd generation aluminium lithium alloys will allow for increased material properties, with considerable weight savings. These materials try to solve some initial isotropic property issues associated with aluminium alloys. Although slightly more expensive and less recyclable, these alloys allow for improvements in the range of 10-18% in specific stiffness and other important properties [45].

For the main aircraft structures being analysed in this report (wingbox and fuselage), aluminium alloys are considered over composites. The main reasons for this selection are the following:

- Aluminium alloys are easier to conduct a preliminary analysis with due to its isotropic properties.
- Aluminium alloys are more recyclable.
- Aluminium alloys are more manufacturable.

Due to the benefits of composites, it would be interesting to consider them in the design of the aircraft and thus would be for a later design phase. As for the type of metal alloy to be implemented, AL7075 (T6) was selected. This selection was based on the failure modes to be considered in the design: yield and buckling. Yield depends on the strength of the material while buckling depends on the stiffness of the material. When observing Table 6.7 it can be seen that the E-modulus and the shear-modulus of all of the aluminium types are relatively close in value. On the other hand, the yield and shear strength of AL7075 (T6) is significantly larger than the other options with regards to percentage difference. Moreover, the density of AL7075 (T6) is not too high and is only outperformed by AL2024 (T4) thus making it relatively lightweight.

**Table 6.7:** Viable Aerospace Industry Materials & Associated Properties

| Material | $\rho$ [g/cm$^3$] | E [GPa] | $\sigma_y$ [MPa] | $\sigma$ [MPa] | $K_c$ [MPa $\cdot$ m$^{0.5}$] | G [GPa] | $\tau$ [GPa] |
|---|---|---|---|---|---|---|---|
| AL2014 (T6) [4] | 2.80 | 72.4 | 415 | 485 | 26.4 | 28 | 290 |
| AL2024 (T4) [5] | 2.77 | 72.4 | 325 | 470 | 22 | 28 | 283 |
| AL7050 (T74) [6] | 2.83 | 70.3 | 450 | 510 | 38.5 | 26.9 | 300 |
| AL7075 (T6) [7] | 2.80 | 71.0 | 505 | 570 | 28.6 | 26.9 | 331 |
| CF Fabric [8] | 1.60 | 70 | - | 600 | - | 5 | 90 |

## 6.4.2. Loading Diagrams

In order to determine the necessary materials to implement in the aircraft, an analysis of the expected loads on the structures needs to be done. In the case of this report, both the wing and the fuselage are analysed and thus loading diagrams are generated for these. Shear and moment diagrams along the half-span of the wing and the entire length of the fuselage were generated. By generating these diagrams, the shear stresses due to the shear loads and the tensile stresses due to the moment loads can be determined. As for the general process of creating these diagrams, the loads distributed along the structures ($F(y)$) had to be determined whereby simplifications/assumptions were made depending on which structure was analysed. Thereafter, the shear and moment loading diagrams can be created using Equation 6.21 and Equation 6.22 [9] respectively. In addition, the torsional loads acting along the fuselage were investigated and a torsional loading diagram was generated. This was done because at times the fuselage can be expected to be an open section when deploying packages, meaning its ability to carry torsional loads decreases. For this reason, torsional loads must be investigated such that the fuselage can be designed accordingly.

$$F(y) = \frac{dV_y}{dy} \tag{6.21}$$

$$V_y = \frac{dM_x}{dy} \tag{6.22}$$

**Wing Loading Diagrams**

From the flight envelope, it was found that the largest load factor that can be expected is 3.5. Therefore, for the generation of the loading diagrams, the largest load factor in combination with a safety factor of 1.5 is considered, leading to a total load factor of 5.25. When approximating the loads acting along the half-span of the wing, several assumptions were made:

- The first assumption was that the wing lift follows an elliptical lift distribution. This leads to the lift of the wing to be represented by Equation 6.23 and hence also Equation 6.24 [18, ch.9].
- The second assumption was that the wings generate all of the lift in order to counteract the weight of the aircraft. This means that the vortex strength constant ($\Gamma_0$) is found by equating Equation 6.24 to the weight of the aircraft and rearranging to find the value.
- The third assumption is that the fuel is all consumed in the wing. This means that no relieving load from the fuel weight is present in the wing. However, the maximum take-off weight is still considered. Therefore, the analysis looks at a more critical loading case.

$$L = \rho V_\infty \int_{-\frac{b}{2}}^{\frac{b}{2}} \Gamma_0 \sqrt{1 - \left(\frac{2y}{b}\right)^2}\, dy \tag{6.23}$$

$$L = \rho V_\infty \Gamma_0 \frac{\pi b}{4} \tag{6.24}$$

With all of these assumptions, it became possible to calculate the loads acting along the half-span of the wing during cruise. This included both the lifting loads acting along the half-span, and the weight of the wing itself. When determining the vortex strength constant for the lift distribution, the maximum take-off mass was considered by equating it to Equation 6.24 and determining the constant as this is the limiting case. Once the vortex strength constant was determined, Equation 6.25 was used to represent the lift load per span along the half-span of the wing. When calculating the relieving force caused by the weight of the wing, the wing was split into sections whereby the weight of each section acted as a point load. With knowledge of the loads acting along the wing, the shear and moment diagrams were constructed for cruise using Equation 6.21 and Equation 6.22 whereby integration was performed to

---

[4]URL: `https://asm.matweb.com/` [cited 21 June 2022]

[5]URL: `https://asm.matweb.com/` [cited 21 June 2022]

[6]URL: `https://asm.matweb.com/` [cited 21 June 2022]

[7]URL: `https://asm.matweb.com/` [cited 21 June 2022]

[8]URL: `http://www.performance-composites.com/carbonfibre/mechanicalproperties_2.asp` [cited 21 June 2022]

[9]URL: https://engineeringstatics.org/VM_relations.html [cited 13 June 2022]

find the values for shear and moment along the half-span of the wing. The shear loading and moment loading diagrams along the half-span of the wing of the aircraft designed can be found in Figure 6.11 where a load factor of $5.25$ was applied as it combines both the ultimate load factor of $3.5$ and the safety factor of $1.5$. These values can be observed in section 6.3. Using these loading diagrams, a stress analysis of the wing could be done and led to the design of the wing described in section 7.2. It is important to note that from inspecting the diagrams, it can be seen that the maximum loads act at the wing root. Table 6.8 presents what these maximum loads at the root are.

$$L(y) = \rho V_\infty \Gamma_0 \sqrt{1 - \left(\frac{2y}{b}\right)^2} \tag{6.25}$$
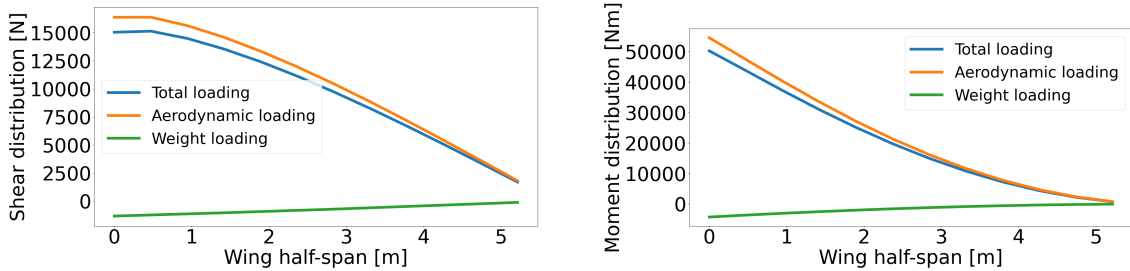


(a) Shear loading diagram of wing along half-span during cruise with load factor of n = $5.25$

(b) Moment loading diagram of wing along half-span during cruise with load factor of n = $5.25$

**Figure 6.11:** Shear loading (left) and moment loading (right) diagrams of wing in cruise with load factor of n = $5.25$

**Table 6.8:** Magnitude of maximum shear and moment loads acting on the wing

| Maximum absolute load at n = 5.25 | Magnitude of load |
|---|---|
| Shear load [kN] | 7.66 |
| Moment load [kNm] | 21.13 |

**Fuselage Loading Diagrams**

For the case of fuselage loading diagrams, two cases were considered: when the aircraft is subject to the largest load factor in combination with the safety factor ($n = 5.25$ in total), and the case when the fuselage is stationed on land. For the first scenario, shear and moment are once again considered in addition to torsion. More importance is put on torsion for the design of the fuselage than the wingbox because the fuselage is an open structure when deploying packages and thus problems relating to torsion are expected. For the case where the fuselage is stationed on the ground, shear and moment are only considered. The reason this scenario is considered is due to the potentially high loads that the landing gear may exert on the fuselage, thus making it worth investigating.

**Flying with Total Load Factor of 5.25**

In order to determine the loads acting along the fuselage, both the masses and position of the different components that make up the aircraft had to be known. This can be found documented for the aircraft designed in this report in Table 6.9. It should be noted that this analysis was not done at the final phase of the design and thus changes to the components masses can be expected. Due to no significant changes to the design being done this late in the design process, the impacts on the loading diagrams will be negligible. It should also be noted that in other analyses performed, the location of the center of gravity of the fuselage is not considered at half of its length but rather at forty percent. However, to simplify the analysis of the fuselage loading diagram, it was assumed that the weight of the fuselage was equally distributed along its length and has a centre of gravity location at half of its length. Moreover, the payload is not considered in Table 6.9, the details regarding its positioning can be found in Table 6.10 whereby it should be known that each payload box has a mass of $20\,kg$. When constructing the fuselage loading diagrams, the following assumptions were made:

- The fuselage mass is equally distributed along the length of the fuselage.

- The mass of all of the aircraft components besides the fuselage acts as a point load.
- The aircraft mass is the maximum take-off mass. This was in order to assess a critical case.
- All of the lift produced by the aircraft is carried by the main wing and the horizontal tail.

**Table 6.9:** Masses and locations of aircraft components used for generation of fuselage loading diagram

| Component | Mass [kg] | Location relative to fuselage length [-] |
|---|---|---|
| Power system | 136.2 | 0.05 |
| Flight control | 75.3 | 0.10 |
| Avionics | 22.3 | 0.20 |
| Electronics | 48.4 | 0.30 |
| Fuselage | 50.0 | 0.5 |
| Wing | 40.5 | 0.18 |
| Fuel | 59.6 | 0.18 |
| Landing Gear | 14.6 | 0.30 |
| Horizontal Tail | 12.3 | 0.92 |
| Vertical Tail | 3.5 | 0.92 |

**Table 6.10:** Number and location of payload boxes used for generation of fuselage loading diagram

| Number of boxes at location | 3 | 3 | 2 | 2 |
|---|---|---|---|---|
| Location of payload boxes [m] | 0.875 | 1.325 | 1.925 | 2.475 |

Using all of the described information, the shear and moment loading diagrams were constructed and can be found in Figure 6.12. In these diagrams, both a load factor of $1$ and the ultimate load factor including the safety factor of $5.25$ were illustrated.



**(a)** Shear loading diagram of fuselage during flight     **(b)** Moment loading diagram of fuselage during flight
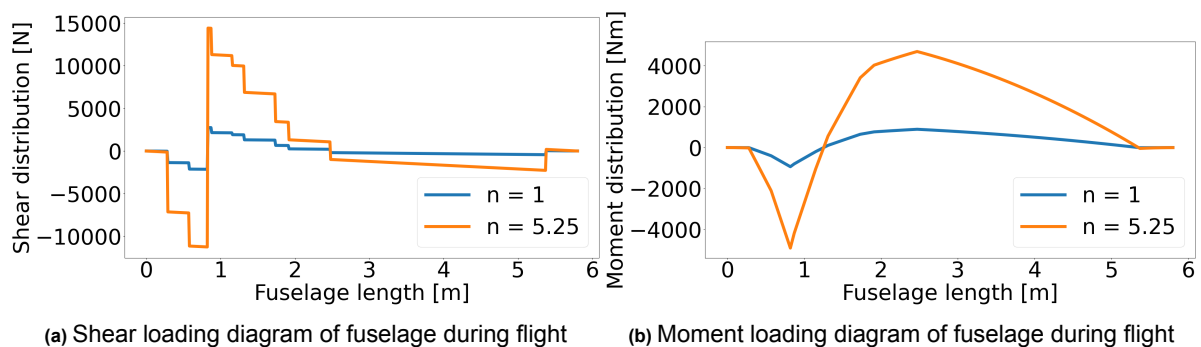
**Figure 6.12:** Shear loading (left) and moment loading (right) diagrams of fuselage during flight including critical load factor

From the shear loading and moment loading diagrams depicted in Figure 6.12, the largest absolute values for the shear and moments, in addition to the location of these, can be found. The results of these can be found in Table 6.11.

**Table 6.11:** Location and magnitude of maximum shear and moment loads acting on the fuselage

| Shear Data | |
|---|---|
| Location of maximum absolute shear load [m] | 0.83 |
| Maximum absolute shear load at n = 1 [N] | 2747.0 |
| Maximum absolute shear load at n = 5.25 [N] | 14421.6 |
| **Moment Data** | |
| Location of maximum absolute moment load [m] | 0.82 |
| Maximum absolute moment load at n = 1 [Nm] | 935.5 |
| Maximum absolute moment load at n = 5.25 [Nm] | 4911.3 |

In order to generate the torsional loading diagram, additional assumptions had to be made:

- Torsion is generated only by the engine, the main wing, and the vertical tail.
- The torsional loads act as point loads.
- The torsional load at the main wing ensures equilibrium with those generated by the engine and vertical tail.

In reality, it can be expected that there are many more sources of torsional loads at the fuselage. However, these assumptions were made in order to allow for a simplified analysis while still giving an impression of the expected torsional loads that the fuselage will be subject to. When determining the torsional load caused by the engine, an inspection of the engine specifications during operation was done and it was found that the torsional load caused by it is equal to $317.9398\ Nm$. As for the determination of the torsional load caused by the vertical tail, the gust load that the aircraft must be able to withstand according to CS-VLA was used. As stated by CS-VLA 443(a), the vertical tail must be able to handle gusts of $15.24\ m/s$ during cruise [11]. Knowing this, the angle of sideslip could be determined which in turn allows for the calculation of the vertical tail side force and thus the torsional load. The resulting torsional loading diagram can be found in Figure 6.13 with an applied safety factor of $1.5$ whereby the maximum absolute torsional load along the fuselage was found to be equal to $2160.492\ Nm$. In this case, only cruise was considered because requirements relating to gusts could not be found for other flight conditions. An important thing to note was that the case where the torsion of the engine and the torsion caused by the vertical tail are in the same direction was considered. This was done so to look at a more critical case.
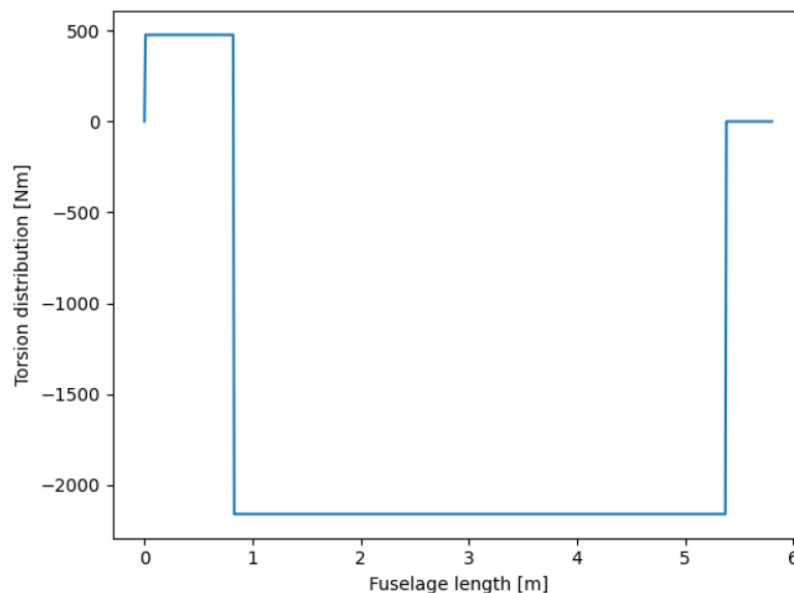


**Figure 6.13:** Torsional loading of fuselage during cruise with applied safety factor of 1.5

**On-land**

In addition to flight conditions, loads acting on the fuselage when on the ground were also considered. In this case, no lift is being produced by the main wing or the horizontal tail, but rather, vertical forces are being exerted by the landing gear to counter the weight of the aircraft. The forces exerted by the landing gear ensure both vertical force equilibrium and moment equilibrium. Using this knowledge, the values provided in Table 6.9 and the locations of the nose and main landing gear (being $0.1\ m$ and $1.55\ m$ respectively), the shear and moment diagrams could be determined. It should be noted that one important assumption was made in the determination of these loading diagrams which was that the total weight of the landing gear was distributed as $60\%$ main landing gear and $40\%$ nose landing gear. This was done as the main landing gear is generally larger than the nose landing gear and thus assuming an equal distribution would be unrealistic. The determined shear and moment diagrams, with an included safety factor of $1.5$, can be found in Figure 6.14. The location and magnitude of the

maximum shear and moment loads acting on the fuselage when the aircraft is grounded can be found in Table 6.12. When inspecting these results, it can be seen that the most critical case is when the aircraft is flying at the critical load factor of $5.25$.



(a) Shear loading diagram of fuselage on-land



(b) Moment loading diagram of fuselage on-land
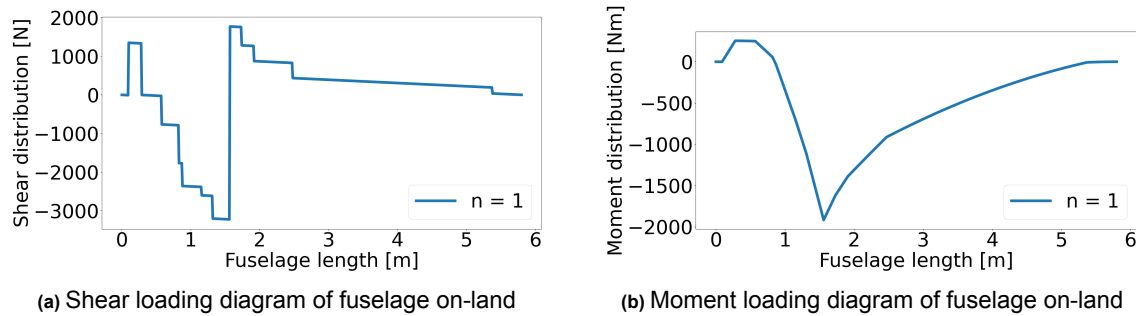
**Figure 6.14:** Shear loading (left) and Moment loading (right) diagrams of fuselage on-land with applied safety factor of 1.5

**Table 6.12:** Location and magnitude of maximum shear and moment loads acting on the fuselage on-land

| Shear Data | |
|---|---|
| Location of maximum absolute shear load [m] | 1.56 |
| Maximum absolute shear load [N] | 4839.267 |
| **Moment Data** | |
| Location of maximum absolute moment load [m] | 1.56 |
| Maximum absolute moment load [Nm] | 2878.519 |

Once the shear, moment and torsional loads along the wing and fuselage were determined, a deeper analysis could be made. This involved creating design tools that analysed the different stresses that the structures would be subject to. In addition, design tools for additional failure modes in the form of buckling and crippling were made. By creating such design tools, design iterations could be made leading to a design for the wing and fuselage. The rest of this section will explain how each of these design tools functioned by going into detail regarding the calculations performed and the results produced.

### 6.4.3. Tension and Compression Due to Bending

One of the main loading types to be considered for long and slender structures such as wingbox and fuselage is tensile and compressive stresses due to bending. These stresses not only allow to evaluate failure by yield but also buckling performance as described in subsection 6.4.8.

To calculate the stresses a simple beam model is used. According to this model the stress in point of a cross-section of the beam can be found using Equation 6.26 and the second derivative of deflection can be found using Equation 6.27. In order to understand the accuracy and applicability of the results the assumptions used are given [10]:

- Beam is initially straight , and has a constant cross-section.
- Beam is made of homogeneous material and the beam has a longitudinal plane of symmetry.
- Resultant of the applied loads lies in the plane of symmetry.
- The geometry of the overall member is such that bending not buckling is the primary cause of failure.
- Elastic limit is nowhere exceeded and 'E' is same in tension and compression.
- Plane cross - sections remains plane before and after bending.

$$\sigma_{bending} = \frac{My}{I_{xx}} \qquad (6.26)$$

---

[10] https://theconstructor.org/structural-engg/theory-of-simple-bending/

$$\frac{d^2y}{dz^2} = -\frac{M}{EI} \tag{6.27}$$

In Equations 6.26 and 6.26 $z$ is the longitudinal coordinate, $y$ is coordinate normal to $z$ in line with the deformation, $M$ is the internal moment load, $I_{xx}$ is the moment of area and $E$ is the stiffness modulus.

### 6.4.4. Shear Stress Due to Torsion

In a wingbox the box structure is usually used to create torsional stiffness. To calculate this stiffness and the resulting stresses in the material a Python program was created. The program looks at two different types of structures, closed sections and open sections. To determine if an section is open or closed the last point of the design is checked with the first point of the design. If they have the same coordinates, the section is considered closed. The open and closed sections both have different equations for the twist and stress. First the equations for an open section are presented.

$$\tau_{max} = \frac{3T}{st^2}$$
$$\frac{d\theta}{dz} = \frac{3T}{Gst^3} \tag{6.28}$$

In these equations $T$ is the torsional moment, $s$ is the length of the section of the design, $G$ is the material shear modulus and $t$ is the thickness of the section. For a given geometry the shear stress, $\tau_{max}$, in each individual element of the design can be calculated. Note that this is the maximum shear stress in the element. Therefore it causes a bit of over engineering. The second equation is not as straight forward to implement. It assumes the design is only one plate and not a more complex geometry. To implement this calculation was avoided as the wingbox design would revolve around a closed section, as a wingbox is usually closed for stiffness purposes.

The equations for closed thin walled sections are described below in Equation 6.29.

$$\tau = \frac{3T}{2tA_m}$$
$$\frac{d\theta}{dz} = \frac{T}{4GA_m^2} \oint_{L_m} \frac{1}{t} ds \tag{6.29}$$

The Python program will take these equations and use them to calculate the twist and stress for the given design. For closed sections the internal area $A_m$ is used. However as geometries become more complex, simple area calculations cannot be used anymore. The cross-section of a wing is not easily approximated by calculating squares and triangles. Therefore a mathematical theorem is used, the shoelace theorem, or Gauss's area formula. This equation uses the coordinates of the geometry to calculated the area. The equation is given in Equation 6.30 for $n$ number of coordinates.

$$2A = \begin{matrix} x_1 & x_2 \\ x_1 & y_2 \end{matrix} + \begin{vmatrix} x_2 & y_3 \\ x_2 & y_3 \end{vmatrix} + \begin{vmatrix} x_3 & y_4 \\ x_3 & y_4 \end{vmatrix} + ...... + \begin{vmatrix} x_n & y_1 \\ x_n & y_1 \end{vmatrix} \tag{6.30}$$

These stresses are then superimposed with the stresses from the other loads on the wingbox.

### 6.4.5. Shear Stress Due to Shear Force

The calculations described in the previous subsection are for torsion. However shear force also causes shear stress. The main equation to relate force to stress first expresses the shear stress as shear flow. This equation is given in Equation 6.31.

$$q_b = -\frac{V_y I_{yy} - V_x I_{xy}}{I_{xx} I_{yy} - I_{xy}^2} \int_0^s tyds - \frac{V_x I_{xx} - V_y I_{xy}}{I_{xx} I_{yy} - I_{xy}^2} \int_0^s txds \tag{6.31}$$

In this equation $I_{xy}, I_{xx}, I_{yy}$ are the moment of inertia of the geometry. These can be calculated by the computer code. $V_y$ and $V_x$ are the forces applied to the structure in y and x direction respectively. The integral in this equation is done per part of the design. This integral starts at the first defined part and adds the previous shear flow from the previous part to the next. This means that counting from a

certain part changes the shear flow of the structure. For an open section this does not matter as the first part usually has no shear flow on the start. However for a closed section this does matter as no 0 shear flow location can be identified by default. To correct for this mistake the shear flow in a closed section must also have a $q_{s0}$ factor. This is a constant shear flow that can be determined by using the formula in Equation 6.32.

$$q_{s0} = -\frac{\oint (q_b/Gt)ds}{\oint ds/Gt} \tag{6.32}$$

In this equation G is dropped as it is assumed that the whole structure is made of the same material everywhere.

### 6.4.6. Shear Center

By using the equations it is assumed that the load is applied in the shear center. This may however not always be true. To correct for this the shear center must be calculated. This is done by calculating the distance of each part to the geometric center. The relationship used is given in Equation 6.33. This first equation describes a line which can be constructed by using the two point on the ends of the part.

$$ax + by + c = 0 \quad distance = \frac{ax_0 + by_0 + c}{\sqrt{a^2 + b^2}} \tag{6.33}$$

After that two load cases are studied, one in y direction and one in x direction. This allows for the positioning of the shear center both in y and x direction. A horizontal force does not have any moment contributions due to their horizontal position with respect to the geometric center. This principle is also used for the vertical position. The moment from the shear center to the geometric center must be the same as the moment from the shear flow. Reverse engineering reveals the location of the shear center. Once this is known, the torsion calculations can be used to introduce a correction for the forces being applied in the geometric center and not the shear center. At the end the list with all the shear flows over the whole geometry can be divided by the local thickness and thus produce the shear stress.

### 6.4.7. Yield Failure

The goal of estimating stresses and buckling of structures is to be able to predict at what loading can the component be expected to fail. During the design of wingbox and fuselage it is attempted to predict the loads which the aircraft is required to sustain and find the lightest and otherwise best performing structural configurations to handle these loads. The way the failure load and type was estimated for metal and composite wingbox design differs substantially. In this subsection it is described how failure of a structure was predicted and how that was used to perform high level design of the wingbox and fuselage.

As described in subsection 6.4.1 it was decided to proceed with an Aluminium 7075(T6) design. This simplifies the analysis as the orientation of the material does not have to be considered as it would have to be for composite materials. It is not denied, though, that composite design might be considered for further design iterations.

**Aluminium Design**

Because Aluminium is a ductile, isotropic and uniform material, Von Mises [10] yield criterion was used. It allows to combine tensile load resulting from bending and shear loads caused by shear loading and torsional loading. The full equation for Von Mises stress is given in Equation 6.35. In this stresses in only two dimensions were considered and thus the equation is simplified to Equation 6.34 where $\sigma_{11}$ is tensile stress caused by buckling and $\sigma_{12}$ is shear stress caused by torsional and shear loads.

$$\sigma_v = \sqrt{\frac{1}{2}\left[(\sigma_{11} - \sigma_{22})^2 + (\sigma_{22} - \sigma_{33})^2 + (\sigma_{33} - \sigma_{11})^2\right] + 3\left(\sigma_{12}^2 + \sigma_{23}^2 + \sigma_{31}^2\right)} \tag{6.34}$$

$$\sigma_v = \sqrt{\frac{1}{2}\sigma_{11}^2 + 3\sigma_{12}^2} \tag{6.35}$$

To determine whether a design would fail by yielding for a given loading a mesh was generated with the shape of the design and Von Mises stresses were calculated at every point of the mesh. If the Von Mises stress calculated at some location was found to be larger than the yield strength of the material

the design was considered to fail at that location. If the Von Mises stress was found to be smaller than the yield stress design was considered to potentially not be optimal as it means less material could be used to save weight, increase Von Mises stresses and yet generate a design that does not fail for the given loads.

### 6.4.8. Buckling Analysis for Stringer and Rib Spacing

When designing the wingbox, additional failure modes were considered in addition to the load-carrying capability of the structure to ensure the structural integrity of the design. In this report, it was determined what stringer number and rib pitch was needed in order to ensure sufficient buckling performance of the wingbox. At this stage of the design, only the rib pitch was considered and a detailed design of the ribs was not conducted. For the buckling analysis, the following assumptions were made:

- All curved panels have the same buckling performance as flat panels. Therefore, all buckling analysis is performed assuming a flat panel.
- All empirically derived relationships are sufficiently accurate to design the wingbox. This assumption applies to the Johnson-Euler relationships used.

In order to determine whether the selected wingbox design would fail due to buckling, the critical buckling load of the skin panels needed to be determined. As the skin panels are stiffened skins, both the skin and the attached stiffeners needed to be considered. As for buckling of the the skin, which is a thin plate, Equation 6.36 was used [23]. Equation 6.36 gives the critical buckling stress of the thin plate alone where $C$ is a constant dependent on the boundary conditions, $E$ is the E-modulus of the material, $v$ is the Poisson ratio of the material, $t$ is the plate thickness and $b_p$ is the width of the plate. However, as previously mentioned, the skin will have stiffeners supporting it. For this reason, $b_p$ is the stringer pitch and C can be equated to $4.0$ [23]. This was done because the connection of the plate to the stringers and ribs is equal to a simple support.

$$\sigma_{cr} = C \frac{\pi^2 E}{12(1 - v^2)} \left( \frac{t}{b_p} \right)^2 \tag{6.36}$$

As for how stiffeners and ribs are considered in the buckling performance of the stiffened panel, the Johnson-Euler column curve was utilised. This curve can be found in Figure 6.15 and describes the failure mode of stiffeners. When the ratio of the effective length to the radius of gyration of the stiffener ($L_e/\rho_g$) is less than a critical value, the failure mode of the stiffener is crippling. Otherwise, the failure mode is Euler buckling. When the failure mode is crippling, the critical stress for buckling can be calculated using Equation 6.37 [23]. If the failure mode is Euler buckling, the critical stress can be determined using Equation 6.38 [23]. This directly relates to both the rib spacing and stiffener dimensions as the effective length of the stiffener ($L_e$) is equal to the rib spacing. Moreover, both the radius of gyration of the stiffener and the stiffener crippling stress of the stiffener ($\sigma_{cc}$) are dependent on the stiffener dimensions.
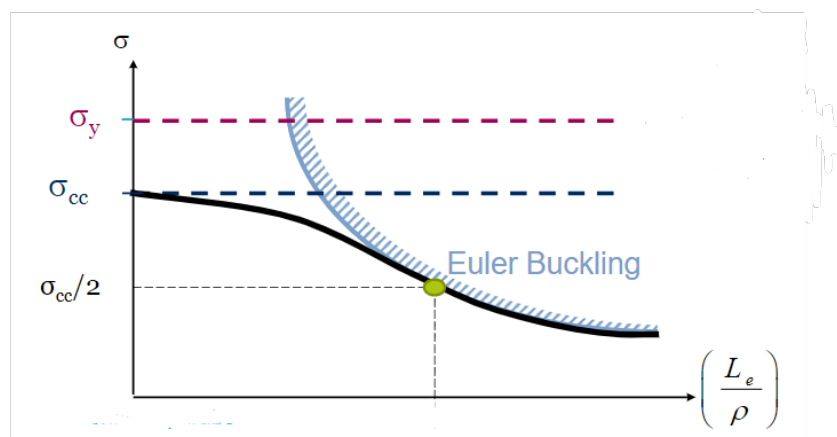


**Figure 6.15:** Johnson-Euler column curve [23]

$$\sigma_{cr} = \sigma_{cc} \left( 1 - \frac{\sigma_{cc}(L_e/\rho_g)^2}{4\pi^2 E} \right) \tag{6.37}$$

$$\sigma_{cr} = \frac{\pi^2 E}{(L_e/\rho_g)^2} \tag{6.38}$$

From Equation 6.37, it can be seem that the crippling stress of the stiffener on its own ($\sigma_{cc}$) needs to be determined. The crippling stress of stiffeners was determined using Equation 6.39 [23] whereby the crippling stress of each component of the stiffener can be found and the total crippling stress is found by finding the weighted average of all the stiffener part crippling stresses with respect to area. $\alpha_c$ and $n$ are material values and were found to be equal to $0.8$ and $0.6$ respectively for aluminium alloys [23].

$$\frac{\sigma_{cc}^{(i)}}{\sigma_y} = \alpha_c \left( \frac{C}{\sigma_y} \frac{\pi^2 E}{12(1 - v^2)} \left( \frac{t}{b_p} \right)^2 \right)^{1-n} \tag{6.39}$$

In addition to the failure stress of the skin and the stiffener (buckling and crippling), another aspect to consider is the local strengthening of the skin where it is attached to the stiffener. At this area, the skin is able to carry load until the crippling stress of the stiffener. The width of the skin whereby local stiffening is found can be calculated using Equation 6.40.

$$2w_e = t\sqrt{\frac{C\pi^2}{12(1 - v^2)}} \sqrt{\frac{E}{(\sigma_{cc})_{stiffener}}} \tag{6.40}$$

Finally, the critical buckling stress of the entire panel can be found by calculating the (area based) weighted average of the buckling/crippling stresses of the plate, stiffener, and locally reinforced plate area. By making a python script using these calculations, it can be confirmed which combination of skin thickness, rib spacing, stringer dimensions, and stringer spacing is required in order to ensure that the wingbox buckles at its design load. More details regarding the implementation of buckling to the design of the wingbox can be found in section 7.2.

### 6.4.9. Geometric Representation of the Design

The design has to be represented geometrically for the computational tools to perform meaningful analysis. To achieve this the components are split up into layer on the longitudinal axis (span-wise for wingbox, nose to tail for the fuselage). The analysis is performed on each of the layers and the layers are stacked on top of each to build the complete geometry. This approach limits the complexity of analysis that can be performed but its is relatively easy to construct and use. In Figure 6.16 a representation of a layer of a geometry is shown. Black lines represents the wingbox body and blue dots show the positioning of stringers. In Figure 6.17 a 3d representation of a wingbox is shown.
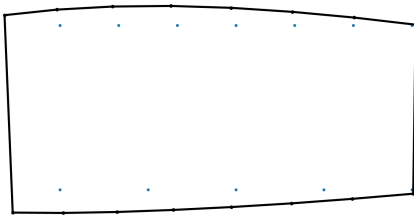


**Figure 6.16:** A layer of 3d geometry representing a wingbox



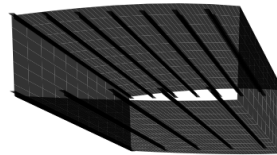**Figure 6.17:** 3d representation of a wingbox

### 6.4.10. Code Verification

For the structural analysis performed in the report, several design tools were created in the form of python scripts whereby each design tool was described in section 6.4. It is essential to perform thorough verification since each script consists of hundreds of lines of code and thus it is likely that mistakes were

made and small errors can be found. As any error could greatly influence the final designs outputted by the python scripts, it is important that there are no errors in the code. For this reason, both unit tests and system tests were performed on each of the python scripts used for the structural analysis of the aircraft.

### Unit Tests

Unit tests are the simplest form of verification tests that verify small parts of the code. This can range from verifying a few lines of code to just one line of code. For the case of all of the python scripts for structural analysis, the same procedure for performing unit tests was used. The unit tests performed were the same as those described in section 6.1 in addition to the following:

- Visual inspection that the correct functions were called with the correct arguments. This was required as multiple functions were made and called upon by different python scripts.
- Place print statements to ensure array lengths are as expected. This was important to test as many arrays were made in order to perform design iterations.

### Loading Diagrams

For the fuselage and wing loading diagrams, a system test was performed using knowledge of the expected loading values at the boundaries. In the case of the shear and moment loading diagrams for the wing, it is expected that there should be zero shear and moment load at the tip and the largest absolute values should be at the root. As for the fuselage, since it should be in equilibrium for the flight states considered, the shear, moment, and torsion values should be zero at the front end and the back end of the fuselage. Upon inspection of the loading diagrams, it can be seen that the diagrams comply to what is expected.

### Shear Flow

For the shear flow calculations a simple case was calculated, a box of 1 meter high and 1 meter wide with thickness everywhere of 0.01 meter. A force of 500 N is applied to the geometric center, to create the test case. To manually calculate the shear flow a number of intermediate answers must be calculated. These intermediate answers are also calculated by the python code and can thus be checked. The intermediate answers that are checked are:

1. Import data correctly (coordinates and thicknesses)
2. Moments of inertia ($I_{xx}$, $I_{yy}$ and $I_{xy}$)
3. Evaluate integrals in Equation 6.31
4. Calculate base shear flow at all points using Equation 6.31
5. Evaluate both integrals in Equation 6.32
6. Calculate $q_{s0}$
7. Determine position of shear center with respect to geometric center
8. Confirm shear flow distribution follow logical and expected distribution when plotted over the distance from the initial point
9. Calculate correction for shear center not being on the geometric center (for shear center on geometric center, correction should be 0)
10. Confirm that shear stress is in an expected and acceptable order of magnitude

Though the python code needed some tweaking, the program was found to be very accurate. For each of these unit test the code was confirmed to work. Once all the unit tests were done, the final data was also compared to the manual calculations. It revealed that the code calculates the shear stress in a non-standard way. Since no sign convention is given to the code, it will create one itself, as it has to define positive and negative numbers. It does this by taking the opposite direction in which the geometry is made. The geometries are made up from plates the travel between two points. These plates can be defined in a clockwise or counter clockwise direction. In the test case that was counterclockwise. It means that during the analysis of the data it must be taken into account that this is the sign convention. However since shear stress does not have a difference between tension en compression as normal stress has, this convention is not considered a problem.

**Buckling**

For the buckling analysis, a simple structure was input into the program and the buckling stress of the stiffened panel was calculated. The same calculation was done by hand and the values for the buckling stresses were compared. The structure considered is illustrated in Figure 6.18 whereby Z-stringers made up of three plates of equal length are used. The values of the different dimensions of the stiffened panel being analysed can be found in Table 6.13. It should also be noted that the material for both the plate and the stringer is aluminium alloy 7075. Upon performing this verification test, it was found that the python script passed the test as both hand calculation and the python script found a stiffened panel buckling stress of $399.82\ MPa$.
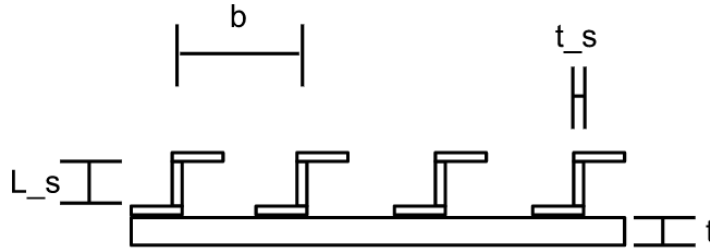


**Figure 6.18:** Stiffened panel design for verification of buckling analysis python script

**Table 6.13:** Values for dimensions of stiffened panel analysed for verification

| Dimension | Symbol | Value [mm] |
|---|---|---|
| Stringer pitch | $b$ | 300 |
| Plate thickness | $t$ | 5 |
| Stringer plate length | $L_s$ | 2 |
| Stringer thickness | $t_s$ | 1 |

**Geometric Representation and Yield Failure**

In order to verify the correct functionality of yield calculations and geometry generation a simple test case is made. The test case consists of a square beam and a uniform lateral loading and uniform torsional loading. Correct functionality is verified by inspecting the shape of the geometry and checking if it is as expected. An image depicting the test geometry is shown in Figure 6.19. In order to verify correct calculation of the stresses, the calculated values are compared at the minimum and maximum stress points of the root and the tip with hand calculated values. Additionally stress distribution both on a single layer and in the span-wise direction is evaluated by inspecting images Figure 6.20 to Figure 6.24 displaying bending, shear and torsional stresses of the beam separately with a relative scale of stresses from 0 to 1.
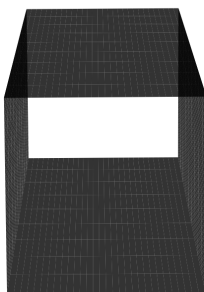


**Figure 6.19:** Geometrical representation verification test case

**Figure 6.20:** Bending stress test case (top view)
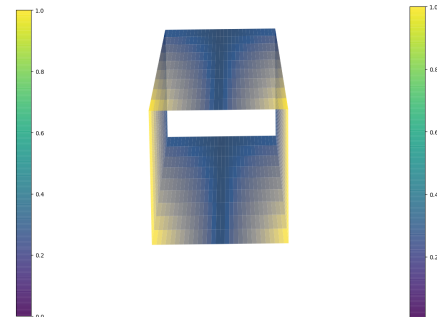
**Figure 6.21:** Bending stress test case (side view)
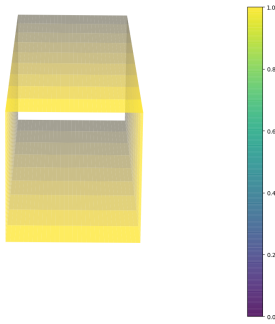
**Figure 6.22:** Torsional stress test case
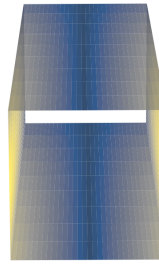
**Figure 6.23:** Shear stress test case (top view)
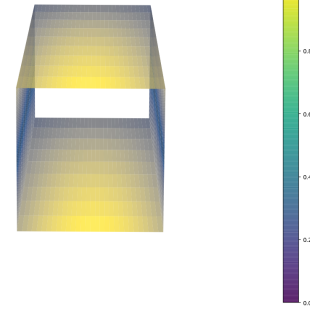
**Figure 6.24:** Shear stress test case (side view)

# 6.5. Stability & Control

In order to size the empennage of the aircraft, a loading diagram and scissor plot need to be created. The loading diagram indicates the shift in the center of gravity range over the mission profile. The scissor plot indicates the center of gravity boundary locations for different horizontal stabilizer sizes. These diagrams can finally be combined to find an optimal location of the wing position and horizontal stabilizer area. The code gives as an output the horizontal stabilizer surface area, location of the leading edge MAC, and the updated tail length. All values are then updated to the data sheet to be used in the next iteration.

## 6.5.1. Assumptions

The assumptions made while designing this tool are the following:

- The aerodynamic center of the wing is at the quarter chord point
- The center of gravity of the wing is at 50% MAC
- All fuel is stored in the wings
- Fuel sloshing is neglected
- Any dynamic effects from losing weight are neglected
- The C.G. of the fuel is always at 50% MAC
- Small angles of attack
- The C.G. of the Vertical and horizontal stabilizer are at 50% of their MAC's respectively.
- Higher order terms of the mach number are neglected

## 6.5.2. Scissor Plot

The scissor plot is a tool used to optimize the size of the horizontal stabilizer, keeping into account the stability and controllability of the aircraft. It consists of two lines, the stability and controllability line, plotted with the center of gravity on the x-axis and horizontal tail surface on the y-axis. When designing the aircraft, the center of gravity range must always lie in between the these two lines.

### Stability

The stability refers to the static longitudinal stability, which is the ability of the aircraft to counteract any disturbances in angle of attack. The static longitudinal stability derivative ($C_{m_\alpha}$) must be negative to be considered stable. In the scissor plot, the right line represents the stability line. The center of gravity must always be to the left of this line, else the aircraft is not statically stable anymore.

The following equation represents the stability line [33], where a stability margin of 5% is included:

$$\frac{S_h}{S} = \frac{1}{\frac{C_{L_{\alpha_h}}}{C_{L_{\alpha_{A-h}}}}\left(1 - \frac{d\epsilon}{d\alpha}\right)\frac{l_h}{\bar{c}}\left(\frac{V_h}{V}\right)^2}\bar{x}_{cg} - \frac{\bar{x}_{ac} - 0.05}{\frac{C_{L_{\alpha_h}}}{C_{L_{\alpha_{A-h}}}}\left(1 - \frac{d\epsilon}{d\alpha}\right)\frac{l_h}{\bar{c}}\left(\frac{V_h}{V}\right)^2} \tag{6.41}$$

Furthermore using Equation 6.42, the longitudinal static stability derivative can be calcuated. For this it will be assumed that the angle of attack is small such that $C_{L_\alpha} \approx C_{N_\alpha}$ [1] [33].

$$C_{m_\alpha} = C_{N_\alpha}(\bar{x}_{cg} - \bar{x}_{np}) \tag{6.42}$$

## Controllability

The controllability refers to the horizontal tail being able to produce sufficient force to trim the aircraft, which is the condition $C_m = 0$. The left line in the scissor plot represents the controllability line. The center of gravity must always be to the right of this line, else the aircraft is too stable and may not be controllable anymore.

The following equation represents the controllability line [34]:

$$\frac{S_h}{S} = \frac{1}{\frac{C_{L_h}}{C_{L_{A-h}}} \frac{l_h}{\bar{c}} \left(\frac{V_h}{V}\right)^2} \bar{x}_{cg} + \frac{\frac{C_{m_{ac}}}{C_{L_{A-h}}} - \bar{x}_{ac}}{\frac{C_{L_h}}{C_{L_{A-h}}} \frac{l_h}{\bar{c}} \left(\frac{V_h}{V}\right)^2} \tag{6.43}$$

Combining Equations 6.41 and 6.43 into one graph produces the scissor plot.

### 6.5.3. Loading Diagram

The loading diagram shows how the aircraft's center of gravity (CG) varies over its mission profile. The diagram starts at the bottom with the CG position at operating empty weight. The CG position is calculated as follows:

$$x_{cg} = \frac{\sum x_{cg_i} W_i}{\sum W_i} \tag{6.44}$$

To calculate the C.G. at operating empty weight the weights and locations of all the aircraft subsystems, such as the avionics, electric systems and engine, need to be known. The weights follow from the Class II weight estimations and other iterations. The locations are estimated or follow from iterations. Once the C.G. at operating empty weight is determined, the shift over the mission profile can be determined. In the mission the fuel and payload change over time. Therefore the center of gravity location must be calculated for different payload configurations, and fuel mass. For this the worst case scenario approach will be taken. These worst case scenarios will be that the packages are dropped from front to back and back to front, which causes the largest shifts in the C.G. Then, the C.G. location and weight can be plotted in a diagram with on the x-axis the center of gravity location and on the y-axis the weight corresponding to that location. From this graph the minimum and maximum C.G. location can be read.

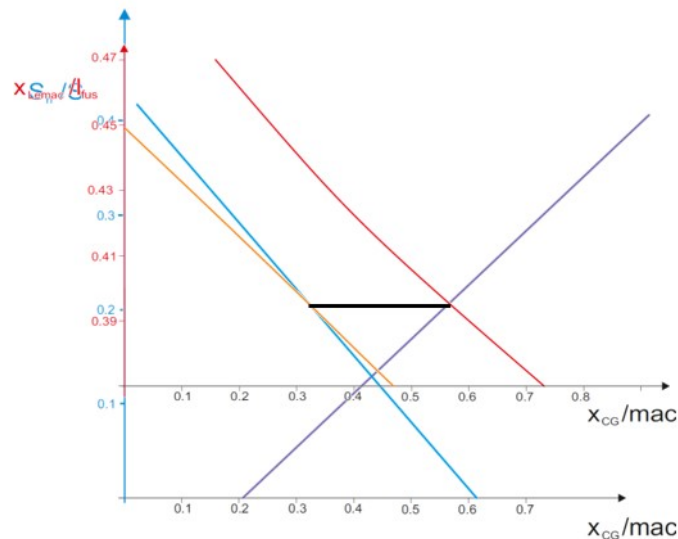### 6.5.4. Combining Scissor Plot and Loading Diagram



**Figure 6.25:** Matching Scissor Plot and Loading diagram [34]

The final step to find the optimal horizontal tail area is to combine the results from the loading diagram and scissor plot. Firstly, the wing position can easily be adjusted to change the C.G. range, which will

be necessary to get the most optimal tail surface area. Therefore the loading diagram will be created for different wing positions, and the C.G. range can be plotted against the wing position. Since the x-axis of this plot and the scissor plot is the same, the graphs can be put on top of each other, and shifted until the tail area is as low as possible, which gives the corresponding wing position. It is important the tail area is as small as possible due to the decrease in weight and drag.

Normally one would combine the two graphs process by hand, however it is desired to automate this, as design iterations occur quite often. Therefore the process is automated with a python script which works as follows. First a set of arrays is obtained from the C.G. range vs. wing position graph. The first two sets of arrays are the minimum and maximum C.G. position and the third array gives the corresponding wing position. The minimum C.G. position is plugged into Equation 6.43, in order to find the smallest possible tail size which keeps the aircraft controllable at this C.G. location. Then, the maximum C.G. position is plugged into Equation 6.41 to find the smallest tail size to ensure stability. Then, the larger of the two values is chosen as the optimal tail size. Note that the smaller of the two tail sizes violates either stability or controllabilty. Finally the wing position corresponding to this tail size can be selected and the sizing method is finished.

### 6.5.5. Code Verification
All the tools presented in this chapter are Python scripts, and therefore they must be verified to ensure the results are reliable.

#### Unit Tests
For the unit tests, both sanity checks and calculations by hand will be performed. The sanity checks are quick unit tests to ensure the output is logical. All the numerical outputs from the python functions will be evaluated and if the result seems off, the code needs to be investigated. The calculations by hand are to ensure the equations are entered correctly. The sanity checks are presented in Table 6.14.

**Table 6.14:** Sanity checks for V&V for stability and control.

| Test description | Pass/fail condition | Pass |
|---|---|---|
| OEW C.G. sanity check | $0 < x_{cg} < l_f$ | Yes |
| Min and max. C.G. sanity check | Min C.G $<$ Max. C.G. | Yes |
| Tail surface area sanity check | Sh/S $<$ 1 | Yes |
| Wing position check | $0 < x_{lemac} < l_f$ | Yes |

Next, the calculations by hand are performed. The result from the hand calculation and from the code are compared, and if the difference is more than a certain margin, the code must be investigated for errors. A margin of 1% will be taken, which is to take into account machine error, and not taking enough decimals in the calculations. The equations that are verified are presented in Table 6.15. The input to the equations are calculated by hand as well and follow from the detailed design.

**Table 6.15:** Verification of equations for stability and control.

| Equation | By hand | By code | Pass |
|---|---|---|---|
| Equation 6.41 C.G. dependent part | 0.97059 | 0.97061 | Yes |
| Equation 6.41 C.G. independent part | 0.1571322 | 0.157136 | Yes |
| Equation 6.43 C.G. dependent part | -1.669959 | -1.669973 | Yes |
| Equation 6.43 C.G. independent part | 0.60689 | 0.52506 | No |
| Equation 6.44 C.G. OEW | 1.1263 | 1.16191 | No |

As can be seen, two equations showed significant differences when calculated by the code and by hand. For the C.G. independent part of the controllability equation, it turned out the $C_{m_{ac}}$ was calculated incorrectly in the code. The flaps contribution was calculated at the quarter chord point instead of at the aerodynamic center, thus this was corrected for in the code. For the CG OEW it turned out the OEW was incorrect. For the sum of the weight the OEW from the Class 1 - Class 2 weight iteration was used, however this value is not the same as the sum of the weights of the subsystems. Therefore, instead of the operating empty weight, the sum of the subsystem weights was used in the calculations.

**System Tests**

For the system tests, the script will be run for different positions of the C.G. at OEW. First, the tail size will be plotted for the C.G. position. This way it can be visualized whether the code as a whole produces the expected result. The expected result is that there is an optimal range for the C.G. location. Furthermore it is expected that the tail size increases rapidly for extreme values as it becomes limited by stability if the C.G. is far aft, or controllability if the C.G. is far forward.
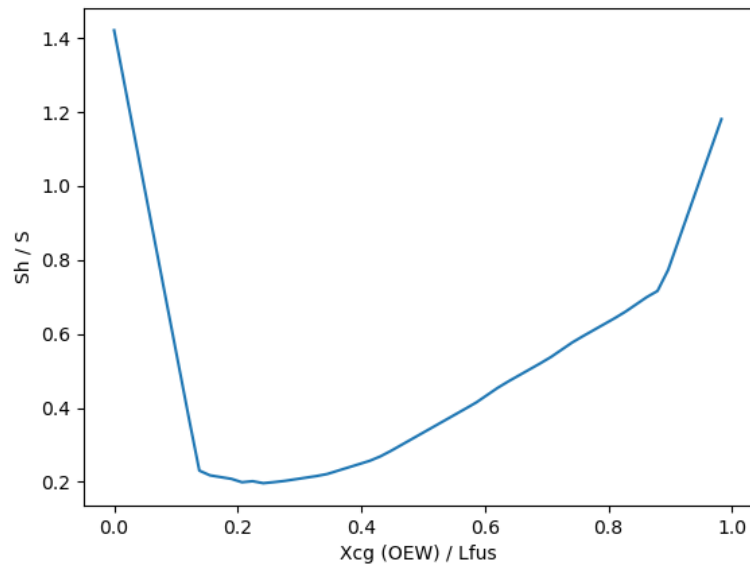


**Figure 6.26:** Plot of tail size against C.G. OEW position

As can be seen, Figure 6.26 follows the expectations. There is an optimum range for the C.G. location between 0.15 and 0.3. At the extreme values of the C.G. location the tail size increases rapidly. The linear increase on the left side is due to controllability, and the linear increase on the right side is due to stability. The part in between these points is not linear, which is because the stability and controllability are alternating limiting.

Next, the scissor plot can be plotted with different C.G. ranges corresponding to the different OEW C.G.'s. This can be done to test whether the C.G. ranges always stay between the stability and controllability bounds, as required.
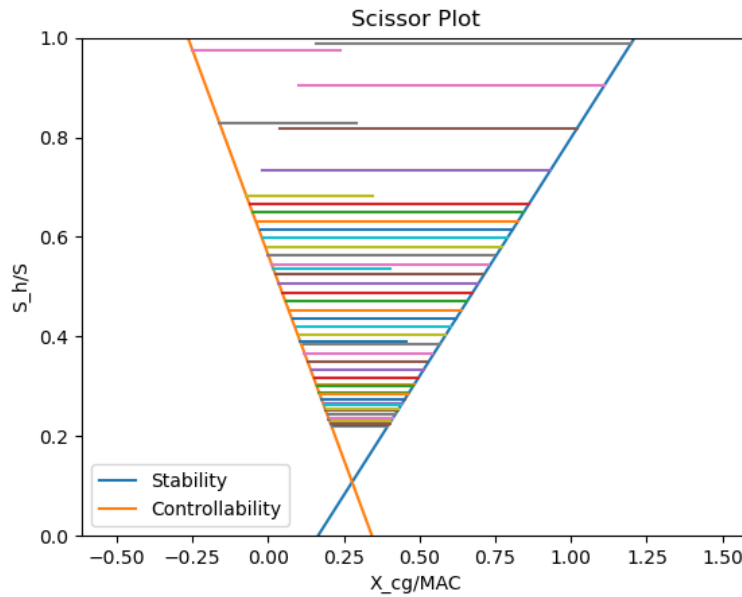
**Figure 6.27:** Different C.G. ranges from OEW C.G. locations plotted on scissor plot

In Figure 6.27 the different coloured lines correspond to the C.G. ranges. As can be seen, all of them fall in the bounds of the stability and controllability line, and therefore this part of the code is verified.

## 6.6. Performance and Propulsion

This section addresses the performance of the primary functions of the design. The aim of this is to demonstrate compliance of a design with the imposed requirements. The assumptions to simplify flight performance analysis are documented below:

- The lift force is equal and in opposite direction to the weight force.
- The thrust force is equal and in opposite direction to the drag force.
- The temperature, pressure and density at varying altitude behaves as modelled by the International Standard Atmosphere model[20].
- The aircraft mass during flight phase varies according to the amount of fuel burnt.
- The aircraft flies under symmetric flight conditions.
- The aircraft drag characteristics can be modelled by a two-term parabolic drag polar, a constant, and a term dependant on the square of the lift coefficient.

### 6.6.1. Equations of Motion

This section discusses the general equations of motion for symmetric flight. To gain a better understanding of the following sections, the reader can refer back to this section to understand the underlying theory behind all calculations. The free body diagram for symmetric flight conditions is illustrated by Figure 6.28.
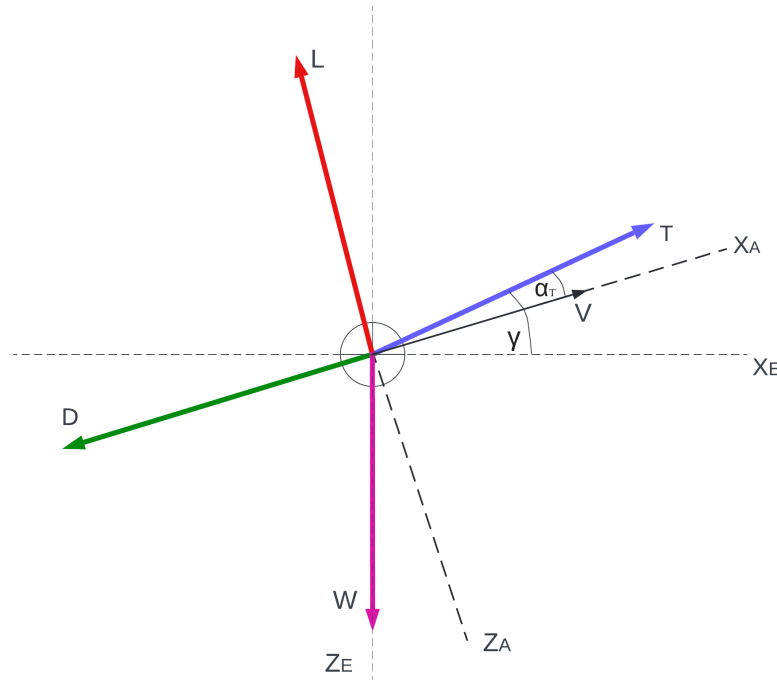
**Figure 6.28:** Symmetric flight free body diagram

The equations for symmetric flight in direction perpendicular and parallel to the airflow are shown by Equation 6.45 and Equation 6.46 respectively. These equations are a relation of the aircraft thrust $T$, drag $D$, lift $L$, weight $W$, flight path angle $\gamma$ and thrust angle $\alpha_T$. The latter is assumed to be negligible at this point in the design, thus $\cos(\alpha_T)$ and $\sin(\alpha_T)$ are approximated to 1 and 0 respectively.

$$\sum F \perp = L - W \cdot \cos(\gamma) + T \cdot \sin(\alpha_T) = 0 \qquad \Rightarrow \qquad L - W \cdot \cos(\gamma) = 0 \qquad (6.45)$$

$$\sum F \parallel = T \cdot \cos(\alpha_T) - W \cdot \sin(\gamma) - D = 0 \qquad \Rightarrow \qquad T - W \cdot \sin(\gamma) - D = 0 \qquad (6.46)$$

The fundamental aerodynamic equations describing the lift and drag are documented below: The equations make use of the aspect ratio $AR$, Oswald efficiency factor $e$, zero-lift drag coefficient $C_{D_0}$, velocity $V$, wing surface area $S$, drag coefficient $C_D$, lift coefficient $C_L$ and atmospheric density $\rho$.

$$k_2 = \frac{1}{\pi \cdot e \cdot AR} \qquad (6.47) \qquad\qquad C_D = C_{D_0} + C_L^2 \cdot k_2 \qquad (6.48)$$

$$D = 0.5 \cdot C_D \cdot \rho \cdot V^2 \cdot S \qquad (6.49) \qquad\qquad L = 0.5 \cdot C_L \cdot \rho \cdot V^2 \cdot S \qquad (6.50)$$

To calculate the power available and break power at a given time Equation 6.51 and Equation 6.52 are used respectively. Where $P_{br}$ and $\eta_{prop}$ are the break power and propeller efficiency respectively.

$$P_{br} \cdot \eta_{prop} = P_a = T \cdot V \qquad (6.51) \qquad\qquad P_r = D \cdot V \qquad (6.52)$$

## 6.6.2. Power and Thrust Functions

To design the the propulsive system, the main emphasis is put on fuel economy. To design for fuel economy two models are used in conjunction. The first model estimates the fuel-flow for a given $P_{br}$ and $RPM$ at which the engine runs. The second estimates the maximum propeller efficiency at a specified flight condition. Then an empirical relation is used to scale the efficiency to all other encountered flight conditions. With the two models and a design propeller efficiency an optimal gear ratio is found and then the model is ready to be used.

**Engine Model**

For the engine model data of the UL260i engine was found to be most elaborate as it provided curves with the relation between hp and fuel flow for a range of rpm values Figure 6.29 [11]. This data was used as a starting point to create a performance map that would be representative of the performance light 4-stroke aviation engines. A second order 2 dimensional least squares regression resulted in Figure 6.30. The function resulting from the regression is shown in Equation 6.53 with the coefficients tabulated in Table 6.16.
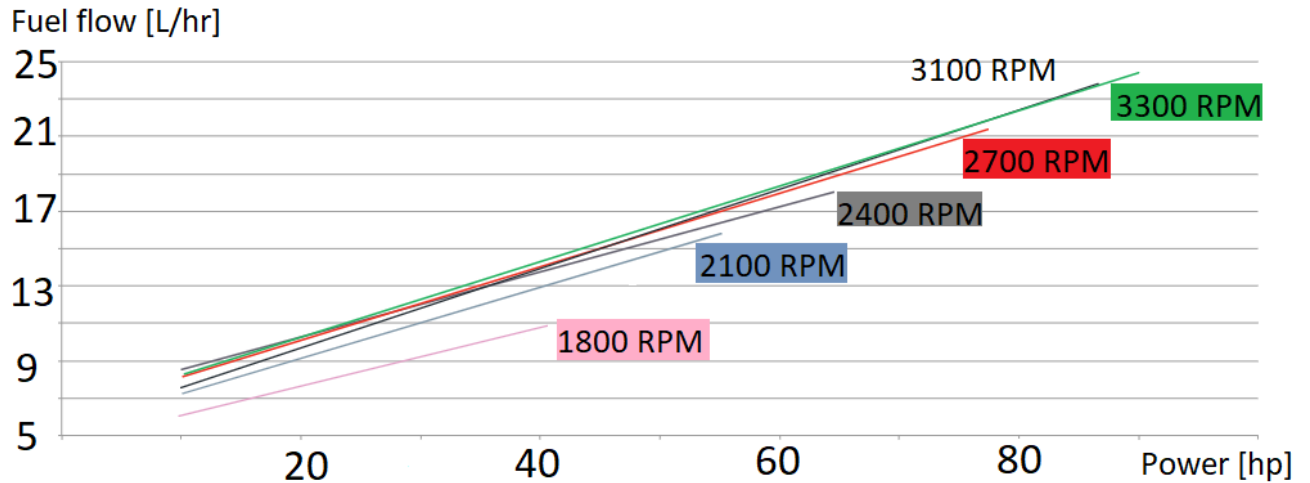


**Figure 6.29:** Fuel flow data UL260i
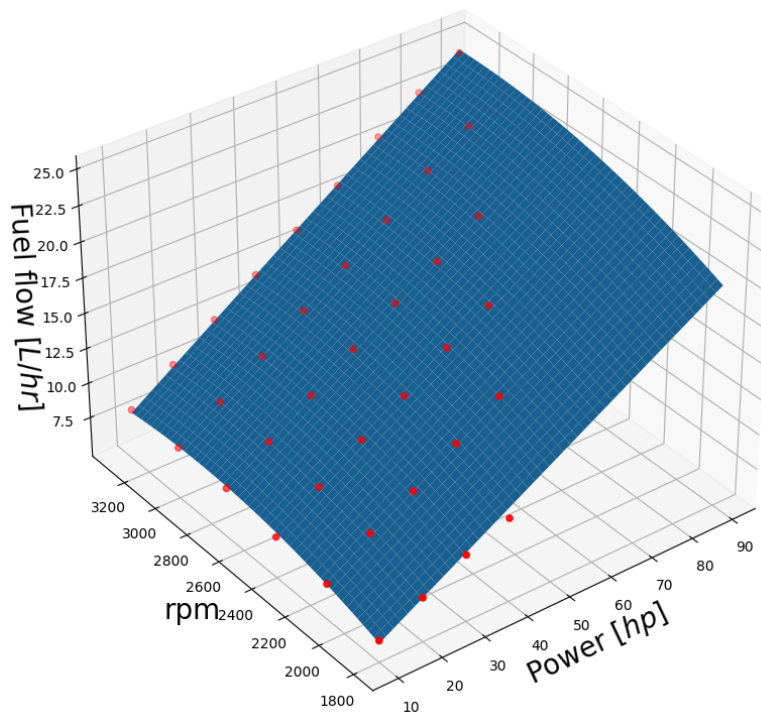


**Figure 6.30:** Performance map regression $R^2$ 0.998

---

[11]https://ulpower.com/en/engines/ul260/ul260i#4-fuel

**Table 6.16:** Coefficients for fuel flow function

| $C_0$ | $C_1$ | $C_2$ | $C_3$ | $C_4$ | $C_5$ |
|---|---|---|---|---|---|
| -9.96594 | 1.469154e-1 | 1.15099e-2 | -1.62514e-05 | -2.02054e-06 | 1.82789e-05 |

$$Fuelflow = C_0 + C_1 \cdot P_{br} + C_2 \cdot RPM + C_3 \cdot P_{br}^2 + C_4 \cdot RPM^2 + C_5 \cdot P_{br} RPM \tag{6.53}$$

**Propeller Model**

The propeller model consists of two parts, first is an estimation for the maximum propeller efficiency and second part corrects for not flying at the design advance ratio. The advance ratio is defined as Equation 6.54 [18, p.624]. The estimate for the maximum propeller efficiency is based upon a relation provided for a generic $1.75\ m$ propeller for a light sport aircraft Equation 6.55 [18, p.638]. The maximum efficiency is found to be $0.858$ at an advance ratio of $0.894$. For the fuel estimation we tweak the rpm of the propeller with a gearing such that we fly at this advance ratio at cruise condition. This gearing is than kept fixed for the simulation.

$$J = \frac{V_\infty}{nD_p} = \frac{60 \cdot V_\infty}{RPM \cdot D_p} \tag{6.54}$$

$$\eta_{prop} = -0.952281 J^2 + 1.703049 J + 0.096574 \tag{6.55}$$

As cost and therefore simplicity are driving in the design, the model assumes a fixed pitch propeller. The problem with a fixed pitch propeller is that you will only fly at your design $\eta_{prop}$ for a single flight condition and $\eta_{prop}$ deteriorates when moving away from that. To correct the propeller efficiency a relation shown on the left of Figure 6.31a [7, p.486] is used. The relation is approximated with a 4th order polynomial resulting in Figure 6.31b. By substituting $\eta_{design}$ and $J_{design}$ in the polynomial a function for $\eta$ in terms of advance ratio can be retrieved.



(a) Fixed pitch efficiency correction



(b) Approximated regression of fixed pitch efficiency
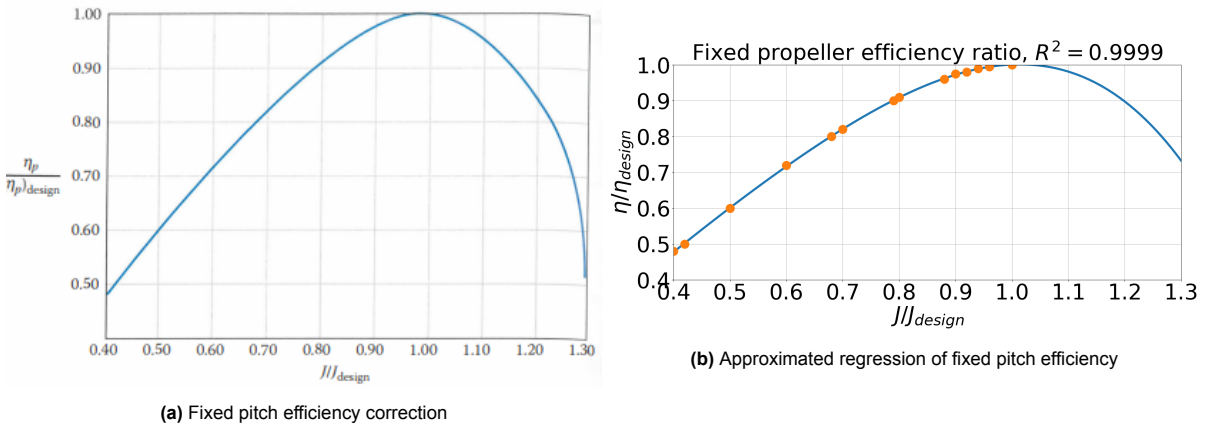
**Figure 6.31:** Correlation to determine propeller efficiency from advance ratio.

**Fuel Optimisation**

The method to optimise for fuel economy is by substitution of $\eta(J) \cdot P_a$ in place of $P_{br}$ in Equation 6.53 and then finding the minimum numerically by using newton's root finding method, Equation 6.56, on the derivative of the fuel flow with respect to $RPM$. Resulting in an optimum $RPM$ and a required $P_{br}$ pair for a given $P_a$ and $V_{TAS}$ which is then used to calculate the fuel flow.

$$RPM_{k+1} = RPM_k - \frac{ff(RPM)'}{ff(RPM)''} \tag{6.56}$$

**Thrust Model**

The Thrust model takes as inputs the velocity and $P_{br}$ and uses both the engine and propeller then optimises for maximum $P_a$, again with the use of Newtons method. Finally the power available is divided by the velocity to obtain the thrust.

Due to Equation 6.51 becoming inaccurate at low velocities, a separate thrust function is created which is only used to calculate the thrust at take-off.

### 6.6.3. Flight Phase Performance

This section discusses all flight phase equations and models used to determine the aircraft performance. The purpose is to estimate the amount of fuel necessary and the time needed to perform one mission. The phases of flight considered are take-off, climb, cruise, descent and landing. For each different phase a sample scenario created to show its capabilities, and all relevant inputs and outputs are tabulated. However only for take-off and landing the corresponding figures are shown, as these are the most interesting. For all other phases is was assumed that the aircraft is in equilibrium and thus all graphs display either constant or linear behaviour with time.

**Take-off Performance**

During take-off the aircraft will not be in force equilibrium as it needs to accelerate from zero velocity to the lift of velocity. After the aircraft is able to lift of it must be able to clear an obstacle with a certain screen height.

Take-off is divided into four different parts as shown in Figure 6.32: The ground roll, rotation, transition and the climb phase. The first two belong to the total ground phase and the last two belong to the airborne phase. The distance covered during ground roll is approximated using a simulation, while the horizontal distance covered during the airborne phase is determined by using analytical equations [22]. During the ground roll the aircraft is accelerated to the lift-off velocity, which is calculated with Equation 6.57. Right before this velocity is reached, the aircraft rotates such that enough lift is produced to take-off. Then the aircraft enters transition phase which is described by a circular motion. Once the optimal climb angle is reached it will climb in a straight line over the screen height.
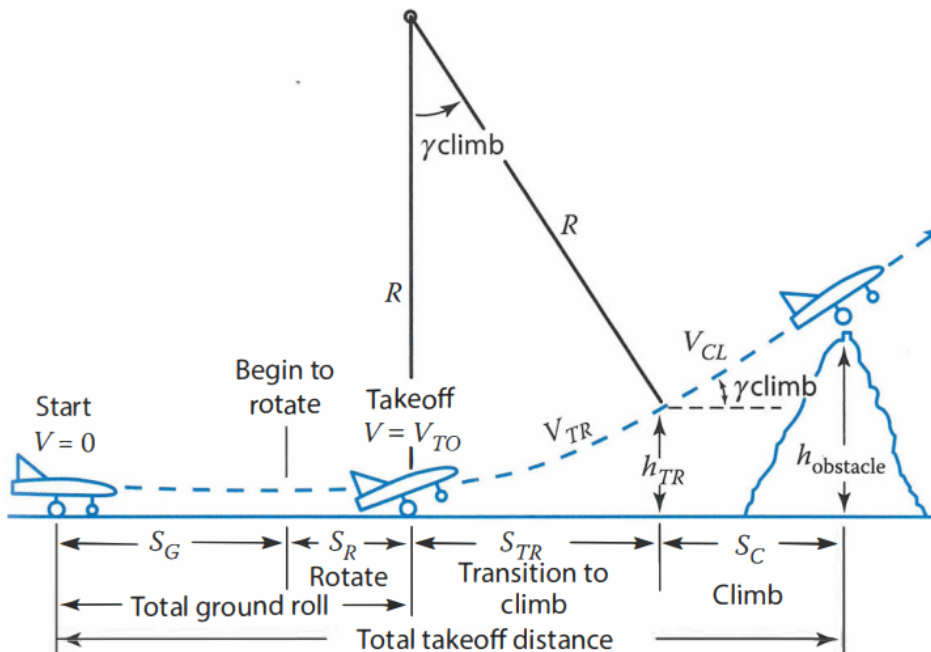


**Figure 6.32:** General take-off procedure [7, p.671]

$$V_{LOF} = \sqrt{\frac{W}{S}\frac{2}{\rho}\frac{1}{CL_{takeoff}}} \qquad (6.57) \qquad\qquad CL_{takeoff} = \frac{CL_{max}}{1.21} \qquad (6.58)$$

The optimal lift coefficient to accelerate with is determined by maximizing Equation 6.59. Furthermore it is assumed that the thrust is independent of $C_L$, such that the optimal value for lift coefficient is found by differentiating $F_{fric} + D$ with respect to $C_L$ and finding the minimum. The friction force is modelled by taking a coefficient dependent on the landing surface and multiplying it with the normal force.

$$F_{res} = T - D - F_{fric} \tag{6.59}$$

This results in the following derivation:

$$F_{fric} + D = C_{fric} \cdot F_{normal} + \tfrac{1}{2} \cdot C_D \cdot \rho \cdot V^2 \cdot S = C_{fric} \cdot (W - \tfrac{1}{2} \cdot C_L \cdot \rho \cdot V^2 \cdot S) + \tfrac{1}{2} \cdot (C_{D_0} + \tfrac{C_L^2}{\pi \cdot AR \cdot e}) \cdot \rho \cdot V^2 \cdot S$$

Differentiating with respect to $C_L$:

$$-C_{fric} \cdot \tfrac{1}{2} \cdot \rho \cdot V^2 \cdot S + \tfrac{2 \cdot C_L}{\pi \cdot AR \cdot e} \cdot \tfrac{1}{2} \cdot \rho \cdot V^2 \cdot S = -C_{fric} + \tfrac{2 \cdot C_L}{\pi \cdot AR \cdot e} = 0$$

Solving for $C_L$:

$$C_L = \frac{C_{fric} \cdot \pi \cdot AR \cdot e}{2} \tag{6.60}$$

Furthermore the aircraft is then accelerated by applying full throttle, thus maximum power. However, Equation 6.51 is inaccurate at very low velocities as the propeller efficiency becomes difficult to approximate. Therefore the ground roll starts at an initial velocity of $2.5 \ m/s$. This will generate some inaccuracy in determining the total ground roll length. This is however insignificant to the total ground roll length and therefore it was decided to continue with this approach.

Once the lift of velocity is reached, the aircraft will enter the airborne phase. The horizontal distance for the transition and climb phase is described by Equation 6.61 and Equation 6.62 respectively [22]. To minimize the horizontal distance covered during the airborne phase, the equations are summed and differentiated with respect to $\gamma$. This results in the optimal climb angle or a specific lift of velocity and load factor. If however the optimal climb angle exceeds the maximum climb angle described in Equation 6.63 [7, p.674], the angle will be set to this value.

$$x_{trans} = \frac{V_{LOF}^2}{n \cdot g} \cdot \sin(\gamma) \tag{6.61} \qquad x_{climb} = \frac{h_{screen} - (1 - \cos(\gamma)) \cdot \frac{V_{LOF}^2}{n \cdot g}}{\tan(\gamma)} \tag{6.62}$$

$$\gamma_{max} = \arcsin \frac{T - D}{W} \tag{6.63}$$

**Climb Performance**

During climb the aircraft must ascend from the screen height to the set cruise altitude. In this climb it is assumed that the aircraft will climb with a constant rate of climb (ROC), while the climb angle $\gamma$ will vary. The velocity is calculated using Equation 6.64, where the lift coefficient at climb $CL_{climb}$ and $\gamma$ are determined by Equation 6.65 and Equation 6.66 respectively. Furthermore the wing surface area $S$ is the only constant value in Equation 6.64, as the weight $W$ decreases with fuel consumed and density $\rho$ decreases with increasing altitude. An arising complication is that the climb angle must be defined before it is calculated. To solve this complication a loop is created that ensures that the climb angle converges to the correct value, with any initial value inputted.

$$V_{climb} = \sqrt{\frac{W \cdot \cos(\gamma)}{S} \frac{2}{\rho} \frac{1}{CL_{climb}}} \tag{6.64}$$

Because the screen height has already been cleared it is not necessary to climb with maximum climb angle. Therefore the lift coefficient is optimized for maximum climb rate which results in Equation 6.65 [27].

$$CL_{climb} = \sqrt{\frac{3 \cdot C_{D_0}}{k_2}} \tag{6.65}$$

From Figure 6.28, the climb angle is easily derived with Equation 6.66. Where ROC is simply the vertical component of the velocity.

$$\gamma = \arcsin\left(\frac{ROC}{V}\right) \tag{6.66}$$

Rewriting Equation 6.46 results in Equation 6.67, the thrust is then multiplied with velocity to calculated the power available, shown in Equation 6.51. This is then used to calculate the mass flow and hereby the fuel consumed. Finally the values for lift, drag, weight and thrust are plugged in Equation 6.45 and Equation 6.46 to verify that the aircraft is indeed in equilibrium. The code is then iterated until the set cruise altitude is reached.

$$T = D + W \cdot \sin(\gamma) \tag{6.67}$$

**Cruise Performance**
During cruise, the aircraft is assumed to be in force equilibrium, and the altitude and attitude is maintained constant. The flight path angle during cruise is assumed to be 0. Thus the equations for force equilibrium can be written as $L = W$ and $T = D$.

It is preferable to travel at the maximum L/D ratio during cruise, as this maximises the cruise range capabilities. According to literature derivations [26], the optimal lift coefficient and drag coefficient can be calculated using Equation 6.68 and Equation 6.69.

$$C_{L_{cruise}} = \sqrt{\frac{C_{D_0}}{k_2}} \tag{6.68} \qquad\qquad C_{D_{cruise}} = 2C_{D_0} \tag{6.69}$$

The flight speed is calculated as a function of decreasing weight using Equation 6.70. This value will decrease in order to maintain altitude and the same $CL_{cruise}$

$$V_{cruise} = \sqrt{\frac{W \cdot \cos(\gamma)}{S} \frac{2}{\rho} \frac{1}{CL_{cruise}}} \tag{6.70}$$

The power available during cruise is equal to the thrust multiplied with the cruise velocity. By definition, this has to be equal to the power required as the thrust equals the drag.

**Descent Performance**
Similar to the climb performance the aircraft has a certain angle, $\gamma$. During descent this is referred to as the descent angle and it is defined as negative due to the convention used. This means that the weight component in Equation 6.46 will contribute to the velocity and thus less thrust is necessary. If the aircraft engine is air-cooled, it is desirable to generate some thrust during descent to avoid large temperature difference cycles. However, the amount of added thrust is a trade-off between a quick descend (minimal thrust), but cruising longer. Or a longer descend and a shorter cruise (higher thrust). Ideally an optimal profile can be determined such that it minimizes the amount of fuel used for the descent procedure, while keeping the engine at the desired temperature. This is however a complex problem that is dependent on the cruise altitude, the target altitude and the fuel consumption during cruise and descent for different thrust levels. It is assumed that the optimal profile will not differ significantly from any other realistic profile in terms fuel and time. Considering the scope of the report and the purpose of the performance calculations it is decided to not optimize this function, but calculate the descent angle with Equation 6.71. Where the target distance is the horizontal distance between the end of cruise and the location where the packages should be dropped. Because all parameters are constant, Equation 6.71 results in a fixed descent angle during the entire descent.

$$\gamma = \arctan\left(\frac{target\ altitude - cruise\ altitude}{target\ distance}\right) \tag{6.71}$$

The lift coefficient is also fixed, by Equation 6.68, as it is chosen to fly at optimum lift over drag. Equation 6.64, Equation 6.67, Equation 6.51 are then used to calculate the remaining forces. Similar to the previous sections the mass flow is calculated by inputting the power available.

**Landing Performance**
Similar during take off, it is assumed that the aircraft is not in equilibrium during landing, but it is decelerating. Furthermore it is divided into three different parts, the approach phase, the flare phase and finally the ground roll. The first two phases are simply described by Equation 6.72, where the radius is calculated using Equation 6.73. To determine the value for $C_{L_{approach}}$, the approach speed is assumed to be 30% higher than the stall speed at maximum lift coefficient. The lift coefficient during approach is then calculated with Equation 6.74. Finally the approach angle is calculated using Equation 6.75 which can be simply derived from Figure 6.28.

$$x_{air} = R \sin{(\gamma_a)} + \frac{h_{scr} - R(1 - \cos{(\gamma_a)})}{\tan{(\gamma_a)}} \quad (6.72) \qquad R = 1.3^2 \cdot \frac{\frac{W}{S} \frac{2}{\rho} \frac{1}{CL_{approach}}}{\Delta n \cdot g} \quad (6.73)$$

$$C_{L_{approach}} = \frac{2 \cdot W}{\rho \cdot S \cdot V_{approach}^2} \quad (6.74) \qquad \gamma_{approach} = \arcsin{\left(\frac{D}{W}\right)} \quad (6.75)$$

The ground roll simulation starts directly after the flare phase and ends when the aircraft is at standstill. It is assumed that the aircraft still flies at $V_{approach}$ and $C_{L_{approach}}$, it however does not touchdown until $C_{L_{max}}$ is reached. Because it is assumed that there is no thrust during the landing phase, the drag will decelerate the aircraft. In turn this increases the lift coefficient by Equation 6.74. When $C_{L_{max}}$ is finally reached, the aircraft will touchdown. To ensure that it does not take-off anymore the lift coefficient is rapidly, but not instantly decreased. The friction force is modelled similarly to the take-off model, by taking a coefficient dependent on the landing surface and multiplying it with the normal force. By decreasing the lift coefficient after touchdown, the lift will decrease as well, which decreases the drag, but will simultaneously increase the friction force.

## 6.6.4. Code Verification
**Unit Tests**
The first step of verification is performing unit tests. These tests are simple and can be performed by inspecting the code or printing a single value of the parameter. It is however crucial that these tests are conducted, as a small error here may lead to a larger error in the final system. For example, during one of the unit tests it was discovered that the unit of a parameter was inputted incorrectly. This resulted in a large, yet feasible take-off distance. This error was found by performing a visual inspection on the units inputted.

**System Tests**
The engine model and propeller models are verified in stages the thing is that the goodness of fit will have to be determined. Secondly both are only possible to be accurate in a bounded domain limited by hardware limitations such as the minimum RPM or physical meaning of the parameter. Lastly the model checked on sensitivity by inputting small deviations and stress tested with extreme value testing. A similar approach is used for each phase of flight. It is verified by creating a sample flight phase and checking if its outputs are as expected. Because take-off and landing are the only phases that are not in force equilibrium certain graphs are displayed as well. For the remaining phases a function is created that breaks the code if the resulting force are above $1~\mu N$. Furthermore extreme value tests are performed as well for the mass flow, thrust and functions for phases of flight to verify the model's response to these values.

***Initial value tests***
Mass flow and thrust
In the engine model the second order polynomial linear least squares regression results in an $R^2$ of 0.998. Although increasing the order of the fit decreases the ability of the $R^2$ parameter to evaluate the goodness of the fit its value is so high and order of the polynomial sufficiently low compared to the amount of data. That the he fit can be accepted. For the propeller model there is no information

given on the quality of the fit from Raymer on the generic propeller efficiency [7] book. Therefore the relation was cross-checked with literature. In two separate annual NACA reports [17] [4] similar magnitude maximum propeller efficiencies for a propeller with a Clark-y airfoil are presented. Figure B.2 Figure B.3. The propeller efficiency correction has a really high $R^2$. Te regression is only limited on the interval $0.4 < J/J_{design} < 1.1$ as it is not proven to be accurate outside the domain.

$$R^2 = 1 - \frac{SSR}{SST} = 1 - \frac{\sum_{i=1}^{n} \left(Y_i - \widehat{Y_i}\right)^2}{\sum_{i=1}^{n} \left(Y_i - \overline{\mathbf{Y}}\right)^2} \tag{6.76}$$

The mass flow function needs as input velocity, power available, gear ratio as shown in Table 6.17a. The power available value is chosen to be start cruise the condition for which the propeller is optimised. The propeller efficiency will therefore be the max efficiency of 0.86. . The fuel efficiency is therefore

**Table 6.17:** Inputs and outputs for mass flow function

**(a)** Inputs for mass flow function

| Parameter | Value | Units |
|---|---|---|
| Velocity | 34 | $m/s$ |
| Power available | 16.8 | $kW$ |
| Gear ratio | 1.98 | – |

**(b)** Outputs of mass flow function

| Output parameter | Value | Units |
|---|---|---|
| Fuel flow | 10.1 | $L/hr$ |
| Mass flow | 7.46 | $kg/hr$ |

To sample the thrust function the same input is used as for take-off. However instead of plotting the thrust against time as on the bottom right of Figure 6.35 the thrust is plotted against airspeed in Figure 6.34. To verify that the thrust is modelled correctly it is compared to Figure 6.33. Because thrust is modelled under different conditions and the units on the axis are different only the shape between the two curves can be compared. Both figures show an increase in thrust when increasing the airspeed, until a certain maximum thrust is reached. If a larger range for airspeed is taken, the curve in Figure 6.34 would also decrease to zero like Figure 6.33 does.

In subsection 6.6.3 it was stated that the ground roll starts at $2.5\ m/s$ due to the thrust function being very inaccurate at low velocities. By making this assumption the distance travelled from $0$ to $2.5\ m/s$ is essentially ignored. To make this assumption it must be verified that that distance is not significant to the overall take-off distance. To calculate the distance a new model is used which assumes the thrust is constant from $0$ to $2.5\ m/s$ and is calculated with Equation 6.77 [18, p.639].

$$T_{static} = K_p \cdot P_{br}^{2/3} \cdot (2 \cdot \rho \cdot A_p)^{1/3} \cdot (1 - \frac{A_p}{A_{spin}}) \tag{6.77}$$

Where $K_P$ is a correction factor that is assumed to be 0.65 [18, p.639] and $A_p$ and $A_{spin}$ are the area of the propeller and spinner respectively. The area of the spinner is assumed to be a value of 0.3 $m$. Using the break power of $90\ hp$ results in a ground roll distance of $2.1\ m$ from $0$ to $2.5\ m/s$. This is less then 1% of the total distance and is thus deemed insignificant.
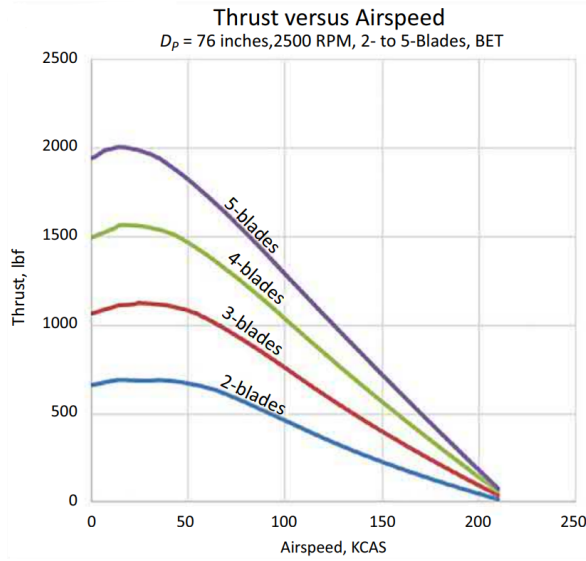
**Figure 6.33:** Thrust against airspeed from [18, p.628]



**Figure 6.34:** Thrust against airspeed from sample code

Take-off

The inputs for the model are shown in Table 6.18a and the model outputs in Table 6.18b. The results are also shown graphically in Figure 6.35. Because the lift coefficient is kept constant until the 10 second mark, the lift, drag and friction force are all quadratic equations and only dependent on the velocity. The initial value for the velocity is $2.5\ m/s$, as mentioned before, and increases slowly at first due the low thrust. Around the 3 second mark the thrust becomes relatively constant, which causes the velocity to increase more or less linearly until the rotation phase. This phase starts at about the 10 second mark, where the lift coefficient is rapidly increased and then kept constant at the value where the normal force will be zero at lift off velocity. The increase in lift coefficient can also been seen in the lift, drag and friction forces. Where at first, a steep increase or decrease is seen, after which it becomes more shallow due to the constant lift coefficient, but still increasing speed. Finally the time and horizontal distance correspond to the values tabulated in Table 6.18b.

**Table 6.18:** Inputs and outputs for take-off performance

**(a)** Inputs for take-off performance

| Parameter | Value | Units |
|---|---|---|
| Mass | 548 | $kg$ |
| $C_{L_{max}}$ | 1.9 | — |
| $C_{D_0}$ | 0.034 | — |
| Wing surface area | 12.35 | $m^2$ |
| e | 0.78 | — |
| AR | 9 | — |
| Propeller diameter | 1.5 | $m$ |
| Take-off altitude | 0 | $m$ |
| Surface coefficient | 0.08 [7, p.672] | — |
| Load factor | 1.15 [22] | — |
| Screen height | 15 | $m$ |
| Time step | 0.01 | $s$ |

**(b)** Outputs of take-off performance

| Output parameter | Value | Units |
|---|---|---|
| Lift off velocity | 26.1 | $m/s$ |
| Ground roll distance | 145 | $m$ |
| Total ground roll time | 11.1 | $s$ |
| Airborne distance | 117 | $m$ |
| Total horizontal distance | 262 | $m$ |

**Figure 6.35:** Take-off performance of the ground roll for the sample script

Climb

The climb model uses the input parameters shown in Table 6.19a and outputs the parameters shown in Table 6.19b.  Because the climb performance is in force equilibrium and the climb rate is fixed, all the graphs are either constant or close to linear and thus not interesting to show.  From a visual inspection it is noticed that the velocity increases slightly.  In Equation 6.64 three parameters change during climb, this includes density, weight and climb angle.  The first two are a function of altitude and power available respectively, while the latter is a function of velocity. If the velocity increases after the first time step, the angle will decrease by Equation 6.66, and vice versa.  For the velocity to then increase the density should decrease relatively more than the weight does.  This is verified by calculating the percentage difference of these two parameters between the first and second time step by hand.  The density decreases by about 0.08 % and the weight by 0.0007 %, this is a difference of two orders of magnitude.  Therefore it is logical that the velocity slightly increases over time.  Furthermore the height plotted against time is a perfect linear line, because the climb rate is constant. This is verified by multiplying the climb rate with the climb time and adding the screen height, which results in $498\ m$. After this value the loop is broken as the height becomes higher than the cruise altitude. Finally the horizontal distance plotted against time seemed linear, which should not be the case as the horizontal velocity is not constant.  However after further inspection it became clear that the gradient slightly increases further in time, this is logical as the velocity also increases with time.

**Table 6.19:** Inputs and outputs for the climb performance sample

**(a)** Inputs for the climb performance sample

| Parameter | Value | Units |
|---|---|---|
| Initial mass | 748 | $kg$ |
| Cruise altitude | 500 | $m$ |
| Initial fuel weight | 100 | $kg$ |
| Propeller diameter | 1.5 | $m$ |
| $C_{D_0}$ | 0.034 | – |
| Wing surface area | 12.35 | $m^2$ |
| e | 0.78 | – |
| AR | 9 | – |
| Rate of climb | 2.1 | $m/s$ |
| Screen height | 15 | $m$ |
| Time step | 1 | $s$ |

**(b)** Outputs of the climb performance sample

| Output parameter | Value | Units |
|---|---|---|
| Fuel consumed | 1.1 | $kg$ |
| Time to climb | 230 | $s$ |
| Horizontal distance covered | 5.89 | $km$ |

Cruise

This sample cruise performance uses the input parameters as described by Table 6.20a and outputs the parameters in Table 6.20b.

**Table 6.20:** Inputs and outputs for the cruise performance sample

**(a)** Inputs for the cruise performance sample

| Parameter | Value | Units |
|---|---|---|
| Initial mass | 748 | $kg$ |
| Cruise altitude | 500 | $m$ |
| Initial fuel weight | 100 | $kg$ |
| Propeller diameter | 1.5 | $m$ |
| $C_{D_0}$ | 0.034 | – |
| Wing surface area | 12.35 | $m^2$ |
| e | 0.78 | – |
| AR | 9 | – |
| Cruise distance | 50 | $km$ |
| Time step | 5 | $s$ |

**(b)** Outputs of the cruise performance sample

| Output parameter | Value | Units |
|---|---|---|
| Fuel consumed | 4.3 | $kg$ |
| Cruise time | 24.42 | $min$ |

A back-of-the-envelope calculation determines that the average fuel consumption for this sample cruise mission is around $14.27\ L/h$, which is reasonable considering the engine was chosen such that cruise performance efficiency is maximised. Compared to the Rotax 912 which has an approximate fuel consumption of $16\ L/hr$ at 75% power [35].

Descent

Another sample script is tested for descent by inputting the parameters in Table 6.21a which outputs the parameters shown in Table 6.21b. Similar to climb and cruise the descent is assumed to be in equilibrium. However this time the descent angle is set to a fixed value as described in Equation 6.6.3. In contrast to climb, the density will now increase instead of decrease, which results in a decreasing velocity and descent rate. This means that the horizontal distance covered against time should be perfectly linear and the height against time should have a small changing slope. This is verified by computing the gradient at certain points on the graphs and comparing it with the others. And indeed the horizontal distance against time had constant value for the gradient, while the height against time varied.

**Table 6.21:** Inputs and outputs for the descent performance sample

**(a)** Inputs for the descent performance sample

| Parameter | Value | Units |
|---|---|---|
| Initial mass | 748 | $kg$ |
| Cruise altitude | 500 | $m$ |
| Initial fuel weight | 100 | $kg$ |
| Propeller diameter | 1.5 | $m$ |
| $C_{D_0}$ | 0.034 | – |
| Wing surface area | 12.35 | $m^2$ |
| e | 0.78 | – |
| AR | 9 | – |
| Target altitude | 100 | $m$ |
| Target distance | 10 | $km$ |
| Time step | 1 | $s$ |

**(b)** Outputs of the descent performance sample

| Output parameter | Value | Units |
|---|---|---|
| Fuel consumed | 0.52 | $kg$ |
| Time to descend | 294 | $s$ |

Landing

The inputs for the model are tabulated in Table 9.11a and it outputs the values shown in Table 9.11b. In the sample script the landing surface was assumed to be firm dirt while having already dropped the $200\ kg$ of payload.

**Table 6.22:** Inputs and outputs for landing performance

**(a)** Inputs for landing performance

| Parameter | Value | Units |
|---|---|---|
| Mass | 548 | $kg$ |
| $CL_{max}$ | 1.9 | – |
| $C_{D_0}$ | 0.034 | – |
| Wing surface area | 12.35 | $m^2$ |
| e | 0.78 | – |
| AR | 9 | – |
| Landing altitude | 0 | $m$ |
| Surface coefficient | 0.3 [7, p.672] | – |
| Load factor | 1.15 [22] | – |
| Screen height | 15 | $m$ |
| Time step | 0.01 | $s$ |

**(b)** Outputs of landing performance

| Output parameter | Value | Units |
|---|---|---|
| Airborne distance | 213 | $m$ |
| Ground roll distance | 226 | $m$ |
| Total ground roll time | 14 | $s$ |
| Total horizontal distance | 440 | $m$ |

The corresponding graphs for the landing performance are shown in Figure 6.36. The total horizontal force is the sum of the drag and the friction force. The performance can be separated into two different parts, the first part is before touchdown, which happens around the 7 second mark, the second part is after touchdown until standstill. The rapid decease in lift coefficient is clearly seen in the lift as well as the drag graphs. A result of the decrease is that the normal force increases as well, which increases the friction force. This will mainly characterize the total horizontal force after touchdown, while the drag full characterizes it before touchdown. Another advantage of decreasing the lift coefficient at touchdown, next to the certainty of the aircraft not being able to take-off anymore, is that the friction force has a large magnitude than the drag. Thus the aircraft will decelerate quicker and will need a shorter distance to come to a standstill.
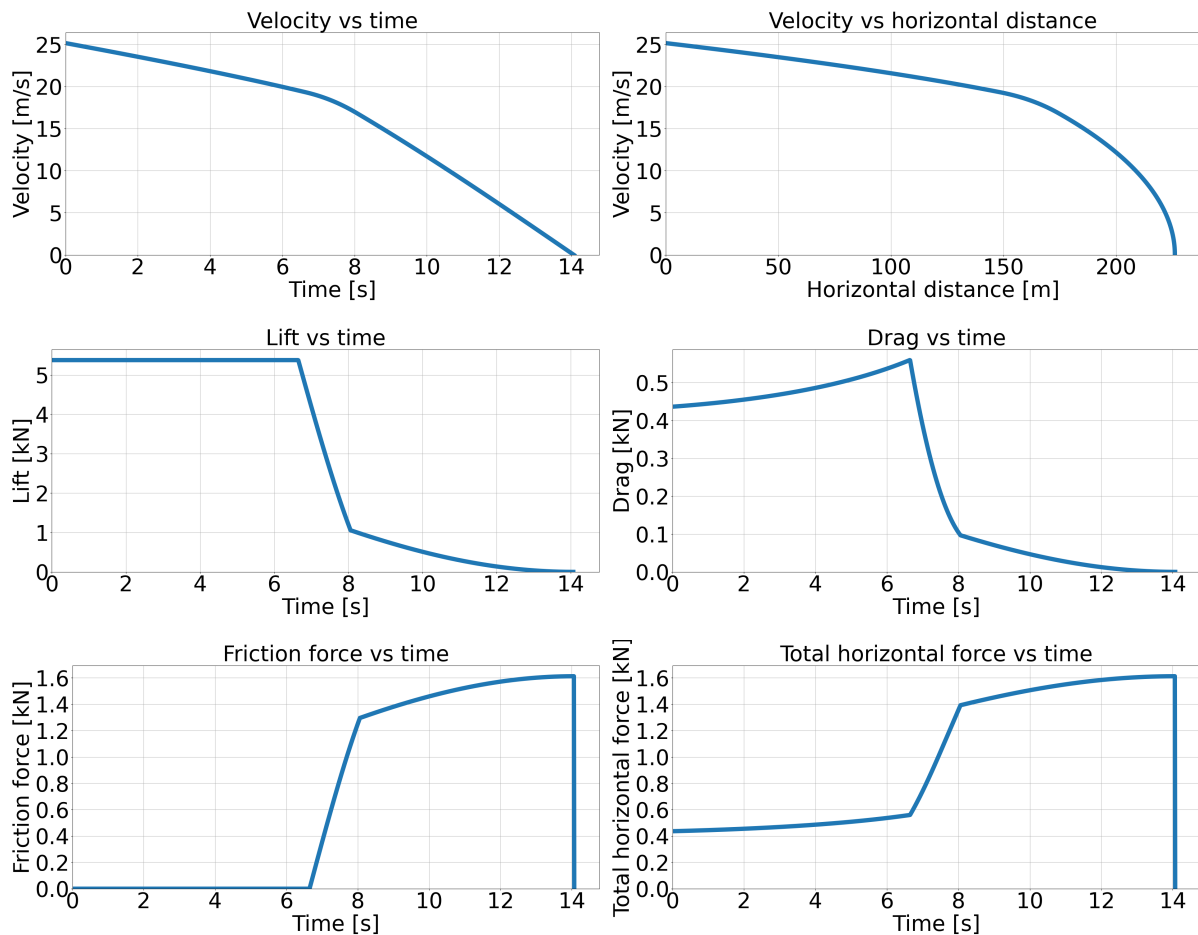
**Figure 6.36:** Landing performance for the sample script

### Extreme value tests

For the extreme value tests each parameter used for the initial value test is multiplied or divided by 100. This will result in nonsensical values for some inputs, for example the Oswald efficiency factor will increase from 0.78 to 78, while the theoretical maximum is 1. If the output is then nonsensical or results in an error corresponding to the input, the test is given a pass.

Other parameters such as the surface area may increase to unreasonable values for the design, a pass is then given if the output is unreasonable as well or a corresponding error is showed.

Very few parameters may still have reasonable values after applying the multiplication, such as the screen height, which decreases from $15\ m$ to $0.15\ m$. Because of the small absolute change the output may not change considerably. If even a small, but reasonable change is detected the test is given a pass as well.

A fail is given if no change is detected in the outputs or the change does not logically follow from the extreme input. An example of a non logical change would be if the velocity decreases while the weight has significantly increased, and the density, surface area and lift coefficient stay relatively constant.

Massflow and thrust

In Table 6.23 all inputs have passed the test and thus both functions are verified for the extreme values.

**Table 6.23:** Extreme values test results for the massflow and thrust.

| | Velocity | | Design velocity | | Propeller diameter | | Power available | | Max power | | Efficiency guess | |
|---|---|---|---|---|---|---|---|---|---|---|---|---|
| Extreme values [%] | 1000 | 0.001 | 1000 | 0.001 | 1000 | 0.001 | 1000 | 0.001 | 1000 | 0.001 | 1000 | 0.001 |
| Massflow | Pass | Pass | Pass | Pass | Pass | Pass | Pass | Pass | - | - | - | - |
| Thrust | Pass | Pass | - | - | - | - | - | - | Pass | Pass | Pass | Pass |

**Phases of flight**

In Table 6.24 the only failed test is the minimal value for the climb angle in the climb code. The fail result is given because no change could be detected in the code output. After inspecting the code the reason was found to be because of the iteration loop created, as stated in Equation 6.6.3, to solve the initial value problem. The fail then confirms that the loop is indeed implemented correctly and the code is still deemed correct.

**Table 6.24:** Extreme values test results for the phases of flight

| Parameter | Extreme value [%] | Take-off | Climb | Cruise | Descent | Landing |
|---|---|---|---|---|---|---|
| MTOW | 1000 | Pass | Pass | Pass | Pass | Pass |
| | 0.001 | Pass | Pass | Pass | Pass | Pass |
| Fuel weight | 1000 | - | Pass | Pass | Pass | - |
| | 0.001 | - | Pass | Pass | Pass | - |
| Surface area | 1000 | Pass | Pass | Pass | Pass | Pass |
| | 0.001 | Pass | Pass | Pass | Pass | Pass |
| $C_{D_0}$ | 1000 | Pass | Pass | Pass | Pass | Pass |
| | 0.001 | Pass | Pass | Pass | Pass | Pass |
| e | 1000 | Pass | Pass | Pass | Pass | Pass |
| | 0.001 | Pass | Pass | Pass | Pass | Pass |
| AR | 1000 | Pass | Pass | Pass | Pass | Pass |
| | 0.001 | Pass | Pass | Pass | Pass | Pass |
| Screen height | 1000 | Pass | Pass | - | - | Pass |
| | 0.001 | Pass | Pass | - | - | Pass |
| Take-off altitude | 1000 | Pass | - | - | - | Pass |
| | 0.001 | Pass | - | - | - | Pass |
| Load factor | 1000 | Pass | - | - | - | Pass |
| | 0.001 | Pass | - | - | - | Pass |
| CL max | 1000 | Pass | - | - | - | Pass |
| | 0.001 | Pass | - | - | - | Pass |
| Climb rate | 1000 | - | Pass | - | - | - |
| | 0.001 | - | Pass | - | - | - |
| Climb angle | 1000 | - | Pass | - | - | - |
| | 0.001 | - | Fail | - | - | - |
| Cruise altitude | 1000 | - | Pass | Pass | Pass | - |
| | 0.001 | - | Pass | Pass | Pass | - |
| Drop altitude | 1000 | - | - | - | Pass | - |
| | 0.001 | - | - | - | Pass | - |
| Target altitude | 1000 | - | - | - | Pass | - |
| | 0.001 | - | - | - | Pass | - |

In this chapter the design of the aircraft will be discussed in detail. Various subsystems are designed and presented in this chapter. Each section analyses each subsystems in multiple disciplines. First the fuselage will be designed by sizing for the payload and constructing for the structural loads. Next the wing is designed by first performing an aerodynamic analysis after which the modularity and structure of the wing are determined. With the wing and fuselage designed the empennage can be sized. Both the vertical and horizontal stabilizer are shaped and the modularity of these stabilizers is analysed. Next to that the stability of the aircraft was also analysed. Next the undercarriage is design. It is sized and positioned on the aircraft. After this the propulsion system is designed. The engine is selected and the propeller is sized. This is followed by the performance analysis of the aircraft. Software and hardware on the aircraft are than sized and a hardware block diagram is created. The electrical system and data handling are than discussed. Finally the final design is summarised with all key design specifications.

## 7.1. Fuselage Design

To design the fuselage various elements and disciplines have to be considered. First the fuselage is shaped to contain the payload. This will be done using the inside out approach. This is than followed up with the structural design of the fuselage. First the goal of the design is established after which the design requirements are presented.

### 7.1.1. Conceptional Fuselage Design

When designing the fuselage of an aircraft, an inside-out approach is adopted. This means that the fuselage is designed to precisely fit the payload and give it an aerodynamic shape. Depending on the layout of the boxes, two distinct fuselage shape were considered.

- **2-3-3-2:** This option increases the frontal area, but reduces the CG range
- **2-2-2-2-2:** Here the fuselage is more slender, but the CG range is larger

With more boxes are positioned closer together, as in option 1, the center of gravity range stays smaller. This means that the horizontal tail volume of the aircraft can remain smaller, so the horizontal tail can be positioned further forward or be sized smaller. Choosing this option than allows for a fixed horizontal tail which does not need to be detached or not completely. The modularity originates from a driving requirement being that the airplane fits inside a $20$ ft container. If the slender design is chosen a bigger horizontal tail is needed and is thus has to be detachable completely or at least more than the wider design as shown in Figure 7.1.
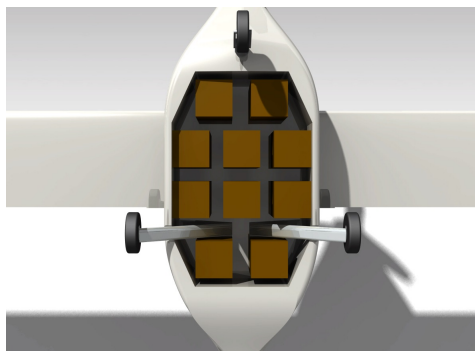


**Figure 7.1:** Cargo configuration of the aircraft

Since a driving requirement is being able to fit inside a $20$ ft container, and the slender fuselage requires a bigger horizontal stabilizer, the wider design was chosen.

Next to box layout the cross-section of the fuselage also has to be determined. For this purpose 4 cross- sections were created. These are displayed in Figure 7.2. Note that they are all made up from simple geometries, corners with constant radii and straight lines. This is done to limit the effort during manufacturing.
A trade-off was performed to find the best fuselage cross-section. Five different criteria were defined.

(a) Design 1



(b) Design 2
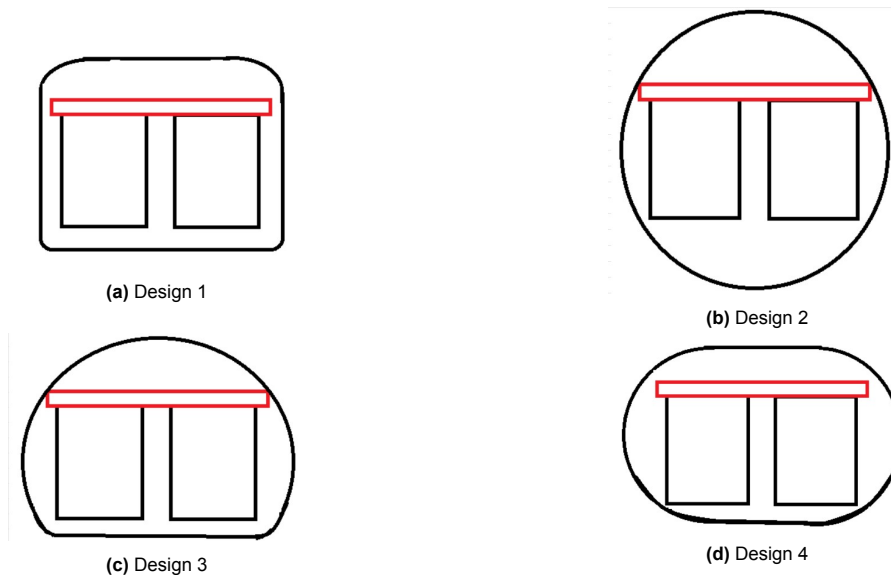


(c) Design 3



(d) Design 4

**Figure 7.2:** Fuselage cross-section options

1. **Wetted area: weight 2**, the zero lift drag is depended on the wetted area of the aircraft. With a CAD model the wetted area of the various design options can be compared. Less area is better, but size drag is depended on more than just the area the weight of this criterion is 2.
2. **Manufacturability: weight 4**, the easier shapes are, the easier they are to make. Straight part can be made of simple sheets. Simple bends can be created simply as well, but it takes more work. Manufacturability is important to keep the aircraft cheap so a weight of 4 is assigned.
3. **Unused volume: weight 1**, the fuselage may also have more volume than is required to store the payload. This unused volume can limit the aircraft from fitting in the container. Since this is more limited by the lengths of the fuselage and the wings, a weight of 1 is assigned.
4. **Aerodynamic shape: weight 4**, next to the wetted area the shape can influence the drag of the fuselage. Square edges can cause flow separation and cause high drag. The weight was therefore considered high and given as 4.
5. **Dropping characteristics: weight 4**, the boxes will be dropped through the bottom of the fuselage. If a lot of volume and edges are below the boxes, the box may get stuck while falling through the airplane. This must be avoided and thus the weight of the criterion is 4.

For each criterion and each design a value was assigned. This resulted in the following point totals in Table 7.1

**Table 7.1:** Final trade-off table for fuselage cross-section

| Concept | Wetted area | Manufacturability | Unused volume | Aerodynamic shape | Dropping characteristics | Score |
|---------|-------------|-------------------|---------------|-------------------|--------------------------|-------|
| Design 1 | 4 | 4 | 5 | 3 | 4 | 57 |
| Design 2 | 3 | 3 | 3 | 5 | 2 | 49 |
| Design 3 | 4 | 3 | 4 | 4 | 4 | 56 |
| Design 4 | 2 | 4 | 4 | 4 | 4 | 56 |

| Poor (1) R | Bad (2) O | Satisfactory (3) Y | Good (4) LG | Excellent (5) G |
|------------|-----------|--------------------|-------------|-----------------|

Even though the difference is small, design option 1 has the biggest score. Since it performs well in many categories. Design 3 is also very good in may categories, but it has a large, round profile which has to be attached to a flat edge. The disadvantage of design 1, that it has relatively square edges,

is less of an issue on low speeds, while the disadvantage of design 3 is more difficult to solve during manufacturing. Therefore it was decided to chose design 1.

## 7.1.2. Structural Fuselage Design

Design of the structure of fuselage is split into two parts at this stage of design: design load carrying part of the fuselage and choose a material for the non load carrying part of the fuselage. Notably, the design of the fuselage at this point is very simplified and is used to find what are the limiting factors for the design, what are the design options and considerations.

**Fuselage Load Carrying Part**

Due to the fact that all considered fuselage designs employ a package dropping mechanism through opening doors at the bottom of the aircraft, it can be assumed that the bottom of the main part of the fuselage is not load carrying. As a consequence, it was decided to design the structural part of the fuselage as a beam-like structure extended through the upper part of the cross-section of the aircraft from the nose to the tail. To find a suitable model of the cross section one must consider the applied types of loads and their magnitudes as well as the load paths.

Normally a fuselage cross-section would be a rectangular or circular section as it provides an easy to manufacture solution with good torsional and bending properties. In contrast to conventional aircraft, this aircraft requires an opening at the bottom of the aircraft in order to be able to drop the packages and openable side sides of the fuselage such that the packages can be conveniently loaded. In order for the aircraft to retain acceptable structural properties these cut-outs have to be addressed. There are two solutions that were considered. Firstly, use load carrying openable doors that effectively negates the effect of the cut-outs. This solution was deemed too complicated and inconsistent. Secondly, the structure has to be built around the holes. The way this could be achieved is shown in Figure 7.3 and Figure 7.4 with the first figure showing a thin sheet structural concept and the second figure demonstrating truss structure design concept. The figures provide a closed cross-section for the parts of the aircraft where there are no openings at the bottom and sides, an open cross-section for the sections with an opening at the bottom and sides, and a side view. Key feature in both designs is the use of a "spine" extending from the front to the back on the upper part of the aircraft. The spine is essentially a closed thin plate structure providing torsional performance. The rest of the structure is there to provide bending performance and connect other key components such as the engine and landing gear.



**Figure 7.3:** Structural concept of the fuselage with load carrying skin



**Figure 7.4:** Structural concept of the fuselage with load carrying truss structure

Additionally, preliminary stress and deflection calculations were performed for the design. The bending stresses and and deflection was evaluated using methodology described in subsection 6.4.3. The calculations assumed constant thickness thin plate structure employing cross-section from Figure 7.3 and overall fuselage shape from Figure A.3. Maximum allowable stress was set to the yield stress of the chosen material Aluminium (subsection 6.4.1) and maximum deflections was chosen arbitrarily to be $5\ cm$. Similarly, torsional analysis was performed with maximum allowable Aluminium shear stress (subsection 6.4.1) and maximum allowable deformation of $1°$. The resulting design is described in

Table 7.2. Despite the values being unrealistic for practical purposes, this is used to give an indication of what are the limiting factors in fuselage design and what is the approximate weight of the fuselage structure.

**Table 7.2**

| Analysis type | Minimum thickness | Unit |
|---|---|---|
| Bending yield limit | $0.4$ | $mm$ |
| Bending deflection limit | $13.3$ | $mm$ |
| Torsion yield limit | $9.5 \cdot 10^{-4}$ | $mm$ |
| Torsion deformation limit | $8.9 \cdot 10^{-2}$ | $mm$ |

**Fuselage Cowling Material Choice**
For non-load-carrying parts of the fuselage that only provide aerodynamic shape, a cheaper and lighter material can be considered. Glass fibre reinforced plastics (GFRP) fit this description very well. To simplify manufacturing, the material can consist of short fibres in resin.

## 7.2. Main Wing Design

The design of an aircraft main wing involves not only aerodynamics and structures, but also requires adequate investigation of the integration and effects on other subsystems. This section will display the final design of the wing planform, modular systems and wing box. The aerodynamics and planform of the wing are used as a constraint and input in the design of the structures. The design of the wingbox involves making decisions relating to spars, skin thickness, ribs, stringers, and material choice. In order to make design choices relating to each of these components, an estimation has to be made regarding the loads that act on the wing. This is done by creating shear and bending load diagrams across the half span of the wing. From there, design iterations can be made to select an optimal wingbox design such that the stresses induced by the loads are carried while minimising weight. In addition, the buckling performance of the wingbox design will be analysed to ensure that the wingbox will not buckle when subjected to the expected stresses.

### 7.2.1. Airfoil Selection

After completing the detailed analysis in XFLR5 on both a two dimensional airfoil and three dimensional wing, the NACA 2415 airfoil was selected. The airfoil characteristics at cruise performance are tabulated in Table 7.5

**Table 7.3:** NACA 2415 Airfoil Characteristics at Criuise Conditions

| Airfoil | $C_{l_{max}}[-]$ | $C_{l_0}[-]$ | $C_{m_{cruise}}[-]$ | $\alpha_{stall}[°]$ | $\frac{C_l}{C_d}_{cruise}[-]$ |
|---|---|---|---|---|---|
| $NACA\ 2415$ | 1.78 | 0.4 | -0.05 | 17 | 80 |

### 7.2.2. Planform Geometry

The planform geometry is defined using the wing area generated from the mission design point. Furthermore the Aspect ratio defines the wing span and root chord. The maximum dimensions of the wing are constrained by the dimensions of a $20\ ft$. Finally The rest of the parameters were defined based on the aerodynamic analysis performed in section 6.2.

**Table 7.4:** Wing Planform Geometry

| Parameter | Symbol | Value | Unit |
|---|---|---|---|
| Wing Area | $S$ | 11.43 | $[m]$ |
| Wing Span | $b$ | 10.14 | $[m]$ |
| Root Chord | $C_r$ | 1.13 | $[m]$ |
| Taper Ratio | $\lambda$ | 1 | $[-]$ |
| Quarter Chord Sweep | $\Lambda_{1/4}$ | 0 | $[°]$ |
| Max Thickness to Chord Ratio | $t/c_{max}$ | 0.15 | $[-]$ |
| Aspect Ratio | AR | 9 | $[-]$ |

An elliptical lift distribution is the most optimum when analysing the induced drag of the wing. In order to achieve an elliptical lift distribution, the wing planform must be shaped in such a way that this is met. An example of this design is the spitfire from World War II. However this required an oval shape wing, which is typically hard to produce and requires thorough quality assurance. In order to still achieve this lift distribution, a taper ratio can be applied to the wing. A taper ratio of 0.4-0.5 will yield an almost perfectly elliptical lift distribution. Moreover, this presents additional challenges with regards to manufacturing as a fully tapered wing requires the manufacture of different ribs along each section of the span. Therefore a compromise was investigated between a wing with a taper ratio of 0 and a wing that has taper 60% along the span of the wing. This taper was set to a value of 0.45.

After conducting 3D wing analysis in XFLR 5 the change in lift to drag ratio was calculated. The addition of taper at the wind tips only amounts to an increase in efficiency of 4.2% in lift to drag ratio. This is deemed to be insignificant when compared to the increase in manufacturing complexity. Therefore the final planform is chosen to be a rectangular wing with geometry defined in Table 7.4.

When considering winglets. Hoerner Wingtips were chosen due to their simplicity and ease of manufacture. Hoerner winglets feature a rounded slant from the bottom side that continue to the top side where a sharp corner is placed. These winglets help provide a drag reduction by inducing a vortex at a small distance displaced from the tip of the wing. This is shown in Figure 7.5
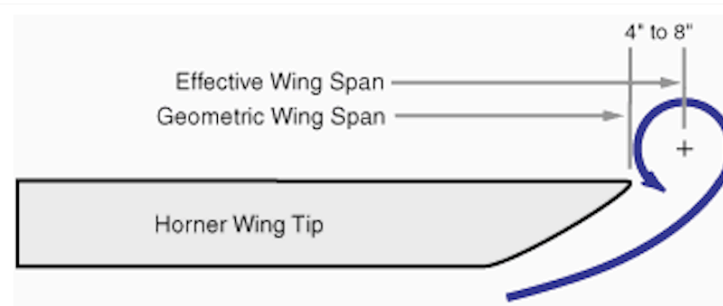


**Figure 7.5:** Hoerner Wing tips and Vortex Generation

These winglets push the induced vortex to the very edge of the wing tip, effectively increasing the wing span. This is extremely useful for the design as the wing span is constrained by the box size. Furthermore this provides a more effective wing while not increasing the geometric wing span. Besides increase efficiency Hoerner wing tips contribute to no net increase in weight, possibly even weight reduction at the tips. The wing tips also allow for ease of manufacture in comparison to more complex geometries; Overall they are the most cost effective, easy to manufacture solution to reducing the induced drag to wing tip vortexes. The final wing planform can be observed in Figure 7.6
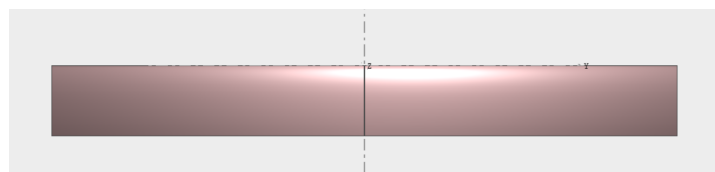


**Figure 7.6:** Final Wing Planform

**Table 7.5:** Final Wing Characteristics at Cruise Conditions

| Angle of attack | $C_{L_{max}}[-]$ | $C_{L_0}[-]$ | $C_{m_{cruise}}[-]$ | $\alpha_{stall}[°]$ | $\frac{C_L}{C_D}_{cruise}[-]$ |
|---|---|---|---|---|---|
| 6.2 | 1.63 | 0.3 | -0.28 | N.A. | 24.5 |

This wing design is an initial estimation which still does not include several factors that may contribute to increase performance. Therefore it is recommended that additional work is performed to see how

wing twist, wing incidence and dihedral contribute to the design.

### 7.2.3. Modularity

At a wing span of $10.14\ m$, the main wing planform is too large to be transported in the standard $20\ ft$ container. Therefore a modular solution allowing the wing to be detached into sections is used. The fuselage and wing are directly integrated together in the midsection. This translates to an effective section of $1.67\ m$ having direct integration with the wing. The two detachable wing sections use long spars that extend out of the section. These spars are inserted into the fuselage mechanism and join together to form one stable structure. Furthermore due to the splitting of the wing, the structure has a more rigid structure at the fuselage root. Splitting the wing further along the span reduces the structural impact as loading decreases along the wingspan. The implementation of this wing structure can be seen in Figure 7.7
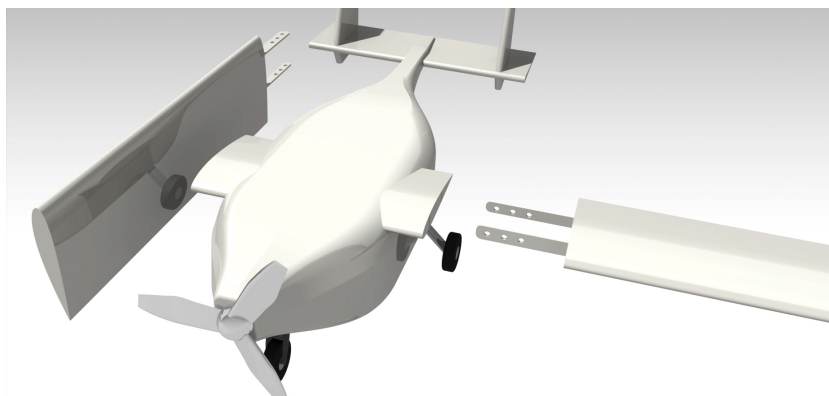


**Figure 7.7:** Modularity of the main wing

### 7.2.4. Wing Stringer Design

Before discussing the design of the aircraft wingbox, the stringers employed will be described. Stringers increase the moment of inertia of a panel, thus improving its loading carrying capability. Figure 7.8 shows different stringer designs that have been previously employed in aircraft [32] whereby it can be noted that many options exist. The stringer design that will be selected for the aircraft design of this report is the extruded Z-stringer (option (a) in Figure 7.8). This selection was based on several reasons:

- The Z-stringer is one of the most popular stringer designs with the J-stringer being the other [32]. The reason why the Z-stringer was selected over the J-stringer is because it is more structurally efficient [32].
- The Z-stringer is easy to attach to aircraft panels [32].
- The Y-stringer, and Hat-stringers are subject to corrosion problems due to difficulties regarding inspection [32].

As for the material choice for the stringers, 7075 aluminium alloy (AA7075) was selected. This was done because this material is typically used for aircraft stringers [1]. By selecting a commonly used material for aircraft stringers, there is high confidence that the stringers will be sufficiently strong. Moreover, the stringers will be more manufacturable relative to stringers made of materials not commonly employed.

---

[1]URL: https://patents.google.com/patent/EP0030070A1 [cited 01 June 2022]
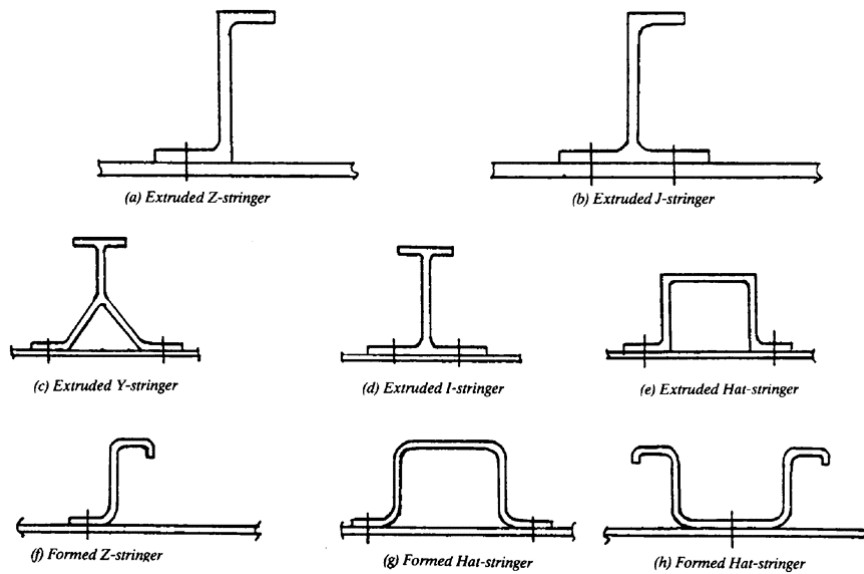
**Figure 7.8:** Stringer designs typically used in aircraft [32]

Regarding the exact dimensions of the stringers utilized in the design process, stringers/stiffeners that can be bought off-the-shelf were inspected. Off-the-shelf Z-stringers could not be found from websites belonging to the amateur builder's market (Vans, Aircraft Spruce), however, L-stringers and T-stringers could be found [2] [3]. These example stringers were used for reference regarding the typical cross-sectional area and thickness of stringers used in aircraft and as such a stringer design as described in Table 7.6 was used. It is important to note that each plate that makes up the stringer are equal in length and thickness.

**Table 7.6:** Stringer design implemented in aircraft

| Stringer type | Thickness [m] | Cross-sectional area [m$^2$] |
|:---:|:---:|:---:|
| Z-Stringer | $1 \cdot 10^{-3}$ | $3.8 \cdot 10^{-5}$ |

## 7.2.5. Wingbox Design

The main structural component of a wing - the wingbox - is usually a single or multi-celled box extended from the root of the wing to the wing tip containing ribs, stringers and other stiffening elements. For the purposes of top level detailed design a wingbox design is hereby produced. The design process and structural analysis is considerably simplified using the following assumptions:

- The stresses are calculated using the methodology described in section 6.4 and thereby utilizes the same assumptions
- Wingbox is said to consists of 2 vertical spars, 2 horizontal skin panels, unknown number of stringers and unknown number of ribs
- The wingbox assumes elliptic aerodynamic load and weight load along the wing span equivalent to the weight of the wingbox (Figure 7.9)

---

[2]URL: https://www.aircraftspruce.com/catalog/mepages/alumangle2.php?clickkey=63992 [cited on 13 June 2022]
[3]URL:https://www.aircraftspruce.com/catalog/mepages/2024t3511.php [cited on 13 June 2022]
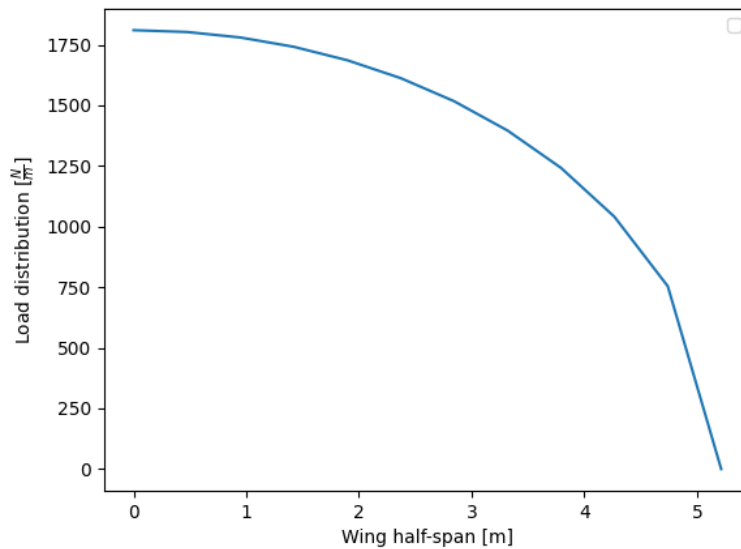
**Figure 7.9:** Assumed aerodynamic load distribution on the wingbox

**Initial Design**

To find how sensitive wingbox design is to each design parameter and to help optimize further design, initial sizing and design option generation is performed. For initial design the tools described in section 6.4 are used alongside visualizing tools such as plots and structure renders together with general engineering judgment.

During initial phase of design it was found that:

- Generally narrower (in chord-wise direction) wingboxes are lighter
- The optimal solution using current design tools results in very thin structures and a minimum allowable thickness has to be defined by considering manufacturability, impact failure and thicknesses used by other aerospace structures
- Some design parameters have to be limited by employing engineering judgment in order to reduce design and calculation time
- Design optimized for yield stress failure are generally very bad at buckling performance and thus a design approach that first considers buckling should be used

After performing the initial design phase of the wingbox, a conceptual design for the wingbox was generated and is represented in Figure 7.10. The wingbox can be seen in orange within the airfoil of the wing. The conceptual design consists of two thin vertical plates accompanied by a top and bottom plate which following the shape of the airfoil. By making such a conceptual design, only the following variables need to be determined during the detailed design phase:

- Rib spacing
- Stringer number
- Thickness of the plates
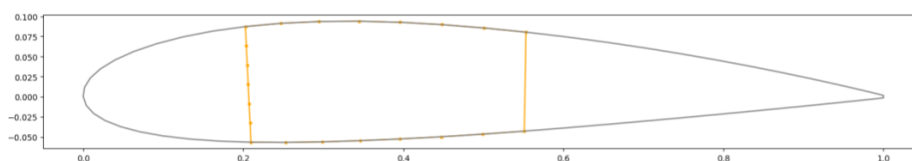


**Figure 7.10:** Conceptual wingbox design before detailed analysis

**Wingbox Design Iterations**

While designing the wingbox there were two main types of failure considered: stress exceeding the allowable material strength and failure through buckling. To find an initial estimate of the design several design parameters were constrained in order to both limit calculation and design time, as well as most efficiently employ engineering judgment. The parameters constrained and the reasoning driving the constraining is presented in the table below Table 7.7:

**Table 7.7:** Wingbox design constrains

| Constraint | Reasoning |
|---|---|
| All of the stringers are identical. | This eases manufacturability of the wingbox and simplifies the design process. |
| The stringer number and cross-sectional area are constant along the span. | This eases manufacturability of the wingbox and simplifies the design process. |
| Top and bottom plates of the wingbox have the same thickness. | To simplify the design process, it was decided to keep the thicknesses the same while varying the stringer number for the top and bottom plates. |
| Side plates have the same thickness. | Any differences in thicknesses would lead to little benefit regarding load carrying capability while increasing the complexity of the design process. |
| The wingbox is divided into four discrete span-wise sections. | This allows for varying thicknesses along the wing to get a lower weight design. In addition, only four sections is selected such that there are not too many thickness changes, making the wingbox more difficult to manufacture. |
| Top and bottom plates of the wingbox take the shape of airfoil at the corresponding location. | Minimises part count and maximises part functionality by implementing wing skin into wingbox. |
| Side plates of the wingbox are vertical. | Optimises the connection of the plates. |
| Stringers have a set cross-sectional area of $3.8 \cdot 10^{-5} \ m^2$ | This was done to limit the number of variables that could be tuned during the design phase. A cross-section was selected as explained in subsection 7.2.4. |
| Rib spacing is set to $0.3 \ m$. | Since there were many adjustable design parameter, rib spacing was given a set value. A spacing of $0.3 \ m$ was selected as this is typical for aircraft structures [24]. In addition, a rib spacing was selected because determining the optimal rib spacing through analytical methods proved to be difficult. |

Once some design constraints have been introduced design iteration loops are performed in order to find an optimized design point. During early wingbox design iterations it was found that if the design is optimized for bending, shear and torsional loads it would perform very poorly for buckling. On the other hand, if the design is optimized for buckling it would most of the time work for the other stresses as well.
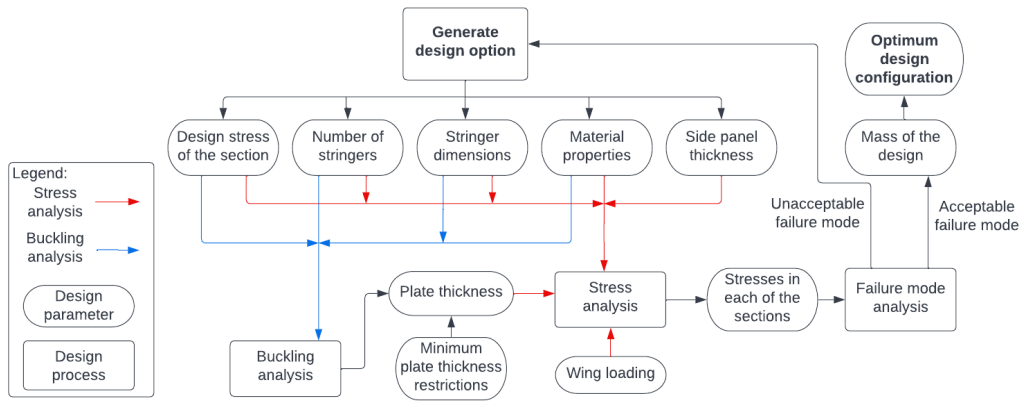
**Figure 7.11:** Wingbox design parameter iteration

A diagram (Figure 7.11) is presented that showcases the design loop used for finding the lightest wingbox design. It demonstrates how the design parameters and analysis affect each other. The design loop starts by generating a design options. Afterwards, buckling analysis is performed for the configuration to determine what are the required thicknesses of horizontal plates to buckle at the design stresses. Then stress analysis (Von Mises for metal design, Tensile/Shear stress analysis of composite designs) is performed to see if the design can meet design stress requirements. If the design produces stresses smaller than the buckling design stresses the mass of the design configuration is recorded and used to compare with other design options. The design parameters given below are combined in order to find the lightest design:

- Design stress in each of the sections
- Number of stringers on each of the horizontal plates
- Material choice
- Side panel thickness
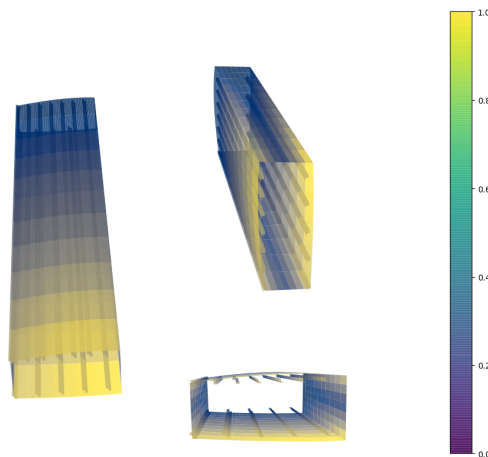


**Figure 7.12:** Wingbox stress distribution

The design that was obtained through performing the design iteration described above is given in Table 7.8. The stress distribution of the final design is shown in Figure 7.12. This preliminary design provides a starting point for further more detailed design.

**Table 7.8:** Design parameters

| Design parameters | Concept 1 |
|---|---|
| Material | Aluminium 7075 (T6) |
| Spar chord-wise positioning | $0.2c$ and $0.6c$ |
| Maximum thickness | $1.4\ mm$ |
| Minimum thickness | $0.6\ mm$ |
| Side panel to horizontal panel thickness ratio | 1.8 |
| Number of stringers | 7 on top, 5 on bottom |
| Stringer cross-sectional area | $3.8 \cdot 10^{-5}\ m^2$ |
| Rib spacing | $0.3\ m$ |
| Mass | $26.8\ kg$ per wing |

# 7.3. Empennage Design

The empennage needs to be designed correctly to ensure the aircraft is stable and controllable. This requires proper sizing following the procedures from section 6.5. This section will first describe the sizing of the horizontal and vertical tails and after that it will look at the modularity of the empennage.

## 7.3.1. Horizontal Tail Sizing

The scissor plot can be generated as described in subsection 6.5.2. When calculating the stability line, the conditions for cruise have to be used, as this is the most crucial phase for stability [33]. For the stability line, the parameters presented in Table 7.9 have to be determined first. The lift slope coefficients are found using the DATCOM method. The downwash is taken from [4]. The velocity ratio, and aerodynamic center location are found using them methods from [33]. The tail length follows from iteration, and is defined as the length between the MAC of the wing and horizontal tail. The MAC follows from the wing design, and finally the stability margin $S.M$ is assumed to be 5%.

**Table 7.9:** Inputs for the stability line. The values are found following the methods of [33]

| Parameter | Value | Unit |
|---|---|---|
| $C_{L_{\alpha_h}}$ | 3.29 | $[1/rad]$ |
| $C_{L_{\alpha_{A-h}}}$ | 5.79 | $[1/rad]$ |
| $1 - \frac{d\epsilon}{d\alpha}$ | 0.90 | - |
| $\frac{V_h}{V}^2$ | 0.85 | - |
| $\bar{x}_{ac}$ | 0.22 | |
| $l_h$ | 3.97 | $m$ |
| $\bar{c}$ | 1.13 | $m$ |
| S.M | 0.05 | - |

For the controllability line, the values from Table 7.10 are the input. For these parameters the conditions at conditions at landing must be assumed, as it is the most critical phase for controllability [34]. The lift coefficient of the tail is taken from [34] assuming a fixed tail. The aircraft-less-tail lift coefficient is found by subtracting the tail lift coefficient from the maximum lift coefficient. The moment about the aerodynamic center is found from [34], which takes into account contributions from the flaps, wings and fuselage. The tail length, MAC, velocity ratio and aerodynamic center are the same as the inputs for the stability line.

When these values are plugged in Equations 6.41 and 6.43, the scissor plot can be found in Figure 7.13.

---

[4]https://ocw.tudelft.nl/wp-content/uploads/Hand-out-Stability_01.pdf

**Table 7.10:** Inputs for the controllability line. The values are found following the methods of [34]

| Parameter | Value | Unit |
|:---:|:---:|:---:|
| $C_{L_h}$ | -0.50 | - |
| $C_{L_{A-h}}$ | 2.40 | - |
| $C_{m_{ac}}$ | -0.31 | - |
| $\frac{V_h}{V}^2$ | 0.85 | - |
| $l_h$ | 3.96 | $m$ |
| $\bar{c}$ | 1.13 | $m$ |
| $\bar{x}_{ac}$ | 0.22 | $/MAC$ |
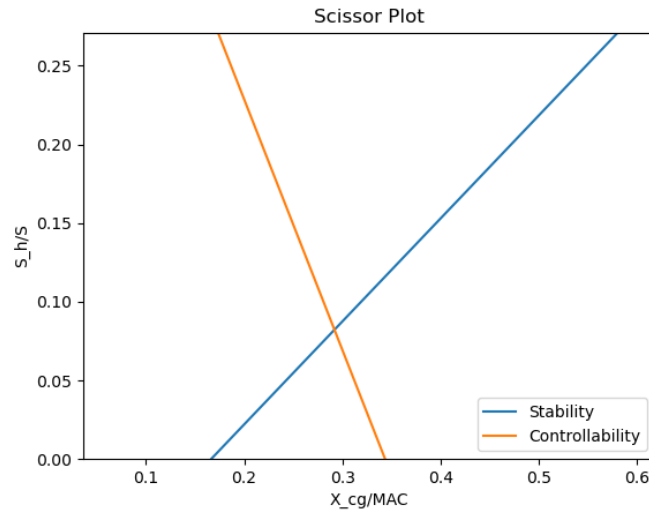


**Figure 7.13:** Scissor plot

Then the loading diagram has to be constructed. If the procedure of subsection 6.5.3 is followed, the centre of gravity of the operating empty weight is found to be $0.84\bar{c}$. This was done by assuming a location of the different subsystems as indicated in Table 7.11. The location of the vertical and horizontal stabilizer and wing follows from iteration. The loading diagram can be found in Figure 7.14, note that the top line represents the fuel being loaded.

**Table 7.11:** Location of the different subsystems

| Component | C.G. [% fuselage length] |
|:---|:---:|
| Fuselage | 40 |
| Landing gear | 30 |
| Power unit | 5 |
| Flight controls | 10 |
| Avionics | 20 |
| Electric systems | 30 |
| Vertical stabilizer | 92.7 |
| Horizontal stabilizer | 92.7 |
| Wing | 25.5 |
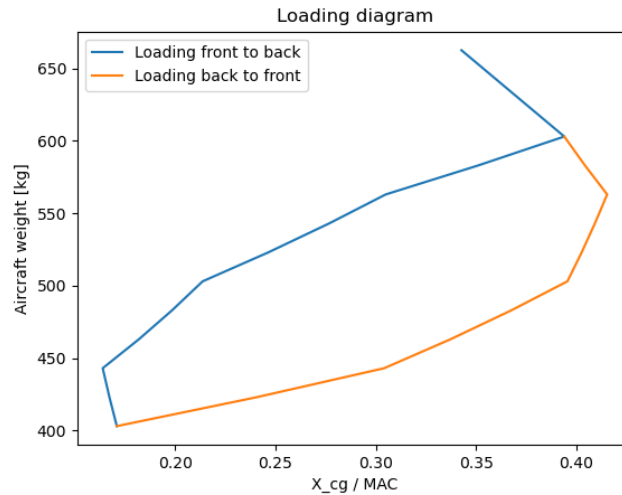
**Figure 7.14:** Loading diagram

The last step before the actual sizing can be performed is to plot the C.G. range against the wing position using the code from the loading diagram. The output is then two almost linear lines with a negative slope. The slope makes sense as the CG locations are with respect to the MAC, which shifts when moving the wing as well.

Finally, the horizontal tail can be sized by combining both graphs, using the algorithm described in section 6.5. The final graph can be found in Figure 7.16
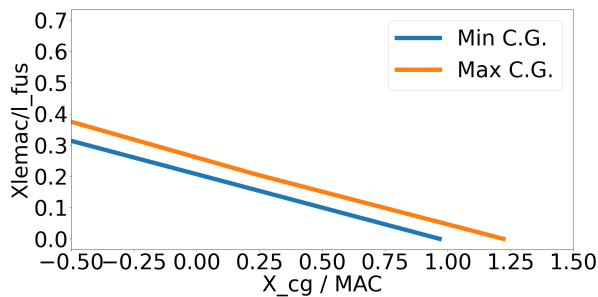


**Figure 7.15:** C.G. range vs. wing position
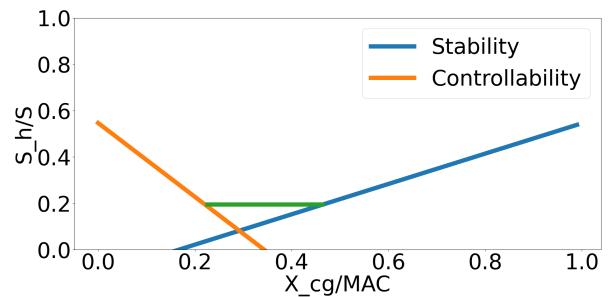


**Figure 7.16:** Scissor plot combined with the loading diagram.

This graph indicates that an optimal $S_h/S = 0.194$ and $X_{LEMAC}/L_{fus} = 0.159$. For the geometry of the horizontal tail it is assumed the taper ratio is 1, and there is zero sweep, as these are the best values for manufacturability and thus price. Furthermore an aspect ratio of 3 is assumed, as this is the smallest aspect ratio within the suggested range from [7]. A small aspect ratio is desired mainly for modularity, as a smaller part of the aircraft needs to be removed. The span and chord are straightforwardly calculated.

**Table 7.12:** Inputs and outputs for horizontal tail sizing

| Inputs | | Outputs | |
|---|---|---|---|
| $S_h/S$ | 0.194 | $S_h\ [m^2]$ | 2.13 |
| $S\ [m^2]$ | 10.94 | $b_h\ [m]$ | 2.53 |
| $AR_h$ | 3.0 | $c_h\ [m]$ | 0.84 |

### 7.3.2. Vertical Tail Sizing

The vertical tail is sized following the procedure of [36]. First a comparable tail volume coefficient has to be found. This value is taken as 0.06 since this is found from statistics for comparable single engine aircraft with comparable wing area [36]. By using the vertical tail volume value, the area of the vertical tail can be deduced from Equation 7.1

$$V_v = \frac{S_v l_v}{Sb} \tag{7.1}$$

For the aspect ratio a value of 1.5 is assumed, which is a typical value for the vertical tail [5]. Furthermore, it is assumed there is no wing sweep and the taper ratio is 1, for the same reasons as for the horizontal stabilizer. Finally it is assumed the vertical tail length is the same as the horizontal tail length. The vertical tail span and the chord can be deducted from the basic wing formula's. The results of the vertical tail sizing can be found in Table 7.13

**Table 7.13:** Inputs and outputs for vertical tail sizing

| Input | | Output | |
|---|---|---|---|
| $V_v$ | 0.06 | $S_v$ $[m^2]$ | 1.78 |
| $AR_v$ | 1.5 | $b_v$ $[m]$ | 1.63 |
| | | $c_v$ $[m]$ | 1.1 |

### 7.3.3. Modularity of the Empennage

According to the the driving requirement WFA-REQ-USE-09 in Table 4.1, the aircraft shall be able to fit in a 20 feet container. The internal dimensions of a 20 ft container are $2.34\ m$ wide, $2.2\ m$ high and $5.89\ m$ long. As the horizontal tail span is $51\ cm$ wider than this, this means that there has to be a cut in the horizontal tail. The aircraft without vertical tail is already $1.47\ m$ high. This means that there can be a vertical tail in the aircraft of $81\ cm$, in other words there has to be a cut about half way the vertical span. This would mean that a conventional tail would take 3 cuts such that it fits in the container. This is not ideal since every cut in the structure means an increase in mass due to that there needs to be an reinforcement in the structure. Therefore it is desirable to have as low of an amount of cuts and as far away from the root as possible.

A design that would have less cuts and fits better in the container is a special type of H-tail. The H-tail would fit in the container by spacing the vertical tails such that they won't have to be removed, so their spacing would be 2.20 metre. The elevator will also only span this spacing in order to keep the mechanical aspect of the empennage is simple as possible. The sizing of the vertical tail will also change since the vertical tail area can be split by two. By keeping the same aspect ratio as described in Table 7.13, the sizing values of one of the vertical fins can be found in Table 7.14.

**Table 7.14:** Sizing of a vertical fin for a H-tail

| Parameter | Value |
|---|---|
| $S_v$ $[m^2]$ | 0.89 |
| $b_v$ $[m]$ | 1.16 |
| $c_v$ $[m]$ | 0.77 |

With a span of 1.16 metres and wanting to leave a margin of $10\ cm$ from the top, this means the vertical tail is $71\ cm$ above the horizontal tail and thus $45\ cm$ below the horizontal tail.

Next to the vertical tails, there will be a detachable part of the horizontal tail. This reduces the amount of cuts and minimizes the amount of added mass since the bending moment at the tip is very small. The vertical tails span $2.20\ m$. This means there is still a span of 65 cm required and thus there should be $16.5\ cm$ detachable from the vertical wing.

The render of the H-tail can be found in Figure 7.17.

---

[5]https://aerotoolbox.com/design-aircraft-tail/
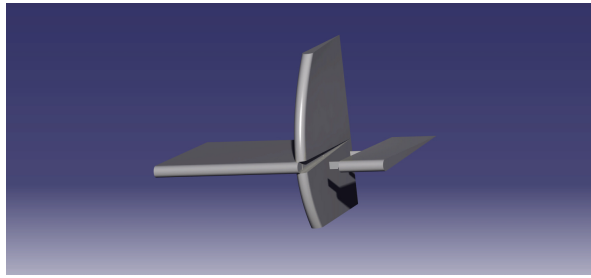
**Figure 7.17:** Render of the H-tail.

### 7.3.4. Stability Analysis

**Longitudinal Stability**

Using the method described in subsection 6.5.2, the static stability derivative $C_{m_\alpha}$ was found to be -2.61 for the most front C.G. and -0.45 for the most aft C.G. Comparing these values to those of the Cessna 172, which has a $C_{m_\alpha}$ for the most front C.G. of -0.97, and a $C_{m_\alpha}$ of -0.89 for the most aft C.G., the stability at the most front C.G. is much better, while the stability at the most aft C.G. is worse [2]. The reason for this is that the C.G. range is much larger than for the Cessna 172, which is because of the large amount of mass being dropped during the mission. Nevertheless, the aircraft is statically stable in the longitudinal direction for every C.G. in the range.

**Lateral Stability**

Next, lateral stability can be investigated. For this, the so called USAF DATCOM method will be used [16], which provides early estimations of stability derivatives using geometric parameters of the aircraft.

**Table 7.15:** Stability derivatives

| Stability Derivative | DATCOM Section | Value | Cessna 172 value [6] |
|:---:|:---:|:---:|:---:|
| $C_{n_r}$ | 7.3.3.3 | -0.3678 | -0.099 |
| $C_{l_r}$ | 7.3.3.2 | 0.078 | 0.096 |
| $C_{n_\beta}$ | 5.6.3.1 | 0.1422 | 0.065 |
| $C_{l_\beta}$ | 5.6.2 | -0.0205 | -0.089 |
| $C_{Y_\beta}$ | 5.6.1 | -0.8336 | -0.31 |

Using these derivatives the lateral dynamic stability can be evaluated as well. For the spiral eigenmotion the following equation must be satisfied for stability [1]:

$$C_{l_\beta} C_{n_r} - C_{n_\beta} C_{l_r} > 0 \tag{7.2}$$

Filling in the values, the result is -0.0035, which means the aircraft is unstable in the spiral motion. However this is not a big issue, as spiral stability is usually so slow that it can be corrected for easily by the (auto) pilot [7].

Wings for aid said during a meeting that their current MiniFreighter is very unstable during the dutch roll. The equation of motion for the dutch roll is given in Equation 7.3.[1]

$$\begin{bmatrix} C_{Y_\beta} - 2\mu_b D_b & -4\mu_b \\ C_{n_\beta} & C_{n_r} - 4\mu_b K_Z^2 D_b \end{bmatrix} \begin{bmatrix} \beta \\ \frac{rb}{2V} \end{bmatrix} = \mathbf{0} \tag{7.3}$$

In Equation 7.3, $\mu_b$ is the relative density for asymmetric eigenmotion and can be found with $\mu_b = \frac{m}{\rho S b}$. Assuming sea level, $\mu_b = 4.25$. $K_z$ is the non dimensional radius of gyration and can be found with $K_z = \sqrt{\frac{I_{zz}}{mb^2}}$. The value for $I_{zz}$ is taken from catia and is $1857\ kg\,m^2$ Therefore, $K_z = 0.17$ According to [1], the characteristic equation of Equation 7.3 can be set in the form of $Ax^2 + Bx + C$ where the coefficient A, B and C are defined as in Equation 7.4

---

[6]https://www.researchgate.net/figure/Stability-derivatives-for-Cessna-172_fig11_309468360

[7]http://www.faatest.com/books/FLT/Chapter17/SpiralInstability.htm

$$A = 8\mu_b^2 K_z^2 \quad B = -2\mu_b(C_{n_r} + 2K_z^2 C_{Y_\beta}) \quad C = 4\mu_b C_{n_\beta} + C_{Y_\beta} C_{n_r} \tag{7.4}$$

When the values of Table 7.15 are used in the quadratic formula the eigenvalues of the dutch roll can be calculated.

$$\lambda_{dutch\ roll} = -0.42 \pm 0.69j$$

In order for the dutch roll to be stable, it is required that the real part of the eigenvalue is small than zero. That is the case for this aircraft so it is stable in dutch roll.

## 7.4. Undercarriage Design

When designing shock absorbers for the landing gear, two main categories can be considered; solid springs or fluid springs. Four categories: simplicity, maintainability, reliability and cost were used as indicators to decide which system was most applicable to the final aircraft. In order to reduce to cost and operational maintenance, a leaf spring design was chosen for the main landing gear. For the nose landing gear, a large central shock absorber with a torsion link to provide stability on landing was chosen. Performance and ability to absorb landing loads can be characterised by 3 main factors, sink speed, load factor and stroke.

Certification methods typically require landing gear validation through vertical drop tests from a predetermined height.The challenge with this system is ensuring that a rapid initial deceleration is possible, followed by a reduced deceleration to ensure smooth motions. Nose landing gear bears the weight of the engine and is a system that can experience significant fatigue and damage. Due to these reasons, the nose landing gear should be designed using significant safety factors, accounting for situations where the loading is greater than calculated. Furthermore the cyclical and abrupt loading that the nose experiences influences the material used. The structure should be able to sustain these fatigue loads for a large operational profile without failing. Other considerations that must be taken into account are:

- Attaching the nose wheel to the engine mount instead of firewall can help provide better structural stability upon landing.
- Prop strikes against ground surface upon landing can result in a mission critical scenario. Therefore it is crucial that adequate margins are used in the engine placement, prop diameter and landing gear height.
- Typically to perform a landing as short as possible, full power is applied then break release.
- Nose wheel loading and system wear can be minimised through adequate elevator deflection.

The sizing of the undercarriage is highly constrained by the internal size of the standard $20\ ft$ storage container. The width of the fuselage is $1.67\ m$ and the internal width of the fuselage is $2.35\ m$. This leaves an internal width of $0.32\ m$ on either side of the fuselage for the landing gear. Furthermore, based off of the sizing of the vertical tail as well as the required propeller size for optimum flight performance, the height of the landing gear is constrained to $0.6\ m$. In order to size the landing gear, the placement between successive box dropping mechanisms is also considered. This is a constraining factor as the landing gear will be placed between these mechanism. This insures that the loading can be transferred into the main fuselage structure and that the dropping of the boxes is not disrupted. Finally there is a constrain placed on the static loading of the nose landing gear. There shall be a minimum loading of 8% of MTOW and a maximum nose loading of 18% of MTOW. These constraints are calculated through statistical data based off of landing gear performance gathered from Roskam [40].

The final dimensions of the landing gear subsystem and the appropriate diagram displaying the size are shown in Table 7.16 and Figure 7.18 respectively. Two other figures, Figure 7.19 and Table 7.17, display information about the scrape angles and tire dimensions respectively.
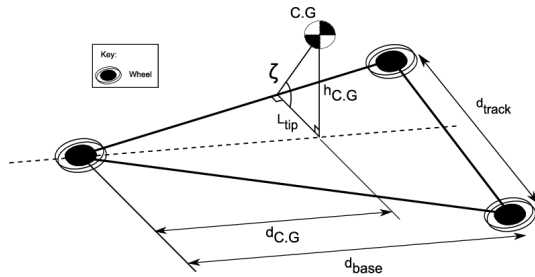
**Figure 7.18:** Landing Gear Geometry [42]
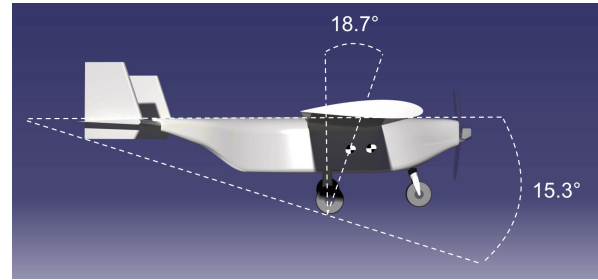


**Figure 7.19:** Aircraft Side-on View Displaying Scrape Angle

**Table 7.16:** Landing Gear Configuration

| Parameter | Value | Unit |
|-----------|-------|------|
| $X_{Nose}$ | 0.1 | $m$ |
| $W_b$ | 2.3 | $m$ |
| $W_t$ | 1.45 | $m$ |
| $Z_{LG}$ | 0.6 | $m$ |

**Table 7.17:** Tire dimensions and Performance

| Parameter | Value | Unit |
|-----------|-------|------|
| $d_t$ | 0.34 | $m$ |
| $W_t$ | 0.17 | $m$ |
| $p_t$ | 20 | $Psi$ |

Given these geometries, the landing gear can expect a minimum static nose load of 8.2% of the MTOW at take-off and a maximum static nose load of 15.4% of the MTOW on landing. In order to fully assess the consequences of the design constraints a full structural analysis must be performed and verification drop tests conducted. When analysing the turning performance of the landing gear, turns of radius 1.85m can be performed with a deflection of 51.6 degrees from the nose wheel. This allows for tight turn while on the runway, ensuring that the aircraft can perform the mission in tight spaces. Furthermore as seen in Figure 7.19, the design has a scrape angle of 15.3 degrees, allowing for adequate clearance during the pitch-up maneuver at take off and during landing.

In order to ensure maximum cushioning and reduction in loads on the nose, Larger tires were chosen. It was concluded that the additional weight and increase in drag were acceptable as the increase in tire size would ensure better operability. This will insure that the aircraft is able to operate in a larger variety of environments, but also reduce the cost of repairs for the Nose landing gear. In order to fully analyse the performance of the subsystem, the structure of both the leaf spring and nose requires detailed design.

## 7.5. Propulsion System

For the propulsive system the AM13 an Suzuki G13 conversion by the company Aeromomentum is chosen. The major considerations were unit and operational costs next to fuel efficiency and time before overhaul TBO. A fixed pith propeller is chosen to keep system simplistic lightweight and low cost. for optimal performance a new propeller will have to be developed with of the shelve fixed pitch propellers its hard to attain desired efficiency as they are designed for a specific engine air-frame combination. However a current of the shelve propellers might suffice and save development cost.

### Engine

The search for an appropriate engine started out with the minimal power required to give adequate take-off performance. In terms of TBO the available 4-stroke engines outperform 2-strokes. Additionally on average the 4-stroke engines on the market have larger max power outputs, thus when chosen are required to run at a lower fraction of their max power limiting wear of the engine. Additionally a four-stroke engine is more sustainable as it does not have excessive oil and partially burned oil in the exhaust gasses. The engines that were considered were the D-Motor, AM13 and as a benchmark the Rotax 912 UL and UL260i were used. The AM13 is clearly the best in terms of price and fuel consumption. Even with the extra weight taken into account the fuel efficiency of the AM13 outperforms the D-motor

as the extra fuel necessary will surpass the weight difference. But maybe even more important is the Price with the below 10,000 USD price tag it is one of the most affordable 4-stroke engines in the 100hp class.

**Table 7.18:** 4-stroke engine comparison *The fuel flow data reflect the most ideal environment for fuel economy as listed the manufactures.

|  | AM13 | D-motor LF26 | Rotax-912 UL | UL260i |
|---|---|---|---|---|
| $P_{max}$ [hp] | 100 | 91.8 | 100 | 97 |
| RPM (prop) | 2240 | 3000 | 2387 | 3300 |
| m[kg] | 77 | 63 | 75 | 72.3 |
| P/m [kW/kg] | 0.97 | 1.1 | 0.99 | 1.0 |
| TBO[hrs] | 2000 | 1500 | 2000 | 1500 |
| price [USD] | 9,995 | approx 16,000 | 19,437 | 22,345 |
| Minimum Octane level | 90 | 91 | 95 | 95 |
| Fuelflow* [L/hp/hr] | 0.13 | 0.18 | 0.14 | 0.13 |
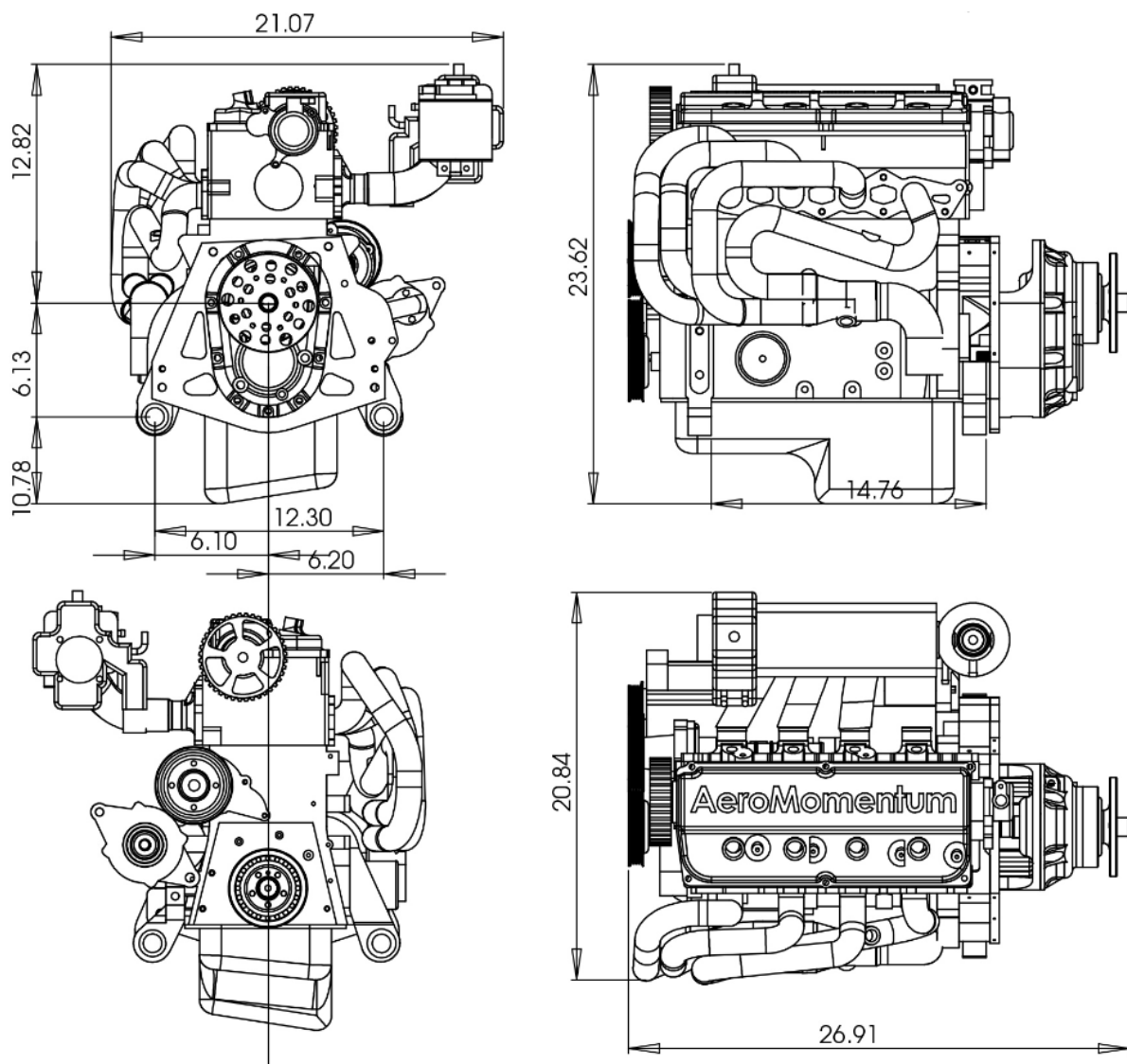


**Figure 7.20:** AM13 engine dimensions in inches [8]

---

[8]https://aeromomentum.com/am13.html[cited 21 jun 2022]

**Propeller**

From the cost and reliability perspective the propeller is made as simple as possible so eliminating the need for a different gearing ratio than the standard on the AM13 engine additionally only fixed pitch propellers are considered. As described in chapter 6 a design choice to optimise the propeller for cruise. Additionally the propeller is limited in size due to ground clearance. EASA VLA [9] ground clearance requirement is taken as guideline and therefore a 18 cm prop-clearance is assumed to be required when the tyres are deflated. This results in a propeller diameter of $1508\ mm$. The propeller model results in a $\eta_{design}$ of 0.86 and total Thrust graph of our propulsion system at sea-level will be the following Figure 7.21.
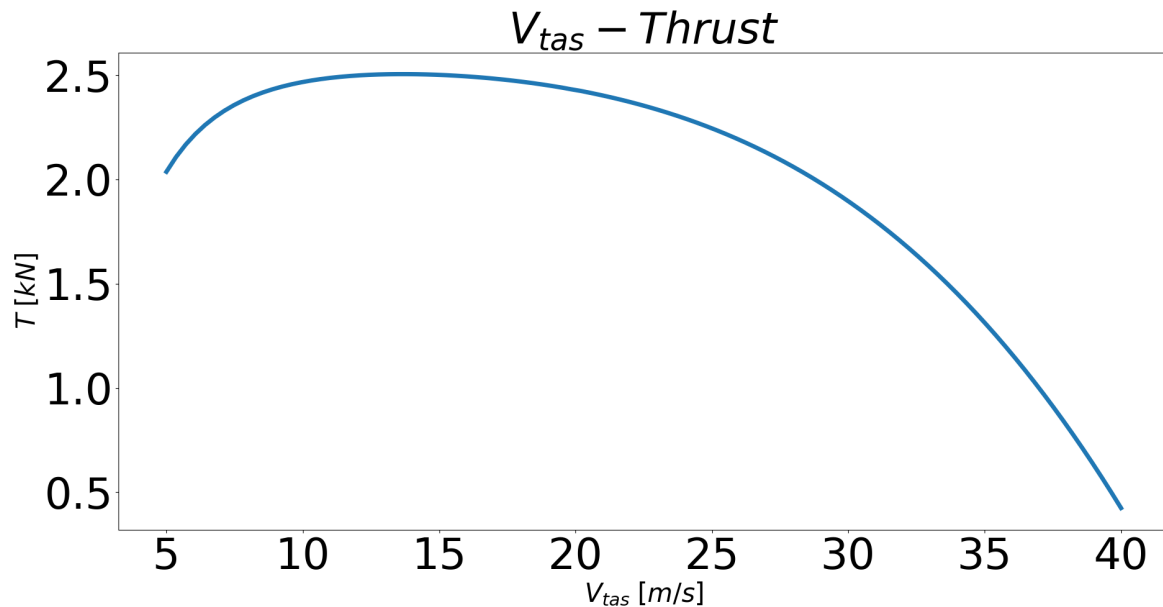


**Figure 7.21:** Max continuous thrust profile of the propulsion system

## 7.6. Performance

The payload range diagram allows for the system user to observe the possible trade off between payload and range within the operational envelope of the aircraft. This trade off is crucial as these operational limits affect the variety of missions that can be performed. When significantly decreasing the payload that the aircraft carries, a larger range is achieved, further expanding the operational range of the system. This can allow the operator to perform a single payload drop of crucial supplies at a distance that is significantly larger that the operational 250 km range.

In order to calculate this diagram, the tools developed for cruise performance were used. The payload range diagram is displayed on Figure 7.22. It should be taken into account that the calculations assumes that the aircraft is only performing cruise for the whole range. Due to the fact that the aircraft is just performing cruise, as opposed to also climbing and descending, the range at nominal amount fuel capacity is slightly higher than $500\ km$, and reaches $730\ km$. As can be seen from the diagram, there is a substantial amount of range possible for the aircraft when all payload is replaced by fuel instead. Reducing the payload to house more fuel could be attractive for missions that require ranges longer than $500\ km$.The range for a mission that replaces all payload mass by fuel mass is approximately $2800\ km$. There is no point in between these two scenarios to describe the case for maximum nominal fuel capacity because the fuel tank sizing has yet to be finalized.

---

[9]https://www.easa.europa.eu/downloads/66874/en
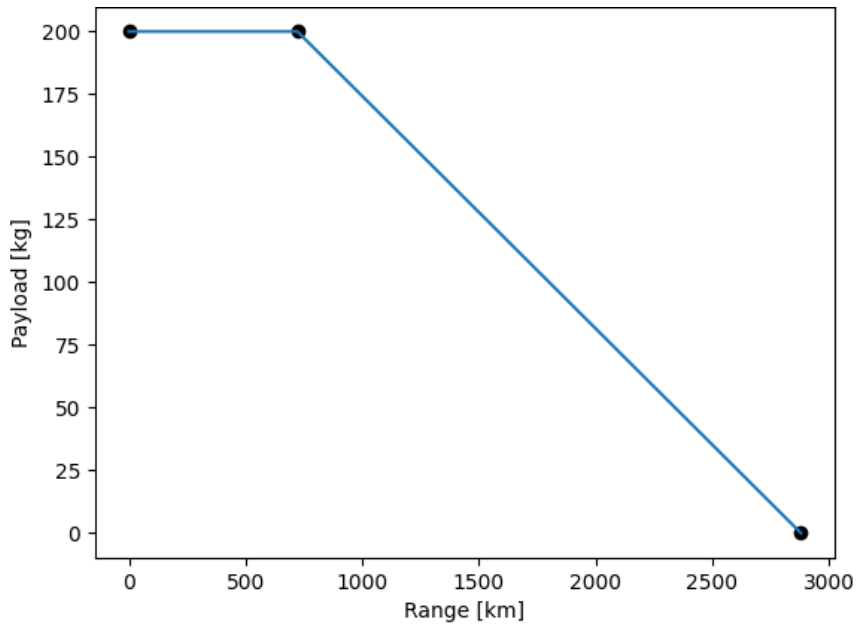
**Figure 7.22:** Payload range diagram

## 7.7. Hardware and Software

To visualize the relations and interactions between the systems onboard, a hardware and software block diagram can be created. These diagram are relatively high level, since the detailed architecture of the whole avionics system is still unknown at this point, however they can be used as guide maps to develop it.
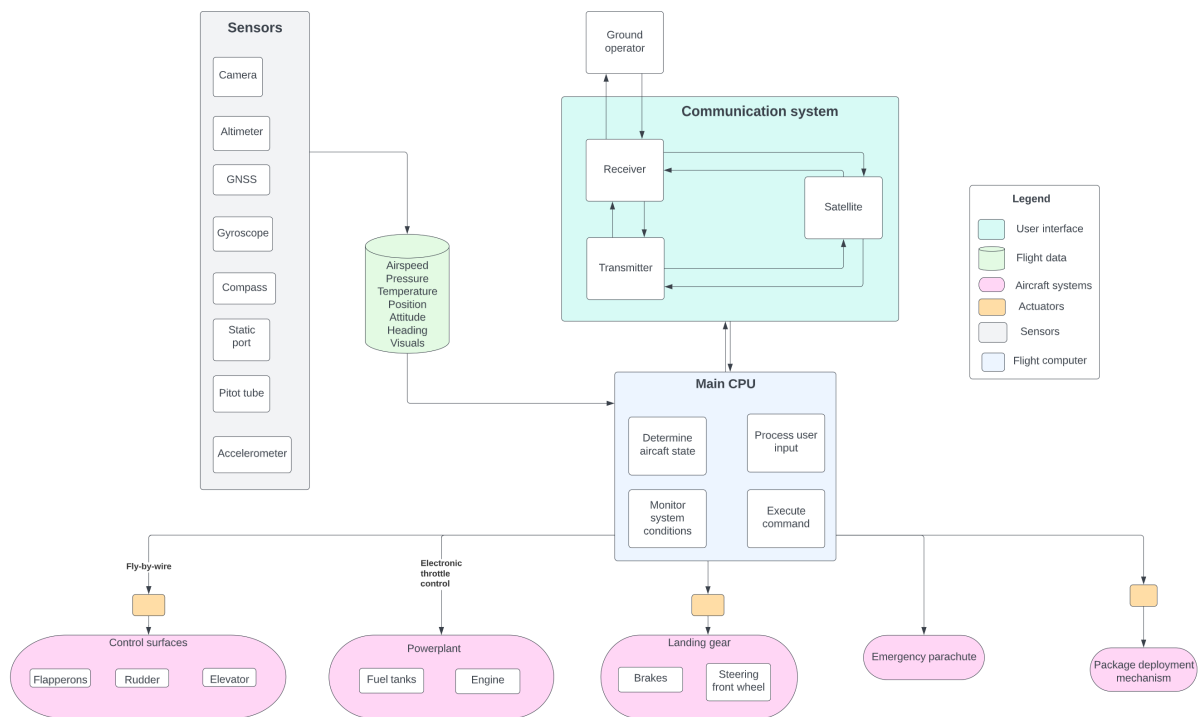


**Figure 7.23:** Hardware block diagram

Based on Figure 7.23, we can establish what components need to go into the avionics system. By searching for products that can the deliver the needed functionality, it is possible to obtain a more ac-

curate prediction for the weight of the avionics system.

One autopilot kit that can be found is the UAVOS AP 10.1[10], which supports UAVs that weigh up to $4000\ kg$. This gives an approximate weight for the control system (incl. sensors, telemetry and communication) of $5.87\ kg$, which can be rounded up to $6.5\ kg$ to account for the flight recorder and power distribution unit.

To estimate the weight of the actuators, heavy duty components that deliver more torque and speed than will be required are looked up, so that a conservative estimate can be obtained. One actuator that has a maximum torque of $10.79\ Nm$ with a power of $59\ W$ and weighs $0.363\ kg$ is the Hitec HS-1100WP[11]. As of now, 5 servos will be needed, so let's assume they are identical. This brings the weight of the actuators to $\approx 1.815\ kg$. One linear actuator which can weigh about $1.42\ kg$ is also needed.

To estimate the mass of the wire harness of the aircraft at this stage will yield very unreliable results, so we will assume the wiring will not exceed $15\ kg$. Based on the size of the aircraft, this number seems reasonable.

weight for avionics thus comes up to about $24.73\ kg$. Including the battery weight from section 7.8, the total weight of the avionics system becomes $42.73\ kg$. Since the methods to estimate this number were so unreliable, a margin of around $50\%$ should be considered, in order to accommodate for any errors. A maximum weight of $64\ kg$ is obtained.

A high level software diagram at this stage of the design would resemble the functional diagram in Figure A.2. At this point, the aircraft is manually operated at take off and landing, with line of sight communication, however, future upgrades would allow for a fully automated flight, where the operator would only need to monitor the flight.

## 7.8. Electrical System

The electric system onboard the aircraft is relatively simple; an alternator driven by the engine provides the electrical power, which is then distributed to all the components that require electricity. Figure 7.24 depicts the electrical system in more detail.
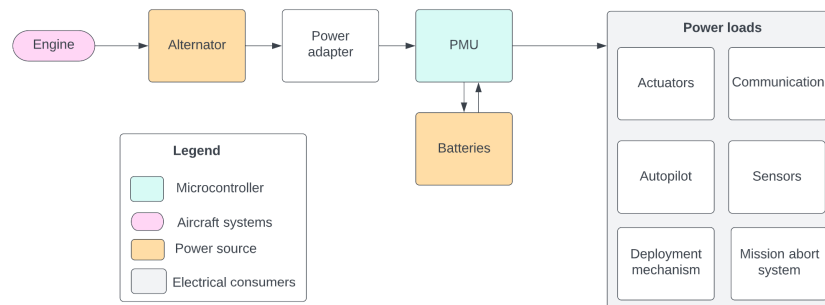


**Figure 7.24:** Electrical block diagram

The batteries will mostly be needed for engine startup and will serve as a backup electrical power supply in case of engine failure. Since the engine is similar to car engines, a reasonable approximation for the battery mass is to take an existing car battery. Most car batteries weigh about $40\ lbs$, which is roughly $18\ kg$.

## 7.9. Data Handling

Since the aircraft needed is an UAV, it is crucial to have sensors onboard that provide the necessary data to operate it. Processing and transmitting the data from the sensors should also be discussed so that an adequate flight computer and communication system can be selected.

---

[10] URL:https://www.uavos.com/products/autopilots/ap10-1-automatic-control-system-for-uav/
[11] URL:https://hitecrcd.com/products/servos/digital/sport-giant/hs-1100wp/product
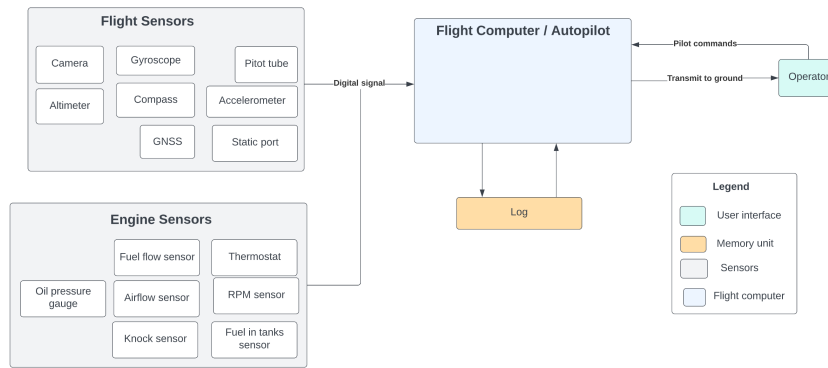
**Figure 7.25:** Data handling diagram

# 7.10. Final Design

This section shows the final design parameters of the aircraft as well as the mission characteristics, in Table 7.19 and Table 7.20 respectively. The final design is however still a preliminary design and requires more iterations to characterize it as an actual final design. Therefor the values in Table 7.19 are not fixed at all and may still change if this design is continued.

The characteristics in Table 7.20 a for a mission where the aircraft will travel $250\ km$ to an isolated destination, drop all the payload and travel back to the ground base. A three view drawing of the full aircraft is shown in Figure A.3.

**Table 7.19:** Final design parameters

| Parameter | Value | Unit | Parameter | Value | Unit |
|-----------|-------|------|-----------|-------|------|
| **Main wing** | | | | | |
| Surface area | 11.43 | $m^2$ | Taper | 1 | − |
| Span | 10.14 | $m$ | x-position leading edge | 0.92 | $m$ |
| Aspect ratio | 9 | − | Sweep | 0 | $rad$ |
| Mass | 40.52 | $kg$ | Material | Aluminium | − |
| Root chord | 1.13 | $m$ | Flap type | Plain | − |
| **Fuselage** | | | | | |
| Length | 5.8 | $m$ | Mass | 49.95 | $kg$ |
| Width | 1.67 | $m$ | Material | Aluminium | − |
| Height | 0.87 | $m$ | Box configuration | 2-3-3-2 | − |
| **Landing gear** | | | | | |
| Nose landing gear position | 0.1 | $m$ | Distance between main wheels | 2.3 | $m$ |
| Main landing gear position | 1.55 | $m$ | Landing gear height | 0.6 | $m$ |
| Mass | 14.59 | $kg$ | Material | Steel | − |
| **Empennage** | | | | | |
| **Horizontal tail** | | | **Vertical tail** | | |
| Surface area | 2.13 | $m^2$ | Surface area | 0.89 | $m^2$ |
| Aspect ratio | 3 | − | Aspect ratio | 1.5 | − |
| Span | 2.53 | $m$ | Span | 1.14 | $m$ |
| Root chord | 0.84 | $m$ | Root chord | 0.77 | $m$ |
| Taper | 1 | − | Taper | 1 | − |
| Mass | 12.28 | $kg$ | Mass | 3.46 | $kg$ |
| **Engine** | | | | | |
| Power | 100 | $hp$ | Mass | 77.1 | $kg$ |
| Fuel consumption | 14.27 | $l/h$ | Max RPM | 5800 | $min^{-1}$ |

**Table 7.20:** Mission characteristics

| Parameter | Value | Unit | Description |
|-----------|-------|------|-------------|
| OEM | 403 | $kg$ | Standard mission |
| MTOM | 663 | $kg$ | Standard mission |
| Mission time | 4.7 | $hours$ | Standard mission |
| Cruise altitude | 500 | $m$ | Standard mission |
| Take-off distance | 240 | $m$ | At sea level |
| Landing distance | 462 | $m$ | At sea level |
| Payload delivered | 200 | $kg$ | Standard mission |
| Fuel consumed | 60 | $kg$ | Standard mission |
| $C_{0_2}$ emissions | 186 | $kg$ | Standard mission |

In this chapter the production plan will be presented. First, the production methodology will be given. Then an overview of the steps will be presented and visualized in a flow chart.

## 8.1. Production Methodology

For production of the Wings for Aid aircraft, line production will be used. Line production is a method where the aircraft move through a main assembly line, and sub-assemblies are fed into this main assembly line at different stages. This can be visually shown in the figure below:
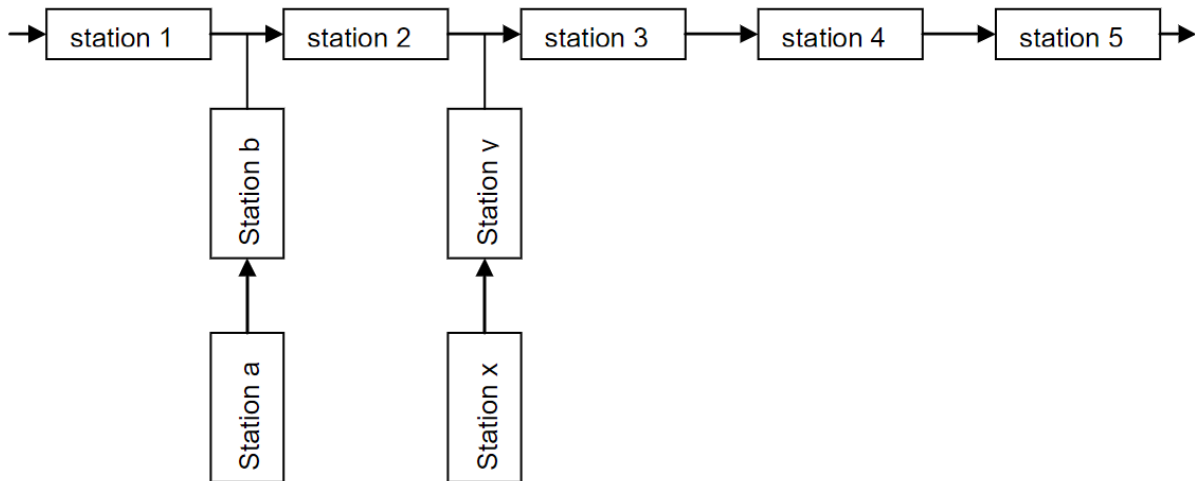


**Figure 8.1:** Visual representation of line production in factories [43]

In this figure, the numbered stations represent the main assembly line. This is where the actual final aircraft moves to. The lettered stations represent sub-assemblies and parts, and are fed into the main assembly line. The key thing about line production is that the time used for each stage of the sub-assembly is the same, and thus the parts and assemblies move at regular intervals, called the delivery interval. The most important advantage for line production is routine forming. When workers perform the same work package over and over again, they start to get faster at it and thus the time needed decreases, and costs go down. Other major advantages are that delays are easily visible, as there will be a gap in the production line, and minimal transport is necessary.

Quality control is a very important aspect of the manufacturing process. It is necessary to make sure all components of the aircraft can perform to its specifications, and any damage can be noticed and fixed in time. For quality control, a process focused method will be used. That means tests are performed at every stage of the production process, thus on the parts themselves, the sub-assemblies and the final product. For performing quality control, non-destructive testing will be employed. In this way tests can be done without breaking the component which keeps the cost low.

Finally, during production, lean manufacturing will be used. This ensures that waste is eliminated as much as possible and efficiency is optimized. During the manufacturing, the 5S method will be used. Lean 5S stands for the following 5 steps [43]:

- Sort: All the items on the workplace have to be looked at an segregated. All the items considered as weight, will be eliminated.
- Simplify: items that are randomly placed have to be identified and put on the right place.
- Shine: The workplace is cleaned on a regular basis and important machinery on a daily basis.
- Standardise: the made improvements to the process are documented
- Sustain: the changes are developed and utilised.

## 8.2. Production Steps

There are five major steps in the production process. These are ordering the parts, preparing them, making them into (sub)assemblies, testing the final system and delivering it to the customer.

### Order Parts

As a first step, the parts must be ordered. The parts to be ordered are basic materials such as metal sheets, blocks and fasteners. Other parts that must be ordered are pre-manufactured components, such as ribs and stringers. Also the off the shelf components such as the engine and landing gear will be ordered. The pre-manufactured parts will be bought from external suppliers. These suppliers will then make the parts in a workshop in batches and are then stored in a warehouse for Wings for Aid to use. Once stock runs low, a new batch will be ordered from the supplier. The off the shelf components will also be bought from an external supplier, and are then stored in a warehouse and brought into the assembly line one by one. The advantage of buying many parts from external suppliers is that the factory can be smaller and less personnel needs to be hired, thus lowering the cost.

### Prepare Parts

Before the parts can be assembled into a sub-assembly they must be prepared. For the pre-manufactured parts and off the shelf components, only quality control will be performed. This will be done by taking a random sample from the components and performing an ultrasonic c-scan to check whether there are any cracks in the part, and radiography will be used to check the thickness variations over the component. The other parts that must be prepared are the bare metals that are to be used in the fuselage, wing and empennage. Forming will be used to get the parts in the right shape, for which a heat treatment may also be used to make it more malleable. Afterwards, the same tests must be performed on these parts for quality control.

### Assembly

Next the prepared parts are made into sub-assemblies by joining them together. This will be done in separate workshops for each sub-assembly. Each subassembly will take the same amount of time to complete. Since the entire aircraft is made out of aluminium, rivets and bolts will be used for assembly as this requires less effort than for example bonding. First, the fuselage will be assembled and moved to the assembly line. In this station, also the engine and other electrical systems will be installed as the inside of the fuselage is more easily accessible. Then it will be moved to the next station where the empennage will be attached. The third station will attach the wing to the aircraft, which preferably is done as late as possible as the wing hinders transport through the assembly line. Finally the landing gear will be installed. Each sub-assembly may also be tested for quality control before moving to the main assembly line. For this visual inspection will be performed to detect any major flaws. Also ultrasonic c-scans and fluorescent dyes will be used to check for any cracks. The final step in the assembly is to paint the aircraft and apply Wings for Aid stickers to the outside. Then the aircraft can be transported to a hangar.

### Deliver System

Finally the aircraft must be delivered to the desired location. Before delivery the aircraft will be prepared by cleaning it, checking oil and tire pressure and disassembling it to fit into a container. Then the aircraft, crew and airbase will be shipped to the customer where it can be assembled again and the mission can be executed.

## 8.3. Production Flow Chart

The production steps in section 8.2 are visually displayed in Figure 8.2. The arrows indicate the order in which the processes take place.
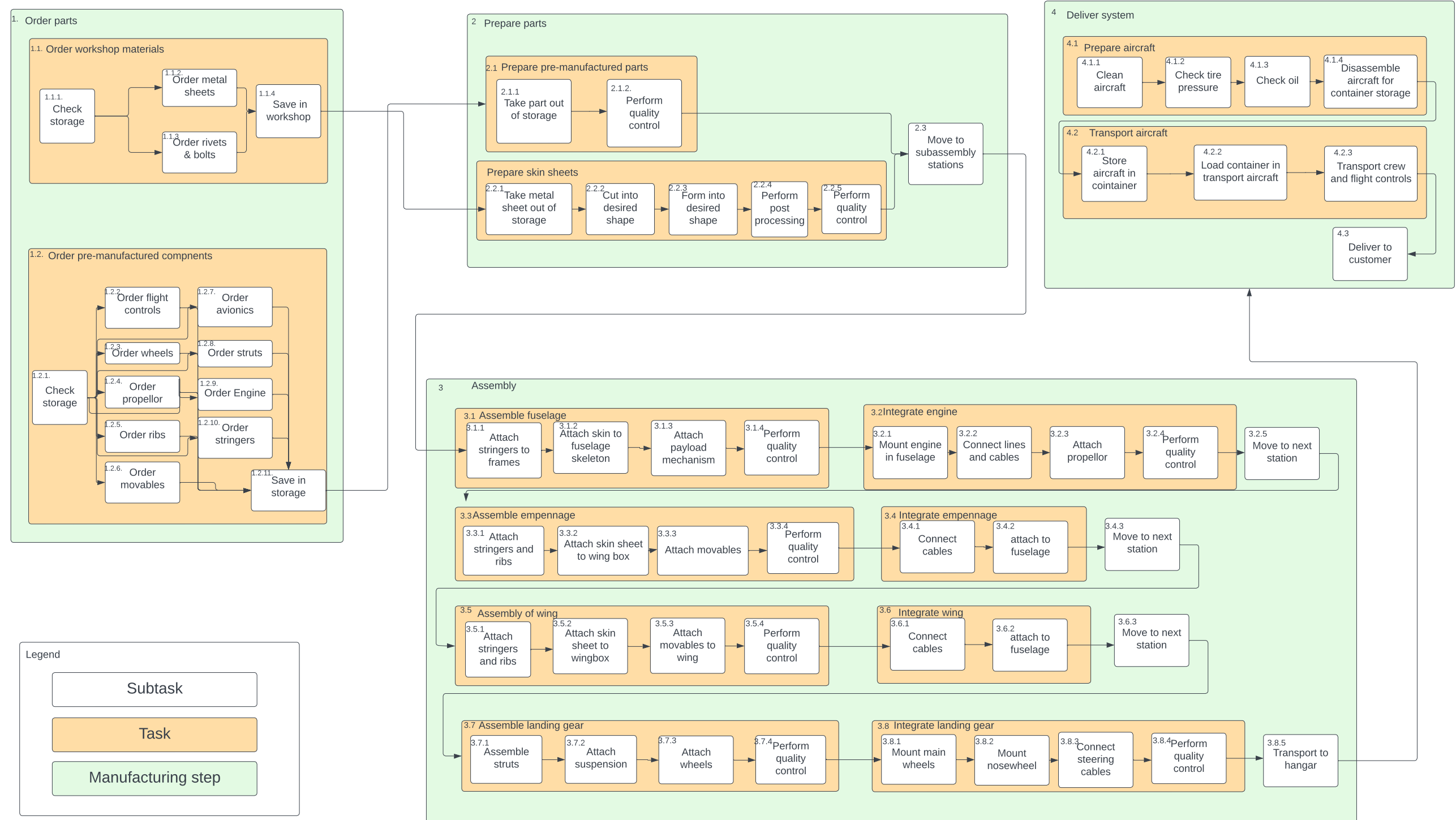
**Figure 8.2:** Production flow diagram

# 9 | Mission Performance Characteristics

This chapter discusses important mission performance characteristics such as: RAMS qualities, resource allocation, technical risk assessment and sustainable development strategy.

## 9.1. Requirement Compliance

The user requirement compliance matrix as requested by the client and the subsystem requirement compliance matrix as imposed by the engineering team are helpful to determine the overall success of the design in reaching the mission goals.

### User, Subsystem and Constraint Compliance Matrix

The compliance matrix is a table containing the user and subsystem requirements, along with the validation methods used to prove requirement compliance. A summary of user and sub-system requirement compliance is documented under Table 9.1 and Table 9.2 respectively. The design constraints compliance matrix is documented in Table 9.3. Requirements which have been complied to will display a green box next to them,as well as their verification method. Requirements that are not complied with will display a yellow box, and those who should be verified as part of post DSE activities display a blue box.

**Table 9.1:** User Requirements compliance matrix

| Requirement ID | Verification method | Check |
|---|---|---|
| WFA-REQ-USE-01 | Aircraft performance analysis as stated in section 7.5 | Yes |
| WFA-REQ-USE-02 | Fuselage design as stated in section 7.1 | Yes |
| WFA-REQ-USE-03 | Fuselage design and mission performance analysis as stated in section 7.1 and section 7.5 | Yes |
| WFA-REQ-USE-04 | Mission description as stated in chapter 2 | Yes |
| WFA-REQ-USE-05 | Cost budget as stated in subsection 9.4.4 | No |
| WFA-REQ-USE-06 | To be calculated during post DSE activities | TBD |
| WFA-REQ-USE-07 | To be calculated during post DSE activities | TBD |
| WFA-REQ-USE-08 | Partial compliance subsection 7.3.4, to be further completed during post DSE activities. | TBD |
| WFA-REQ-USE-09 | Designed to fit in container as stated in chapter 7 | Yes |
| WFA-REQ-USE-10 | Modularity of design as stated in chapter 7 | Yes |
| WFA-REQ-USE-12 | Analysis of the existing deployment mechanism [REF] | Yes |
| WFA-REQ-USE-13 | Camera incorporation with enough 100m fog visibility | Yes |
| WFA-REQ-USE-14 | Landing and take-off performance as stated in section 7.5 | Yes |
| WFA-REQ-USE-15 | Operations and logistics characteristics section 9.2 | Yes |
| WFA-REQ-USE-16 | Mission performance as stated in section 7.5 | Yes |
| WFA-REQ-USE-17 | Operations and logistics characteristics section 9.2 | Yes |
| WFA-REQ-USE-18 | Selected engine requires octane number of 90 as stated in section 7.5 | Yes |
| WFA-REQ-USE-19 | RAMS characteristics as stated in section 9.3 | Yes |
| WFA-REQ-USE-20 | Operations and logistics characteristics section 9.2 | Yes |
| WFA-REQ-USE-21 | RAMS characteristics as stated in section 9.3 | Yes |

**Table 9.2:** Subsystem requirements compliance matrix

| Requirement ID | Verification method | Check |
|---|---|---|
| WFA-UREQ1-SysTe-FP-1 | Mission performance characteristics as stated in section 7.5 | Yes |
| WFA-UREQ1-SysTe-FP-1-1 | Wing structure and fuel integration design as stated in section 7.2 | Yes |
| WFA-UREQ3-SysTe-PD-1 | Fuselage design, mission performance given the payload capacity as stated in section 7.1 and section 7.5 | Yes |
| WFA-UREQ3-SysTe-PD-1-1 | Fuselage design as stated in section 7.1 | Yes |
| WFA-UREQ3-SysTe-PD-1-2 | Fuselage design section 7.1 | Yes |
| WFA-UREQ4-SysTe-SEN-1 | Sensors described in section 7.9 | Yes |
| WFA-UREQ4-SysTe-SEN-2 | Sensors described in section 7.9 | Yes |
| WFA-UREQ4-SysTe-SEN-3 | Sensors described in section 7.9 | Yes |
| WFA-UREQ4-SysTe-SEN-4 | Sensors described in section 7.9 | Yes |
| WFA-UREQ8-SysTe-SB-1 | To be yet verified as part of future DSE plans | No |
| WFA-UREQ8-SysTe-SB-2 | Not as statically stable as a Cessna 172, for the most aft C.G. | No |
| WFA-UREQ8-SysTe-SB-2-1 | Not as statically stable as a Cessna 172, for the most aft C.G. | No |
| WFA-UREQ8-SysTe-SB-2-2 | Lateral stability will be performed post-DSE | No |
| WFA-UREQ11-SysTe-FP-1 | Comparison between UH-1 helicopter condition to be performed during post DSE activities | TBD |
| WFA-UREQ11-SysTe-FP-1-1 | Gust speed calculations performed section 6.3 | Yes |
| WFA-UREQ11-SysTe-FP-1-5 | Take-off and landing performance analysis as stated in chapter 7 | Yes |
| WFA-UREQ11-SysTe-FP-1-7 | Take-off and landing assumed to occur in wet grass (worst conditions) | Yes |
| WFA-UREQ12-SysTe-FP-1 | Mission performance analysis constrained drop altitude to be 50 m above ground | Yes |
| WFA-UREQ12-SysTe-PD-1 | Consultation with WFA lead engineer | Yes |
| WFA-UREQ12-SysTe-PD-2 | Consultation with WFA lead engineer | Yes |
| WFA-UREQ13-SysTe-FP-1 | Use of sensors and camera to aid pilot during landing & takeoff as stated in section 7.7 | Yes |
| WFA-UREQ17-SysTe-PD-1 | Operations and logistics as explained under section 9.2 | Yes |
| WFA-UREQ17-SysTe-PD-1-1 | SORA approach as documented under section 9.6 | Yes |
| WFA-UREQ20-SysTe-PD-1 | Mission capacity discussed in section 9.2 | Yes |
| WFA-REQ-SysTe-CT-1 | As explained in chapter 7 | Yes |
| WFA-REQ-SysTe-CT-1 | As explained in chapter 7 | Yes |
| WFA-REQ-SysTe-CT-1-2 | As explained in chapter 7 | Yes |
| WFA-REQ-SysTe-FP-3 | Rate of climb characteristics as stated in chapter 7 | Yes |
| WFA-REQ-SysTe-FP-4 | Take-off performance characteristics as stated in chapter 7 | Yes |
| WFA-REQ-SysTe-FP-5 | Landing performance characteristics as stated in chapter 7 | Yes |
| WFA-REQ-SysTe-FP-6 | Screen height designed for take-off and landing chapter 7 | Yes |

**Table 9.3:** Design constraints compliance matrix

| Requirement ID | Verification method | Compliance |
|---|---|---|
| WFA-UREQ5-SysCo-FI-1 | The aircraft's unit cost documentation documented in subsection 9.4.4 | No |
| WFA-UREQ9-SysCo-DIM-1 | Outer dimensions of disassembled aircraft in chapter 7 | Yes |
| WFA-UREQ9-SysCo-DIM-1-1 | Detachment points discussed in section 7.2 and section 7.3 | Yes |
| WFA-UREQ14-SysCo-OP-3-1 | Wet grass considered for take off and landing section 6.6 | Yes |
| WFA-UREQ15-SysCo-TI-1 | Operation breakdown in section 9.2 | Yes |
| WFA-UREQ15-SysCo-TI-1-1 | Operation breakdown in section 9.2 | Yes |
| WFA-UREQ15-SysCo-TI-1-2 | Model uses given cruise speed in section 6.6 | Yes |
| WFA-UREQ16-SysCo-OP-5 | Model uses cruise altitude of 500 m in section 6.6 | Yes |
| WFA-UREQ18-SysCo-OP-1 | Engine selected in section 7.5 | Yes |
| WFA-UREQ18-SysCo-OP-1-1 | Engine selected in section 7.5 | Yes |
| WFA-UREQ19-SysCo-OP-6 | Operation breakdown in section 9.2 | Yes |
| WFA-REQ-SysCo-TI-1-2-1 | Engine selected in section 7.5 | Yes |
| WFA-REQ-SysCo-TI-1-2-2 | As explained in section 6.4 | Yes |
| WFA-REQ-SysCo-TI-1-2-2-1 | Aeroelastic effects to be investigated during future DSE plans | No |
| WFA-REQ-SysCo-TI-2 | Operation breakdown in section 9.2 | Yes |
| WFA-REQ-SysCo-TI-2-1 | Operation breakdown in section 9.2 | Yes |
| WFA-REQ-SysCo-TI-2-2 | Operation breakdown in section 9.2 | Yes |
| WFA-REQ-SysCo-OP-2 | The aircraft shall be an unmanned aerial vehicle | Yes |
| WFA-REQ-SysCo-OP-2-1 | Aircraft architecture shown in section 7.7, section 7.9 | Yes |
| WFA-REQ-SysCo-OP-3-2 | Wet grass considered for take off and landing section 6.6, better quality runway decreases rolling distance | Yes |
| WFA-REQ-SysCo-OP-4 | Maintenance of high risk elements described in section 9.3 | Yes |
| WFA-REQ-SysCo-SA-1 | Aircraft architecture shown in section 7.7, section 7.9 | Yes |
| WFA-REQ-SysCo-SA-2 | Flight planning described in section 9.2 | Yes |
| WFA-REQ-SysCo-SUS-1-1 | Aircraft production emissions to be calculated during post DSE activities | TBD |
| WFA-REQ-SysCo-SUS-1-2 | Aircraft emissions during standard mission as documented in section 7.10 | Yes |
| WFA-REQ-SysCo-SUS-1-3 | End of life emissions of aircraft handling procedures to be calculated during post DSE activities | TBD |
| WFA-REQ-SysCo-SUS-2 | Aircraft recyclabylity to be assessed during post DSE activities | TBD |
| WFA-REQ-SysCo-SUS-2-1 | Aircraft recyclabylity to be assessed during post DSE activities | TBD |

# 9.2. Mission Operation and Logistics

## 9.2.1. Grand Scale Mission Planning

Before airplane can be loaded and landing strips can be used, the mission must be planned on a much bigger scale. The planes are stored and maintained in a hangar somewhere in the world until the delivery services are needed. To structure the work that needs to be done before and after the mission, 9.1 was created. In this diagram the external sources and dependencies are given in the light-blue boxes. The steps under the deploy base block should also be performed in roughly the prescribed order as for example assembling the aircraft in an open field is not recommended. The preparations can be performed simultaneously, but the work plan is create to show what the planing is for the mission deployment.
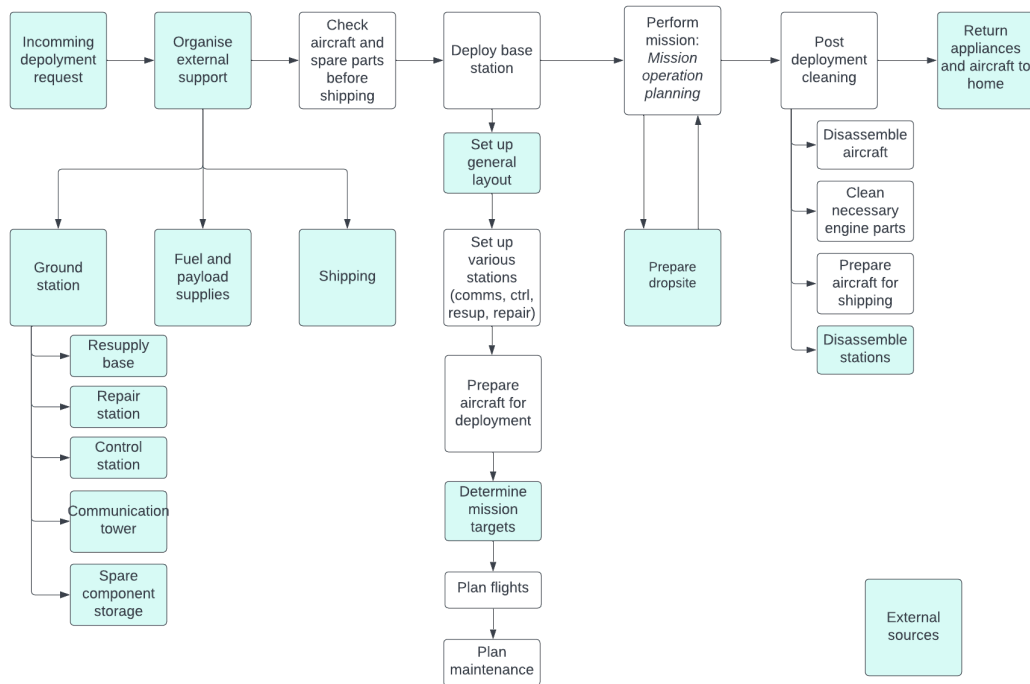
**Figure 9.1:** Mission organisation work plan

Note that the *mission operation planning* is written in italics. This is because it references to the next section in which the operation of the mission is planned out. Furthermore the block *Clean necessary engine parts* can be seen. The necessary references to the certain parts of the plane that require cleaning after operation, such as the engine, fuel tanks, hydraulics and parts that can get dirty such as the tyres. Avionics and other electronics usually do not perform well after being exposed to water, so it would be recommended to clean these parts.

During a meeting with the client the deployment strategy was discussed. It was found that during the off time, the time that the drone will not be used for aid programs, the aircraft are used as commercial delivery drones. This can be done at multiple places in the world. However whenever the drones are needed for aid delivery, the commercial operation will be stopped. From an organisational standpoint there are certain places in the world which could help the transport speed. Places such as Florida, South Africa, Italy, Spain or India have central locations with access to airports or harbours. Taking into account the flight time and loading and unloading of the drones it may take up to 12 hours to transport drone with an aircraft. Noting that the operational cost of a C17 Globemaster transport aircraft is $ 23,811 [38]. This means that using a C17 for 12 hours costs 288,000 dollars. Since this is only for the first few planes, shipping the complete operation with airplanes may prove to be a financial bottleneck. To avoid this, a large part of the mission may be shipped by ocean. Shipping on ships is cheaper and allows for large containers as well, but the travel time is significantly longer. For example a trip from Melbourne to Jakarta, which may be a disaster struck zone, will take 6 to 8 days over seas. With this option available it is most optimal for the first containers to be transported by plane, to set up a base camp and start emergency deliveries. In one or two weeks containers with the rest of the fleet may arrive. In this way the financial cost can be limited while preparing of the base may already start. It seems like a good option as the fleet size is 32 and shipping 32 drones by plane would take 4 round trips and may cost more than a million dollars. This is not viable and the plan to split up the shipment between plane and ship is financially more interesting.

For the drones 20ft containers are used for transport. As an immediate response to an emergency planes would rather be used for transport than ships. If a standard military transport plane as used, a Boeing C17 Globemaster III will be the transport aircraft. The cargo hold of the Globemaster has dimensions of 5.48 by 26.82 meters with a height of 3.76 meters and a maximum payload weight of

77519 $kg$ [5]. This means that 8 20ft containers can be placed in the cargo hold. With an empty mass of the drones of 403 $kg$ and an empty mass of 2180 $kg$ for the container the total mass of this combination is 2583 $kg$. This means that 8 containers weigh 20664 $kg$ which is well within the payload capacity of the C17. Even if the 2583 $kg$ is considered very lean and the weight doubles per container, the total weight, 41382 $kg$, can still be transported with a C17. It is recommended to send the first two deliveries of drones by plane. This also includes all equipment for the forward operating base, the base that is used by the aircraft to operate from. This means that 10 to 12 aircraft can be airlifted for half a million dollars as the emergency response. The other 17 aircraft, which are calculated in subsection 9.2.3, can be transported by ship. This is cheaper and as the operating base is not finished yet, there is no advantage of having 29 airplanes collecting dust while the base is being constructed.

## 9.2.2. Mission Operation Planning
To estimate the time that a full mission takes, a mission planning was created. A block diagram was used to plan the mission. This diagram can be found in Figure 9.2 . It can be seen that the mission has some loops or side paths. This makes it difficult to give and an exact answer on the mission planning as it depends on the deployment. For example the number of drop zones that are planned along the flight path can be as high as the number of aid packages. It could also be that all packages are only dropped in one or two locations. The variation in this means that no 100 % accuracy can be provided.
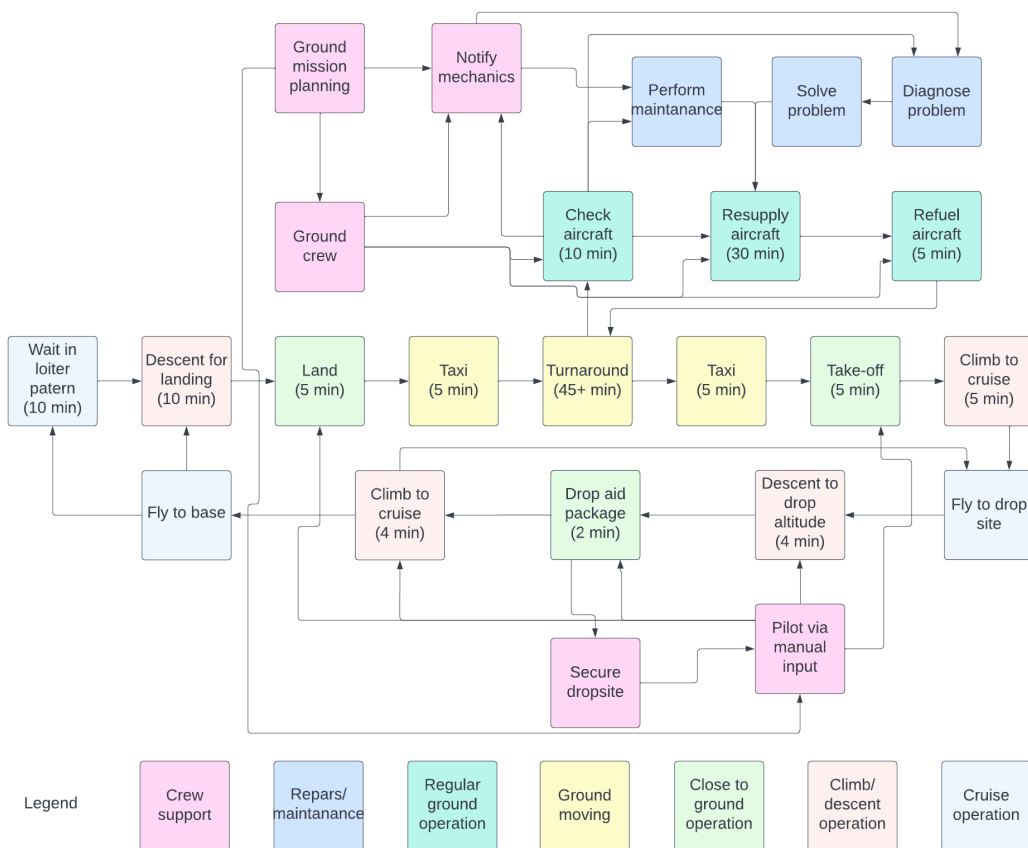


**Figure 9.2:** Mission operation planning

To estimate the time the mission would take, the time it would take to fly the mission was needed. This came from an iteration and a close analysis of the flight planning in Table 7.20. With the iteration the mission would take 5.45 hours. With this mission time 4.40 missions can be executed per day. This means that during one day one airplane can drop 200 $kg$ of aid 4.40 times per day and thus drops 880.73 $kg$ of aid per day. If the dropping capacity requirement of the C-130 Hercules, 20,000 $kg$, must be matched, the whole fleet must consist of 23 aircraft which all operate 24 hours per day.

### 9.2.3. Ground Organisation Planning

The timeline must also be organised with maintenance in mind. Some time will be used for repairs or maintenance. Since no maintenance times are known, it is derived from the an information letter of Continental Motors in which it is recommended to do an overhaul every 1,200 to 2,000 hours [12]. This information can be combined with the time it takes to do one overhaul. Not much information can be found on this from big companies, however multiple private websites have information on the overhaul time. The estimates range from 15 to 25 hours [6], [46], [9]. Note that this is an estimate from car engines which are more difficult to access. However this extra time also evens out with the extra time spend on the aircraft for working on other subsystems, such as avionics or control surfaces. Dividing these numbers, 15 by 1200 and 25 by 2000, results in 1.25 hours of service per 100 hours of flying. This means that after 19 flights the aircraft will be serviced. As 23 aircraft all do their trips in 4.70 hours, one aircraft will take-off each 14.22 minutes, if drones are not swarming. If a service takes 1 hour to perform, 5.28 aircraft cannot take-off because of it. This means that the fleet should be expanded with an additional 6 aircraft, bringing the total fleet size to 29 aircraft, of which 6 are back-up or spare. They can be used in regular planning, but this will temporally decrease the mission capacity when services are performed. For this reason they are considered spare or back-up aircraft and only perform instead of another aircraft.

It should also be noted that if 1 aircraft takes off every 14.22 minutes, one aircraft also lands every 14.22 minutes. This means the runway will be used for landing or take-off every 7.11 minutes. However if the aircraft are deployed in swarms, they may take-off and land within seconds of each other. This may cause the need to revise the ground base resupply station. If a swarm of 5 aircraft is used, the current base size will be sufficient. It is recommended to reevaluate the ground base once the swarm capabilities determined. Though this swarm size is not sized, as it depends on the user needs and the auto pilot of the airplane, some notes on this swarm performance can be made. In the stability analysis, subsection 7.3.4, it was shown that the aircraft is stable in Dutch roll. Though a more thorough analysis is needed in the future, this stability can influence how close airplanes can stay together in swarm. Unstable airplane should not be close to other airplane to avoid possible mid-air collisions. Next to that the sensors on board of the aircraft need to be accurate enough to know where the other airplanes are so it can avoid them. All these subsystem designs and analyses have to be performed in the future to prove that the airplane is completely capable of swarm deployment.

The capacity of the resupply station can also be calculated now. As calculated it takes 45 minutes to check, resupply and refuel the aircraft and it takes 4.70 hours for the aircraft to perform their mission. This means 23 aircraft are supplied every 4.70 hours. With one station which takes 0.75 hours to resupply the plane, only 7.27 planes can be resupplied. To match the flow of planes the station should have a capacity of 3.17 planes. Rounding up and adding one extra for safety means that the resupply station should have a capacity of 5 planes at the same time to match the mission timeline.

Next to a resupply station the ground station also needs a communication station to the aircraft. This includes a communications relay with a tower to improve the communication range and a control base from which the airplanes are controlled. These can be transported in containers just as the aircraft are. This means that for the complete ground station 3 to 4 containers are needed, 2 for the communication station and an additional 1 or 2 for the tents of the resupply station.

### 9.2.4. Temporary Landing Strip Deployment

Runway quality is a driving characteristic that determines the performance of the aircraft at both take-off and landing. When the system is deployed in a new location, suitable places for the forward operating base must be located. These locations must have a general proximity that is close to a range of affected communities within the $250\ km$ radius. Operating out of existing infrastructure is desirable as it requires low levels of preparation as well as already contains multiple facilities needed for the mission. Existing infrastructure can be defined as a preexisting surface that has specifically been assigned for the purpose of aircraft take-off and landing. However sometimes operating out these locations presents additional challenges such as navigating the controlled airspace and interacting with external aircraft. Furthermore this existing infrastructure may not always be available for the full duration of the mission. Therefore an advance temporary landing strip that can be quickly deployed in a variety

of environments must be investigated and designed. Considering the environment, infrastructure and access to specialised tools, an assessment of the location can be performed and an specific solution can be formulated. In Table 9.4, ground friction coefficients for a variety of different surfaces are listed. Lower friction coefficients for free roll lead to lower take-off distances, while higher values for braking lead to lower landing distances. These values demonstrates how performance of the aircraft will change based off of the runway conditions. For take-off the free roll coefficient is taken and it is preferred that it is a low as possible. While during landing the braking coefficient is used and a high coefficient is preferred. For both manoeuvres wet grass is the worst ground surface.

**Table 9.4:** Ground surface friction coefficients [18, p.795]

| | Ground Friction Coefficient $\mu$ | |
|---|---|---|
| **Surface Type** | **Free roll** | **Braking** |
| Dry Asphalt | 0.03-0.05 | 0.3-0.5 |
| Wet Asphalt | 0.05 | 0.15-0.3 |
| Icy Asphalt | 0.02 | 0.06-0.1 |
| Hard Turf | 0.05 | 0.4 |
| Firm Dirt | 0.04 | 0.3 |
| Soft Turf | 0.07 | 0.2 |
| Wet Grass | 0.08 | 0.2 |

Considering available airports and runway strips, these can be used as locations for the forward operating base; typically runway strips will be built utilising either hard asphalt or firm dirt. Domestic airports that have high traffic are not desirable as they limit the amount of possible landings per day. Once the delivery area is identified, operators can search for areas that are usable; these will include flat, smooth areas of preferably dirt or short grass. This method is however only applicable when environmental conditions are optimum. Utilisation of dirt runways is not always desirable, especially if the aircraft must perform the respective mission through seasons of especially high rain and bad weather. These Dirt runways can erode easily as well as become muddy, which will prevent continued operation of the mission. Furthermore, runways that deteriorate to this state, force the operator to be more careful during take off and landing; increasing the distance for take off and landing.

When considering the long term application of the aircraft in an environment that is heavily affected by natural or humanitarian disasters, the need for an advance temporary landing strip may become apparent. The natural surfaces may be damaged and unusable to the point that an additional surface must be placed on top to create a proper runway. Furthermore in a long term operation, the frequent use of the runway by multiple aircraft in a swarm solution will cause significant degradation based off the quality of the ground surface. The most common ground surfaces available will be dirt, clay, grass and gravel. The surface layer will constantly change after multiple operations, leading to a very high runway maintenance. Therefore alternative materials that can be laid on top of or Incorporated into the ground material will provide higher runway quality characteristics and decreased operating costs. This runway is to be utilised in long term operations or when no temporary runway can be identified within the operational zone.

There are already pre-existing solutions designed by the military for this application. Therefore a range of ideas can be sourced from literature. During World War 1, 2 and the Vietnam war, the American military developed landing strip solutions that were cheap and rapidly deployable. Commonly referred to as advance landing ground or ALG, these systems involved multiple sections of metallic panels joined together. These sections of metallic panels are quickly deployable by an onsite operator; sections are linked together to from a desired length, width and afterwards are secured down through steel stakes. Furthermore these flat panels are stackable on a standard transport palate, which can then be flown and driven to the forward operating base. Not only would the use of this type of runway reduce maintenance and operation costs, it would also reduce the need for substantially large landing gear improving weight and drag characteristics. It is recommended that further design is conducted on this type of runway, or a partnership with pre-existing companies specifically working on this product be established. Faun Trackway presents an interesting solution, which can be seen in both the stacked and assembled states

in Figure 9.3 and Figure 9.4 respectively.



**Figure 9.3:** Stacked Runway Panels [44]



**Figure 9.4:** Assembled Temporary Runway [44]

### 9.2.5. Data Handling Block Diagram

The aircraft will need to communicate with the ground station. It should also be able to perform missions or parts of a mission by itself. To achieve this the aircraft needs to know certain things about itself, altitude, attitude, airspeed, location and various other parameters. Though the exact design of this avionics system will be decided later, the handling of the produced data will be discussed here. In 9.5 the data flow between the aircraft and the ground is described.
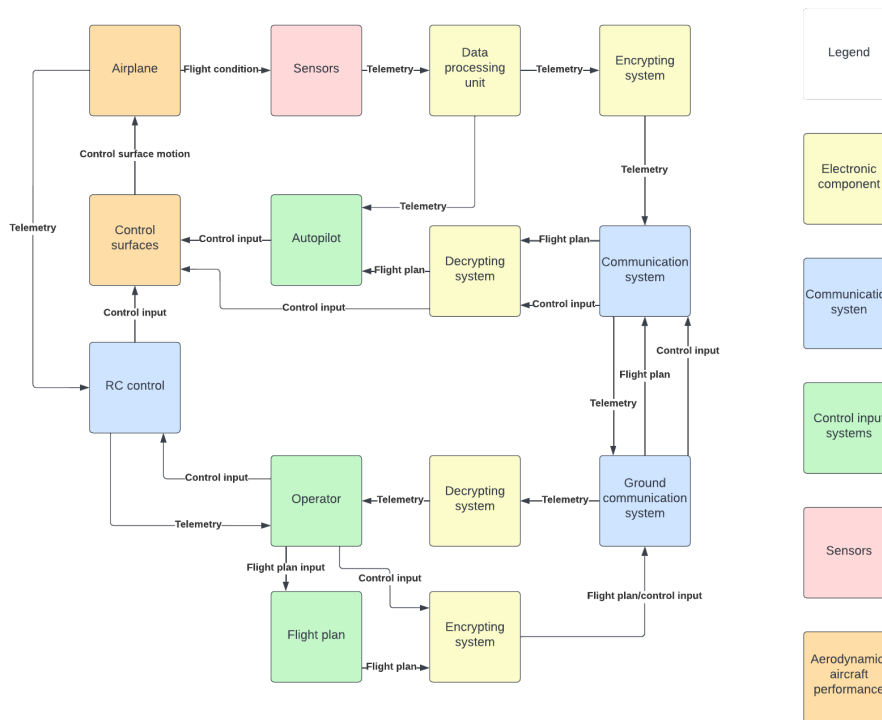


**Figure 9.5:** Data handling diagram

The different types of subsystems are each given a different color as can be seen in the legend. Since it is unknown how much data flows through the whole system, the type of data is presented. Note that there are multiple ways to control the aircraft. For automatic flight the pilot can upload a flight plan to the drone and the autopilot will adhere to this plan. A direct control is also possible. This means that the aircraft is directly controlled by a pilot. This can be done through the same long range system as for the flight plan or it can be used on take-off and landing via an radio control (RC) connection. With an uploaded flight plan the aircraft can control itself. The loop of the autopilot to the data processing unit through the aircraft can be build in such a way that the autopilot will execute the flight plan while

controlling the aircraft. If this is done with a locally installed autopilot, the plane can also operate without communication to the mission base. This, however is undesirable, since the location and course of the aircraft would be unknown. Therefore, a link to the aircraft must be established at all times. To explain the diagram, the subsystems are listed below with a short description.

- Airplane: The plane with certain behavioural characteristics
- Control surfaces: Ailerons, flaps, elevator, rudder, engine control. All systems used to control the aircraft
- Autopilot: On board autopilot programmed into the flight computer. Shall be able to work without communication
- Sensors: Measuring the behaviour of the aircraft
- Data processing unit: Unravels the outputs from the sensors and organises the output for quick use in the other subsystems
- Encrypting/decrypting systems: Package/open the data in encrypted format for safe and robust communication. Reduces chance of hacking and loss of communication
- Communication system: The antenna/other communication system on board the aircraft
- Ground communication system: The communication system on the ground
- Operator: The pilot/flight planner that decides the next move of the aircraft. Pilot may also land the aircraft
- Flight plan: Predetermined route the aircraft will follow. Also includes drop locations. Is uploaded to the plane before flight, so no communication is necessary for the mission
- RC control: For close range control Radio Control will be used

# 9.3. RAMS

In order to give the operator an understanding of the potential faults of the aircraft and its operations, including the mitigation tasks performed to overcome these, details regarding reliability, availability, maintenance, and safety are provided in this section.

## 9.3.1. Reliability

When estimating the reliability of a system, ideally a large sample size of similar systems would be needed, which provides data on their performance over time. This way, the reliability can be calculated empirically based on the number of systems that have failed over their lifetime. This data however may not be available, which would mean that the only way left of estimating the reliability of the system is qualitatively. It is therefore important to have redundancies in place so that no single point of failure exists.

**Airframe**

When adequately designed and built, the airframe will withstand all loads during operation without failing. Fatigue is usually the main cause of damage to the airframe. However the number of cycles before failure can be approximated through study of the materials used. Through maintenance and inspection, risk of failure of the airframe due to fatigue during flight is mitigated . What could cause damage to the airframe is unforeseeable external factors, such as bird strikes, heavy hailstorms, enemy fire, etc. One place that is more prone to failure is the joint where the wing tips detach from the main wing.

**Landing Gear**

Even though the landing gear is used for only a couple of minutes per flight, it is a critical system, because faults there can very quickly cause failure and even the destruction of the aircraft. After meeting with the client, it was established that the landing gear of the current Mini Freighter design is particularly susceptible to breaking and lead to the loss of a drone. Therefore, apart from being overdesigned, the landing gear will also be thoroughly tested before production starts. Drop tests are a common way of testing landing gears.

**Ground Control System**

Being on the ground, the opportunity to perform maintenance on the control station is always present. It is also possible to have more redundant subsystems than on the drone, since there is no mass constraint. The ground station is therefore the most reliable part of the mission.

**Engine**

Being the system with the most moving parts and operating at the harshest conditions (high temperatures and pressure), the engine is (one of) the most likely system(s) to fail unpredictably. Inspection after each flight will improve the confidence in the engine. Four stroke engines, like the one that is chosen have more moving parts compared to two stroke or Wankel engines and are therefore less reliable. Still, modern engines are relatively robust, with failure rates between 1 in 1000 and 1 in 10,000 flight hours according to the FAA[39].

**Avionics**

Since the avionics system includes the electrical components, as well as sensors, wiring, actuators and power source, redundant subsystems need to be implemented, such as a backup cable harness in case the wiring fails, a backup power supply and alternative sensors which can provide the necessary data for flight in case individual sensors fail.

## 9.3.2. Availability

Availability describes the time during which the aircraft operates and fulfills its mission. This depends mostly on how much time the aircraft is grounded. In order for the mission to be as time efficient as possible, the down time, or unavailability, should be as low as possible. Maintenance is the primary reason for unavailability. It is important to note that the maintenance is performed in order to improve the reliability of the system. subsection 9.3.3 further elaborates on the maintenance process.

## 9.3.3. Maintainability

In order to ensure that maintenance can occur efficiently and in a low-cost manner, the aircraft has to be designed accordingly. One way in which the aircraft is designed to allow for ease of maintenance is the modularity of its different parts. By allowing parts to be easily taken out, replacement of parts when subject to damage can be done quickly.

In addition to designing for an easily maintainable aircraft, an outline of the different maintenance activities needs to be generated. Since the aircraft being designed has to fly multiple times in a day, maintenance is necessary in order to ensure the mission can always be performed without failure of any aircraft components. However, as stated by user requirement WFA-REQ-USE-19, the aircraft shall have a 24/7 operational window. Therefore, the aircraft cannot afford to be under maintenance for long or else its availability will be hindered. Furthermore, the maintenance costs may be too high if maintenance is conducted too frequently which will increase the operational cost of the aircraft and may lead to a violation of user requirement WFA-REQ-USE-06. It can thus be said that a balance should be achieved with respect to the amount of maintenance that the aircraft being designed should be subject to. Regardless, both corrective and preventive maintenance strategies have been adopted and designed in a way such that the mentioned user requirements are considered.

In general, regular preventive maintenance shall be adopted in order to ensure that failure of any of the critical aircraft subsystems/parts is avoided. For this reason, it is planned that corrective maintenance shall not occur often. In the case that the aircraft does experience an unexpected failure of any of its parts, replacement of parts shall be accommodated as a result of the modularity of the aircraft design. By having many of the aircraft parts being interchangeable, the replacement of parts is a relatively quick process and the hindering of availability is minimised.

As for preventive maintenance, both calendar-based and condition-based strategies will be adopted. As for the calendar-based approach, generally maintenance checks are broken down into different groups which vary depending on frequency of checks and activities done. These groups are: line maintenance checks, A-checks, B-checks, C-checks, and D-checks[1]. In addition, pre-flight checks are often considered too which are more frequent and less thorough than line maintenance checks [3]. In order to ensure high availability of the aircraft only pre-flight checks, line maintenance checks, B-checks, and D-checks will be considered for the aircraft with regards to calendar-based preventive maintenance. This is acceptable as B-checks incorporate the activities of A-checks [3] and the activities of D-checks

---

[1]URL: https://www.naa.edu/types-of-aviation-maintenance-checks/ [cited 31 May 2022]

are more thorough while less frequent than C-checks [3]. To explain what these maintenance checks are and what they entail:

- Pre-flight checks: These are maintenance checks that occur before every flight and only include a simple visual inspection by the mechanics and pilots[3]. For this reason, only the main structural components will be inspected to ensure no obvious cracks are present before flight.

- Line maintenance checks (Daily checks): These are regular inspections that occur every 24-60 hours of flight time [2]. As each designed aircraft of the fleet is expected to fly close to this range on a daily basis, line maintenance checks are planned to be conducted daily during night. As for the activities performed during line maintenance, inspection of the aircraft filters (air and fuel) will be done. In addition, checking of the aircraft wheels and brakes will be done as well as an inspection of the aircraft oil and hydraulics fluid levels as suggested by the National Aviation Academy [3]. Moreover, the avionics will be inspected to ensure that all of them are calibrated correctly.

- B-checks: These maintenance checks occur every 750 flight hours and are also a lot more thorough than the previously mentioned types of maintenance checks [3]. In this case, B-checks will include a more thorough inspection of the main structural components to check for cracks, corrosion, and any deformations. Furthermore, recommended B-check activities will be done such as engine oil spectra analysis and part lubrication [3].

- D-checks: This form of maintenance check is done every 20,000 flight hours and is the most thorough form of maintenance[3]. This form of maintenance involves heavy inspections and a repair of the entire aircraft is done [4].

As previously mentioned, condition-based strategies will be considered in combination with calendar-based maintenance. The reason this is done is to be more time efficient with maintenance by avoiding unnecessary maintenance and thus increasing the availability of the aircraft. Condition-based maintenance is a strategy whereby the condition of a part is monitored and based on its results maintenance may occur. Since calendar-based maintenance is still being conducted, condition-based maintenance is planned to only be performed for critical aircraft components. Therefore, important components (those which lead to mission failure if the component fails) and those subjected to high loads are considered. Therefore, the components that will be checked with condition-based maintenance are: the engine, propeller blades, the wing, the empennage, and the landing gear. As for how monitoring of these different components will be conducted, different sensors will be equipped depending on the component. For the engine, sensors will be equipped to monitor the temperature, noise and exhaust levels. For structural components and the propeller blade, sensors will be equipped that monitor for cracks (visually), vibrations, and sound. If any of these sensors detect abnormal readings, the need for maintenance will be signalled.

A table outlining the different aircraft components and the different maintenance checks applied can be found in Table 9.5.

**Table 9.5:** Maintenance checks on different aircraft components (PF = pre-flight, LM = line-maintenance, B = B-checks, D = D-checks, CB = condition-based).

| Component | Maintenance Check |
|---|---|
| Airframe | PF, B, D |
| Wings | PF, CB, B, D |
| Empennage | PF, CB, B, D |
| Landing gears | PF, LM, CB, B, D |
| Engine | LM, CB, B, D |
| Propeller blades | PF, CB, B, D |
| Hydraulics | LM, D |
| Avionics | LM, D |

[2]URL:https://www.naa.edu/types-of-aviation-maintenance-checks/ [cited 31 May 2022]
[3]URL: https://www.naa.edu/types-of-aviation-maintenance-checks/ [cited 31 May 2022]
[4]URL:https://www.naa.edu/types-of-aviation-maintenance-checks/ [cited 31 May 2022]

### 9.3.4. Safety

In order to improve both the reliability and safety of the aircraft, redundancy is incorporated for a number of the aircraft subsystems. This ensures that continued operation of the aircraft can occur in the case of subsystem failure. The reason why redundancy is not incorporated for every aircraft subsystem is due to the additional weight that redundancy adds. For this reason, redundancy was added to the design of the aircraft based on which subsystems aircraft generally add redundancy for and which subsystems are more critical regarding its functioning.

As for where redundancy is typically added to aircraft, additional sources of electricity and hydraulics are typically included in addition to redundant software [5]. As the aircraft is expected to have many electrical components, and the landing gear of the aircraft is considered a critical component whereby hydraulics are used to control the landing gear, redundancy for both sources of electricity and hydraulics are required. As for software, since the aircraft is a UAV, redundancy is a necessity to ensure loss of control never occurs. This is generally done by implementing two of the same type of software created by different manufacturers [6].

For the aircraft being designed, the landing gear is considered a critical component/subsystem. This is reasoned because the aircraft is expected to take-off and land on poor quality landing strips. This makes the landing gear more susceptible to failure due to the large loads and debris expected to be encountered with such landing strips. Therefore, redundant systems generally considered for this component will be implemented for the aircraft. This includes an emergency landing gear release and emergency braking [7].

For additional safety measures, a flight termination system is designed as a contingency in case the aircraft is compromised or veers off of the allocated flight path. It can be either automatically triggered, in case the aircraft exits its flight corridor or loses communication for an extended period of time, or manually activated by the operator.

## 9.4. Resource Allocation

To ensure that the project can be continued after the preliminary design phase, it is important to demonstrate that the budget is not exceeded in terms of the available resources. Enough margin should be given so that in case more resources are needed in a certain domain, e.g. detailed design shows that the OEW will increase, the aircraft is still a feasible design.

### 9.4.1. Mass Budget

During the detailed design of the aircraft, the weights of the various systems were updated to more accurate and reliable estimates compared to the Class II weight estimation. Since one of the key requirements is for the aircraft to have a maximum weight of $750\ kg$, the difference between this number and the maximum take off mass will give us the margin. Table 9.6 shows the mass budget breakdown, which shows that the margin left is $157\ kg$, which is $26.5\%$ of the current maximum take-off mass. The weight of the avionics system was estimated in section 7.7 and section 7.8.

---

[5]URL: https://medium.com/swlh/forget-about-the-cost-aircraft-systems-redundancies-to-the-rescue-2a2b77c99110 [cited 31 May 2022]

[6]URL: https://medium.com/swlh/forget-about-the-cost-aircraft-systems-redundancies-to-the-rescue-2a2b77c99110 [cited 31 May 2022]

[7]URL: https://orschelnproducts.com/redundant-aircraft-systems/ [cited 31 May 2022]

| Element/System | Weight [kg] |
|---|---|
| Wing | 42.4 |
| Fuselage | 52.3 |
| Empennage | 16.5 |
| Avionics | 64 |
| Undercarriage | 15.3 |
| Power system | 142.5 |
| Fuel | 59.6 |
| Payload | 200 |
| Total | 593 |
| Margin | 157 |

**Table 9.6:** Mass budget

### 9.4.2. Power Budget

Apart from the mechanical power needed for the propulsion of the aircraft, electrical power is also needed for the avionics onboard. It is therefore necessary to estimate the power needed by every component to ensure that the engine can provide enough power for both the propulsion and avionics. Actuators for the control surfaces and the steering of the nose gear will require most of the electrical power, therefore it is important to correctly estimate the control forces. Based on available products that deliver the required accuracy, functionality and performance, the following table was generated:

| Component | Power required [W] | Brand | Note |
|---|---|---|---|
| Camera | 4 | GoPro[8] | |
| GNSS | 0.2 | UAVOS[9] | |
| Telemetry module | 2.4 | | |
| Navigation computer + magnetometer + IMU + compass | 2 | | |
| Autopilot | 2.5 | UAV Navigation [10] | |
| Transponder | 11 | Sagetech XPC Mode S Transponder [11] | |
| Linear actuator | 63 | Robotzone 115 lb Thrust Linear Servo [12] | Probably over-powered |
| Servomotor | 94 | HS-1100WP Servo [13] | Probably over-powered |
| Total (incl. 5 servos) | 555.1 | | Conservative estimate |

**Table 9.7:** Power budget

From Table 9.7, the power required from the alternator will be roughly $0.56 \ kW$. Even though this number is highly overestimated (since the servo considered is likely too powerful and every component consumes maximum power at the same time), it is still relatively low compared to the power required for flight. However, it should be taken into account when estimating the fuel needed for a flight.

### 9.4.3. Drag Budget

From the determination of the drag coefficient conducted in subsection 6.2.4, values for the zero-lift drag coefficient of the main aircraft components was found. At the start of the project, a contingency margin of $20\%$ was taken as less accurate methods were used. At the current stage of the design, more accurate methods for estimating the aircraft drag coefficient is used and thus the contingency margin

---

[9]https://gopro.com/en/us/shop/cameras/hero10-black/CHDHX-101-master.html
[10]URL: https://www.uavos.com/images/brochures/AP10.1Datasheet$_R03 - 2021 - 900MHz.pdf$
[11]URL: https://www.uavnavigation.com/products/autopilots/vector-600
[12]URL: https://sagetech.com/transponders/xpc/
[13]URL: https://www.servocity.com/12-stroke-115-lb-thrust-linear-servo/

was reduced to $15\%$. These values can be found documented in Table 9.8 and displayed as a pie chart in Figure 9.6 to show the relative contributions toward the total aircraft zero-lift drag coefficient.

**Table 9.8:** Contribution of different aircraft components to zero-lift drag coefficient including $15\%$ margin

| Component | $C_{D_0}$ contribution | $C_{D_0}$ contribution with 15% margin |
|:---:|:---:|:---:|
| Wing | 0.00972 | 0.0112 |
| Horizontal Tail | 0.00129 | 0.00149 |
| Vertical Tail | 0.000850 | 0.000978 |
| Fuselage | 0.0116 | 0.0134 |
| Landing Gear | 0.00590 | 0.00678 |
| Excrescence and Leakage | 0.00294 | 0.00338 |
| **Total** | 0.0323 | 0.0372 |
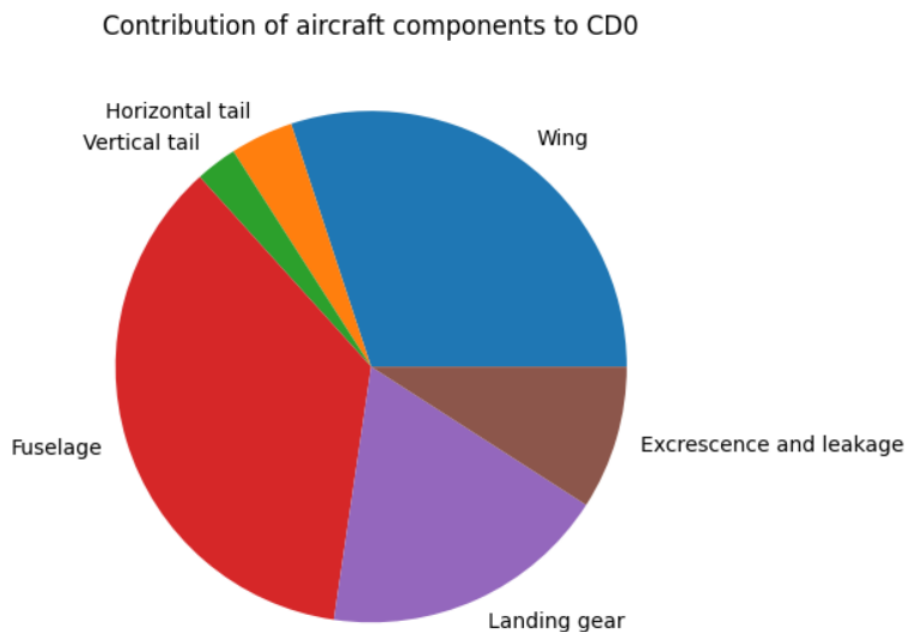


**Figure 9.6:** Pie chart displaying contribution of different aircraft components to zero-lift drag coefficient of aircraft

## 9.4.4. Cost Budget

It is important to obtain a more accurate cost estimate compared to the one performed in the midterm report [25]. To do that, we can look up the price of of-the-shelf parts and components that deliver the desired functionality. Where no parts can be readily found, the cost estimation will be more unreliable and be based more on material costs, statistics and the size of the system.

The cost of the airframe is the hardest to estimate, since this system contains little to no off-the-shelf components with available prices. The result will therefore be very volatile. The approach was to first approximate the weight of the airframe. Since aluminium alloys will be predominantly used in the structure, a pure aluminium airframe is assumed.

The power system consists of the engine with the alternator, wiring, sensors, etc. As mentioned in section 7.5, the selected power system costs $9,995$ \$, which is around $9,540$ €.

The avionics system is another system whose price is relatively inaccurate, since not every part has the price listed. By finding prices for products from the same class, the price came at around $4,300$ €. The parts considered are also discussed in subsection 9.4.2.

Finally, the undercarriage cost was estimated based on the parts that go into it, i.e. a leaf spring for the main landing gear, the oleo-pneumatic shock absorber, the nose strut, the wheels, brakes and tires,

which amounted to $2,500$ €.

The total cost thus becomes $19,340$ €; this price however only covers materials and parts and ignores the manufacturing process, which will likely add around $20,000 - 30,000$ €. It should also be mentioned that this estimation is fairly inaccurate and would require some margin ( $50$%) in order to cover the worst cases.

| System | Price [€] |
|--------|-----------|
| Airframe | 3,000 |
| Power system | 9,540 |
| Avionics | 4,300 |
| Undercarriage | 2,500 |
| **Total** | 19,340 |

**Table 9.9:** Cost breakdown

Operational costs also have to be discussed. For this, the method used in the midterm [25] will be used. For the calculations the same inputs will be assumed as in the mid term report. However the flight hours are updated, and it is now assumed that 23 aircraft are operating at all times, see subsection 9.2.2. Furthermore the fuel consumption is updated using the current fuel consumption from section 7.5, where a value of 14.27 liters per hour on average is taken.

**Table 9.10:** Annual operational cost for 23 drones[25]

| Component | Cost [€] |
|-----------|----------|
| Fuel | 3,447,268 |
| Salary cost | 2,528,640 |
| Maintenance | 1,020,652 |
| Depreciation | 955,018 |
| Insurance | 238,547 |
| **Total** | 8,190,126 |

# 9.5. Technical Risk Assessment

This section describes the technical risk assessment of the system from the design phase to its end of life. It is important to identify and analyse the risks associated with the mission because those that are attributed a high likelihood and severity require mitigation strategies to prevent the mission goal from being compromised.

## 9.5.1. Risk Management Process

Following the procedure described in Figure 9.7, the risks are first to be identified, after which their probability and severity are estimated. By plotting the risks onto a risk map, the severity and likelihood of each risk can be visualised and adequate mitigation procedures can be considered. These procedures will affect the probability and/or impact of the dangerous risks and a post-mitigation risk map can be obtained to assess the mitigation strategy success.

# Risk management process
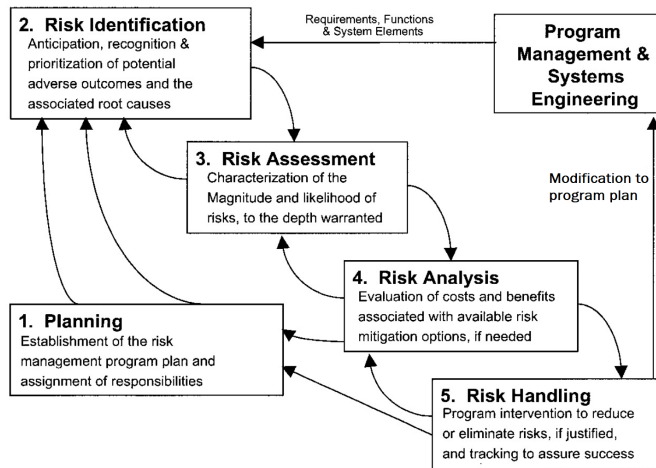


**Figure 9.7:** Risk management process [28]

## 9.5.2. Risk Identification & Assessment

The functional flow diagram presented in Appendix A defines the main phases of the mission, and the functions of the system. This can used as a tool to identify technical risks that stem from system functions during the mission duration. Each risk can be associated to a specific phase during the mission, therefore it has a unique risk ID. The convention used for risk IDs can be explained by analysing the risk ID $R.DSTR.STR.4$. The ID begins with an $R$ that stands for the word 'risk'. It is used to distinguish risk IDs from other mission IDs, such as requirement IDs. Second part of the ID $DSTR$ contains information about which of the 5 main mission phases the risk belongs to, in this case $DSTR$ corresponds to the abbreviation for the distribution phase as shown in the top level functional flow diagram in Figure A.1. The third part of risk ID $STR$ stands for the secondary functions that stem from the 5 main mission functions, in this case $STR$ corresponds to storage, which occurs within the distribution phase. The fourth part of risk IDs contains a number to distinguish different risk form the same secondary phase. The complete list of main secondary mission phases is presented in Table 9.11.

**Table 9.11:** Shortened abbreviation for main and secondary mission phases

**(a)** Shortened versions of secondary mission phases used in risk IDs

| Abbreviation | Full name |
|---|---|
| PART | Part manufacture |
| SAS | Sub-assembly manufacture |
| (PRO.)ASM | Part assembly |
| QA | Quality assurance |
| STR | Storage |
| MIS | Mission definition |
| SHP | Ship aircraft |
| (OPS.)ASM | Assemble aircraft |
| PREP | Prepare for flight |
| TOFF | Take-off |
| CLB | Climb |
| CRS | Cruise |
| DES | Descend |
| DRP | Deploy payload |
| NXT | Set next target |
| LAN | Land |
| POF | Post flight operations |
| (OPS.)DIS | Disassemble aircraft |
| (EOL.)DIS | Dismantle into components |
| SOR | Sort components |
| INS | Inspect components |
| DSS | Dispose/sell component |
| CAL | Calculation/modelling |
| GEN | General design |

**(b)** Shortened versions of main mission phases used in risk IDs

| Abbreviation | Full name |
|---|---|
| PRO | Production |
| DSTR | Distribution |
| OPS | Operations |
| EOL | End of life |
| DES | Design |

All risks have a cause, this cause could create a risk event which, as a consequence, effects promises such as the mission technical performance, schedule, or cost. In order to identify if a risk endangers the mission to an unacceptable level, a set of five risk severity and likelihood criteria were developed to assess every risk. These criteria are summarised and documented in Table 9.12. The reason to adopt a qualitative approach of assessment is due to the nature of risks and the inherent uncertainty in estimating their actual impacts on the project.

**Table 9.12:** Risk Severity, Definition and Probability

| Consequence | | Probability |
|---|---|---|
| Severity | Definition | Class |
| Catastrophic (CAT) | Complete failure of project objective, direct harm to surrounding environment and population, Complete degradation of performance | Very High (VH) |
| Critical (CR) | Significant degradation to performance, major damage that results in serious injuries, mission success is questionable | High (H) |
| Moderate (MOD) | Substantial degradation to performance, impact on primary mission objective is noticeable | Moderate (M) |
| Minor (MIN) | Degradation and under-performance of secondary mission, small reduction in technical performance | Low (L) |
| Negligible (NEG) | Inconvenience that does not affect the progress of the project, no reduction in technical performance, non-operational impact | Very Low (VL) |

There is now a plan on how to identify and characterise risks based on their likelihood and severity. A more detailed description of the identified risk $R.DSTR.STR.4$ during storage is presented in Table 9.13. This risk was chosen as an example due to its high influence on the design, which drove the team to design an aircraft that can easily be stored inside a 20 ft container. For a fuller list of identified risks

and their descriptions the reader is directed to Table A.1 under Appendix A, as it contain the complete list of over 100 risks identified.

**Table 9.13:** Description of risk #20 with ID: R.DSTR.STR.4

| # | Risk ID | Cause | Risk event | Consequence | Promise | L | S |
|---|---------|-------|------------|-------------|---------|---|---|
| 20 | R.DSTR.STR.4 | Aircraft design is large | The aircraft is damaged during storage | Drone integrity is compromised | Performance, schedule, cost | M | CAT |

The risk description convention from Table 9.13 was adopted to document every risk identified. By describing the cause, risk event and consequence associated to it, a complete risk understanding and assessment can be attained. Risk cause and consequence descriptions are used for estimating the likelihood and severity of a risk event. Assigning a likelihood and severity for every risk makes it possible map out risks and identify which ones need a mitigation strategy. The complete risk map for all identified risks during the five main phases is provided in Figure 9.8.
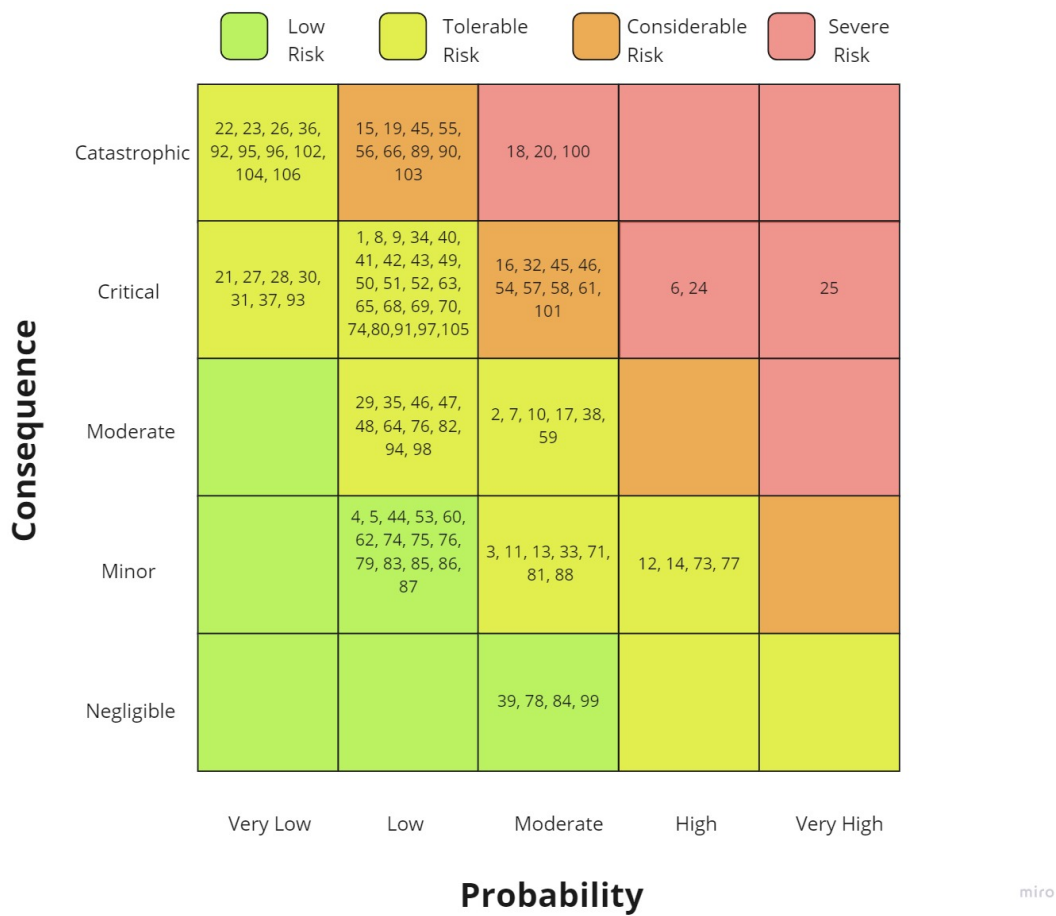


**Figure 9.8:** Technical risk map

The risk makes use of four colours: green, yellow, orange and red in ascending order of impact. risks with a high severity and high probability of occurrence would be mapped close to the top right corner of the map, and vice-versa. The allocation of risks into one of these risk areas determines the class of risk dealt with. Depending on each risk's class, mitigation could be necessary. As seen in Figure 9.8, risk #20 R.DSTR.STR.4 lies within the moderate probability and catastrophic severity, making it a severe risk that requires mitigation. A complete list of all severe risks is shown below:

- **#6 - R.PRO.PART.6:** Qualified personnel is not available

- **#18 - R.DSTR.STR.2:** The aircraft is damaged during transportation
- **#24 - R.DSTR.STR.4:** The aircraft is damaged during storage
- **#25 - R.DSTR.SHP.1** Aircraft does not make it to desired destination on time
- **#26 - R.DSTR.SHP.2** The condition of the infrastructure is inadequate for delivery of the containers containing the aircraft
- **#100 - R.OPS.PREP.11** Aircraft propeller suddenly rotates, injuring personnel

## 9.5.3. Risk Analysis & Handling

During the process of risk analysis and risk handling, it is important to analyse the impact of the risk on the mission as a whole, if a risk's severity and likelihood are both high, it is crucial to create a mitigation plan to lower one or both of these factors. To facilitate and aid in risk handling decisions, risks have been associated to one of the four respective classes as documented by Table 9.14, where the adopted mitigation strategies are described. As previously explained, the risk map determines what class a risk will belong to.

**Table 9.14:** Risk class and respective mitigation strategy required

| Risk Class | Mitigation |
|---|---|
| Severe Risk | Requires mitigation. Operation should not continue until valid mitigation is completed |
| Considerable Risk | Requires Mitigation. Should only be acceptable when mitigation is not possible/or complicated |
| Tolerable Risk | Acceptable with possible mitigation |
| Low Risk | Acceptable with no mitigation needed |

It is important to understand how risk mitigation measures are able to aid with dealing with risk. Risk handling involves the development of mitigation strategies that have an influence on the likelihood and/or severity of risks with the aim of lowering its impact on the project. The four mitigation strategies considered to aid in risk handling are:

- Treat: This risk mitigation strategy focuses on reducing the likelihood and/or severity of the risk
- Accept: This risk mitigation strategy involving accepting the consequence with/without a contingency plan
- Transfer: This risk mitigation strategy involves the transfer of risks to a third party
- Terminate: This risk mitigation strategy will prevent the risk from having the opportunity to manifest itself

For a complete list of mitigation strategies on all severe and considerable risks we refer the reader to Table A.2 under Appendix A.

A post mitigation strategy risk map is generated and displayed on Figure 9.9, where the effectiveness of all proposed mitigation measures can be obtained by a comparison to the initial risk map. The risk numbers denoted by bold font are the ones that have been mitigated.
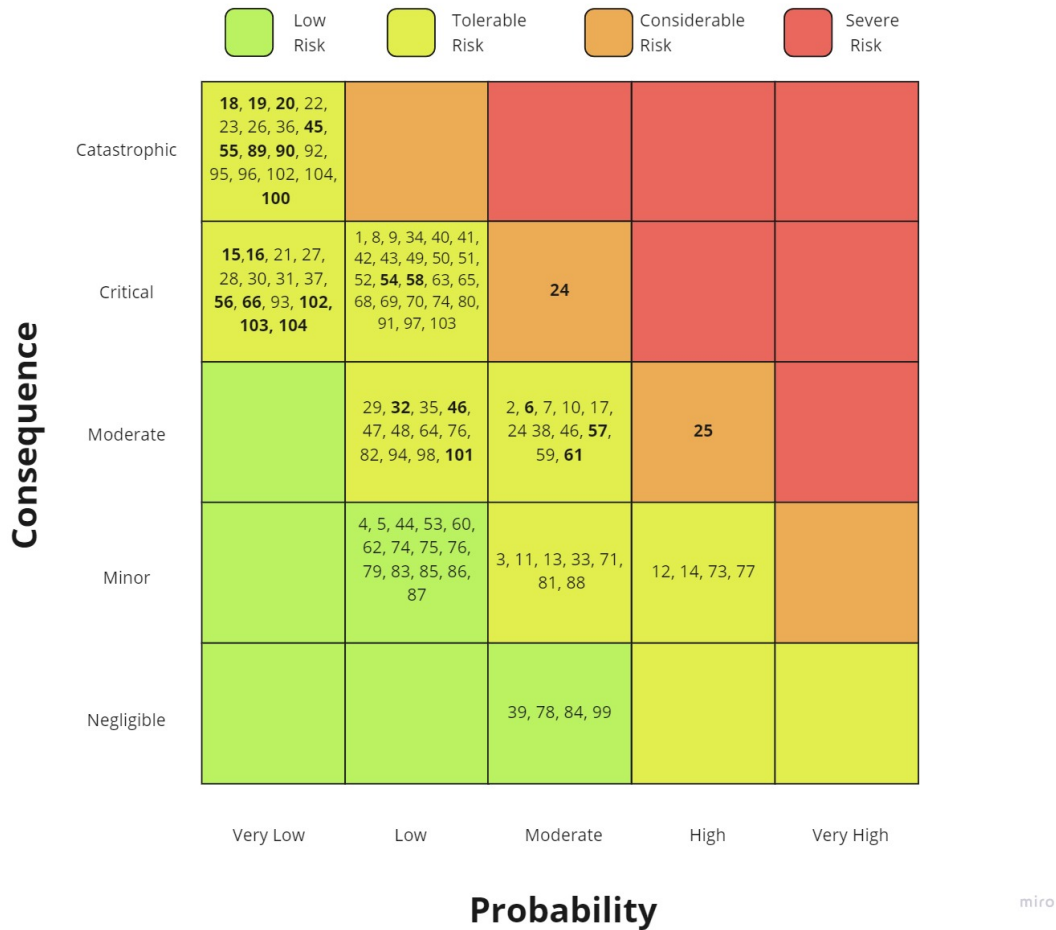
**Figure 9.9:** Post-mitigation technical risk map

Two important mitigation effectiveness will be described, these concern to risks #24 and #25 as shown in Figure 9.9. The reason why these are the only two risks left in the considerable class of risks is due to their high initial values for severity and likelihood. Their considered mitigation strategies are able to reduce their impact to a considerable extent where any more mitigation measures lead to an excessively increased system complexity and/or additional costs, thus reducing their efficiency. For these reasons, risks #24 and #25 are accepted to remain as considerable risks.

## 9.6. SORA Approach

There are three EASA drone categories: the open category, specific category and certified category. The Wings for Aid aircraft will likely fall under the specific category, as it is too heavy to be considered in the open category ($< 25\ kg$), and the risk is not high enough to be considered in the certified category. According to EASA, UAV's in the "Specific Category" may receive operational authorisation from the authorities by means of a risk assessment [14]. The recommended risk assessment to perform is the so called SORA approach. First an operational volume must be defined for the aircraft. This is essentially a corridor in space through which the operation will be performed. This is visualized in Figure 9.10. The main steps taken to obtain approval for operation of the mission are summarized below [15]

1. First the ConOps must be defined, which describes the technical and operational information of the UAV as well as information about the operator themselves.
2. The ground risk class (GRC) must be determined. The GRC relates to the risk of a person getting hit on ground by the drone. It is found by determining the operational scenario and characteris-

---

[14] https://www.easa.europa.eu/domains/civil-drones/drones-regulatory-framework-background/specific-category-civil-drones
[15] https://eudronebewijs.nl/blogs/actueel/zo-voer-je-een-sora-uit-deel-1-van-5

tic dimension (wingspan in this case), from which the intrinsic GRC can be found. If there are mitigation measures to decrease the ground risk the score may be reduced by a certain number depending on the level of robustness. The level of robustness is a function of the level of integrity and the level of assurance.

3. Next the air risk class (ARC) can be determined. This represents the risk of a collision with another aircraft in air. The initial ARC is chosen by looking at several factors such as the airspace and altitude. Then, this score can be decreased if the drone flies in atypical airspace, which can be the case if the there are little manned aircraft in the area. Therefore the airspace in which the operation takes place needs to be investigated.

4. Next the Tactical Mitigation Performance Requirement (TMPR) must be determined based off the ARC. Based off the TMPR tactical migitations must be performed, which are mitigations to actively avoid other aircraft

5. From the GRC and ARC the Specific Assurance and Integrity Level (SAIL) can be determined.

6. From the SAIL, the Operation Safety Objectives (OSO) must be determined together with their level of robustness. Then the safety objectives to be met can be read from a table depending on the level of robustness

7. Then, the risks that exist when leaving the operational volume must be evaluated. It is important that any type of system failure does not cause the drone to fly outside of the ground risk buffer

8. Finally the outcomes of the SORA risk analysis must be put in a Comprehensive Safety Portofolio and handed in to the authorities.
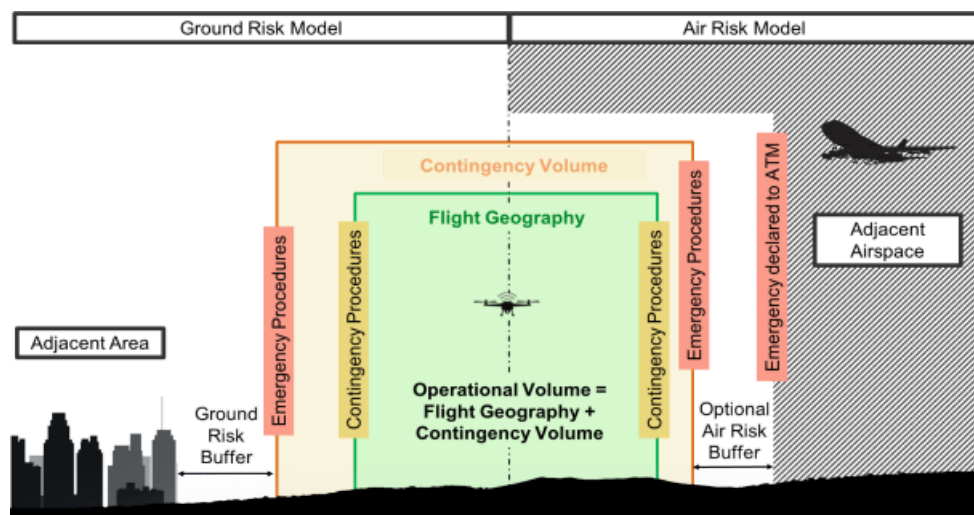


**Figure 9.10:** Operational volume for the SORA approach [41]

## 9.7. Sustainable Development Considerations

This section discusses the sustainability considerations that influenced the decisions towards the final detailed design. Sustainability is a broad term, therefore the definition provided by the United Nations during the 1987 Brundtland Commission: "meeting the needs of the present without compromising the ability of future generations to meet their own needs." [14]. To meet our sustainability requirements the social, economical and environmental sustainability considerations is considered.

### 9.7.1. Design Sustainability Considerations

**Fuel Consumption**

Striving for low fuel consumption is essential to ensure a sustainable design; this is not only beneficial economically by reducing the amount spent on fuel, but also has environmental benefits by reducing the emissions. Fuel consumption is mainly affected by the engine choice and the aerodynamic properties, namely drag. Between a four stroke, a two stroke and a Wankel engine, the four stroke has the lowest fuel and oil consumption for the same power output, therefore it was the engine of choice. By comparing

the performance of different engines found on the market, their fuel consumption was modelled and the best option was chosen. This process is described in detail in subsection 6.6.2. It should be noted that the fuel choice is not the most environmentally sustainable, however, in the context of the mission, it makes sense to use the fuel that is locally available, which is mostly gasoline and diesel. This not only eliminates costs for the shipping of fuel, but also supports the local economy.

**Lightweight Structure**
Minimizing the structural weight of the aircraft is a complex task, since it requires finding the optimal geometry that provides the needed structural stiffness and strength. It is also important to note that the best structure in terms of weight will not necessarily be the best structure in terms of cost or manufacturability. When designing the structure of the aircraft (section 6.4), the weight, cost, manufacturability and recyclability were taken into account and the optimal design was chosen.

**Manufacturability**
The material choice, as well as the geometric properties of the structure, have an impact on the manufacturability and by consequence on the sustainability. Table 9.15 shows how much energy is required to produce various materials that are commonly used in the aircraft industry. Naturally, less energy required for manufacturing a certain material is preferred, so carbon fibre reinforced polymers (CFRP) will be avoided. chapter 8 also explains how lean manufacturing will be implemented, which will reduce waste.

Table 9.15: Embodied energy of several materials typically used in aerospace [21]

| Material | Embodied energy (MJ/kg) |
| --- | --- |
| Carbon fibre | 183-286 |
| Glass fibre | 13-32 |
| Polyester resin | 63-78 |
| Epoxy resin | 76-80 |
| Aluminium alloys | 196-257 |
| Stainless steel | 110-210 |

**Modularity**
Ensuring the disassembled aircraft can fit in a 20 ft container contributes significantly to the economic sustainability of the design. This container is the most used shipping container, along with the 40 ft container, so being able to use it for transportation allows for a lot of different transport options, such as flying it to the destination with a C130 or C17.

## 9.7.2. Sustainability Contribution
Sustainability in aviation has tends to the focus on the reduction of greenhouse gas emissions during the operational life of aircraft's. Due to the strict cost requirement and the necessity to utilise cheap available fuel such as diesel and gasoline, the sustainability approach during manufacturing and end of life procedures should be given special attention. The social aspect of the development strategy will cover the impact of the design on the lives of the people in disaster struck areas.

**Sustainable Development Goals**
The design, but most importantly the mission it carries out is a huge step towards meeting the 17 sustainability goals (SDGs) proposed by the Unites Nations [29]. Within the 17 goals, this mission is contributing to meet the following:

- **SDG goal #2 - Zero hunger:** One of the targets of this goal is: 'By 2030, end hunger and ensure access by all people, in particular the poor and people in vulnerable situations, including infants, to safe, nutritious and sufficient food all year round' [30]. Wings for aid is a mission to deliver aid to disaster struck areas, therefore contributing to ensuring as much people in vulnerable situations get access to aid, which also comes in the form of food.
- **SDG goal #3 - Good health & well being:** Target 3.8 of this goal is to 'Achieve universal health coverage, including financial risk protection, access to quality essential health-care services and

access to safe, effective, quality and affordable essential medicines and vaccines for all'[31]. The delivery aid packages are equipped with medicinal items, the mission is able to quickly reach and treat injured and sick people effectively within hours of disaster. '

- **SDG goal #6 - Clean water and sanitation:** Target 6.1 of this goal states: 'By 2030, achieve universal and equitable access to safe and affordable drinking water for all' [13]. As mentioned previously the aid packages delivered by the wings for aid mission contain food supplies, which come in the form of clean water and sanitation products. Clean water and sanitation equipment are often scarce when the area has been struck by a natural disaster such as an earthquake, which can quickly make the spread of diseases lethal.

**Circular Design Approach**

When talking about circular design approach, the goal is to repair, reuse, recycle. Since the design is highly modular and uses off-the-shelf components where possible, repairability will be very easily implemented. Electrical components, engine parts and tires can be found readily on the market, as for components such as the wing and other load carrying structures, maintenance and repairs can be performed depending on the material used.

The modularity also helps with reusability. When one drone can no longer be operated for whatever reason, various parts and systems can be salvaged and used as spares for the rest of the fleet. Finally, whatever parts do not allow for reuse in other aircraft units, will be recycled. Here, a distinction between upcycling and downcycling needs to be made.

When developing a procedure for the end of life cycle, an important concept to introduce is the upcyling and downcycling of components. Ensuring that a system contains both procedures allows for multiple uses and ultimately choices for recycling once the aircraft is retired from service. One option when considering a sustainability approach is the upcycling of components that no longer meet the required performance. Large components such as the fuselage, wing or tailplane can be converted into usable structures. These up cycled components can be sold to academic institutions, aerospace companies and individuals who have a strong interest in aircrafts. The profit on these up-cycled components can then be further invested into the project allowing for ongoing research and development. Examples of previously up-cycled aircraft components are shown in the Figure 9.11



**Figure 9.11:** Upcycled furniture from Aero-Design[8]

Downcycling on the other hand means re-purposing of the materials, e.g. using the aluminium from the wing and fuselage to cast other products. Downcycling is less desirable, since sometimes the cost of processing the material can be greater than the value of the final product.

## 10.1. Project Development and Design Logic

The project development and design logic presents the flow of tasks to be performed post-DSE. The start of this chart is the preliminary design which is the output of this report. Then, the tasks to be performed from this point, to the final point, which is delivery to the customer, are presented. The tasks presented are still quite general and at a high level description, primarily due to not having all the information to give a more detailed description at the current stage.

### Final Design

The preliminary design can be iterated upon using more sophisticated tool such as computational fluid dynamics (CFD) to analyse the aerodynamics and finite element methods (FEM) to analyse loads on the structure. From the final design, a final CAD model will be created, which is also used to create the prototype aircraft, which will be used in several tests. These first tests will be both flight tests and on ground tests, and will be reported. Lastly, the aircraft has to be certified, for which a report has to be made according to the SORA approach, to receive certification.

### Company Development

After the preliminary design also the company needs to start up by using marketing and crowdfunding for example. Furthermore, engineers need to be hired to perform the detailed design, as well as customer service and pilots to operate the aircraft once they are ready to be used. Finally, the customers should be established. Wings for Aid will then look for fit customers such as the UN and the Red Cross, and will propose a deal to them.

### Operations and Logistics

For operations and logistics a number of facilities and contractors need to be acquired. The facilities include offices to operate from, hangars and movable bases to store the plane. Contractors are needed to provide for the fuel and transport to the right location.

### Manufacturing

After the final design the manufacturing plan has to be performed, which was outlined in chapter 8.

### Delivery to Customer

After the aircraft are manufactured, the final step is to deliver the service to the customer. For this everything including personnel, the airbase and aircraft has to be shipped to the location. Then finally, the aircraft has to set up and the mission can be performed.

## 10.2. Post-DSE Gantt Chart

In the post-DSE Gantt chart the tasks and sub-tasks from section 10.1 are given an estimated time range. The times are given in terms of quarters, as it is not possible to make an accurate estimate of the time needed at this point. The post DSE Gantt chart can be found in Figure 10.2

POST DSE GANTT CHART                    Wings for aid

| ID | Task | 2022 | | | 2023 | | | 2024 | | |
|----|------|------|--|--|------|--|--|------|--|--|
| | | Q3 | Q4 | Q1 | Q2 | Q3 | Q4 | Q1 | Q2 | Q3 | Q4 |
| 1. | Final design | | | | | | | | | | |
| 1.1 | Perform detailed analysis | | | | | | | | | | |
| 1.1.1 | Perform CFD on aircraft | | | | | | | | | | |
| 1.1.2 | Perform CFD on boxes | | | | | | | | | | |
| 1.1.3 | Perform FEM analysis on structure | | | | | | | | | | |
| 1.1.4 | Perform stability analysis | | | | | | | | | | |
| 1.1.5 | Iterate design | | | | | | | | | | |
| 1.2 | Make final CAD model | | | | | | | | | | |
| 1.2.1 | Design parts | | | | | | | | | | |
| 1.2.2 | Construct assembly | | | | | | | | | | |
| 1.2.3 | Create technical drawings | | | | | | | | | | |
| 1.3 | Perform tests | | | | | | | | | | |
| 1.3.1 | Manufacture prototypes | | | | | | | | | | |
| 1.3.2 | Perform aircrafts structure test | | | | | | | | | | |
| 1.3.3 | Perform flight tests | | | | | | | | | | |
| 1.3.4 | Evaluate test results | | | | | | | | | | |
| 1.4 | Perform certification | | | | | | | | | | |
| 1.4.1 | Establish UAV category | | | | | | | | | | |
| 1.4.2 | Perform SORA Risk analysis | | | | | | | | | | |
| 1.4.3 | Hand in report to autorities | | | | | | | | | | |
| 2. | Company development | | | | | | | | | | |
| 2.1 | Marketing | | | | | | | | | | |
| 2.1.1 | Determine audience | | | | | | | | | | |
| 2.1.2 | Create ads | | | | | | | | | | |
| 2.1.3 | Create crowdfunding page | | | | | | | | | | |
| 2.2 | Hire personell | | | | | | | | | | |
| 2.2.1 | Hire pilots | | | | | | | | | | |
| 2.2.2 | Hire customer service | | | | | | | | | | |
| 2.2.3 | Hire engineers | | | | | | | | | | |
| 2.3 | Establish customers | | | | | | | | | | |
| 2.3.1 | Determine fit customers | | | | | | | | | | |
| 2.3.2 | Make proposal | | | | | | | | | | |
| 2.3.3 | Approach customers | | | | | | | | | | |
| 2.3.4 | Close deal | | | | | | | | | | |
| 3. | Operations and logistics | | | | | | | | | | |
| 3.1 | Acquire facilities | | | | | | | | | | |
| 3.1.1 | Rent offices | | | | | | | | | | |
| 3.1.2 | Rent hangar | | | | | | | | | | |
| 3.1.3 | Acquire movable bases | | | | | | | | | | |
| 3.2. | Acquire contractors | | | | | | | | | | |
| 3.2.1 | Acquire transport contractors | | | | | | | | | | |
| 3.2.2 | Acquire fuel contractors | | | | | | | | | | |
| 4. | Manufacturing | | | | | | | | | | |
| 4.1 | Perform production plan | | | | | | | | | | |
| 5. | Delivery to customer | | | | | | | | | | |
| 5.1 | Prepare mission | | | | | | | | | | |
| 5.1.1 | Receive job from client | | | | | | | | | | |
| 5.1.2 | Send aircraft to site | | | | | | | | | | |
| 5.1.3 | Send personell to site | | | | | | | | | | |
| 5.1.4 | Send airbase to site | | | | | | | | | | |
| 5.1.5 | Setup airbase | | | | | | | | | | |
| 5.1.6 | Build aircraft | | | | | | | | | | |
| 5.2 | Execute mission | | | | | | | | | | |
| 5.2.1 | Load cargo | | | | | | | | | | |
| 5.2.2 | Refuel aircraft | | | | | | | | | | |
| 5.2.3 | Check aircraft | | | | | | | | | | |
| 5.2.4 | Perform mission | | | | | | | | | | |

| | | |
|---|---|---|
| Major task | X. | |
| Task | X.X. | |
| Subtask | X.X.X | |

**Figure 10.2:** Post DSE Gantt chart

## 10.3. Technical Recommendations

Within the scope of this project, several subsystems have been designed and sized at an initial level. In order to ensure the design progresses to the detailed proof of concept stage, a series of further technical analysis must be completed. In this section recommendations for the subsystems of aerodynamics, structures, flight performance & propulsion, control & stability and operations are listed in order of importance utilising identifiers with the format of Project - Department - Recommendation - Number; WFA-AERO-REC-01.

### 10.3.1. Aerodynamics

- WFA-AERO-REC-01: Complete further analysis on empennage airfoil selection.
- WFA-AERO-REC-02: Conduct in depth analysis of subsystem interactions, ie. wing, fuselage, empennage, landing gear. Optimise geometry between these sections to provide minimum drag while still optimising weight and structural performance.
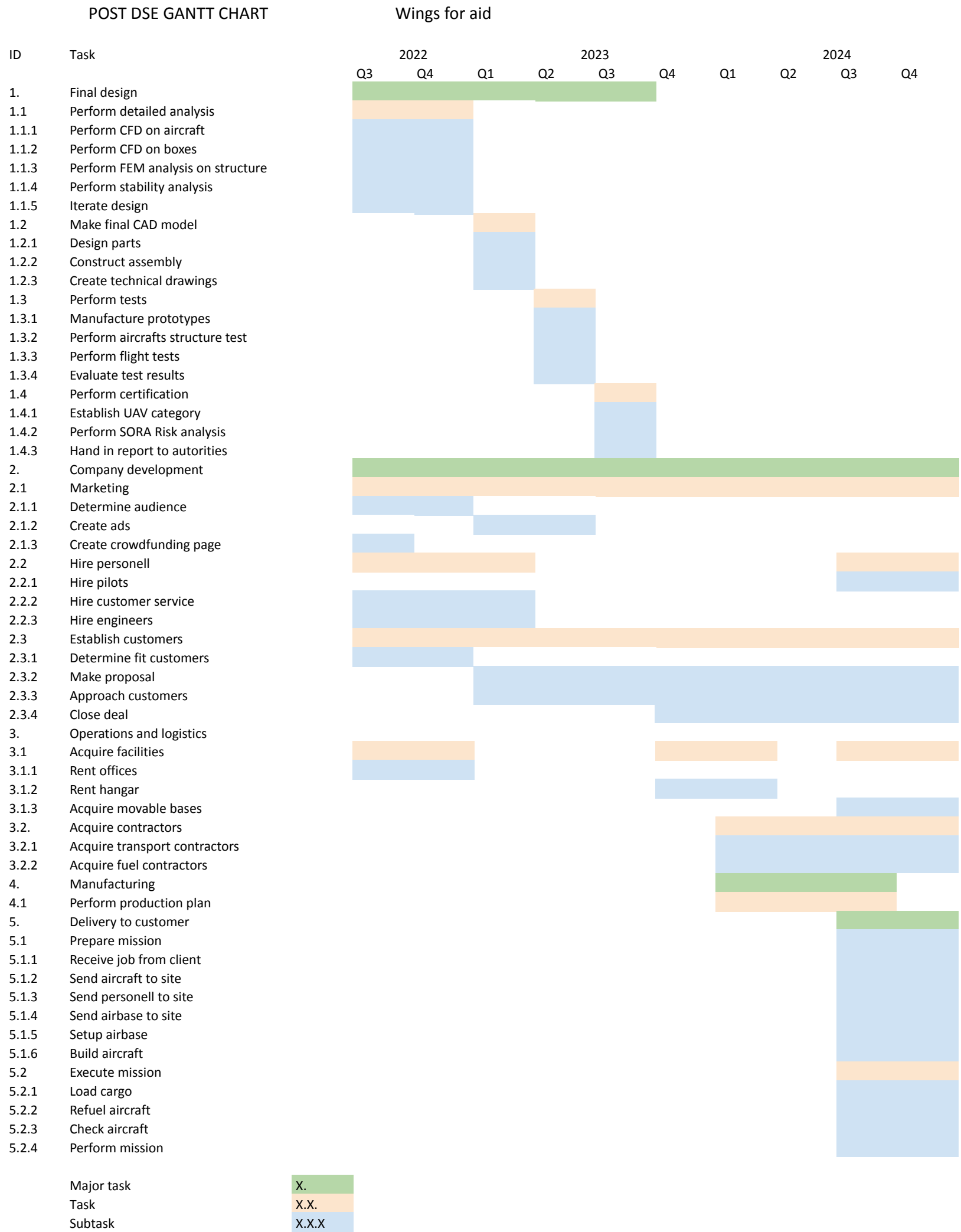- WFA-AERO-REC-03: Construct complete drag budget using CFD to characterise drag coefficients at each stage in the flight profile.
- WFA-AERO-REC-05: Complete Wind tunnel analysis to validate aerodynamic predictions. It will be useful to test a preliminary complete design at varying angles of bank, angle attack and sideslip, further validating the performance of the simulation and model at every point within operational profile.
- WFA-AERO-REC-06: Complete Wind tunnel analysis to validate aerodynamic predictions. It will be useful to test a preliminary complete design at varying angles of bank, angle attack and sideslip, further validating the performance of the simulation and model at every point within operational profile.
- WFA-AERO-REC-07: Complete Wind tunnel analysis to validate aerodynamic predictions. It will be useful to test a preliminary complete design at varying angles of bank, angle attack and sideslip, further validating the performance of the simulation and model at every point within operational profile.
- WFA-AERO-REC-08: Utilise wind tunnel test to validate optimum position of external flaps in junker flap wing configuration. This analysis will help with the precise positioning of the external junker flap in relation to the lower surface of the trailing edge.
- WFA-AERO-REC-09: Utilise wind tunnel test to validate optimum position of external flaps in junker flap wing configuration. This analysis will help with the precise positioning of the external junker flap in relation to the lower surface of the trailing edge.
- WFA-AERO-REC-10: Complete aerodynamic analysis of chosen propeller. This will allow for the efficiency, drag effects and thrust of the propeller to be calculated, allowing further development in the flight performance model.
- WFA-AERO-REC-11: Conduct analysis of open fuselage and closed fuselage. This analysis will verify if the affects on aircraft drag for an open fuselage are significant and if a closed hatch dropping mechanism is required.
- WFA-AERO-REC-12: Take current NACA 2415 airfoil and optimise for drag and mission performance. It is possible to investigate which pressure distribution along the airfoil is most optimal for the mission profile, then use methodologies and analysis tools such as XFLR5 to reverse engineer the airfoil geometry.

### 10.3.2. Structures

- WFA-STRUC-REC-01: Create complete CAT model for structural analysis. With this complete model FEM (Finite Element Method) analysis can be done and a more detailed design can be made.
- WFA-STRUC-REC-02: Consider bending and torsional stiffness in the design process.
- WFA-STRUC-REC-03: Consider more stress considerations and failure modes such as inter-rivet buckling, fatigue failure, impact damage, shear buckling, and stress concentrations.
- WFA-STRUC-REC-04: Look into performing vibrational and flutter analysis.
- WFA-STRUC-REC-05: Consider designs that consist of more than one material.
- WFA-STRUC-REC-06: Introduce more varied and accurate aerodynamic loads.
- WFA-STRUC-REC-07: Perform structural analysis on a more detailed level.
- WFA-STRUC-REC-08: Consider more flight stages.
- WFA-STRUC-REC-09: Consider complete structural analysis of the aircraft.
- WFA-STRUC-REC-10: Introduce environmental effects. This includes temperature, light damage, water damage, and corrosion.
- WFA-STRUC-REC-11: Consider manufacturability at a more detailed level.
- WFA-STRUC-REC-12: Look into option for closed fuselage bottom. More structural integrity can be achieved with a closed fuselage, but no such option was analysed as it is creates a more complex design. A more in depth analysis is recommended.

### 10.3.3. Flight Performance & Propulsion

- WFA-PP-REC-01: Further research into a better fitted engine.
- WFA-PP-REC-02: Further research into a specific propeller design.
- WFA-PP-REC-03: Further research into propeller performance characteristics.
- WFA-PP-REC-04: Optimize the performance such that fuel and time are minimized.
- WFA-PP-REC-05: Perform noise calculations.
- WFA-PP-REC-06: Perform more elaborate emissions calculations.
- WFA-PP-REC-07: Research in the application reverse thrust, flaps, speed brakes during landing.
- WFA-PP-REC-07: Implement a wind model for performance calculations.

### 10.3.4. Stability & control

- WFA-SC-REC-01: Find other static stability derivatives in lateral direction using the DATCOM method, to assess the lateral static stability.
- WFA-SC-REC-02: The subsystems should be correctly positioned by sizing the inside of the fuselage, which will give a more accurate C.G. OEW location.
- WFA-SC-REC-03: Dynamic stability should be analysed by using the equations of motion to calculate the eigenvalues corresponding to all the eigenmotions.
- WFA-SC-REC-04: Dynamic effects of dropping the payload should be investigated.
- WFA-SC-REC-05: Dynamic effects of fuel sloshing should be investigated.
- WFA-SC-REC-06: The C.G. location of the fuselage and landing gear should be updated from a final CAD model.
- WFA-SC-REC-07: A more accurate C.G. location of the vertical and horizontal stabilizer, and wing should be found

### 10.3.5. Operations

- WFA-OPS-REC-01: Complete analysis of optimum distribution center locations to reduce logistical challenges.
- WFA-OPS-REC-02: Develop a complete operating profile program that allows the operator to input the package delivery location and receive the flight performance plan, fuel required, contingency plans as well as if the current operating range is feasible.
- WFA-OPS-REC-03: Perform a complete SORA risk analysis for the operations to receive approval for operations.

After the end of the 10 week DSE project period, the DSE Group 12 Wings For Aid successfully developed a preliminary design for an aid delivery aircraft. The aircraft is capable of delivering ten $20\ kg$ packages within an effective range of $250\ km$ from the forward operating base. This aircraft is an unmanned aerial vehicle (UAV) which utilises a proprietary payload box dropping technology developed by the client organisation Wings for Aid. These boxes are deployed from the aircraft at a minimum height of $50\ m$. Afterwards 4 aerodynamic flaps deploy to slow down the payload to a speed of $40\ km/h$ before reaching the landing zone. This payload can be accurately delivered in a drop zone of $25\ m$ by $25m$. This is considerably more accurate than typical aerial delivery systems such as the C-17 globe master, which can require up to a 1 km large drop zone. This characteristic of our system makes it uniquely suited to performing the "last mile" aid delivery service.

Using XFLR5, a range of commonly selected general aviation aircraft airfoils were analysed based off of performance indicators. It was concluded that a NACA 2415 airfoil provided the best combination of performance when comparing both 2D aerofoil analysis and 3D Wing analysis. Based off of the design point calculated with wing loading, power loading, and a finalised MTOW, the wing surface area and span were calculated to be $11.43\ m^2$ and $10.14\ m$ respectively, with an aspect ratio of 9. The aircraft will fly at a lift coefficient of 0.84 and a cruise speed $34.01\ m/s$. Flaperons were designed to act as High Lift devices and ailerons. Further aerodynamic analysis on wing and empennage interaction must be done to develop a complete lift and drag profile.

From the static stability and control analysis, it was determined that the required optimum tail area ratio was $0.194$. To ensure that the aircraft fits into the container, two unconventional design decisions were made. First of all, instead of placing the ten packages arranged in 5 rows of 2, the width of the fuselage was increased such that two rows contain three packages and thus one row could be removed. This decreased the length of the fuselage and allowed the tail to fit in the container in length wise direction. Furthermore an H-tail was chosen such that the vertical tail area can be divided over two parts. This way the tail fits in the container height wise, while also allowing a high scrape-back angle. Based on the calculated wing surface area, a horizontal stabilizer area of $2.13\ m^2$ is required to provide stability. However the span of the horizontal stabilizer is larger than the width of the container. Therefore, the horizontal stabilizer are designed to be removed when transporting the aircraft.

The main structural components of the aircraft were analysed and a preliminary design was made. This included the fuselage, wing, and the landing gear. For the fuselage, preliminary design calculations were conducted followed by a structural design concept. The design process of the wingbox was more thorough whereby an initial detailed design was made accompanied by details of the skin thicknesses, stringer number, stringer dimensions, rib spacing, and a mass estimation. In addition, a landing gear design was optimized for stability on ground as well as repeated operations. Additionally the wing is modular and can be disassembled into two pieces. This allows for ease of transport and operations.

After the aircraft was designed in higher detail, the performance of the aircraft is analysed and an engine and propeller are chosen. The most common flight-profile was determined after consultation with the client. This consists of flying to a location, located at a maximum of $250\ km$ away from the ground base. Here all the payload will be dropped and the aircraft will return back. The current engine is a 4-stroke AM13 from Aeromomentum, and it is chosen because it is relatively efficient, has low maintenance and can take low octane levels. Furthermore the propeller decision is driven by ground clearance and efficiency. And in the end a fixed pitch, three bladed propeller is chosen, which will be optimized for cruise such that the amount of fuel is limited. By combining the profile, engine and propeller into one simulation the total time is approximately $4.7\ hours$ and the fuel consumption is estimated at $60\ kg$.

Transporting the complete organisation requires a lot of planning. For quick transport an aircraft can be used, however this is expensive. Therefore it is recommended to airlift the first 2 batches of aircraft and the Forward Operating Base and send additional aircraft and equipment by ship. This is both cost effective and it allows the local crew to set up the ground base without have many aircraft standing idly by. The aircraft performance dictates how many aircraft need to be transported. From the performance analysis is was found that an aircraft can perform 4.4 mission in a 24 hour cycle. To match the dropping capacity of the C-130 Hercules, 23 aircraft are needed and 6 aircraft are needed to not lose capacity

when maintenance is performed. The ground base needs a resupply station with space for 5 aircraft at a time. However if swarms of planes are used, more resupply stations are needed. Initially the mission must be performed with the locally available runways. If the mission will be performed for a longer time or in increasingly more challenging conditions such as a winter or rain seasons, more permanent runways can be created as certain performance advantages start to weigh more.

[1] J.A. Mulder et al. *Flight Dynamics Lecture Notes*. Delft University of Technology, 2013.

[2] P Vadivelu et al. *Numerical study on Longitudinal control of Cessna 172 Skyhawk aircraft by Tail arm length*. Tech. rep. Department of Aeronautical Engineering, Bannari Amman Institute of Technology, 2020.

[3] Ramesh Bapu B. R. "Evaluation of Aircraft Maintainability and Aircraft Maintenance". In: Nov. 2007.

[4] David Biermann and Edwin P Hartman. *The aerodynamic characteristics of six full-scale propellers having different airfoil sections*. Tech. rep. US Government Printing Office, 1939.

[5] *C-17 Globemaster III*. last checked: 14/06/2022. url: `https://www.af.mil/About-Us/Fact-Sheets/Display/Article/1529726/c-17-globemaster-iii/`.

[6] Nally C. *How Long Does It Take To Overhaul An Engine?* McNally Institute. Apr. 2022. url: `https://www.mcnallyinstitute.com/how-long-does-it-take-to-overhaul-an-engine/`.

[7] Raymer D.P. *Aircraft Design: A Conceptual Approach*. Ed. by Schetz J.A. Sixth edition. American Institute of Aeronautics and Astronautics, Inc., 2018.

[8] Aero Design. *Luxury creations inspired by aerospace industry*. url: `https://www.aero-design.fr/en/`.

[9] Ruth Doyle. *How long does it take to do a top overhaul?* MSI. url: `https://mysweetindulgence.com/common-questions/how-long-does-it-take-to-do-a-top-overhaul/`.

[10] Johnson E.R. et al. *Mechanics of Materials*. Eigth edition. McGraw-Hill, 2020.

[11] *Easy Access Rules for Very Light Aeroplanes (CS-VLA) (Initial issue)*. Initial issue. EASA. Nov. 2018. url: `https://www.easa.europa.eu/downloads/66873/en`.

[12] Continental Motors Aircraft Engine. *Service Information Letter*. Online. July 2013.

[13] *Ensure availability and sustainable management of water and sanitation for all*. 2022. url: `https://sdgs.un.org/goals/goal6`.

[14] World Commission for Environment and Development. *Our Common Future*. 1987. url: `http://www.un-documents.net/our-common-future.pdf`.

[15] Oliviero F. *Aircraft aerodynamic analysis - Lift & Drag*. Lecture slides of Aerospace Design and Systems Engineering Elements II, TU Delft. 2021.

[16] R.D. Finck. *USAF STABILITY AND CONTROL DATCOM*. Tech. rep. McDonell Douglas Corporation, 1978.

[17] Hugh B Freeman. *Comparison of Full-Scale Propellers Having RAF-6 and Clark Y Airfoil Sections*. Tech. rep. 1931.

[18] Snorri Gudmundsson. *General Aviation Aircraft Design*. Second Edition. Butterworth-Heinemann, 2022. isbn: 978-0-12-818465-3.

[19] Thomas Haberkorn. "Aircraft separation in uncontrolled airspace including human factors". PhD thesis. Apr. 2016.

[20] Prof.dr.ir. Jacco Hoekstra. *The standard atmosphere*. Lecture slides of AE1110-I Intro to Aerospace Engineering, TU Delft. 2019.

[21] Jack Howarth, Sada S.R. Mareddy, and Paul T. Mativenga. "Energy intensity and environmental analysis of mechanical recycling of carbon fibre composite". In: *Journal of Cleaner Production* 81 (2014), pp. 46–50. issn: 0959-6526. doi: `https://doi.org/10.1016/j.jclepro.2014.06.023`. url: `https://www.sciencedirect.com/science/article/pii/S0959652614006118`.

[22] Dr. Ir. Mark Voskuijl Ir. P.C. Roling. *Airfield performance*. Lecture slides of AE2230 – I Flight & Orbital Mechanics, TU Delft. 2021.

[23] C.D. Rans J.A. Melkert. *Buckling*. Lecture slides of AE2135-I Structural Analysis & Design, TU Delft. 2020.

[24] Arunkumar K N, N. Lohith, and Ganesh B B. "Effect of Ribs and Stringer Spacings on the Weight of Aircraft Structure for Aluminum Material". In: *Journal of Applied Sciences* 12 (Oct. 2012), pp. 1006–1012. doi: `10.3923/jas.2012.1006.1012`.

[25]  G. Luc et al. *Wings For Aid Mid-term report*. Tech. rep. TU Delft, May 2022.

[26]  Ir. Joris Melkert. *Part 2: Horizontal flight*. Lecture slides of AE1110-I Intro to Aerospace Engineering, TU Delft. 2019.

[27]  Ir. Joris Melkert. *Part 3: Climbing and descending flight*. Lecture slides of AE1110 – I Introduction to Aeronautical Engineering, TU Delft. 2019.

[28]  Erwin Mooij. *PMSE Lecture Slides Workshop 2*. 2022.

[29]  United Nations. *Do you know all 17 SDGs?* 2022. url: `https://sdgs.un.org/goals`.

[30]  United Nations. *End hunger, achieve food security and improved nutrition and promote sustainable agriculture*. 2022. url: `https://sdgs.un.org/goals/goal2`.

[31]  United Nations. *Ensure healthy lives and promote well-being for all at all ages*. 2022. url: `https://sdgs.un.org/goals/goal3`.

[32]  Michael Chun-Yung Niu. *Airframe Structural Design - Practical Design Information and Data on Aircraft Structures (2nd Edition)*. AD Adaso/Adastra Engineering LLC, 1999. isbn: 978-962-7128-09-0. url: `https://app.knovel.com/hotlink/toc/id:kpASDPDID1/airframe-structural-design/airframe-structural-design`.

[33]  Dr. Fabrizio Oliviero. *Requirement Analysis and Design principles for A/C stability & control (Part 1)*. AE3211-I Systems Engineering and Aerospace Design. Mar. 2020.

[34]  Dr. Fabrizio Oliviero. *Requirement Analysis and Design principles for A/C stability & control (Part 2)*. AE3211-I Systems Engineering and Aerospace Design. Mar. 2020.

[35]  *Operators manual for Rotax engine type 912 series*. 2013.

[36]  J.A. Melkert R. Vos. *Wing Positioning, Landing gear design and empennage design*. Slides AE1222-II. Mar. 2019.

[37]  R. et al Raj. "A Review of Aluminum Alloys in Aircraft and Aerospace Industry". In: (June 2021).

[38]  Colin Ritsick. *C-17 Facts: Everything You Need To Know*. last checked: 14/06/2022. Jan. 2020. url: `https://militarymachine.com/c-17-facts/`.

[39]  A. Romeyn. *Aircraft Reciprocating-Engine Failure: An Analysis of Failure in Complex Engineered System*. Tech. rep. Australian Transport Safety Bureau, Nov. 2007.

[40]  Roskam. *Airplane Design Part I: Preliminary Sizing of Airplanes*. DarCorporation, 1989.

[41]  Joint Authorities for Rulemaking of Unmanned Systems. *JARUS guidelines on Specific Operations Risk Assessment (SORA)*. Tech. rep. Joint Authorities for Rulemaking of Unmanned Systems, 2019.

[42]  Tariq Saeed. "Conceptual design for a laminar-flying-wing aircraft". In: (Nov. 2012).

[43]  Jos Sinke. *Production of Aerospace Systems (AE3211-II) reader*. TU Delft, 2022.

[44]  *UAV Landing Mat*. 2022. url: `https://fauntrackway.co.uk/defence/air/uav-landing-mat`.

[45]  Russell Wanhill. "Aerospace Applications of Aluminum–Lithium Alloys". In: Dec. 2014, pp. 503–535. isbn: 9780124016989. doi: `10.1016/B978-0-12-401698-9.00015-X`.

[46]  Home X. *How Many Hours Does It Take To Rebuild An Engine?* url: `https://homex.com/ask/how-many-hours-does-it-take-to-rebuild-an-engine`.
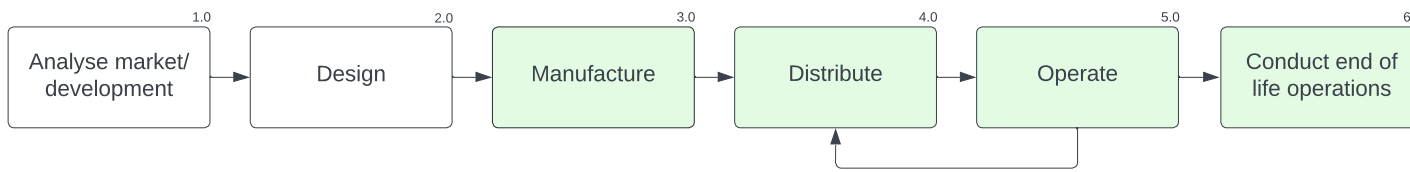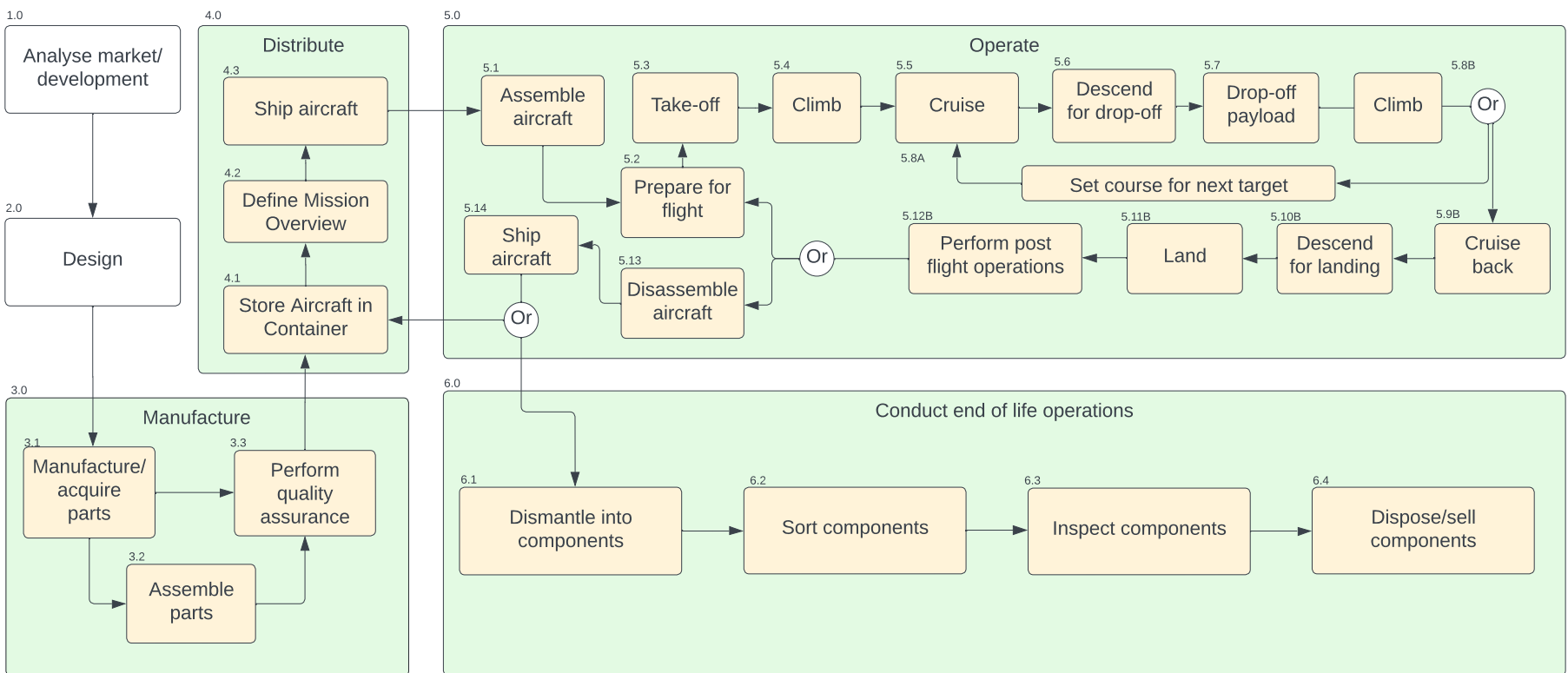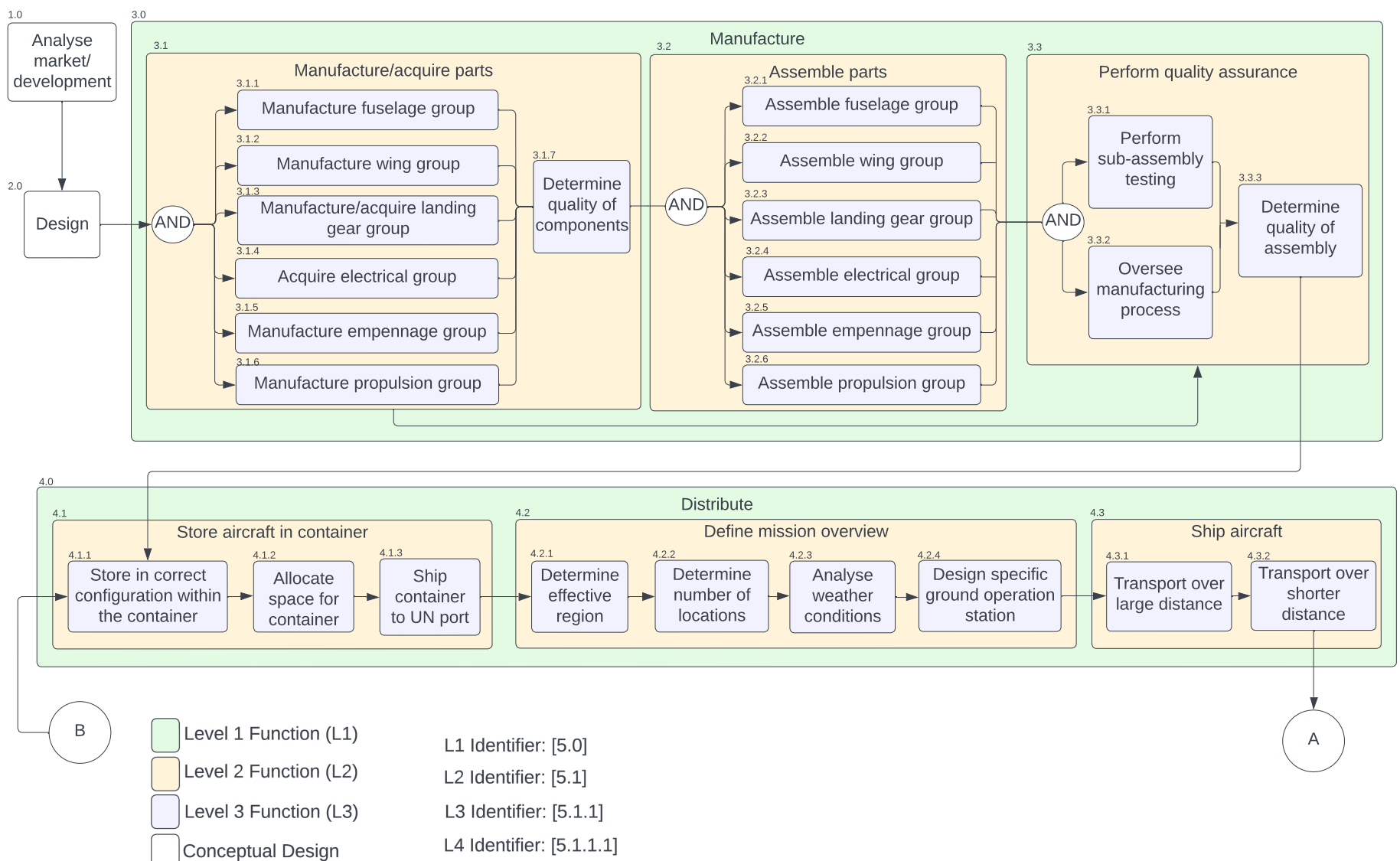
**Figure A.1:** DSE Functional flow diagram of level 1, 2 and the first part of level 3.
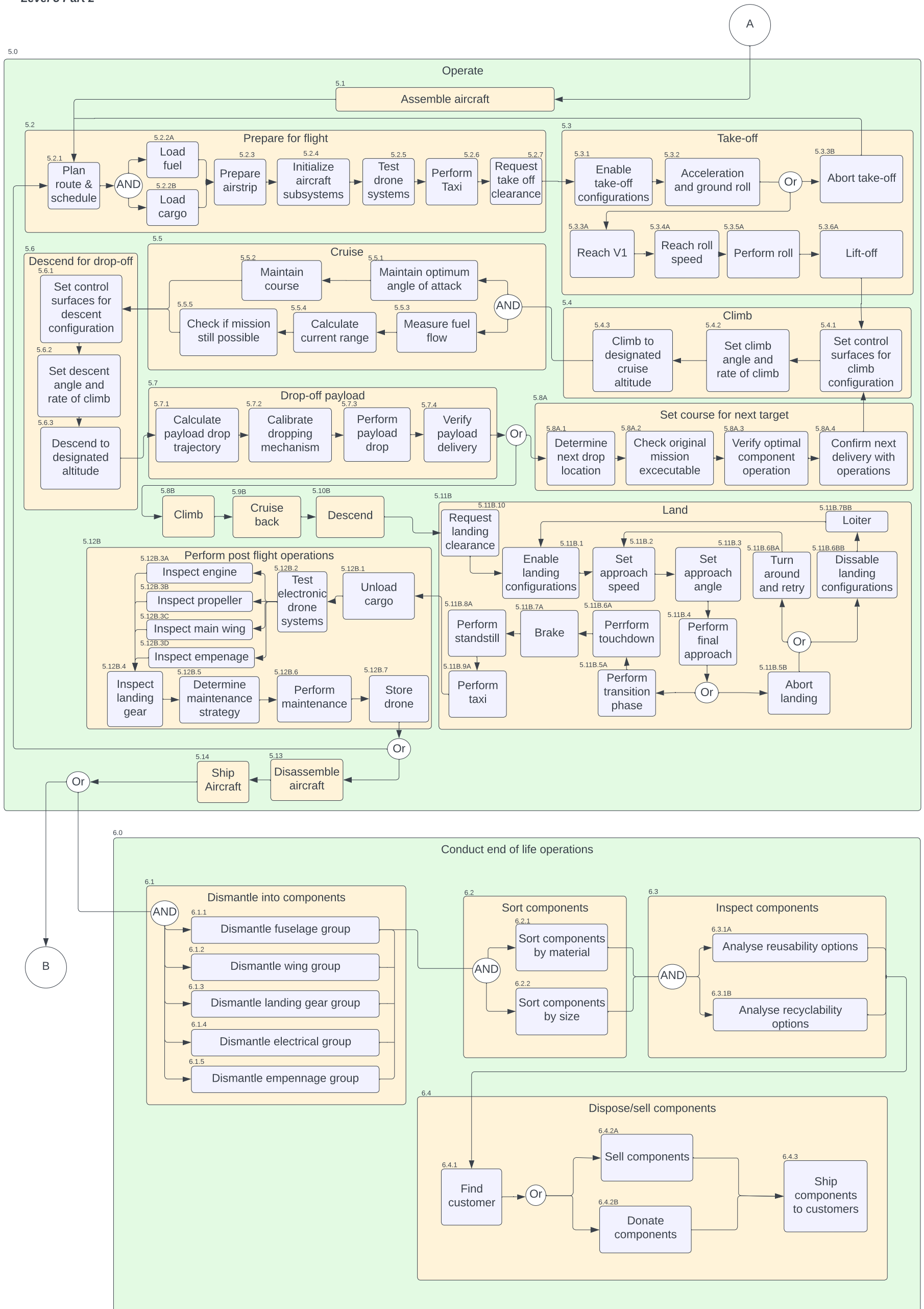
*Level 3 Part 2*



**Figure A.2:** DSE Functional flow diagram of the rest of level 3.

**Table A.1:** Technical risk summary

| # | Risk ID | Cause | Risk event | Consequence | Promise | L | S |
|---|---------|-------|-----------|-------------|---------|---|---|
| 1 | R.PRO.PART.1 | Errors made during the manufacturing process | A manufactured part does not have the expected structural performance | Failure loads of the aircraft cannot be accurately predicted | Performance | L | CR |
| 2 | R.PRO.PART.2 | Inadequate handling procedures, personnel errors | A part is damaged during transportation | A replacement part has to be procured | Schedule, cost | M | MOD |
| 3 | R.PRO.PART.3 | Supply shortages, economic variability | Part is not available | Aircraft manufacture has to be delayed | Schedule | M | MIN |
| 4 | R.PRO.PART.4 | Inadequate handling procedures, personnel errors | Part is lost | Aircraft manufacture has to be delayed | Schedule, Cost | L | MIN |
| 5 | R.PRO.PART.5 | Supply shortages, economic variability | Required equipment is not available | Aircraft manufacture has to be delayed | Schedule | L | MIN |
| 6 | R.PRO.PART.6 | Sickness, transportation issues, miscommunication, etc. | Qualified personnel is not available | Aircraft manufacture has to be delayed | Schedule | H | CR |
| 7 | R.PRO.PART.7 | Errors made during the manufacturing process | Manufacturing schedule is not met | Part is not manufactured on time | Schedule, cost | M | MOD |
| 8 | R.PRO.PART.8 | Insufficient health and safety measures | Personnel injury | Aircraft manufacture delayed | Cost, schedule | L | CR |
| 9 | R.PRO.PART.9 | Inadequate manufacturing procedures | Insufficient part tolerance | The part cannot be used in the final product | Schedule, cost | L | CR |
| 10 | R.PRO.ASM.1 | Inadequate handling procedures, personnel errors | A part is damaged during assembly | A replacement part has to be procured | Schedule, cost | M | MOD |
| 11 | R.PRO.ASM.2 | Inadequate joining procedures, personnel errors | Parts are joined incorrectly | A replacement part has to be procured | Schedule, cost | M | MIN |
| 12 | R.PRO.ASM.3 | Supply shortages, economic variability | Required equipment is not available | Aircraft manufacture has to be delayed | Schedule | H | MIN |
| 13 | R.PRO.ASM.4 | Errors made during the manufacturing process | Manufacturing schedule is not met | Part is not manufactured on time | Schedule | M | MIN |
| 14 | R.PRO.ASM.5 | Sickness, transporttion issues, miscommunication, etc. | Qualified personnel is not available | Aircraft manufacture has to be delayed | Schedule | H | MIN |
| 15 | R.PRO.ASM.6 | Insufficient health and safety measures | Personnel injury | Aircraft manufacture delayed | Cost, schedule | L | CAT |
| 16 | R.PRO.QA.1 | Inappropriate quality assurance plan, personnel error | Low quality parts or assemblies are used in the final product | Failure loads of the aircraft cannot be accurately predicted | Performance | M | CR |

| No. | ID | Cause | Event | Consequence | Affected | Likelihood | Severity |
|---|---|---|---|---|---|---|---|
| 17 | R.DSTR.STR.1 | Supply shortages, economic variability | Required container type is not available | Delay in transportation, increase in cost, storage is not possible | Schedule, cost | M | MOD |
| 18 | R.DSTR.STR.2 | The conditions in a container are not appropriate for the storage of the aircraft | The aircraft is damaged during transportation | Drone integrity is compromised | Performance, schedule, cost | M | CAT |
| 19 | R.DSTR.STR.3 | Inadequate container handling procedures, operator error | The container experiences a structural failure | Drone is damaged | Performance, schedule, cost | L | CAT |
| 20 | R.DSTR.STR.4 | The storage location is not safe | The aircraft is damaged during storage | Drone integrity is compromised | Performance, schedule, cost | M | CAT |
| 21 | R.DSTR.MIS.1 | There is little available information about the area needing aid | Inappropariate mission plan, poor resource alloaction | Mission delayed, mission goal cannot be fulfilled | Schedule, cost | VL | CR |
| 22 | R.DSTR.MIS.2 | Key mission locations are chosen incorrectly | Mission base cannot be set up, flight plans are set-up incorrectly | Aid cannot be delivered to the correct recipients | Schedule | VL | CAT |
| 23 | R.DSTR.MIS.3 | The type or amount of aid is assessed incorrectly | The delivered aid is not sufficient | Mission delayed, mission goals cannot be fulfilled | Schedule, cost | VL | CAT |
| 24 | R.DSTR.SHP.1 | Shipping delays, bad weather, pirates | Aircraft does not make it to desired loaction on time | Mission delayed, mission goals cannot be fulfilled | Schedule, cost | H | CR |
| 25 | R.DSTR.SHP.2 | The mission is expected to take place in a location with some infrastructure disruptions | The condition of infrastructure is inadaquate for delivery of the containers containing the aircraft | Drone integrity is compromised, mission delayed, mission goals cannot be fulfilled | Performance, schedule, cost | VH | CR |
| 26 | R.DSTR.SHP.3 | Poor communication | The aircraft is delivered to the incorrect location | Mission delayed, mission goals cannot be fulfilled | Schedule, cost | VL | CAT |
| 27 | R.OPS.ASM.1 | Inadequate assembly manuals, untrained personnel | Structural damage to parts/sub-assemblies | Mission delayed, mission goals cannot be fulfilled | Performance, schedule, cost | VL | CR |
| 28 | R.OPS.ASM.2 | Inadequate assembly manuals, untrained personnel | Incorrect/incomplete assebly of components/parts | Mission delayed, mission goals cannot be fulfilled | Schedule, performance | VL | CR |
| 29 | R.OPS.ASM.3 | Sickness, transportation issues, miscommunication, etc. | Qualified personnel is not available | Aircraft assembly has to be delayed | Schedule | L | MOD |
| 30 | R.OPS.PREP.1 | Inadequate testing manuals, personnel errors | Incomplete tests of the aircraft systems | Aircraft can fail unpredictably | Performance | VL | CR |
| 31 | R.OPS.PREP.2 | Inadequate fueling manuals, personnel errors | Incorrect fuel type loaded | Possbile engine damage | Performance, schedule, cost | VL | CR |
| 32 | R.OPS.PREP.3 | Fuel scarcity | Insufficient fuel availability | Mission delayed, mission goals cannot be fulfilled | Schedule | M | CR |

| # | Code | Cause | Effect | Affected | Prob. | Severity |
|---|------|-------|--------|----------|-------|----------|
| 33 | R.OPS.PREP.4 | Inadequate handling procedures, personnel errors | Damage to cargo while loading | Mission delayed, mission goals cannot be fulfilled | Schedule, cost | M | MIN |
| 34 | R.OPS.PREP.5 | Inadequate mission plan, miscommunication | Incorrect type of aid/ amount loaded into package | Mission delayed, mission goals cannot be fulfilled | Schedule, cost | L | CR |
| 35 | R.OPS.PREP.6 | Inadequate handling procedures, personnel errors | Incorrectly loaded cargo | Mission delayed, mission goals cannot be fulfilled | Schedule, cost | L | MOD |
| 36 | R.OPS.PREP.7 | Miscalculations on required amount of fuel, incorrect fuel measurements | Incorrect fuel amount loaded | Risk of crashing, mission delayed, mission goals cannot be fulfilled | Schedule, cost | VL | CAT |
| 37 | R.OPS.PREP.8 | Inadequate mission plan, personnel errors | Too poor airstrip preparation | Damaged aircraft, unable to take-off/land | Schedule, cost | VL | CR |
| 38 | R.OPS.PREP.9 | Miscommunication/ unforeseen weather | Change in planned schedule and/or route | Mission delayed | Schedule | M | MOD |
| 39 | R.OPS.PREP.10 | Weather conditions, Undetected damage | Loss of communication with local authorities | Mission delayed, mission goals cannot be fulfilled | Schedule | M | NEG |
| 40 | R.OPS.TOFF.1 | Undetected damage, poor take off conditions, pilot error, environmental conditions | Propulsion system failure | Aborted take off, Drone damange | Schedule, cost, performance | L | CR |
| 41 | R.OPS.TOFF.2 | Undetected damage, poor take off conditions, pilot error | Control system failure | Aborted take off, Drone damange | Schedule, cost, performance | L | CR |
| 42 | R.OPS.TOFF.3 | Undetected damage, poor take off conditions, pilot error | Electronics failure | Aborted take off, Drone damange | Schedule, cost, performance | L | CR |
| 43 | R.OPS.TOFF.4 | Undetected damage, poor take off conditions, pilot error | Sensor failure | Aborted take off, Drone damange | Schedule, cost, performance | L | CR |
| 44 | R.OPS.TOFF.5 | Inadequate flight manuals, personnel errors | Incorrect take off thrust setting | Aborted take off | Schedule, cost, performance | L | MIN |
| 45 | R.OPS.TOFF.6 | Poor ground infrastructure, airstrip, organisation, miscommunication | Collision with obstacle | Aborted take off, Drone damange | Schedule, cost, performance | L | CAT |
| 46 | R.OPS.TOFF.7 | Signal/power loss | Loss of communication | Drone damange | Schedule, cost, performance | M | CR |
| 47 | R.OPS.CLB.1 | Inadequate flight manuals, personnel errors, compromised communication channels | Incorrect configuration setting | Drone damange, sub-optimal climb procedure | Schedule, performance | L | MOD |

| No. | ID | Cause | Failure | Effect | Impact | L/M | Severity |
|---|---|---|---|---|---|---|---|
| 48 | R.OPS.CLB.2 | Inadequate flight manuals, personnel errors, compromised communication channels | Incorrect climb angle/ rate of climb selected | Drone damange, sub-optimal climb procedure | Schedule, performance | L | MOD |
| 49 | R.OPS.CRS.1 | Undetected damage, pilot error, environmental reasons | Propulsion system failure | Mission delayed, mission goals cannot be fulfilled, drone damage possible | Schedule, performance, cost | L | CR |
| 50 | R.OPS.CRS.2 | Undetected damage, pilot error, software errors | Control system failure | Mission delayed, mission goals cannot be fulfilled, drone damage possible | Schedule, performance, cost | L | CR |
| 51 | R.OPS.CRS.3 | Undetected damage, pilot error, software errors | Electronics failure | Mission delayed, mission goals cannot be fulfilled, drone damage possible | Schedule, performance, cost | L | CR |
| 52 | R.OPS.CRS.4 | Undetected damage, pilot error, software errors | Sensor failure | Mission delayed, mission goals cannot be fulfilled, drone damage possible | Schedule, performance, cost | L | CR |
| 53 | R.OPS.CRS.5 | Undetected damage, pilot error, software errors | Loss of measured fuel flow information | Mission delayed, mission goals cannot be fulfilled, drone damage possible | Schedule, performance, cost | L | MIN |
| 54 | R.OPS.CRS.6 | Weather conditions, Undetected damage | Communication issues | Mission delayed, mission goals cannot be fulfilled, drone damage possible | Schedule, performance, cost | M | CR |
| 55 | R.OPS.CRS.7 | Poor mission flight path planning, undetected damage, operator errors | Defence strategy failure | Drone is damaged/ destroyed | Schedule, performance, cost | L | CAT |
| 56 | R.OPS.DES.1 | Undetected damage, pilot error, software errors | Incorrect angle of descent and rate of descent | Collision with ground, mission delayed | Schedule, performance, cost | L | CAT |
| 57 | R.OPS.DES.2 | Sensor failure | Failure of altitude detection systems | Collision with ground, mission delayed | Performance, cost | M | CR |
| 58 | R.OPS.DRP.1 | Undetected damage, pilot error, software errors | Deployment mechanism failure | Mission delayed, mission goals cannot be fulfilled, drone damage possible | Schedule, cost | M | CR |
| 59 | R.OPS.DRP.2 | Weather, innapropiate speed, Geo-location services, miscommunication | Innacurate drop location | Mission delayed, mission goals cannot be fulfilled, drone damage possible | Schedule, cost | M | MOD |

| # | ID | Causes | Failure mode | Consequence | Impact | Likelihood | Severity |
|---|---|---|---|---|---|---|---|
| 60 | R.OPS.DRP.3 | Faulty payload deployment mechanism, miscommunication | Incorrent amount/ type of aid dropped | Mission delayed, mission goals cannot be fulfilled, drone damage possible | Schedule, cost | L | MIN |
| 61 | R.OPS.NXT.1 | Weather conditions, Undetected damage | Communication issues | Mission delayed, mission goals cannot be fulfilled, drone damage possible | Schedule, cost | M | CR |
| 62 | R.OPS.NXT.2 | Inadequate flight plan | Sub-optimal flight path | Mission delayed, mission goals cannot be fulfilled, drone damage possible | Schedule, cost | VL | MIN |
| 63 | R.OPS.LAN.1 | Pilot error, undetected damage | Landing gear failure | Drone is damaged/ destroyed, airstrip damage | Schedule | L | CR |
| 64 | R.OPS.LAN.2 | Undetected damage, pilot error, software errors | Propulsion system failure | Mission delayed, mission goals cannot be fulfilled, drone damage possible | Schedule, performance, cost | L | MOD |
| 65 | R.OPS.LAN.3 | Undetected damage, pilot error, software errors | Control systems failure | Mission delayed, mission goals cannot be fulfilled, drone damage possible | Schedule, performance, cost | L | CR |
| 66 | R.OPS.LAN.4 | Undetected damage, pilot error, software errors | Electronics failure | Mission delayed, mission goals cannot be fulfilled, drone damage possible | Schedule, performance, cost | L | CAT |
| 67 | R.OPS.LAN.5 | Undetected damage, pilot error, software errors | Sensor failure | Mission delayed, mission goals cannot be fulfilled, drone damage possible | Schedule, performance, cost | L | CAT |
| 68 | R.OPS.LAN.6 | Undetected damage, pilot error, software errors | Brake system failure | Mission delayed, mission goals cannot be fulfilled, drone damage possible | performance, cost | L | CR |
| 69 | R.OPS.LAN.7 | Inadequate flight manuals, personnel errors, compromised communication channels | Incorrect configuration setting | Drone damange, sub-optimal landing procedure | Schedule, performance | L | CR |
| 70 | R.OPS.POF.1 | Inadequate inspection manuals, personnel errors | Incomplete/poor inspection | Aircraft can fail unpredictably | performance | L | CR |
| 71 | R.OPS.POF.2 | Inadequate maintenance manuals, personnel errors, poor maintenance logs | Maintenance takes longer than expected | Aircraft maintenance/ operations have to be delayed | Schedule | M | MIN |
| 72 | R.OPS.POF.3 | Unexpected component failure, lack of spare components | Lack of adequate maintenance equipment | Aircraft maintenance/ operations have to be delayed | Schedule | H | MIN |

| # | ID | Causes | Event | Consequence | Impact | Likelihood | Severity |
|---|---|---|---|---|---|---|---|
| 73 | **R.OPS.POF.4** | Inadequate maintenance manuals, personnel errors, poor maintenance logs | Incorrect/ incomplete maintenance logs | Aircraft maintenance/ operations have to be delayed | Schedule, performance | L | MIN |
| 74 | **R.OPS.DIS.1** | Inadequate disassembling manuals, untrained personnel | Structural damage to parts/sub-assemblies | Mission delayed, mission goals cannot be fulfilled | Performance, schedule, cost | L | CR |
| 75 | **R.OPS.DIS.2** | Inadequate handling procedures, personnel errors | Part is lost | Future aircraft missions have to be delayed, a replacement part has to be acquired | Schedule, Cost | L | MIN |
| 76 | **R.OPS.DIS.3** | Insufficient health and safety measures | Personnel injury | Mission delayed, mission goals cannot be fulfilled, morale loss | Cost, schedule | L | MOD |
| 77 | **R.OPS.DIS.4** | Sickness, transportation issues, miscommunication, etc. | Qualified personnel is not available | Aircraft dissasembly has to be delayed | Schedule | H | MOD |
| 78 | **R.EOL.DIS.1** | Inadequate disassembling manuals, untrained personnel | Part/component is damaged | Sustainability goals are not met | Cost | M | NEG |
| 79 | **R.EOL.DIS.2** | failure of security system, Inadequate disassembling manuals, untrained personnel | Component is lost | Sustainability goals are not met | Cost | L | MIN |
| 80 | **R.EOL.DIS.3** | Failure of security system | Unauthorized people entering storage facility | (Fatal) Injury | Cost | L | CR |
| 81 | **R.EOL.DIS.4** | Inadequate storage conditions, poor long term design considerations | It is not possible to safely dismantle components | Sustainability goals are not met, injury, loss of economic value | Cost | M | MIN |
| 82 | **R.EOL.DIS.5** | Unexpected customer order, supply shortages, economic variability | Lack of adequate dismantling equipment | Delay in dismantling, sustainability goals not met, loss of customer | Cost | L | MOD |
| 83 | **R.EOL.SOR.1** | Inadequate inspection manuals, personnel errors | Material of component is determined incorrectly | Delay in sorting, sustainability goals are not met | Cost | L | MIN |
| 84 | **R.EOL.SOR.2** | Sickness, transportation issues, miscommunication, etc. | No qualified personnel to sort parts | Delay in sorting, sustainability goals are not met | Cost | M | NEG |
| 85 | **R.EOL.INS.1** | Inadequate inspection manuals, personnel errors | Component quality is assessed incorrectly | Sustainability goals not met, loss of economic values | Cost | L | MIN |
| 86 | **R.EOL.INS.2** | Inadequate inspection manuals, personnel errors | Reusability/recylability of a component is not assessed correctly | Sustainability goals not met, loss of economic values | Cost | L | MIN |
| 87 | **R.EOL.DSS.1** | Supply shortages, economic variability | The component cannot be transported | Sustainability goals not met, loss of economic values | Cost | L | MIN |

| # | Code | Cause | Consequence | Effect | Type | | |
|---|------|-------|-------------|--------|------|---|---|
| 88 | R.EOL.DSS.2 | Poor long term design considerations | The component cannot be sustainably disposed of | Sustainability goals not met, loss of economic values | Cost | M | MIN |
| 89 | R.DES.CAL.1 | Inadequate methodology and/or process | The structural performance of the aircraft is overestimated | The aircraft breaks during operations | Performance | L | CAT |
| 90 | R.DES.CAL.2 | Inadequate methodology and/or process | The main wing and empennage performance are overestimated | The aircraft is not able to take-off | Performance | L | CAT |
| 91 | R.DES.CAL.3 | Inadequate methodology and/or process | The engine performance is overestimated | The aircraft is unable to generate enough thrust | Performance | L | CR |
| 92 | R.DES.CAL.4 | Inadequate methodology and/or process | The reliability of the aircraft is overestimated | The aircraft has a lot of unexpected failures | Performance | VL | CAT |
| 93 | R.DES.CAL.5 | Inadequate methodology and/or process | The material selection is done incorrectly | The aircraft becomes to heavy | Performance | VL | CR |
| 94 | R.DES.GEN.1 | Inadequate trade-off CReria, trade-off weights and/or scores | The trade-off is not performed correctly | The optimal design choice is not chosen | Performance | L | MOD |
| 95 | R.DES.GEN.2 | Incorrect or no verification tests | The system is not verified correctly | The aircraft does not perform as expected during operation | Performance | VL | CAT |
| 96 | R.DES.GEN.3 | Not reading or interpretation the top level requirements | The system is not validated correctly | The aircraft does not perform as intended during operation | Performance | VL | CAT |
| 97 | R.DES.GEN.4 | Inadequate methodology and/or process | The costs are significantly underestimated | The high costs make it impossible to produce the aircraft | Cost | L | CR |
| 98 | R.DES.GEN.5 | Regulatory bodies impose strict regulations that can change with time and vary by location | The product does cannot meet regulatory requirements | The aircraft may not be able to operate in some areas | Performance | L | MOD |
| 99 | R.DES.GEN.6 | There are considerable economical, political and technological challenges limiting possible sustainability solutions | The design is not sufficiently sustainable | Some of the design goals are not mate | Performance | M | NEG |
| 100 | R.OPS.PREP.11 | Communication error between ground crew and pilot | Airplane propeller suddenly rotates, hurting personnel | Dangerous situations for the ground crew develop | Safety | CAT | M |
| 101 | R.OPS.CRS.8 | Navigation system fails | Airplane starts diverting from prescribed airspace | Endangers people on the ground | Safety | CR | M |
| 102 | R.OPS.CRS.9 | Insufficient software security | Drone is hijacked | Possible usage of the aircraft as weapon | Safety | CAT | VL |

| | | | | | | CAT | |
|---|---|---|---|---|---|---|---|
| 103 | **R.OPS.CRS.10** | Stall characteristics are considered bad | Stall may become unrecoverable | Hull loss | Safety | CAT | L |
| 104 | **R.OPS.POF.5** | Damage to the fuel tank by enemy fire | Fuel can leak on the landing strip and ground station | Dangerous situations for the ground crew and other aircraft | Safety | CAT | VL |
| 105 | **R.OPS.DRP.4** | Drop operator not present at drop site on time | Unable to deploy packages | Mission not fulfilled | Schedule | CR | L |
| 106 | **R.DEV.SAS.1** | Chosen engine becomes unavailable | Plane cannot be produced | Plane cannot be used | Operation | CAT | L |

**Table A.2:** Severe risk mitigation strategies

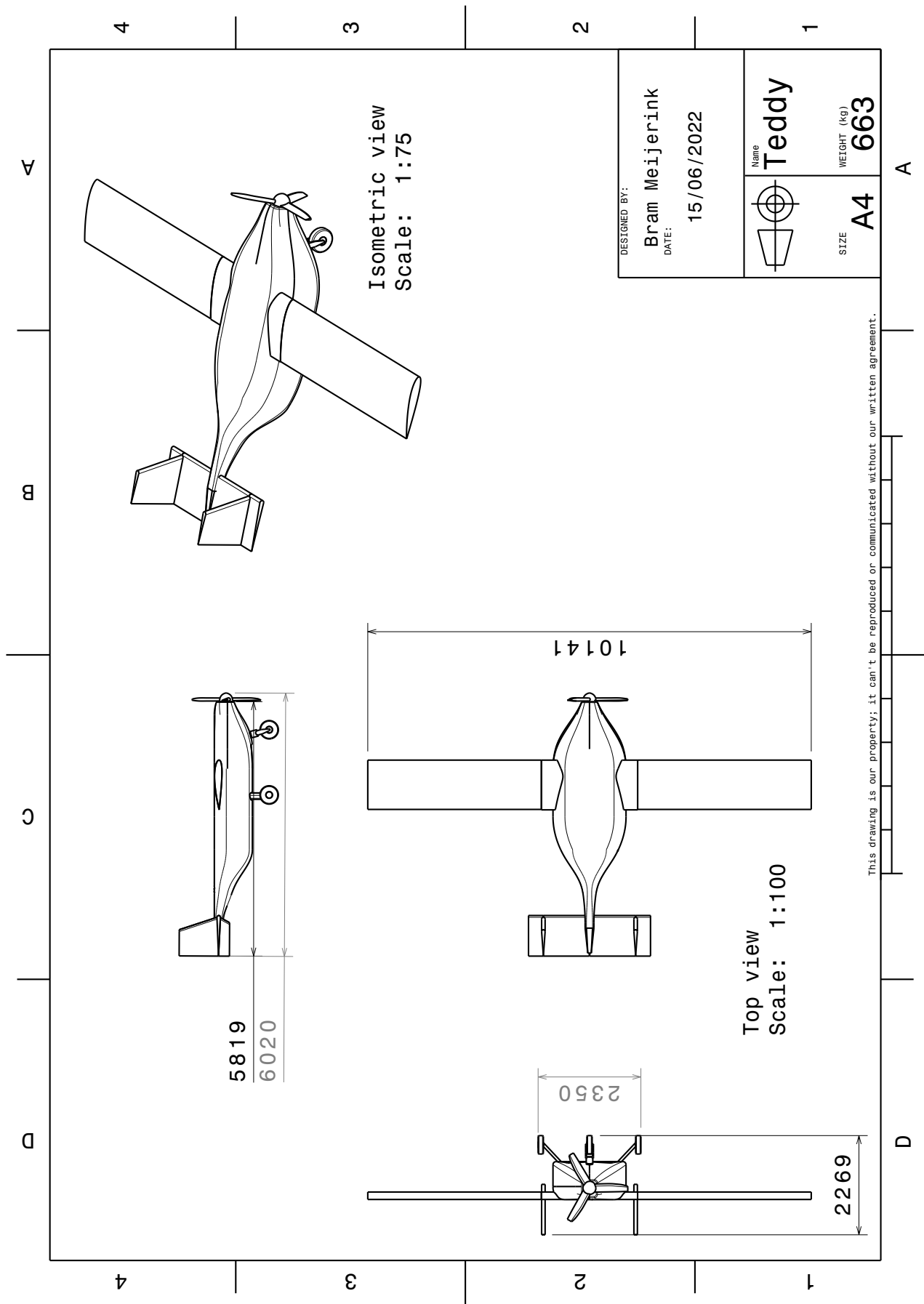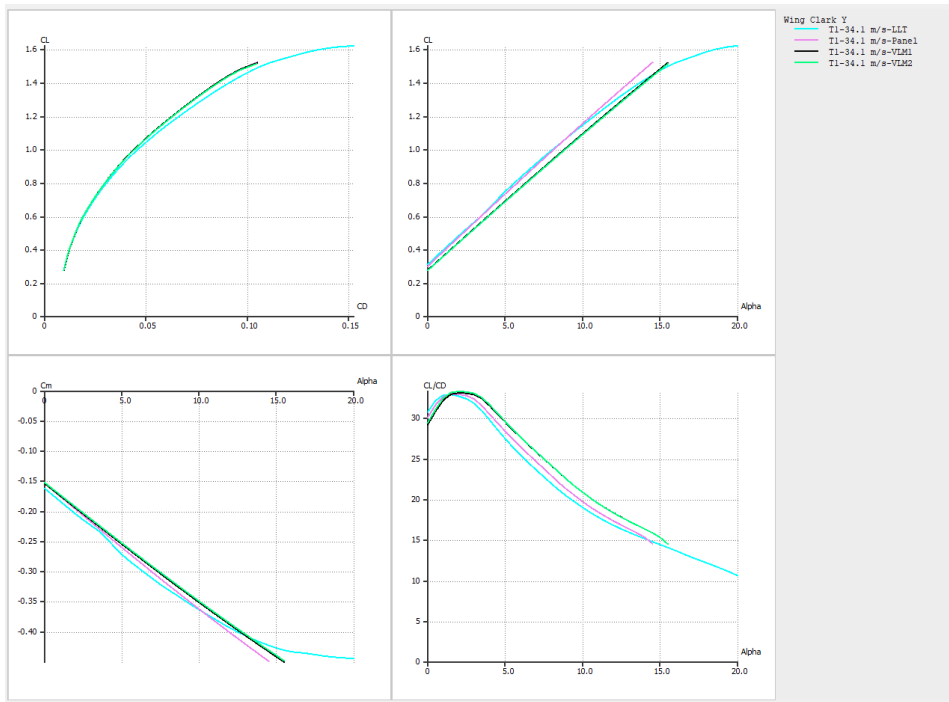| # | Risk ID | Mitigation strategy | L | S |
|---|---------|---------------------|---|---|
| 6 | **R.PRO.PART.6** | Sickness: have standby personnel available. Transport issues: have backup transport available. miscommunication: verify of other persons understood | M | MOD |
| 15 | **R.PRO.ASM.6** | Train personnel to prevent injury; better health and safety measure; have reserve workers on standby | VL | CR |
| 16 | **R.PRO.QA.1** | Inappropriate quality assurance plan: revise plan until quality matches required quality, personnel error: material and parts are checked by multiple employees | VL | CR |
| 18 | **R.DSTR.STR.2** | Drone is checked before storage in container and after transport. Shipping material, such as foam is used to ensure safe travels. | VL | CAT |
| 19 | **R.DSTR.STR.3** | Tightly secure UAV to prevent damage; use reliable shipping companies that assure safe delivery; include stiffening structure inside the container when using unreliable shipping companies | VL | CAT |
| 20 | **R.DSTR.STR.4** | Provide a loading checklist, loading and unloading handbook to ensure aircraft parts are handled and constrained correctly. Add padding to container were parts can come in contact. Constrain the aircraft parts inside the container. Have yearly container inspection to ensure integrity of the container. | VL | CAT |
| 24 | **R.DSTR.SHP.1** | Include extra range capabilities to circumnavigate bad weather. | M | CR |
| 25 | **R.DSTR.SHP.2** | Allow the system capable to setup operations using a make-shift airstrip by flying the system in. Fly the aircraft in from a larger/established airport or make the system capable to be airdropped from larger cargo craft. Allow for large air drops to re-supply the ground base. Optimize ground base location selection process | H | MOD |
| 32 | **R.OPS.PREP.3** | Store backup fuel in tanks | L | MOD |
| 45 | **R.OPS.TOFF.6** | Check airstrip visually before usage | VL | CAT |
| 46 | **R.OPS.TOFF.7** | Have backup antennas | M | MOD |
| 54 | **R.OPS.CRS.6** | Perform maintenance more often, avoid flying in bad weather | L | CR |
| 55 | **R.OPS.CRS.7** | hire person to do flight plans, perform maintenance more often, give operators extra training | VL | CAT |
| 56 | **R.OPS.DES.1** | Check aircraft structure regularly for damage, pilot error: disallow extreme movement of the aircraft with software. Test software extensively. Create a safe mode in which the aircraft always stays operational. | VL | CR |
| 57 | **R.OPS.DES.2** | Add possibility for manual control at all stages of flight. Keep accurate record of flight characteristics at each point of the profile, eg. velocity, heading, altitude, position, fuel. | M | MOD |
| 58 | **R.OPS.DRP.1** | Redundant deployment system; extensive pre-departure inspection; possibility for robust deployment mechanism that reduces probability eg. no payload hatch doors. | L | CR |
| 61 | **R.OPS.NXT.1** | Automatic deploy or return system, climb to 10,000 ft and return to base. Use secondary short range communication system for landing. | M | MOD |
| 66 | **R.OPS.LAN.4** | Redundant electrical system, monitor electric flow and charges | VL | CR |
| 89 | **R.DES.CAL.1** | Take bigger margins | VL | CAT |
| 90 | **R.DES.CAL.2** | Take bigger margins | VL | CAT |
| 100 | **R.OPS.PREP.11** | Mechanical limiting of the aircraft when moving in the ground station with the use of a dead man's switch | CAT | VL |
| 101 | **R.OPS.CRS.8** | Use of a ballistic parachute will prevent the aircraft from drifting too far from course and it limits the danger to the people on the ground | MOD | L |
| 102 | **R.OPS.CRS.9** | Ballistic parachute that is operated remotely or will be deployed when the plane does not adhere to predetermined rules | CR | VL |
| 103 | **R.OPS.CRS.9** | Stall prevention software to aid pilot | CAT | VL |
| 104 | **R.OPS.POF.5** | Fire prevention equipment shall be ready on the airfield and fuel adsorbing material shall be available | CR | VL |
| 105 | **R.OPS.DRP.4** | Begin mission when there is confirmation that the drop operator is expected to be ready at the drop site. Use additional fuel to loiter | CR | VL |
| 106 | **R.DEV.SAS.1** | Keep in contact with the engine manufacturer on status of the production | CAT | L |

Isometric view
Scale: 1:75

Top view
Scale: 1:100

DESIGNED BY:
Bram Meijerink
DATE:
15/06/2022

Name
Teddy

WEIGHT (kg)
663

SIZE
A4

This drawing is our property; it can't be reproduced or communicated without our written agrement.

10141

5819
6020

2350

2269

**Figure A.3:** 3 View drawing of the final design

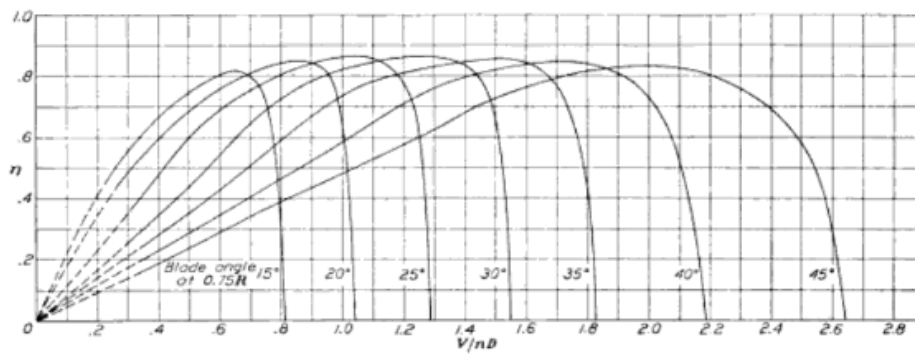**Figure B.1:** Comparison of 3D Wing Analysis in XFLR5 Using Finalised Wing Planform



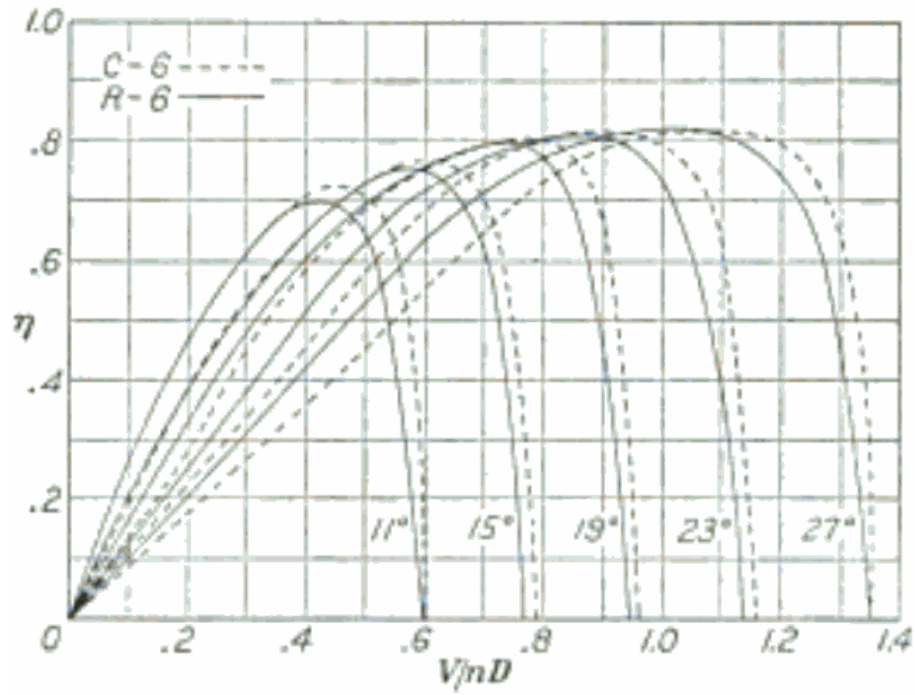**Figure B.2:** Propeller efficiency Clark-Y airfoil [4]

FIGURE 13c.—Efficiency

**Figure B.3:** Propeller efficiency Clark-Y airfoil [17]